



**A University of Sussex DPhil thesis**

Available online via Sussex Research Online:

<http://sro.sussex.ac.uk/>

This thesis is protected by copyright which belongs to the author.

This thesis cannot be reproduced or quoted extensively from without first obtaining permission in writing from the Author

The content must not be changed in any way or sold commercially in any format or medium without the formal permission of the Author

When referring to this work, full bibliographic details including the author, title, awarding institution and date of the thesis must be given

Please visit Sussex Research Online for more information and further details

**Investigations into the Biochemical and Cellular Biology  
of a Cytoplasmic Dynein Mutation,  
Abnormal Rear Leg (*Ar1*)**

**By**

**Amelia Philpott  
(BSc Hons)**

**Thesis submitted for the degree of Doctor of Philosophy  
University of Sussex**

**September 2010**

I hereby declare that this thesis has not been submitted in whole or part to another university for any other degree.

This work is my own, except where stated otherwise.

Amelia Philpott

September 2010

## Acknowledgements

I would like to thank my supervisor, Dr Majid Hafezparast for all his support and guidance during this project. I am grateful to Drs Ali Morsi El-Kadi, Wenhan Deng and Violetta Soura for their invaluable help. I am extremely grateful to Professor Viki Allan, who kindly gave me much of her time and expertise during my learning and optimisation of the dynein purification protocol and MT gliding assay. I am also indebted to Professor Rob Cross for generously allowing me to use his VE-DIC microscopy equipment and also offering invaluable advice and guidance. I am also tremendously grateful to all of his lab group for their help, particularly Kase (Dr Kuniyoshi Kaseda) for kindly giving his time to help with the MT gliding assay. I am appreciative of the help and explanations provided to me by Professor Tony Pullen which have helped me to better analyse TEM micrographs and learn new fixation techniques, and to Dr Julian Thorpe for patiently teaching me to use the TEM. I am grateful to Professor Tony Moore for his help with the mitochondrial assays and for allowing me to use his equipment for the assays and mitochondrial preparations. I would like to thank the University of Sussex for providing me with the studentship to allow me to undertake this project. Finally, I would like to thank my family, particularly my parents and David Whitner for all their support and encouragement.

## Contents

List of figures and tables

Abbreviations

Abstract

### **Chapter I - Introduction**

<b>I.1</b>	Motor proteins	<b>1</b>
<b>I.2</b>	Dyneins	<b>1</b>
<b>I.2.1</b>	Cytoplasmic dynein	<b>2</b>
<b>I.2.1.1</b>	Dynein heavy chain	<b>2</b>
<b>I.2.1.2</b>	Dynein accessory chains	<b>7</b>
<b>I.2.2</b>	Dynein in neurons	<b>9</b>
<b>I.3</b>	Dynein regulators and adaptors	<b>11</b>
<b>I.3.1</b>	Dynactin	<b>11</b>
<b>I.3.2</b>	Lis1, NudE and NudEL	<b>16</b>
<b>I.4</b>	Dynein cargos	<b>19</b>
<b>I.4.1</b>	Golgi	<b>19</b>
<b>I.4.2</b>	Mitochondria	<b>20</b>
<b>I.4.3</b>	Endosomes	<b>22</b>
<b>I.4.3.1</b>	Receptor mediated endocytosis	<b>23</b>
<b>I.4.3.1.1</b>	EGF/EGFR endocytosis	<b>24</b>
<b>I.5</b>	Dynein mutations	<b>24</b>
<b>I.5.1</b>	Legs at odd angles ( <i>Loa</i> ) and Cramping 1 ( <i>Cral</i> )	<b>25</b>
<b>I.5.2</b>	Sprawling ( <i>Swl</i> )	<b>28</b>
<b>I.5.3</b>	Motor neuron disease and SOD1	<b>30</b>
<b>I.5.4</b>	Dynein mutations and SOD1	<b>32</b>
<b>I.5.5</b>	Abnormal rear leg ( <i>Arl</i> )	<b>35</b>
<b>I.5.6</b>	<i>Arl</i> and SOD1	<b>38</b>
<b>I.5.7</b>	Axonemal dynein mutation	<b>38</b>
<b>I.6</b>	Aims of project	<b>40</b>

## **Chapter II - Materials and methods**

<b>II.1</b>	Buffers and media	<b>41</b>
<b>II.2.1</b>	Genotyping	<b>44</b>
<b>II.2.2</b>	SDS-PAGE and Western Blotting	<b>45</b>
<b>II.2.3</b>	Dynein quantification in brain tissue	<b>46</b>
<b>II.2.4</b>	Dynein quantification in spinal cord tissue	<b>46</b>
<b>II.2.5</b>	Sucrose density gradient analysis	<b>47</b>
<b>II.2.6</b>	Dynein purification	<b>47</b>
<b>II.2.7</b>	Tubulin polymerisation	<b>49</b>
<b>II.2.8</b>	MT gliding assay	<b>49</b>
<b>II.2.9</b>	MT dependent ATPase assay	<b>50</b>
<b>II.2.10</b>	MT binding assay	<b>50</b>
<b>II.3.1</b>	Collection and culture of MEFs	<b>50</b>
<b>II.3.2</b>	Golgi reassembly	<b>51</b>
<b>II.3.3</b>	Endosomal trafficking	<b>51</b>
<b>II.3.4</b>	Endosomal trafficking in live cells	<b>52</b>
<b>II.3.5</b>	Tracking mitochondria in live cells	<b>53</b>
<b>II.3.6</b>	Culturing of motor neurons	<b>54</b>
<b>II.4.1</b>	Perfusion fixation	<b>55</b>
<b>II.4.2</b>	Preparation of mitochondria and O <sub>2</sub> assay	<b>55</b>

## **Chapter III - Investigating the effect of the *Ar1* mutation on dynein heavy chain protein**

<b>III.1</b>	Introduction	<b>57</b>
<b>III.2</b>	Effect of the mutation on mice	<b>57</b>
<b>III.3</b>	Dynein heavy chain protein	<b>58</b>
<b>III.4</b>	Integrity of the dynein complex	<b>59</b>
<b>III.5</b>	Purifying the dynein complex for analysis of its function	<b>60</b>
<b>III.6</b>	MT gliding assay	<b>62</b>
<b>III.7</b>	MT dependent ATPase assay	<b>63</b>
<b>III.8</b>	MT binding assay	<b>64</b>
<b>III.9</b>	Discussion	<b>65</b>

## **Chapter IV - Investigating the effect of the *Arl* mutation on cargo transport**

<b>IV.1</b>	Introduction	<b>70</b>
<b>IV.2</b>	<i>In vitro</i> cell system	<b>71</b>
<b>IV.3</b>	Golgi reassembly	<b>72</b>
<b>IV.4</b>	EGF trafficking in fixed cells	<b>73</b>
<b>IV.5</b>	EGF trafficking in live cells	<b>74</b>
<b>IV.6</b>	Transport of Mitochondria	<b>75</b>
<b>IV.7</b>	Transport of cargo in motor neurons	<b>76</b>
<b>IV.8</b>	Discussion	<b>76</b>

## **Chapter V - Investigating the effect of the *Arl* mutation on the Golgi apparatus and mitochondria using transmission electron microscopy**

<b>V.1</b>	Introduction	<b>78</b>
<b>V.2</b>	Ultrastructural analysis of Golgi	<b>78</b>
<b>V.3</b>	Ultrastructural analysis of mitochondria	<b>80</b>
<b>V.4</b>	Measuring rates of respiration	<b>81</b>
<b>V.5</b>	Discussion	<b>82</b>

## **Chapter VI - Final Discussion**

<b>VI.1</b>	Summary of data	<b>88</b>
<b>VI.2</b>	Significance of results and conclusions	<b>89</b>
<b>VI.3</b>	Future directions	<b>93</b>

<b>Bibliography</b>	<b>95</b>
---------------------	-----------

<b>Publications</b>	<b>105</b>
---------------------	------------

## Figures and Tables

### Chapter I

#### Tables:

<b>Table 1</b>	Comparisons between <i>Loa</i> and <i>CraI</i>	<b>28</b>
----------------	--	-----------

#### Figures:

<b>Figure 1</b>	Schematic of cytoplasmic dynein	<b>2</b>
<b>Figure 2</b>	Diagram showing the arrangement of domains of C-terminus of the heavy chain	<b>4</b>
<b>Figure 3</b>	Schematic demonstrating the model for a linker domain in the dynein powerstroke	<b>6</b>
<b>Figure 4</b>	Schematic showing structure of dynactin	<b>12</b>
<b>Figure 5</b>	Schematic of cytoplasmic dynein showing sites of interaction with regulators and adaptors	<b>17</b>

### Chapter II

#### Tables:

<b>Table 2</b>	Antibodies	<b>44</b>
----------------	------------	-----------

### Chapter III

#### Tables:

<b>Table 3</b>	Motility assay conditions	<b>62</b>
----------------	---------------------------	-----------

#### Figures:

<b>Figure 6</b>	Genotypes of a selection of mice used in this project	<b>58</b>
<b>Figure 7 A and B</b>	Quantification of DHC in brain and spinal cord tissue from WT and <i>Arl/+</i> mice	<b>59</b>
<b>Figure 8</b>	Western blot of sucrose density gradient	<b>60</b>
<b>Figure 9</b>	Western blots of WT and <i>Arl/+</i> dynein complex from dynein isolation	<b>60</b>
<b>Figure 10</b>	Coomassie gels of WT and <i>Arl/+</i> dynein complex from dynein isolation	<b>61</b>
<b>Figure 11 A and B</b>	Graphs showing average motility speeds from MT gliding assays	<b>62</b>
<b>Figure 12</b>	Summary of ATP/NADH coupled assay	<b>64</b>

<b>Figure 13 A and B</b>	Binding of dynein to MTs in WT and <i>Arl/+</i> , western blot and graph	<b>65</b>
--------------------------	--	-----------

## **Chapter IV**

### **Figures:**

<b>Figure 14</b>	Golgi reassembly after disruption with NZ in WT, <i>Loa/+</i> , <i>Arl/+</i> and <i>Arl/Loa</i> MEFs	<b>72</b>
<b>Figure 15 A and B</b>	Quantification of Golgi reassembly after disruption with NZ in WT, <i>Loa/+</i> , <i>Arl/+</i> and <i>Arl/Loa</i> MEFs, graph and table	<b>73</b>
<b>Figure 16</b>	Endosomal trafficking chase of Alexa Fluor 555 conjugated EGF in WT, <i>Loa/+</i> , <i>Arl/+</i> and <i>Arl/Loa</i> MEFs	<b>73</b>
<b>Figure 17</b>	Graph showing number of EGF positive vesicles remaining in WT, <i>Loa/+</i> , <i>Arl/+</i> and <i>Arl/Loa</i> MEFs after indicated timepoints	<b>74</b>
<b>Figure 18 A and B</b>	Endosomal trafficking chase of Alexa Fluor 555 conjugated EGF in WT, and <i>Arl/+</i> MEFs, and trajectories	<b>75</b>
<b>Figure 19</b>	Quantification of speed of endosome movement in WT and <i>Arl/+</i> MEFs	<b>75</b>
<b>Figure 20</b>	Still frames from movies showing movement of mitochondria in WT and <i>Arl/+</i> MEFs	<b>75</b>
<b>Figure 21</b>	Graph showing mean mitochondrial speeds in WT and <i>Arl/+</i> MEFs	<b>76</b>

## **Chapter V**

### **Figures:**

<b>Figure 22</b>	TEM micrographs showing Golgi structure in WT and <i>Arl/+</i> cells	<b>79</b>
<b>Figure 23</b>	Graph of quantification of number of mitochondria in cell body of WT and <i>Arl/+</i> neuronal cells	<b>80</b>
<b>Figure 24</b>	Graph showing average neuron soma diameter in WT and <i>Arl/+</i> spinal cord neurons	<b>80</b>
<b>Figure 25</b>	TEM micrographs of mitochondria in WT and <i>Arl/+</i> neuronal cells	<b>81</b>
<b>Figure 26</b>	Graph showing O <sub>2</sub> consumption of WT and <i>Arl/+</i> mitochondria	<b>82</b>

## **Chapter VI**

### **Figures:**

- |                  |  |           |
|------------------|--|-----------|
| <b>Figure 27</b> | Flow chart of suggested effects of mutation on dynein structure and function | <b>90</b> |
| <b>Figure 28</b> | Diagram showing suggested effects of mutation on dynein structure            | <b>91</b> |

## Abbreviations

AAA	ATPase associated with various cellular activities
ADP	Adenosine diphosphate
ALS	Amyotrophic lateral sclerosis
AMP.PNP	Adenylyl-imidodiphosphate, tetralithium salt
AP	Adaptor protein
<i>Arl</i>	Abnormal rear leg
Arp	Actin related protein
ATP	Adenosine triphosphate
BDNF	Brain derived neurotrophic factor
BFP	Blue fluorescent protein
BICD	Bicaudal D
BSA	Bovine serum albumin
CAP-Gly	Cytoskeleton-associated protein, Glycine rich
CC1	Coiled-coil chain 1 of dynein stalk
CC2	Coiled-coil chain 2 of dynein stalk
CCP	Clathrin coated pit
CHAPS	3-[(3-cholamidopropyl)dimethylammonio]-1-propanesulfonate
CLIP-170	CAP-Gly domain containing linker protein 170
<i>Cral</i>	Cramping 1
DAPI	4',6-diamidino-2-phenylindole
DHC	Dynein heavy chain 1
DMEM	Dulbecco's modified eagles medium
Dnah11	Axonemal dynein heavy chain 11
DRG	Dorsal root ganglion
Drp1	Dynamin related protein
DTT	Dithiothreitol
<i>Dync1h1</i>	Dynein heavy chain gene 1
E13	Embryonic age day 13
EB1	MT end binding protein 1
EDL	Extensor digitorum longus muscle
EDTA	Ethylenediamine tetracetic acid
EEA1	Early endosomal antigen 1
Eg5	Kinesin 5 family member
EGF	Epidermal growth factor
EGFR	EGF receptor
EGTA	Ethyleneglycol tetracetic acid
EM	Electron microscopy
ENU	N-ethyl-N-nitrosurea
ETC	Electron transport chain
GARS	Glycyl-tRNA synthetase
GFP	Green fluorescent protein
GTP	Guanosine triphosphate

HEPES	4-(2-hydroxyethyl)-1-piperazineethanesulfonic acid
HSP	Hereditary spastic paraplegia
IC	Dynein intermediate chain
IFT	Intraflagella transport
<i>iv</i>	situs inversus viscerum
LC	Dynein light chain
LDH	Lactate dehydrogenase
LIC	Dynein light intermediate chain
Lis1	Lissencephaly 1
<i>Loa</i>	Legs at odd angle
MEF	Mouse embryonic fibroblast
MFN	Mitofusin
MND	Motor neuron disease
MOM	Mitochondrial outer membrane
MOPS	3-(N-morpholino)propanesulfonic acid
MT	Microtubule
MTBD	Microtubule binding domain
MVB	Multivesicular body
NADH	Nicotinamide adenine dinucleotide
NCV	Nerve conductance velocity
NF	Neurofilament
NudE	Nuclear distribution protein E
NudEL	NudE-like
NZ	Nocodazole
OPA1	Optic atrophy 1
p150 <sup>Glued</sup>	Dynactin subunit
PBS	Phosphate buffered saline
PBSG	PBS containing gelatin from coldwater fish skin
PCD	Primary ciliary dyskinesia
PEP	Phosphoenolpyruvate
PFA	Paraformaldehyde
PIPES	piperazine-N,N'-bis(2-ethanesulfonic acid)
PK	Pyruvate kinase
RILP	Rab interacting lysosomal protein
SB	Sample buffer
SBMA	Spinal bulbar muscular atrophy
SDH	Succinate dehydrogenase
SDS	Sodium dodecyl sulphate
SDS-PAGE	SDS-polyacrylamide gel electrophoresis
SMA	Spinal muscular atrophy
SOD1	Cu/Zn superoxide dismutase 1
SOD1 <sup>G93A</sup>	Mutant SOD1
<i>Swl</i>	Sprawling
TA	Tibialis anterior muscle

TEM	Transmission electron microscopy
TfR	Transferrin receptor
TGN	Trans-Golgi network
TMPD	N,N,N',N'-tetramethyl-p-phenylenediamine
Tris	Tris (hydroxymethyl) aminomethane
Trk	Tropomyosin-receptor kinase
VDAC	Voltage dependent anion selective channel
VE-DIC	Video enhanced differential interference contrast microscopy
vi	Vanadate
WD repeat	Tryptophan-aspartate repeat
WT	Wildtype
$\beta$ III	Golgi specific spectrin isoform
$\Delta\psi$	Membrane potential

Amelia Philpott

DPhil

Investigations into the Biochemical and Cellular Biology of a Cytoplasmic  
Dynein Mutation, *Abnormal Rear Leg (Arl)*

Abstract

The aim of this project was to investigate the effects of a novel mouse cytoplasmic dynein mutation; *Abnormal rear leg (Arl)*. Cytoplasmic dynein is a microtubule (MT) based motor protein important for diverse cellular processes including Golgi maintenance and retrograde transport of organelles. *Arl* is a mouse point mutation in the heavy chain subunit of dynein (*Dync1h1*). Homozygous *Dync1h1<sup>Arl/Arl</sup>* die at embryonic day 10. *Dync1h1<sup>Arl/+</sup>* heterozygotes have a normal life span, but exhibit abnormal gait and hindlimb clasp during tail suspension, typical of neuronal dysfunction. Protein purification from wildtype and heterozygous brain tissue showed increased MT binding in *Dync1h1<sup>Arl/+</sup>* compared to wildtype. Delayed endosomal trafficking was observed in EGF stimulated *Dync1h1<sup>Arl/+</sup>* mouse embryonic fibroblasts (MEFs) compared to wildtype, in both fixed cells and using live cell imaging. Similarly, a delay in the reassembly of the Golgi complex after disruption with a MT depolymerisation agent, nocodazole, was observed in *Dync1h1<sup>Arl/+</sup>* MEFs compared to wildtype. In addition, the Golgi complex was observed as being structurally perturbed in *Dync1h1<sup>Arl/+</sup>* lumbar spinal cord neurons using transmission electron microscopy (TEM) compared to the wildtype. TEM also revealed that the mitochondria were structurally perturbed in *Dync1h1<sup>Arl/+</sup>* lumbar spinal cord neurons compared to wildtype, and O<sub>2</sub> consumption assays investigating their function showed the *Dync1h1<sup>Arl/+</sup>* mitochondria to have increased respiration rates compared to wildtype. Thus, these data highlight the *Arl* mouse as an invaluable model for studying the mechanism of dynein function and the subsequent outcomes when they are compromised.

## **CHAPTER I**

## **Chapter I**

### **INTRODUCTION**

#### **I.1 Motor Proteins**

The often large size and complex organisation of eukaryotic cells requires a system of efficient directed transport. This transport is provided by motor proteins that power the movements of subcellular components such as organelles and chromosomes. Movement is along the two polarised cytoskeletal fibres - actin filaments and microtubules.

There are three families of motor proteins; myosins, kinesins and dyneins. Kinesins and dyneins move along MTs, with kinesins mainly moving towards the plus ends (anterograde transport) and the majority of dyneins moving towards the minus end (retrograde transport). Most myosins move along actin filaments towards the barbed, plus end.

#### **I.2 Dyneins**

There are two classes of dyneins - axonemal dyneins are responsible for the movements of cilia and flagella, while cytoplasmic dyneins are involved in a number of processes, for example, transport of organelles, nuclear migration and mitosis.

Cytoplasmic dynein has two forms, designated as cytoplasmic dynein 1 and 2. Cytoplasmic dynein 2 is involved in retrograde intraflagella transport (IFT), a process required for assembly and maintenance of lower eukaryotic cilium/flagellum, first identified in *Chlamydomonas* (Pazour, Dickert et al. 1999; Porter, Bower et al. 1999). It is now also well established in the generation and maintenance of mammalian cilia (Grissom, Vaisberg et al. 2002; Mikami, Tynan et al. 2002; Perrone, Tritschler et al. 2003). Cytoplasmic dynein 1 is the more abundant of the two complexes and is responsible for multiple activities such as transport of organelles, chromosome segregation and positioning of Golgi apparatus.

## **I.2.1 Cytoplasmic dynein**

### **I.2.1.1 Dynein Heavy Chain**

Dyneins are members of the AAA family (ATPase associated with various cellular activities) of ATPases (Neuwald, Aravind et al. 1999). They consist of extremely large heavy chains of more than 500kDa each. The C terminal 380kDa fragment contains the motor domain with the C terminal 2350 residues forming 6 linked AAA modules (AAA1-AAA6) each 35-40kDa in a ring structure. There is also thought to be a seventh domain, C terminal to AAA6 which is not an AAA module. When a truncated motor domain was engineered without the C terminal sequence, the overall motor domain structure under EM was mainly unchanged and no gap was left in the ring, which would be expected if it were a heptameric ring structure (Roberts, Numata et al. 2009). The ring consisting of the six AAA modules forms the globular head of dynein. Between the AAA4 and AAA5 modules, the dynein heavy chain forms a rod-like loop with a small, globular, ATP-sensitive microtubule-binding site at the tip. The stalk, or the stem, is formed by an anti-parallel coil of the folded back heavy chain and can be up to 15nm in length (Gee, Heuser et al. 1997).

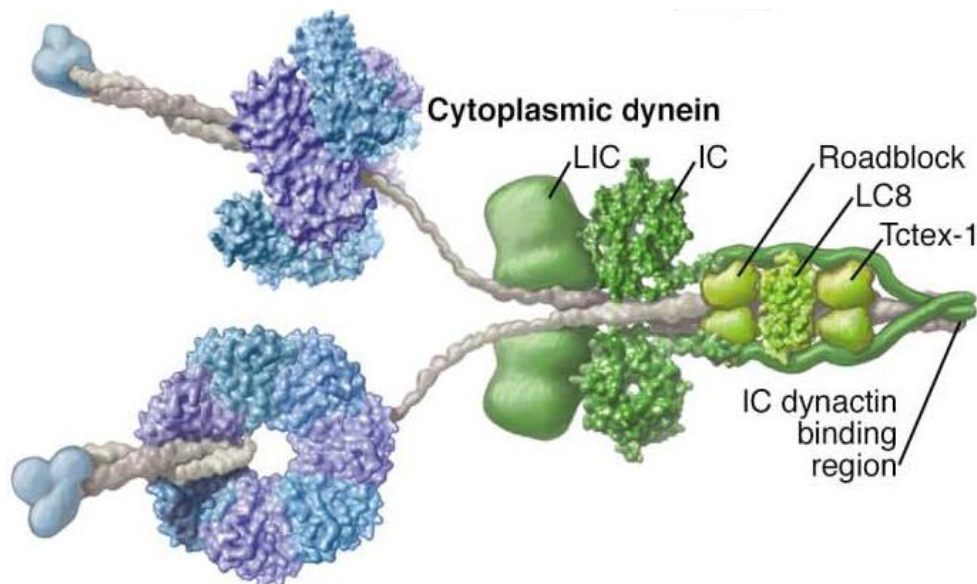


**Figure 1. Schematic of cytoplasmic dynein.**

Schematic diagram of cytoplasmic dynein showing dimerised heavy chains and sites of accessory chain binding. Adapted from (Vale 2003). LIC refers to light intermediate chain, IC refers to intermediate chain and LC refers to light chain of the dynein complex.

The N terminal 1800 residues form a tail that interacts with accessory chains and cargo. Modules 1 to 4 bind ATP, but only AAA1, nearest the N terminus, hydrolyses ATP during the interactions with microtubules that generate movement (Gibbons, Lee-Eiford et al. 1987; Ogawa 1991; Gee, Heuser et al. 1997). The other domains may regulate the ATPase cycle at AAA1. These four modules contain a highly conserved Walker A motif, also called a P loop, and a Walker B motif.

Walker motifs are 3 different, non-contiguous stretches of sequence known as Walker A, B and C that bind phosphates and are found in a number of ATP- and GTP-binding proteins. Walker A defines the binding site for the triphosphate and is important in the removal of the  $\gamma$ -phosphate of ATP during hydrolysis, and the B and C motifs interact with the base of the nucleotide (Gee, Heuser et al. 1997; Petsko and Ringe 2004). Evidence of a functional role for the first P loop came from molecular dissection of cytoplasmic dyneins in which mutation of the P loop caused loss of their motor activities (Silvanovich, Li et al. 2003). Dyneins have a high affinity for ADP bound to vanadate (vi), which can absorb light in the UV region. Illumination of dynein bound to ADP-vi causes a break in the heavy chain near the AAA1 domain (Vallee and Hook 2006). When the AAA1 was destroyed through UV photocleavage, most of the ATPase activity of the dynein was lost (Gibbons, Lee-Eiford et al. 1987). It is thought that the other P loops have a regulatory role binding either ATP or ADP. Removal of the extreme C-terminal portion of the heavy chain eliminates the AAA1 photocleavage by vanadate, suggesting the AAA ring needs to be intact to function fully (Gee, Heuser et al. 1997).

More recently, Reck-Peterson and Vale have used systematic mutagenesis of nucleotide binding sites in the non-essential *DYNI* gene of budding yeast to elucidate the functions of the individual AAA nucleotide binding sites. They showed that AAA2 and AAA4 can be made hydrolysis-incompetent without affecting function, but ATP hydrolysis is required in AAA1 and AAA3 for dynein function. Nucleotide binding at AAA2 and AAA4 is needed for maximal levels of MT binding *in vitro* (Reck-Peterson and Vale 2004).

In cytoplasmic dynein the MT binding domain at the end of the stalk is far away from the site of ATP hydrolysis in the AAA ring. This is in contrast to both myosins and kinesins, where the nucleotide binding site and filament binding site are relatively close together, allowing direct communication. In dynein this may be dealt with by the ATPase activity affecting the MT binding through conformational changes in adjacent AAA domains that are passed around the ring structure.

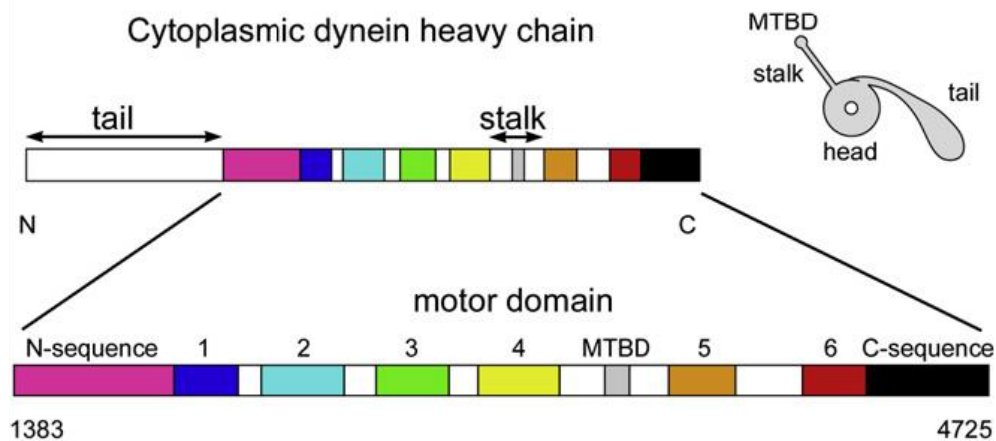


**Figure 2. Diagram showing arrangement of domains of C terminal of the heavy chain.**

Diagram showing the arrangement of the AAA domains, stalk and MTBD in the C-terminus of DHC. From (Roberts, Numata et al. 2009).

Another suggestion of how MT-binding affinity could be affected by ATP-hydrolysis and/or the powerstroke which occurs from the stem, comes from axonemal dyneins. In the axoneme, the globular heads appear to rotate during the mechanochemical cycle (Goodenough and Heuser 1984). Thus, if the powerstroke of cytoplasmic dynein contained a rotary and linear component, the rigid MT-binding stalk would dramatically change its orientation in relation to the MT axis. This could disrupt the interaction with the MT and cause a significant change in the affinity of the dynein stalk for the MT (King 2000).

Gibbons et al (Gibbons, Garbarino et al. 2005) have suggested that the alignment of the two strands of the coiled-coil, CC1 and CC2, directly affects the affinity of the MT binding domain (MTBD) for MTs. In using a number of expressed fragments that contained different lengths of the coiled-coils, which placed them out of alignment, the authors were able to show that only one conformation gave maximum MT binding, one

other gave intermediate binding, whilst all others showed greatly reduced affinity. A model for how the coiled-coil stalk mediates “communication” between the ATP binding site and the MTBD proposes a small sliding movement between CC1 and CC2, changing the alignment and therefore the MTBD affinity for MTs.

The “powerstroke mechanism” has become the generally accepted model for force generation in cytoplasmic dynein. Using EM analysis of axonemal dynein, it has been proposed that the dynein tail assumes two different positions relative to the head - the prestroke or primed and poststroke or unprimed positions - depending on the binding of the nucleotides at the head (Imamura, Kon et al. 2007; Roberts, Numata et al. 2009). Burgess et al (Burgess, Walker et al. 2003) have shown that the stem and stalk are closer together in dynein-apo ( $136^\circ$ ) than dynein-ADP-vi molecules ( $160^\circ$ ). As there was negligible change in the length of either the stalk or stem, it appeared the change in their relative distances must be due to translational movement between the two domains. The tail therefore acts as a lever arm for the powerstroke due to conformational changes originating in the head. Movement of the stalk in cytoplasmic dynein has also been seen to be nucleotide dependent, with a shift of 5nm in a clockwise direction upon nucleotide binding (Roberts, Numata et al. 2009).

Whilst using a rare, long-stemmed form of axonemal dynein, termed dynein-c, it was noticed that there was often a sharp, approximately  $90^\circ$  bend in the stem which corresponded to the position of the bend normally seen in typical molecules. A previously unnoticed structure was seen between the bend and the head, of approximately 10nm in length and a width similar to the neck of 2 nm (Burgess, Walker et al. 2003). This structure was termed the linker and suggested to undergo a swinging movement across the head, depending on nucleotide binding, thus facilitating the powerstroke.

Evidence for a linker domain in cytoplasmic dynein has recently been proposed. To determine if a linker exists in cytoplasmic dynein, the function of the top of the stem was investigated. A truncation construct of *Dictyostelium discoideum* that lacks 542 residues N terminal to the AAA1 ( $\Delta N$ ) was engineered. This region is known to be essential for motor activity. Using negative stain EM, removal of the N terminal sequence changed the shape of the ring structure of the head, causing it to become more

symmetrical in shape with well defined “wedge-shaped” domains (Roberts, Numata et al. 2009). Fusion proteins were also constructed, in which GFP and BFP were inserted at specific locations in the motor domain sequence, including the N terminal region at residue 1383, allowing the location of the N terminal to be mapped by EM. In unprimed motor the N terminal region tag was consistently found close to the periphery of the head near the base of the stalk at AAA4, which is close to the tail-linker junction in axonemal dynein-c, suggesting that a similar linker exists in cytoplasmic dynein. When ATP and vanadate were added to form the primed conformation, the N terminal tag shifted towards AAA2 by a distance of approximately 16-18 nm. Based on this, a model is proposed where the linker portion of the N terminal is closest to AAA2 when ATP is bound to the motor (prestroke or primed conformation) then, during the powerstroke the linker swings across the head towards AAA4 pulling cytoplasmic dynein forwards, resulting in the post-stroke conformation (Roberts, Numata et al. 2009).

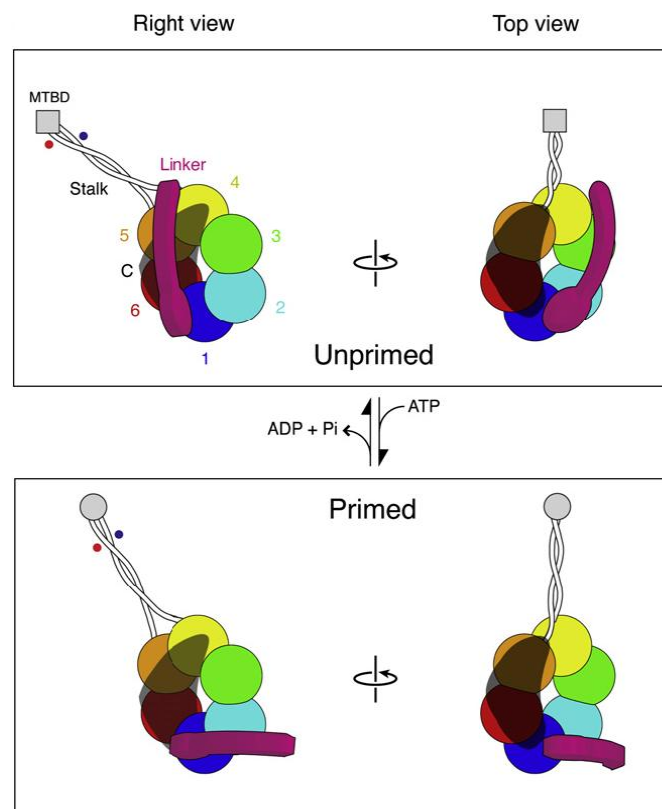


**Figure 3. Schematic demonstrating the model for a linker domain in dynein powerstroke.**

The 6 AAA domains form a ring, with a 7<sup>th</sup> non-AAA domain, here shown in shaded black. The purple domain represents the linker which is positioned across the motor head from AAA1 (blue) to AAA4 (yellow) when in the unprimed position. This linker domain moves down across the ring towards AAA2 (light blue) in the primed conformation, thus causing the N-terminus of DHC to move by ~17 nm [From (Roberts, Numata et al. 2009)].

To investigate step size, Mallik et al (Mallik, Carter et al. 2004), used purified dynein bound to beads. The beads allowed the position of the motor head to be tracked during the experiment. An optical trap was used to determine the force exerted by dynein based on the distance moved at different stiffness of the trap. It was found that the size of the step taken by dynein is dependent on the cargo load. At low load, dynein took steps of 24 – 32 nm. However, under high load ( $>0.8$  pN) the step size measured was 8 nm. This suggests that dynein can act as a molecular gear where nucleotide binding at AAA1-AAA4 leads to a “tighter” conformation of the AAA ring, which results in a smaller, but stronger dynein step. Kinesin takes 8 nm steps, so under low load, the 32 nm steps taken by dynein suggest that dynein can be four times more efficient, in terms of ATP usage, at transporting cargo, compared to kinesin (Mallik, Carter et al. 2004).

#### **I.2.1.2 Dynein Accessory Chains**

At the N-terminal base of the heavy chain stems there are a number of accessory chains. These comprise a number of intermediate, light intermediate and light chains. At least 10 genes are known to encode the components of the dynein complex (King, Bonilla et al. 2002).

The intermediate chains are 70-74kDa polypeptides that are encoded by 2 genes, *Dync1i1* (encoding DYNC1I1, from this point onwards referred to as IC1) and *Dync1i2* (encoding DYNC1I2, from this point onward represented as IC2), which undergo much splicing and phosphorylation to produce a number of structural isoforms. Nurminsky et al have shown, using *Drosophila*, that there are at least 10 structural isoforms of IC produced by alternative splicing from one IC gene, and that the splicing is tissue specific. The variation in structure of the isoforms is specific to the N-terminus of the IC, where it interacts with dynactin, the dynein activator, suggesting differences in the dynactin-mediated organelle binding by IC isoforms (Nurminsky, Nurminskaya et al. 1998).

More recently, Kuta (Kuta, Deng et al. 2010), have reported new splice isoforms for both IC genes and detailed the expression of isoforms in a range of mouse embryonic and adult tissues. Their data corroborates the theory that alternative splicing of the N-

terminus of ICs is important for dynein function. Neural specific isoforms identified indicate that specialised regulation may occur in neurons.

The conserved N-terminus of IC interacts with dynactin (King, Bonilla et al. 2002) while the C-terminus contains multiple WD repeats that are thought to fold into a  $\beta$ -propeller structure. This predicted domain is conserved between all ICs (cytoplasmic and axonemal) and is thought to play a part in subunit-subunit interactions with the dynein molecule (Paschal, Mikami et al. 1992; King, Bonilla et al. 2002).

The light intermediate chains are 52-61 kDa polypeptides with 2 genes *Dync1li1* (encoding DYNC1LI1, referred to from now as LIC1) and *Dync1li2* (encoding DYNC1LI2, referred to now as LIC2), which through alternative splicing give rise to at least seven isoforms. The LIC chains bind directly to the heavy chain and are thought to interact with cargos, as LIC1 chains have been shown to directly interact with pericentrin, a centrosomal protein. This suggests LICs may have a cargo targeting function (Tynan, Gee et al. 2000).

Studies performed in COS7 cells have demonstrated that LICs bind directly to the N-terminus of the HCs, adjacent to and overlapping with the IC binding site. No direct interaction has been seen, but both ICs and LICs are present in the same complexes, suggesting that LICs and ICs need to be independently located on DHC to allow necessary interactions with other proteins, but without sterically interfering with each other (Tynan, Gee et al. 2000).

The light chains (referred to from now as LC) are 10-13 kDa polypeptides, thought to be encoded by three gene families and currently accepted to contain 6 different genes (See refs included in (Banks, Bros-Facer et al. 2009). The gene families are, Tctex1 (t), Roadblock (rb) and LC8 (l). Current evidence suggests that LCs are common to cytoplasmic and some axonemal dyneins (King, Bonilla et al. 2002), therefore they are designated as: *Dynlt1* (referred to as Tctex1), *Dynlt3* (rp3), *Dynlrb1* (Robl1), *Dynrb2* (Robl2), *Dynll1* (LC8-1) and *Dynll2* (LC8-2) (Pfister, Fisher et al. 2005). However, some variation in nomenclature still exists.

Both Tctex-1 and LC8 have very similar structures and are homodimers in solution (King, Bonilla et al. 2002). They both bind ICs at non-overlapping sites that have sequence homology. Tctex-1 has some role in cargo binding as it has been shown to directly interact with retinal opsin and is needed for correct opsin localisation (Tai et al 2001). LC8 interacts with a number of other polypeptides, but these have not yet been confirmed as definite cargos of dynein.

Different isoforms of the dynein complex may exist, as components of the complex are differentially expressed in different tissues. This suggests that dynein complexes consisting of different combinations of subunits may exist (Vaughan and Vallee 1995; Vaisberg, Grissom et al. 1996; King, Barbarese et al. 1998). The variety in composition of dynein sub-complexes may allow for the large range of cargos that it binds and transports.

### **1.2.2 Dynein in neurons**

Co-ordinated active transport systems are extremely important in neurons due to their enormous size in comparison to other somatic cells. Neurons are numerous in size and shape, but can have tremendously long axons and the neuronal cytoskeleton is exceptionally important in maintaining the specialised and polarised morphology necessary for their proper functioning.

The neuronal cytoskeleton is comprised of networks similar to those in non-neuronal cells, such as actin filaments and MTs, but also contains specialised intermediate filaments known as neurofilaments. The actin filaments are important during development for axonal outgrowth and cell motility, and in mature neurons for integrity of the cell. Actin filaments can also provide tracks for short range movement by myosins for distribution of vesicles and organelles. The MTs are essential to maintain the processes that extend from the cell and to provide polarity, distinguishing axonal and dendritic areas of the neuron, as well as providing tracks for kinesins and dynein to move along. Neurofilaments (NFs) are necessary for resistance to stress and cell integrity and accumulate as the neuron matures (Levy and Holzbaur 2006).

In neurons anterograde movement, mainly by kinesins, transports newly synthesised synaptic vesicles and proteins, and organelles from the cell body along the axon to areas where they are needed, such as the synapse. Retrograde transport, predominantly by dynein, is responsible for translocating cargo from the cell periphery and distal axon back to the cell centre, often for degradation and recycling.

Retrograde signaling in neurons is very important and the dynein/dynactin complex plays a key role in transporting neurotrophic factors from the synapse to the cell body. Neurotrophins are a family of small molecules, such as nerve growth factor (NGF), brain derived neurotrophic factor (BDNF) and neurotrophin-4 (NF-4), that are secreted by target tissues, then bind to receptor tyrosine kinases (Trk receptors) on the surface of the neuron. The neurotrophin/Trk receptor complex is then internalized and transported by dynein to the cell centre, beginning signalling cascades that regulate growth and survival (Levy and Holzbaaur 2006). When dynein function was blocked in cultured sensory neurons, the transport of activated Trk receptors was inhibited, demonstrating dynein is required (Heerssen, Pazyra et al. 2004).

Degradation and recycling of misfolded or degraded proteins is particularly important in neurons as many neurodegenerative diseases have been linked to defective accumulation of protein aggregates. Dynein has been established as the motor responsible for transporting proteins back to the cell body for lysosomal degradation or autophagy (Burkhardt, Echeverri et al. 1997; Levy and Holzbaaur 2006).

Because of the unique size and morphology of neurons, anterograde and retrograde transport systems are extremely important. This makes neurons acutely sensitive to defects in, or disruption to, motor proteins, but particularly dynein as the predominant retrograde motor.

### **I.3 Dynein regulators and adaptors**

#### **I.3.1 Dynactin**

Dynactin is a multisubunit complex, required for most, if not all, types of cytoplasmic dynein activity in eukaryotes (Schroer 2004). It binds dynein and allows the motor to move long distances along the MTs.

The dynactin complex consists of 11 different polypeptide subunits, some of which are present in more than one copy, resulting in a 1.2 MDa, 20S complex with more than 20 polypeptide chains (Schroer 2004). It consists of 2 morphologically distinct domains - a rod shaped domain that binds cargo, and an extended arm projection that binds MTs and dynein (Kim, Ling et al. 2007).

The rod part of the dynactin molecule is a ~10x40 nm rod that resembles a short actin filament. It is an octameric polymer of Arp1 - the actin related protein. Arp1 filaments are very stable, short and of uniform length, meaning they are far less dynamic than conventional actin. On one end of the Arp1 rod is the conventional actin capping protein, CapZ, and on the other end is another actin related protein, Arp11, and the dynactin subunit p62 (Schroer 2004).

P62 primary sequence predicts a 53 kDa protein with a zinc-binding motif near the N-terminus. These motifs usually allow protein-protein interactions, so the N-terminus of p62 may be involved in binding to Arp1, Arp11, other dynactin subunits, or to other subcellular structures. Its loss from the complex does not, however, affect the stability of dynactin (Lee, Kumar et al. 2001). P62 and Arp11 associate with the two smallest dynactin subunits, p25 and p27, forming a heterotetrameric complex that is positioned at the end of the Arp1 rod, opposite CapZ (Schroer 2004).

The components of the rod - Arp1, Arp11, p62, p25, p27, and CapZ are more highly conserved, in comparison to the arm projection of dynactin, and therefore may have important structural roles (Schroer 2004).

The arm structure that projects from the Arp rod is both flexible and extendable and consists of 3 subunits: p150<sup>Glued</sup>, dynamitin (p50) and p24/22, with each dynactin

molecule containing 4 copies of dynamin and 2 copies each of p150<sup>Glued</sup> and p24/22 (Schroer 2004). Based on the sequences, all three polypeptides are predicted to form  $\alpha$ -helices with coiled-coils responsible for the interactions between the subunits.

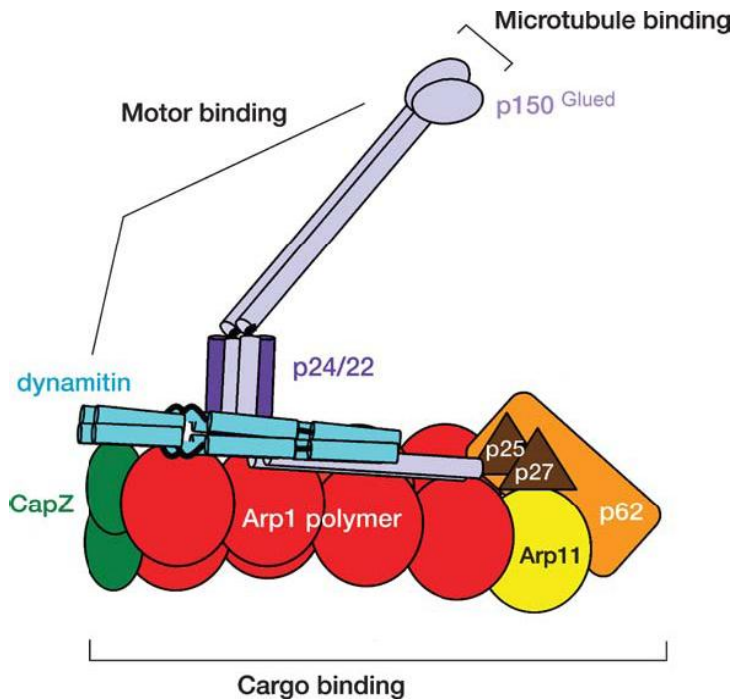


**Figure 4. Schematic showing structure of dynactin**

Schematic illustration of dynactin showing the arrangement and structure of the subunits in the complex. The structure and arrangement of dynactin have been inferred from EM studies and results combined from published results [From (Schroer 2004)].

Of all the dynactin subunits, p150<sup>Glued</sup> is the largest and is thought to form an elongated dimer containing 2 central coiled-coils (~50 and ~20nm long respectively), with regions of unknown structure in between. At the tip of the dynactin arm are 2 globular heads which contain a conserved CAP-Gly (cytoskeleton-associated protein, glycine rich) domain, which is at the far N-terminus (aa1-110) (Schroer 2004).

The CAP-Gly motif is important for MT binding, which is necessary for dynactin to enhance the processivity of dynein. This is demonstrated through the use of antibodies against the CAP-Gly domain which have been shown to abolish dynactin's ability to increase the run length of dynein coated beads (King and Schroer 2000). Truncation of p150 polypeptides have also been used to demonstrate that only fragments containing the CAP-Gly domain are able to bind to MTs (Culver-Hanlon, Lex et al. 2006).

Dynactin enhancement of dynein transport over long distances is necessary for proper neuronal function, indicating the importance of dynactin.

Apart from MTs, the CAP-Gly domain also binds proteins such as the MT plus-end binding proteins EB1 and CLIP-170. It is currently not known if p150<sup>Glued</sup> binds both MTs and associated binding proteins at the same time, or only one at a time, which could suggest that the binding of associated proteins offers some form of regulation of dynactin. This could be through either the promotion of enhancement of processivity, or binding of plus ends possibly to anchor the MTs (Schroer 2004).

Another form of regulation may come from phosphorylation. p150<sup>Glued</sup> affinity for MTs is reduced by phosphorylation of p150<sup>Glued</sup> at S19, suggesting that protein kinases can associate with and affect the activity of the CAP-Gly domain (Vaughan, Miura et al. 2002).

The N-terminal third of p150<sup>Glued</sup>, past the CAP-Gly motif (aa~220-550), is predicted to form an  $\alpha$ -helical coiled-coil of approx. 50 nm length. As the well defined arm of dynactin is known to be 24 nm in length, it suggests that the C-terminal half (aa~380-550) of the arm is involved in the flexible shoulder located on top of the Arp rod (Schroer 2004).

The middle part of p150<sup>Glued</sup> is involved with binding dynein, as an antibody to the p150<sup>Glued</sup> subunit blocks binding of dynein to dynactin, demonstrating that this region is important for binding (Waterman-Storer, Karki et al. 1997). Also, a 123 aa fragment of DIC has been shown to bind a recombinant fragment of p150<sup>Glued</sup> (aa 150-811) (Vaughan and Vallee 1995). Vaughan et al found a serine residue (S84) in DIC that is thought to regulate, via phosphorylation, the ability of DIC to bind to p150<sup>Glued</sup> (Vaughan, Leszyk et al. 2001).

p150<sup>Glued</sup> has been shown to interact with members of the kinesin family - p150<sup>Glued</sup> aa 410-811 binds Eg5 and aa 600-811 binds kinesin II, suggesting p150<sup>Glued</sup> may allow dynactin to interact with multiple MT based motors.

The C-terminal third of p150<sup>Glued</sup> (aa ~900-1300) is less well defined than the N-terminal region, but seems to allow a number of protein-protein interactions. It is also proposed to play a role in linking the arm to the rod of dynactin, as it contains a conserved actin-binding motif which has been suggested to bind to the Arp1 filament. In addition, a mutation in *Drosophila* of the Glued gene product (which has sequence homology and functional similarities with p150<sup>Glued</sup>) in a region that corresponds with the C-terminal third of p150<sup>Glued</sup> results in it not binding to the complex (McGrail, Gepner et al. 1995). This suggests that the C-terminal region of p150<sup>Glued</sup> is important for attachment of the arm projection to the Arp rod in dynactin.

Also important for linking the arm to the Arp rod is dynamitin (p50). In each dynactin molecule there are four subunits of dynamitin which are thought to tightly associate with each other and p24/22 via 3 coiled coils, forming the shoulder of dynactin. P24/22 is one of the smallest subunits of dynactin at only 21 kDa and is thought to be  $\alpha$ -helical in structure (Karki, LaMonte et al. 1998). The dynamitin-p24 complex interacts with p150<sup>Glued</sup> and components of the Arp rod to hold the complex together (Maier, Godfrey et al. 2008). Free dynamitin disrupts the structure, displacing p150<sup>Glued</sup> and p24/22 from dynactin and leaving the remaining structure non-functional (Echeverri, Paschal et al. 1996). This demonstrates that dynamitin is essential in maintaining the structure of dynactin.

There are a number of theories suggesting how dynactin might aid the function of dynein. A number of studies have shown dynactin is involved in binding to some cargos, such as Arp1 binding to  $\beta$ III, a Golgi specific spectrin isoform (Holleran, Ligon et al. 2001). Bicaudal D (BICD) is a protein involved in Golgi-ER transport and has binding sites for both dynein and dynamitin. Also, the BICD binding partner, Rab6 binds to p150<sup>Glued</sup> (Short, Preisinger et al. 2002) suggesting Rab6 may function as a tethering or specificity factor controlling the recruitment of dynactin to membranes. Rab7 and its effector protein Rab interacting lysosomal protein, RILP, recruit the dynein/dynactin complex to late endosomes and lysosomes, allowing their transport to the  $-$ end of MTs. When this interaction is blocked, it results in late endosomes being transported towards the cell periphery by kinesin. A direct interaction between dynein/dynactin and Rab7 or RILP has not been identified, but it suggests the existence

of a linker protein that mediates the association of the two complexes with each other (Jordens, Marsman et al. 2005).

Another proposed function of dynactin is in increasing the processivity of dynein along MTs. It has been shown that dynactin does increase the processivity of dynein, through increasing the run length of coated beads, but without affecting the velocity or ATPase kinetics of dynein (King and Schroer 2000). The MT binding activity of dynactin is required for the increased processivity which indicates that dynactin aids processivity by providing an extra contact with MTs, reducing the risk of detachment from the MT (King and Schroer 2000).

Further investigations into dynactin's MT binding found that there are two MT binding domains in p150<sup>Glued</sup> - the CAP-Gly domain and a previously unknown basic region in the N-terminus. This basic region binds to MTs, even in the absence of the CAP-Gly domain and is sufficient to increase processivity of dynein by demonstrating a "skating" behaviour along MTs (Culver-Hanlon, Lex et al. 2006). This suggests that the two different MT binding domains in p150<sup>Glued</sup> may play different roles in aiding dynein's movement, with the basic domain maintaining contact between dynein, cargo and MTs, and the CAP-Gly domain allowing stable binding of MTs at the plus end to allow loading of cargo (Culver-Hanlon, Lex et al. 2006).

A recent study by Ross et al (Ross, Wallace et al. 2006) has suggested that dynactin may play a role in the directionality of dynein. The movement of GFP tagged dynein/dynactin complexes along MTs was tracked by single-molecule fluorescent microscopy. The data suggests that dynactin may allow reversals in dynein's movement as significant plus-end directed motion was detected in addition to the expected minus-end directed movement (Ross, Wallace et al. 2006). However, a more recent study by Kardon et al, using yeast, suggests that although the dynein/dynactin complex is more processive than dynein alone, it does not increase the plus-end directed movement (Kardon, Reck-Peterson et al. 2009). These differences may result from dynactin having different roles depending on its cargo, or simply from differences between mammalian and yeast dynactin.

### **I.3.2 Lis1, NudE and NudEL**

A number of proteins have been found to interact with dynein, and studies have shown them to be necessary for its proper functioning, suggesting them to be adaptors or regulators of dynein. Lissencephaly 1 (Lis1) is a protein that directly interacts with dynein. Mutations in the *Lis1* gene are linked to the disease lissencephaly 1 which causes severe malformation of the cortex of the brain due to defective neuronal migration (Reiner, Carrozzo et al. 1993). Nuclear distribution protein E (NudE) is involved in kinetochore function and along with the homologous protein NudE-like (NudEL) function with Lis1, interacting with dynein.

Studies have shown that Lis1, NudE and NudEL are extremely important for a number of dynein functions, including organelle transport, kinetochore activity, and nuclear and spindle positioning (Liang, Yu et al. 2004). Loss of function mutations in all three proteins result in very similar phenotypes affecting dynein function, which suggests they act as important co-factors. They directly interact with dynein and have been shown to be involved in dynein mediated transport of kinetochore proteins (Howell, McEwen et al. 2001). However, their exact mechanisms are not currently well understood.

NudE and NudEL mutants defective for Lis1 or DHC binding cause phenotypes similar to those seen from dynein disruption, such as Golgi fragmentation and reduced vesicle trafficking. Studies have also shown that in the absence of NudE/NudEL, dynein is still able to bind to MTs and cargo, but movement is impaired (Liang, Yu et al. 2004), suggesting that the interaction of Lis1, NudE, NudEL with dynein is important in regulating a number of dynein functions.

Complete inhibition of NudE and NudEL function prevents dynein, dynactin and Lis1 from localising to kinetochores, which leads to cell arrest at metaphase and misorientation of the kinetochores (Stehman, Chen et al. 2007). This suggests that NudE and NudEL are important for recruiting dynein/dynactin and Lis1 to kinetochores.

In neural progenitor cells, Lis1, NudE and dynein are responsible for the proper positioning of nuclei and spindles for cell division. The resulting neurons require Lis1, NudEL and dynein for the movement of the centrosome and nucleus during migration [Refs in (Kardon and Vale 2009)].

A unique feature of Lis1 is that it binds directly to the motor domain of dynein. Lis1 comprises an N-terminal coiled-coil attached to seven WD40 repeats (40 amino acids with a C-terminal Trp-Asp dipeptide), which dimerises at the coiled-coil. The WD40 repeat binds to the AAA1 domain of the dynein motor. Lis1 interacts with both NudE and NudEL, but exact sites of interaction have yet to be identified (Sasaki, Shionoya et al. 2000).

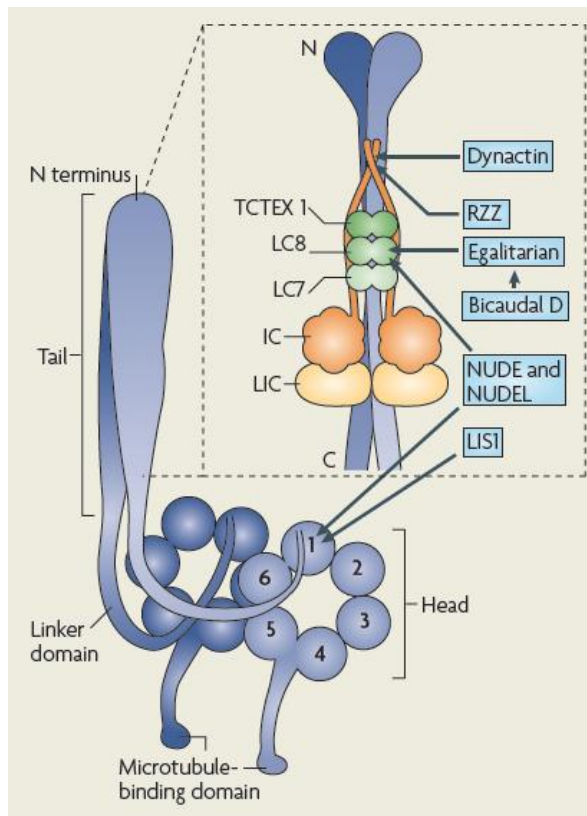


**Figure 5. Schematic of cytoplasmic dynein showing sites of interaction with regulators and adaptors.** The dimerised dynein heavy chain is shown in blue. The sites of interaction with the dynein regulators dynactin, Lis1, NudE and NudEL are shown, as well as other proteins proposed to regulate and adapt dynein function [From (Kardon and Vale 2009)].

NudE and NudEL are highly homologous, both containing an N-terminal coiled-coil, which is important for dimerisation, as well as Lis1 binding. The C-terminus is

unstructured, but binds to the AAA1 domain of dynein. This region also interacts with the light chain, LC8 and DIC (Sasaki, Shionoya et al. 2000), as well as kinetochore proteins, centromere protein F (CENPF) and ZW10. ZW10 also interacts with dynamitin in dynactin (Starr, Williams et al. 1998). Lis1 has been shown to be necessary for dynein to localise to MT plus ends (Markus, Punch et al. 2009).

Recent studies have indicated that Lis1 may be involved in regulating the ATPase activity of dynein, however, there are conflicting results from the different studies. Mesngon et al (Mesngon, Tarricone et al. 2006), showed that in using native brain dynein and recombinant Lis1, the two proteins bind and Lis1 significantly increases the MT stimulated ATPase activity of dynein. Their data showed that Lis1 must be dimerised for this ATPase regulation to occur, as a C-terminal fragment lacking the dimerisation domain, but retaining the dynein interaction site was unable to alter ATPase activity.

However, the Hirotsune group showed that Lis1 suppressed the motility of native dynein (purified from porcine brain tissue) along MTs and it is NudEL that releases this effect by blocking Lis1 suppression. Lis1 increased ATPase activity at concentrations that inhibit motility, suggesting Lis1 separates the mechanical-chemical coupling of dynein. NudEL reduced by ~60% the MT stimulated ATPase activity, which is in keeping with data showing NudEL is involved in dissociating dynein from MTs (Yamada, Toba et al. 2008).

It appears that Lis1, in conjunction with NudE and/or NudEL, is involved in regulating ATPase function in the dynein motor, but further work is needed to determine the exact mechanism of this regulation.

It has been proposed that Lis1 and NudE or NudEL complexes may affect the conformation of dynein. As Lis1/NudE and Lis1/NudEL are dimers, they could possibly bridge across two AAA1 domains, bringing them into closer proximity. Another possibility is that the motor and tail domains of dynein could be brought together into a folded conformation, as the C-terminus of NudE and NudEL is able to bind LC8 and Lis1 binds the motor (Kardon and Vale 2009), although if this occurs, and how it might affect regulation remains to be determined.

## **I.4 Dynein Cargos**

As the main retrograde motor in cells, cytoplasmic dynein is responsible for the transport and localisation of an enormous range of cargos. These include large membrane organelles such as the Golgi, mitochondria and nuclei; small vesicles and tubular intermediates in the endocytic and secretory pathways; and cytoskeletal filaments such as MTs and actin filaments.

### **I.4.1 Golgi**

The Golgi apparatus consists of a network of flattened membrane cisternae that are interconnected and associated with tubules and vesicles. The Golgi is responsible for the post-translational modifications of proteins and macromolecules transported from the rER which are then packaged for transport to the plasma membrane (e.g. for exocytosis) or the secretory or endocytic pathways.

The Golgi maintains a perinuclear position, often close to the MT organising centre (MTOC). MTs are known to have an important role in maintaining the location and integrity of the Golgi as disruption of MTs using depolymerising drugs causes the Golgi to fragment and disperse throughout the cell. Upon removal of the depolymerising drug, the MTs are able to repolymerise and the Golgi fragments move along the MTs towards the centrosome to re-form the membrane network.

Dynein was proposed to be the MT motor responsible for maintaining the structure of Golgi and repositioning it after disruption, and a number of studies have confirmed this. Burkhardt et al overexpressed the dynactin subunit, dynamitin, which caused fragmentation of the Golgi, despite the MT complex remaining intact. Also, the microinjection of function blocking DIC antibodies resulted in the same Golgi fragmentation and dispersal (Burkhardt, Echeverri et al. 1997). A similar phenotype was also identified in blastocysts cultured from DHC knockout mice (Harada, Takei et al. 1998), confirming that dynein is the motor responsible for maintaining integrity and localisation of Golgi.

There appear to be a number of factors that play a role in the recruitment of dynein/dynactin to Golgi membranes. Arp1 of dynactin has been shown to directly bind a Golgi specific isoform of spectrin,  $\beta$ III (Holleran, Ligon et al. 2001). Spectrins are cytoskeletal proteins that provide structure and integrity to many membranes. There are two Arp1 binding sites in  $\beta$ III spectrin, one of which overlaps with the well conserved actin binding site (Holleran, Ligon et al. 2001). The interaction between  $\beta$ III spectrin and Arp1 provides a direct link between the dynein/dynactin complex and its Golgi cargo.

#### **I.4.2 Mitochondria**

The correct distribution of mitochondria throughout a cell is essential for proper cell functioning and survival. Mitochondria have a number of crucial roles in the cell-energy production, cell signalling, calcium homeostasis and apoptosis. Different types of cells have different requirements, and thus the distribution of mitochondria is specific to the energy needs of that cell. For example, in neurons, high energy demands at the synapse mean more mitochondria are required at this location (Hollenbeck and Saxton 2005).

Dynein and kinesin motors play important roles in the transport of mitochondria and are essential for proper distribution throughout the cell. Mitochondria are synthesised in the cell body and must be transported to the location of energy requirement. In neurons they need to be distributed along the axon, which occurs through a combination of transport, at velocities of  $0.3\text{-}2.0\mu\text{m}\cdot\text{s}^{-1}$ , and stopping as over half of mitochondria are stationary [Refs in (Miller and Sheetz 2004)]. Disruption of axonal transport leads to non-uniform distribution of organelles, including mitochondria, along the axon.

Mitochondrial potential drives the production of ATP. The potential is generated by oxidative phosphorylation through the electron transport chain (ETC) and varies in response to changes in metabolic demand. Using the potential-sensitive dye JC-1 Miller and Sheetz have shown that  $\sim 90\%$  of mitochondria with a high potential move anterogradely towards the growth cone in neurons, while  $\sim 80\%$  of low potential mitochondria move retrogradely towards the cell body (Miller and Sheetz 2004). Depolarised mitochondria are retrogradely transported to lysosomes to be recycled by

autophagy. Aged mitochondria become, on average, more depolarised and so retrograde transport by dynein is essential to ensure that non-functioning mitochondria are removed from cells.

Tctex-1 can interact with the voltage dependent anion-selective channel (VDAC1) in the mitochondrial outer membrane (MOM). This interaction could regulate the binding of dynein when the mitochondrial membrane potential is decreased, and may contribute to increased retrograde transport (Boldogh and Pon 2007).

Mitochondria are highly dynamic organelles that constantly alter their morphology using fission and fusion in response to a range of signals (Santel and Frank 2008). The main factors required for fusion of mammalian mitochondria are the large mitochondrial GTPases, mitofusin (MFN) 1 and 2, and optic atrophy 1 (OPA1). The protein mainly responsible for fission is dynamin related protein 1 (DRP1), also a large GTPase (Santel and Frank 2008).

MFN 1 and 2 localise to the mitochondrial outer membrane, while OPA1 is located at the inner membrane, suggesting that MFN1 and 2 are involved with outer membrane fusion and OPA1 is involved with fusion of the inner membrane. MFN1 and 2 contain coiled-coil regions that project from the outer membrane allowing tethering of two mitochondria together (Suen, Norris et al. 2008) ultimately resulting in fusion.

Mitochondrial fission consists of a number of steps. Drp1 is recruited to the outer membrane, where multimerisation of the protein occurs, which finally results in fission of the membrane bilayers. A neuronal isoform, Drp1p, is important for the correct distribution of mitochondria to the synapse. In HeLa cells it has been shown that disruption of dynein via DIC, or dynactin through dynamitin, results in the repositioning of Drp1 from the mitochondria to other cytoplasmic membranes. Also seen is the transport of mitochondria from the cell cortex to a perinuclear region (Varadi, Johnson-Cadwell et al. 2004). This suggests that dynein might contribute to the targeting of Drp1 to mitochondria in addition to its more established roles (Boldogh and Pon 2007).

### **I.4.3 Endosomes**

Endosomes are transport vesicles formed during the process of endocytosis. This is the uptake of material into a cell by invagination of the plasma membrane and its internalisation in a membrane bound vesicle (Alberts, Johnson et al. 2002).

Mammalian cells contain many complex intracellular structures, which means diffusion can only occur at slow rates. Cells have therefore developed active intracellular transport systems to move and target macromolecules to their correct destinations. This can either result in transport to the lysosomes for degradation of the contents of the vesicle, or recycling of the vesicle back to the cell membrane.

Endocytosis encompasses various forms of uptake of extracellular material by cells, including phagocytosis, the uptake of large particles, usually carried out by specialist cells (such as macrophages), and pinocytosis, the internalisation of fluids. It also includes uptake into membrane pits which can either be coated, as with clathrin-dependent and caveolin-dependent endocytosis, or uncoated, as with clathrin-independent and caveolin-independent endocytosis (Mukherjee, Ghosh et al. 1997).

Clathrin and caveolin are coat proteins that cause curvature of the membrane to form vesicles (Parkar, Akpa et al. 2009). Clathrin forms the structural backbone of clathrin-coated pits (CCPs), but adaptor proteins (APs) are required that can attach to both the pit and the cargo. It is currently unclear as to whether existing vesicles trap and internalise cargo, or the presence of cargo causes vesicle formation. In clathrin-dependent endocytosis it appears to depend on the cargo. EGF receptor stimulates the formation of new CCPs, but transferrin receptor (TfR) stabilises existing CCPs and is then internalised into them (Benmerah and Lamaze 2007). Caveolae are mainly pre-existing vesicles, but need to be stimulated for internalisation of cargo to occur. There are a number of different isoforms of caveolin that are important for the proper formation of caveolae.

Once the pits have formed, dynamin, a large GTPase, is involved in scission of the pits into vesicles. Once the vesicles are released from the membrane, the clathrin coat is released and recycled back to the plasma membrane. Caveolae do not strip caveolin

upon internalisation, but fuse with existing endosomes and release their contents, before recycling back to the cell surface.

#### **I.4.3.1 Receptor mediated endocytosis**

Receptors that use existing CCPs are thought to internalise by constitutive endocytosis, regardless of whether they are bound to their ligands. However, in receptor-mediated endocytosis, the ligand binding to its receptor stimulates the formation of the clathrin-coated vesicle and the internalisation of the ligand-receptor complex (Benmerah and Lamaze 2007).

A large range of receptors are internalised in clathrin-coated vesicles (CCVs), for example, epidermal growth factor receptor (EGFR), transferrin receptor (TfR), low-density lipoprotein receptor (LDL-R),  $\beta_2$  adrenergic receptors and insulin receptor. By controlling cell-surface receptors such as these, CCPs can regulate cell signalling (Parker, Akpa et al. 2009). CCVs also play a role in protein sorting and are found at the trans-Golgi network (TGN).

Once the CCV is internalised and pinched off from the membrane by dynamin, the clathrin coat recycles back to the plasma membrane and the CCVs fuse to form early endosomes. Fusion of these early endosomes gives rise to multi-vesicular bodies (MVBs), and it is from these that proteins either recycle back to the cell surface, or continue in the degradative pathway to the lysosomes.

Rab proteins are involved in regulating fusion and fission of vesicles and are involved in sorting cargo in vesicles by creating subdomains (Jordens, Marsman et al. 2005). Rab5 has been shown to be present on early endosomes and through its interaction with its effector protein, early endosome antigen (EEA1), it is involved in endosomal fusion (Woodman 2000). Rab5 is also important for the transport of early endosomes as it interacts with DIC and may be involved in tethering early endosomes to the dynein complex for transport. Once vesicular sorting has occurred, early endosomes or MVBs fuse together to form late endosomes. This is coupled to the loss of Rab5 and the gain of Rab7. Rab7 and its effector protein, Rab7-interacting lysosomal protein (RILP),

recruit the dynein/dynactin complex to late endosomes for transport and fusion to the lysosomes for degradation (Jordens, Marsman et al. 2005).

#### **I.4.3.1.1 EGF/EGFR endocytosis**

The epidermal growth factor (EGF) receptor (EGFR) is a widely expressed transmembrane receptor tyrosine kinase. It is activated via binding of a number of ligands, such as EGF, which promotes receptor dimerisation and autophosphorylation. EGF receptor-ligand binding can activate signalling of a wide variety of pathways that can lead to cell proliferation, differentiation, motility or survival, depending on the ligand and cell involved.

Once activated, EGFR is endocytosed into clathrin-coated pits. EGFRs remain active after internalisation and remains so until they reach the lysosome for degradation. Transport to the lysosomes is dynein dependent as disruption of the dynein complex in HeLa cells inhibits retrograde movement of EGF-positive endosomes (Driskell, Mironov et al. 2007). Delay in reaching the lysosomes for degradation has been shown to result in prolonged EGFR signalling, that in turn leads to sustained activation of downstream targets (Taub, Teis et al. 2007).

#### **I.5 Dynein mutations**

The importance of dynein in cellular function is well documented, but its exact mechanism of function and interaction with other proteins is not fully understood. To provide a better understanding of the functional interplay between dynein and cellular mechanisms in organisms, mutagenesis of dynein in model organisms has provided invaluable information about the downstream effects of disrupted dynein. Many of these mutations in animal models have resulted in phenotypes that mimic, or are similar to human diseases, providing insight into the importance of the protein and the many cellular functions it participates in. This can also provide information about possible mechanisms of disease that may involve dynein.

### **I.5.1 Legs at odd angles (*Loa*) and Cramping 1 (*Cra1*)**

Hafezparast et al (2003) described two new DHC mutations in mice that help provide further information about the functioning of dynein, as well as how defects in dynein can lead to phenotypes that are similar to human disease.

Two independent ENU mutagenesis programmes resulted in two mouse mutants that exhibited a similar, unusual twisting and clenching of the hindlimbs when suspended by the tail. Due to their phenotypes they were named Legs at odd angles (*Loa*) and Cramping1 (*Cra1*). Both mutations are autosomal dominant traits that in heterozygotes cause progressive loss of muscle tone and locomotor ability, but without significant reduction in lifespan. The homozygotes are much more severely affected with inability to move or feed properly and die within 24 hours of birth (Hafezparast, Klocke et al. 2003).

Both mutations were confirmed as being due to single amino acid substitutions in *Dync1h1*. *Loa* results from a T-A transversion in *Dync1h1* changing a phenylalanine to tyrosine at residue 580. *Cra1* is due to a change of A-G in *Dync1h1* resulting in tyrosine to cysteine at residue 1055. The two mutations were found to be allelic, as when crossed together, they produced compound heterozygotes with the same phenotypes as the homozygotes and all died within 48 hours of birth (Hafezparast, Klocke et al. 2003).

The *Loa* mutation occurs within the highly conserved region thought to be the binding site for *Dync1i1* chains and the site for homodimerisation, and the *Cra1* mutation is in a potential area of homodimerisation.

No differences were identified in the amounts of DHC and DIC protein between *Loa* and *Cra1* homozygous, heterozygous and WT mice, and the localisation of DHC and DIC was not affected by the mutations. This suggests that the phenotypes caused by the *Loa* and *Cra1* mutations are not due to changes in the amount of protein or its location in the cell (Hafezparast, Klocke et al. 2003).

As the hindlimb clenching is typical of a neuromuscular defect, and progressive motor impairment is seen, the motor neurons were checked. The number of  $\alpha$ -motor neurons (the large calibre neurons that innervate muscle), in the spinal cord anterior horn were compared between heterozygote and wildtype littermates at 3 months and then at 19 months in *Loa* and 16 months in *Cral*. A significant decrease was detected in both sets of mice over these timeframes (Hafezparast, Klocke et al. 2003).

The anterior horn cells (AHCs) of *Loa* and *Cral* homozygous embryos, at embryonic age E18.5, and wildtype littermates were compared, with the *Loa/Loa* embryos showing 50% fewer AHCs compared to WT, while the *Cral/Cral* embryos showed an 80% decrease. The AHCs in these homozygous mutants also had increased rates of apoptosis and the surviving neurons contained intracellular inclusions. These inclusions were found to contain ubiquitin, SOD1, CDK5 and NFs, similar to the inclusions that are characteristic of human amyotrophic lateral sclerosis (ALS) (Hafezparast, Klocke et al. 2003).

Dupuis et al (Dupuis, Fergani et al. 2009) also investigated neuronal degeneration in *Cral/+* mice to fully characterise the motor defect. Motor neurons in adult spinal cord anterior horns were counted to establish cell loss, however, none was established, even in aged mice. Corticalspinal motor neurons from 14 month old *Cral/+* mice were also checked and did not show any difference in number compared to WT littermates. These data suggest that *Cral/+* mice do not in fact display typical motor neuron disease.

The hindlimb grip strength in *Loa/+* has been shown to be reduced by 52%, but forelimb grip strength is unaffected, compared to WT littermates (Chen, Levedakou et al. 2007). In agreement with this, cervical dorsal root ganglion (DRG) neurons are not affected, but lumbar DRG neurons are reduced by 42% in *Loa/+* compared to WT. Muscle spindles are central to the proprioceptive sensory system, allowing perception of the positioning of limbs. In 13 week old *Loa/+* mice, muscle spindles were seen to be reduced by 86% in the hindlimbs compared to WT. Together these data suggest that *Loa/+* mice exhibit a proprioceptive sensory defect (Chen, Levedakou et al. 2007).

To determine the exact timing of the motor axon degeneration identified by Hafezparast et al (Hafezparast, Klocke et al. 2003), lumbar motor roots in young *Loa/+* mice were

examined (from 1.5 months – 22 months). At 1.5 months, *Loa/+* mice exhibited loss of motor axons compared to WT, however, no reduction in  $\alpha$ -motor axons ( $>3.5 \mu\text{m}$  diameter) was observed, but a 55% loss of  $\gamma$ -motor neurons (which innervate muscle spindles) was identified (Ilieva, Yamanaka et al. 2008). No further loss was identified up to 22 months of age.

Despite  $\alpha$ -motor neuron loss not being detected in older mice in this study (Ilieva, Yamanaka et al. 2008), significant loss of sensory neurons was identified in 1.5 month old mice, continuing through to 22 month old mice. No effect on nociception was identified in *Loa/+* mice, so the significant loss of sensory neurons suggests that proprioception may be affected. To confirm this, proprioceptive axonal function was tested by examining the stretch reflex in adult *Loa/+* mice. The expected H wave was entirely absent from all *Loa/+* mice tested, but present in WT, confirming the presence of a defect in proprioception in *Loa/+* mice.

In *Loa* mice, the effect of the mutation on Golgi was investigated. Normal positioning and morphology of Golgi was identified in mouse embryonic fibroblasts (MEFs), however, the ability of dynein to re-position Golgi after disruption was impaired. MTs were depolymerised with the drug, nocodazole, fragmenting the Golgi throughout the cell. Once the nocodazole was removed, the MTs repolymerised and in WT cells the Golgi was reassembled into its perinuclear position by dynein. However, in *Loa/Loa* cells this was significantly impaired. The authors suggest that normal Golgi positioning and morphology, but impaired reassembly after disruption, shows that the *Loa* mutation reduces dynein function only during cellular stress (Hafezparast, Klocke et al. 2003).

Fragmented Golgi complex, similar to that seen in nocodazole treated cells, is a feature of both human ALS and the mutant SOD1 transgenic mice that model ALS. Disrupted Golgi is also seen in embryos from dynein knockout mice (Harada, Takei et al. 1998).

Dynein has a number of roles that are specific to neurons, including neuronal migration and axonal transport of organelles. The effects of the *Loa* mutation on these roles were investigated by analysing the formation of cranial and spinal nerves in E10.5 *Loa/Loa* and WT littermates. Although there was no difference in motor neuron differentiation in the neural tube, a difference was seen in the migration of motor neuron cell bodies

from the face to hindbrain in *Loa* homozygous embryos. This is similar to the facial weakness caused by impaired lower motor neurons in the brainstem of spinal bulbar muscular atrophy (SBMA) patients, and some bulbar subtypes of ALS (Hafezparast, Klocke et al. 2003).

Investigations into retrograde axonal transport using a fluorescent fragment of the tetanus toxin (TeNT H<sub>c</sub>) showed that although retrograde transport was not abolished in *Loa/Loa* neurons, there was a significant reduction in the frequency of high speed carriers and an increase in stationary pauses. This suggests that the *Loa* mutation impairs dynein's ability to maintain fast retrograde transport (Hafezparast, Klocke et al. 2003).

The range of different studies carried out on *Loa* and *Cral* mice suggests that the similar phenotypes observed in both are due to sensory defects, with accompanying motor defects that vary in severity and require further investigation.

### **I.5.2 Sprawling mouse (*Swl*)**

The sprawling mouse (*Swl*) is a radiation induced, autosomal dominant mutation, first identified due to its hindlimb clenching when suspended by the tail, as well as an unsteady, jerky gait (Duchen 1974). It has been shown to be caused by a 9 base pair deletion in *Dync1h1* that changes 4 residues at position 1040-1043 to a single alanine (Chen, Levedakou et al. 2007).

The hindlimb clenching is similar to that seen in *Loa* and *Cral* heterozygotes, but *Swl*/+ mice also develop an abnormal gait, characterised by a jerky, wobbly movement. When stationary the hindlimbs are splayed outwards and forwards, and the hindlimbs have reduced grip strength. The *Swl*/+ mice have a normal lifespan and no obvious progression of the phenotype with age has been identified (Chen, Levedakou et al. 2007).

Due to the hindlimb clenching, and abnormal gait phenotypes, the limbs of *Swl*/+ mice are clearly affected. Motor function and grip strength were investigated using motor nerve conductance velocity (NCV) tests on *Swl*/+ and WT littermates, which showed

<i>Loa</i>	<i>Cral</i>
Autosomal dominant mutation – due to single amino acid substitution in <i>Dync1h1</i> .	Autosomal dominant mutation – due to single amino acid substitution in <i>Dync1h1</i> .
Progressive loss of locomotor ability, but no significant reduction in lifespan.	V. mild effect on gait, no significant reduction in lifespan.
Mutation located in region of DHC involved in DLIC binding and homodimerisation.	Mutation located in region of DHC thought to be involved in homodimerisation.
Significant loss of anterior horn cells (AHCs) in <i>Ar1/+</i> compared to WT. Loss of $\gamma$ -motor neurons, not $\alpha$ -MNs, identified by Ilieva et al.	Conflicting data – reduction in AHCs seen by Hafezparast et al, but none seen by Dupuis et al.
Reduction in lumbar dorsal root neurons	Loss of neurons in dorsal root
Phenotype suggested to be due to proprioceptive defects with accompanying motor defects	Phenotype thought to be due to proprioceptive sensory defects, with lack of motor defects.
Rescue of SOD1 <sup>G93A</sup> phenotype identified	Rescue of SOD1 <sup>G93A</sup> phenotype identified, although less significant than with <i>Loa</i> .

**Table 1. Comparisons between *Loa* and *Cral* mice and phenotypes.**

Table comparing major features of the *Loa* and *Cral* mice as detailed in studies conducted by Hafezparast et al., Ilieva et al. and Dupuis et al. (Hafezparast, Klocke et al. 2003; Ilieva, Yamanaka et al. 2008; Dupuis, Fergani et al. 2009)

forelimb grip strength was unaffected, but a 50% decrease was identified in hindlimbs. Normal peripheral motor nerve function was detected through measuring the velocity and amplification of the compound muscle action potential (M wave). The morphology and number of  $\alpha$ -motor neurons was unaffected, suggesting the reduced hindlimb grip strength is not due to defects in the anterior horn of the lumbar spinal cord (Chen, Levedakou et al. 2007).

Previously, *Swl* mice have been characterised as having thin peripheral nerves and sensory roots, a reduced number of DRG neurons, small dorsal columns of the spinal cord, and a marked reduction in the number of sensory neurons (Duchen 1974). To determine whether specific subpopulations of sensory ganglion neurons are affected, tail flick tests were used to investigate nociceptive sensory function. These showed that nociception was unaffected in *Swl/+* mice compared to WT, and this is backed up by the lack of limb amputations seen in *Swl/+* mice. Sensory NCV, measured to assess sensory nerve function, showed no difference between *Swl/+* and WT, however, the amplitude of the sensory nerve action potential was reduced by 32% (Chen, Levedakou et al. 2007). These data suggest that the *Swl* mutation does not affect the nociceptive or motor function of these mice, but rather some other sensory aspect.

Consequently, the proprioceptive function was assessed using the H reflex in tibial nerves. The H reflex measures the afferent Ia fibres and the efferent  $\alpha$ -motor fibres across the reflex arc, which provides a measure of proprioceptive function. The H reflex was completely absent from the hindlimbs of all the *Swl/+* mice tested, but present in all WT mice. This together with normal motor nerve function suggests that the proprioceptive function of the *Swl* sensory system is affected. In keeping with this data, the number of proprioceptive sensory receptors was significantly reduced in *Swl/+* compared to WT (Chen, Levedakou et al. 2007).

The neuron loss in DRGs was further investigated and the reduction was found to be greater in lumbar segments than cervical segments in *Swl/+*. This is consistent with the hindlimbs being much more affected than the forelimbs in *Swl/+* mice. In these sections the number of proprioceptive sensory neurons is greatly reduced in *Swl*, much more so than for nociceptive sensory neurons. These data suggest that the subpopulation of proprioceptive sensory neurons is much more severely affected than

the subpopulation of nociceptive sensory neurons in *Swl/+* lumbar DRGs (Chen, Levedakou et al. 2007).

Degeneration of muscle spindles during late embryonic development, between E15.5 and P0.5, was identified and found to accompany the loss of lumbar proprioceptive neurons in *Swl/+* mice (Chen, Levedakou et al. 2007).

Taken together, this data suggests that *Swl* is due to an early onset proprioceptive sensory defect and it is this, rather than motor neuron loss, that is probably the cause of the phenotype seen. This indicates that a mutation in DHC can lead to sensory neuron defects. Proprioceptive sensory neurons are a subpopulation of DRG neurons characterised by medium and large soma areas, and like  $\alpha$ -motor neurons, they require a large supply of energy and significant trafficking; this may cause them to be particularly vulnerable to vesicular and axonal transport defects, particularly as previous studies have shown large motor and sensory neurons are more vulnerable to diseased conditions than small sized neurons (McIlwain 1991). As dynein transports vesicles and organelles from nerve terminals to cell bodies, neurons with longer axons are more likely to be affected by *Swl* mutation which may explain why hindlimbs, but not forelimbs are affected.

### **I.5.3 Motor neuron disease and SOD1**

Motor neuron diseases (MND) encompass several adult and juvenile onset neurodegenerative disorders, including amyotrophic lateral sclerosis (ALS), spinal muscular atrophy (SMA), spinal bulbar muscular atrophy (SBMA) and hereditary spastic paraplegias (HSP).

ALS is the most common adult-onset motor neuron disease and leads to selective dysfunction and death of neurons in the cortex, brainstem, and spinal cord, with the large diameter  $\alpha$ -motor neurons in the spinal anterior horns mainly targeted. It is progressive and terminal, causing muscle weakness, atrophy and spasticity, leading to eventual paralysis and death within 2-5 years of onset (Julien and Kriz 2006). ALS generally occurs in middle to late age with a lifetime risk of ~1 in 2000 (Bruijn, Miller et al. 2004).

There are no effective treatments to delay or cure the disease and the causes for the majority of cases are unknown. Clinically they can be highly variable, suggesting that many factors may contribute to the disease mechanism. These are classed as sporadic ALS (SALS) and account for ~90% of cases. The remaining 10% of ALS cases are familial (FALS), and of these, 20-25% are mapped to the Cu/Zn-SOD1 gene on chromosome 21. More than 100 different mutations have been identified (Rosen, Siddique et al. 1993; Gaudette, Hirano et al. 2000).

Superoxide dismutase 1 (SOD1) is a ubiquitously expressed cytosolic metalloenzyme that catalyses the formation of hydrogen peroxide and oxygen via dismutation of superoxide anions. It is thought that this action protects against cellular damage induced by oxygen radicals (Shaw 2001).

Transgenic mice expressing various forms of mutant SOD1 have been generated and mice over-expressing mutant SOD1 develop ALS; with SOD1<sup>G93A</sup>, SOD1<sup>G37R</sup> and SOD1<sup>G85R</sup> the most studied forms, developing many pathological phenotypes seen in human ALS (Turner and Talbot 2008).

The main characteristics of the SOD1<sup>G93A</sup> mice are hindlimb tremor and weakness which develop at around 3 months. This progresses to paralysis and death after approximately 4 months. SOD1<sup>G37R</sup> and SOD1<sup>G85R</sup> show similar phenotypes, but they present at later timepoints, with disease onset visible at 4-6 months and 8-14 months respectively [Reviewed in (Turner and Talbot 2008)].

The mutations in SOD1 are not due to loss of function, as SOD1 knockout mice do not develop motor neuron disease (Reaume, Elliott et al. 1996). Also, expression of a dismutase inactive mutant did not affect onset of disease or survival, and increased levels of WT-SOD1 had no effect, or even accelerated the disease (Bruijn, Houseweart et al. 1998; Jaarsma, Rognoni et al. 2001). This suggests the SOD1 mutations cause a toxic gain of function, and as a common feature of affected mice is the presence of large aggregates and cellular inclusions, it is most likely from the formation of aggregates and misfolded protein. However, the exact mechanism through which SOD1 results in motor neuron degeneration is currently unclear.

To better understand how mutant SOD1 interacts with motor neurons to induce degeneration, the pathology of neuronal cells in SOD1 mice was investigated. A common feature among mutant SOD1 mice is the presence of neuronal and astrocytic inclusions and aggregates highly immunoreactive for SOD1. These inclusions are similar to SOD1-containing aggregates seen in some human sporadic and familial ALS cases (Bruijn, Houseweart et al. 1998).

Defects in axonal transport have been identified in SOD1 mice, with a slowing in tubulin and NF transport occurring just before disease onset and one of the earliest pathologies detected (Williamson and Cleveland 1999).

SOD1 is ubiquitously expressed, but it has been shown that motor neurons from mutant SOD1 mice can avoid degeneration if some surrounding non-neuronal cells are unaffected. Conversely, affected non-neuronal cells expressing mutant SOD1 are able to translate the damage to motor neurons that they surround, suggesting non-cell autonomous excitotoxicity is involved (Ilieva, Yamanaka et al. 2008).

#### **1.5.4 Dynein mutations and SOD1**

Although mutations in dynein have not been found in ALS patients (Ahmad-Annur, Shah et al. 2003; Shah, Ahmad-Annur et al. 2006), mutations in dynactin have been identified in patients with slow progressing forms of ALS (Puls, Jonnakuty et al. 2003), highlighting the relevance of mutations in the dynein complex in ALS. As dynein is the major retrograde motor in neurons and *Loa* and *Cral* have been shown to cause degeneration of motor neurons, and with motor neuron degeneration and axonal transport defects seen in SOD1 mice, a possible link between dynein and mutant SOD1 was investigated.

*Loa* mice were crossed with SOD1<sup>G93A</sup> mice to investigate whether the interaction between the dynein mutation and mutant SOD1 had any effect on disease progression and lifespan in double heterozygote (*Loa*/SOD1<sup>G93A</sup>) mice (Kieran, Hafezparast et al. 2005). Surprisingly, the double heterozygotes showed an improvement over SOD1<sup>G93A</sup> littermates, showing that *Loa* rescues the SOD1 phenotype.

As previously mentioned, *Loa*/+ mice have a normal lifespan (Hafezparast, Klocke et al. 2003), while SOD1<sup>G93A</sup> mice have a reduced lifespan of only 125 days. The *Loa*/SOD1<sup>G93A</sup> mice showed a significant increase in their lifespan of 28% to 160 days, also with significant delay in the onset of the disease (Kieran, Hafezparast et al. 2005).

Axonal transport defects in E13 motor neurons were completely rescued in *Loa*/SOD1<sup>G93A</sup> mice compared to SOD1 mice. There was also a significant increase in motor neuron survival in the spinal cord of *Loa*/SOD1<sup>G93A</sup> adult mice (Kieran, Hafezparast et al. 2005).

The results suggest that defects in axonal transport contribute to motor neuron degeneration in SOD1<sup>G93A</sup> mice and that rescuing these defects can have a favourable effect on both disease progression and lifespan (Kieran, Hafezparast et al. 2005).

To determine if the rescue of the phenotype in SOD1 mice is confined to the *Loa* mutation, or whether other dynein mutations could have the same effect, *Cral* mice were crossed with SOD1<sup>G93A</sup> mice. The resulting double heterozygote (*Cral*/SOD1<sup>G93A</sup>) mice showed a significantly improved lifespan over SOD1 littermates, as well as delayed disease progression. However, neuropathological examination of cervical and lumbar spinal cords at end stage showed both *Cral*/SOD1<sup>G93A</sup> and SOD1<sup>G93A</sup> exhibited striking degeneration of motor neurons. This indicates that further experiments are needed to check motor neuron loss in each genotype group at specific timepoints prior to end stage to identify differences in the degree of motor neuron loss (Teuchert, Fischer et al. 2006).

The data demonstrates that mutations in dynein lead to a decrease in motor neuron death in SOD1<sup>G93A</sup> mice, but that the rescue of the SOD1 phenotype in *Cral*/SOD1<sup>G93A</sup> mice by the *Cral* mutation is less dramatic than with *Loa*/SOD1<sup>G93A</sup> mice. This difference could be due to the difference in locations of the mutations on dynein heavy chain, or due to genetic backgrounds as different strains carry the *Loa* and *Cral* mutations (Teuchert, Fischer et al. 2006).

Establishing that two different DHC mutations, both of which cause axonal trafficking defects, can rescue the phenotype of a SOD1 model of ALS, suggests the importance of axonal transport in understanding the degeneration of motor neurons.

Both *Loa* and *Cral* predominantly affect motor neurons and were demonstrated to rescue the SOD1 phenotype, however, the *Swl* mutation predominantly affects sensory neurons. Chen et al. (Chen, Levedakou et al. 2007), used *Swl* to see if a dynein mutation that is also located in DHC, but affects sensory rather than motor neurons, is also able to rescue the SOD1<sup>G93A</sup> phenotype. They crossed *Swl* with SOD1<sup>G93A</sup> and assessed disease progression and lifespan of the resulting *Swl*/SOD1<sup>G93A</sup> double heterozygote progeny.

Unlike *Loa* and *Cral*, *Swl*/SOD1<sup>G93A</sup> mice showed no difference in average survival time compared to SOD1 mice. Similarly, there was no difference in body weight between *Swl*/SOD1<sup>G93A</sup> and SOD1, indicating no delay in disease progression (Chen, Levedakou et al. 2007). Together, this data indicates that the *Swl* mutation does not rescue the SOD1 phenotype and suggests that a mutation in dynein may only be capable of rescuing the SOD1 phenotype if it causes a defect in motor neurons; a mutation causing a sensory neuronal defect is not sufficient.

Interestingly, mutations in dynein are not unique in being able to rescue the SOD1 phenotype. Human mutations in the essential enzyme, glycyl-tRNA synthetase (GARS), cause motor and sensory axon loss in the peripheral neuron system, leading to a range of phenotypes such as Charcot-Marie-Tooth neuropathy to a severe infantile form of spinal muscular atrophy (SMA) (Banks, Bros-Facer et al. 2009).

A mouse model of this contains a point mutation resulting in a change of cysteine to arginine at residue 201, *Gars*<sup>C201R</sup>. Heterozygous *Gars*<sup>C201R</sup> mice show reduced grip strength, disrupted fine motor control and reduced axon diameter in peripheral nerves. Interestingly, when crossed with SOD1<sup>G93A</sup> mice the double heterozygotes (SOD1<sup>G93A</sup>/*Gars*<sup>C201R</sup>) show a similar rescue of the SOD1 phenotype as seen in *Loa*, with a significantly increased lifespan of approximately 29%. The SOD1<sup>G93A</sup>/*Gars*<sup>C201R</sup> also demonstrates a significant delay in disease progression (Banks, Bros-Facer et al. 2009).

GARS is vital for translation to occur in all cells, and in neurons is active in the periphery as well as the cell body. It is therefore essential for numerous functions of neuronal development and maintenance, such as axon guidance, cell migration and cell polarity (Banks, Bros-Facer et al. 2009). It could therefore be one of these many functions that is defective in *Gars*<sup>C201R</sup> that results in the rescue of the SOD1 phenotype.

This data suggests that a function that is defective in *Loa*, *Cral* and *Gars*<sup>C201R</sup>, but not in *Swl* is likely to play a major role in ameliorating the effect of the SOD1 mutation.

### **I.5.5 Abnormal rear leg (*Arl*)**

A separate ENU mutagenesis programme conducted at the Centre for Modelling Human Disease (CMHD) in Toronto, Canada, resulted in another mouse that exhibited a similar phenotype to *Loa* and *Cral*. Male C57BL/6 male mice were treated with ENU and mated with C3H/HeJ females. A resulting female was identified with twisting and clenching of the hindlimbs when suspended by the tail, and due to the appearance of the phenotype the mutation was named Abnormal rear leg (*Arl*). This mouse was crossed with a WT C3H/HeJ male and the resulting offspring were also affected, confirming this was an autosomal dominant trait.

To map this mutation 85 polymorphic markers were used by the CMHD to genotype 11 affected and 10 unaffected mice. The mutation was mapped to the distal region of Mmu12 between D12Mit167 (47cM; 100.6Mb) and the telomere (116Mb).

Due to the similarity of this mutation to *Loa* and *Cral* it was sent to the Fisher group at UCL for further positional cloning, where much work on *Loa* had previously been conducted. As both *Loa* and *Cral* arise from mutations in *Dync1h1* in the 55cM region of Mmu12 (Hafezparast, Klocke et al. 2003) – the same region as this new mutation – it seemed that *Dync1h1* was a likely candidate gene for this mutation. This gene was sequenced in mutant and WT littermates and a 3616T→C transition mutation was identified, causing a change of tryptophan to arginine at residue 1206 (Bros-Facer, Golding et al. Manuscript in preparation).

*Arl* appears to be more severe than either *Loa* or *Cral* as no homozygous mutants (*Arl/Arl*) have been born. Tests have not identified any *Arl/Arl* embryos after E10.5, whereas in both *Loa* and *Cral* homozygous mutant are born, but die within 24 and 48 hours respectively.

As the twisting and clenching phenotype is typical of a neuromuscular defect and occurs in the hindlimbs, the muscle force of two hindlimb muscles were examined; the EDL and TA muscles. At 90 and 100 days no differences were seen in *Arl/+* compared to WT, but 1 year old *Arl/+* mice exhibited significant reduction in muscle force of TA muscles compared to WT. No significant difference in EDL muscles was identified (Bros-Facer, Golding et al. Manuscript in preparation).

The fact that a decrease in maximum force is not detected in TA muscles in *Arl/+* mice until they are aged 1 year may suggest that a subtle disease phenotype is starting to exhibit in the *Arl/+* mice. Therefore more aged mice need to be used to repeat these experiments.

EDL muscles in 1 year old mice were also checked for functional motor units, which showed no difference in number comparing *Arl/+* and WT. The muscle contraction profiles of these EDL muscles were also investigated. EDL muscles are mainly composed of fast fibres which rapidly fatigue when stimulated repeatedly. In *Arl/+* mice these muscles showed a similar phenotype to WT, with rapid fatigue after repeated stimulation, resulting in Fatigue Index (FI) values that are not significantly different for each genotype (Bros-Facer, Golding et al. Manuscript in preparation).

Due to the reduction in TA muscle force in *Arl/+* mice, the oxidative capacity of TA muscle fibres was tested by staining with the oxidative enzyme, succinate dehydrogenase (SDH). This showed that in *Arl/+* the TA muscles had a normal pattern of staining, indicating a low oxidative capacity, similar to the TA muscles in WT (Bros-Facer, Golding et al. Manuscript in preparation).

A significantly greater number of motor units innervate the TA muscles making measurements of motor unit number unreliable. Although this meant a comparison could not be made between *Arl/+* and WT, a difference seemed unlikely as motor

neuron survival assays have shown no significant motor neuron loss in *Arl/+* mice compared to WT littermates.

Motor neuron survival in 1 year old *Arl/+* mice was compared against WT mice in lumbar spinal cord sections. Nissl staining showed no significant difference in the number of motor neurons, however, a significant difference was identified in the area of the motor neuron soma which were ~ 20% smaller in *Arl/+* neurons compared to WT. Overall, a greater number of smaller motor neurons were identified in *Arl/+* compared to WT (Bros-Facer, Golding et al. Manuscript in preparation).

Consequently, the cross-sectioned area of sciatic nerves from 1 year old *Arl/+* and WT littermates were analysed and compared. Cross sections immunolabelled for NFs showed a 50% reduction in sciatic nerve area in *Arl/+* compared to WT (Bros-Facer, Golding et al. Manuscript in preparation). However, because mice younger than 1 year did not show any deficit in muscle physiology, they were not further tested. Therefore, it is currently not established whether this smaller cross sectional area in sciatic nerve develops over 1 year, or if it presents at developmental stages.

The decrease in sciatic nerve area is likely to be due to the increase in motor neurons with smaller soma areas, however, the reason for the decrease in motor neuron soma area is unclear. Further studies are required to establish the cause of the reduction in motor neuron soma and sciatic nerve areas seen in *Arl/+* mice. Also, more aged mice should be used to repeat these experiments to identify if any motor neuron loss is exhibited at later stages and whether the sciatic nerve area shows any change in size in *Arl/+* compared to WT at later stages.

Peripheral nerve excitability was measured in 14 week and 1 year old *Arl/+* and WT mice, using the caudal nerve of the tail. *Arl/+* mice exhibited abnormal excitability properties compared to WT mice, particularly at 1 year. The difference between the *Arl/+* and WT became more significant with age, as WT excitability recordings change over time, but the *Arl/+* recordings remained mainly the same. This apparent lack of normal development could be related to the smaller cell bodies of motor neurons and reduced cross-sectional area of the sciatic nerves in *Arl/+* compared to WT, but the

exact nature of the phenotype is currently unclear (Bros-Facer, Golding et al. Manuscript in preparation).

As with the other dynein mutations, *Loa* and *Swl*, the retrograde axonal transport was investigated using the fluorescent fragment of tetanus toxin (TeNT H<sub>c</sub>). Using motor neurons cultured from E13 *Arl*/+ and WT embryos, the analysis showed similar speeds in both genotypes (Bros-Facer, Golding et al. Manuscript in preparation).

### **I.5.6 *Arl* and SOD1**

To determine whether *Arl* was similar to *Loa* and *Cra1* in attenuating disease in SOD1<sup>G93A</sup> mice, or whether it was similar to *Swl* in being unable to delay disease, the *Arl* was crossed with SOD1<sup>G93A</sup>.

Assessment of muscle force and motor neuron units was used to determine whether *Arl*/SOD1<sup>G93A</sup> double heterozygotes were able to rescue the SOD1 phenotype. The muscle force was compared between *Arl*/SOD1<sup>G93A</sup> and SOD1 in both TA and EDL muscle. Despite a trend in improvement of muscle performance of *Arl*/SOD1<sup>G93A</sup> mice compared to SOD1, it is not significant. Similarly, the number of motor units and the fatigue profiles of *Arl*/SOD1<sup>G93A</sup> mice show a similar trend in improved performance compared to SOD1, but it is not significant (Bros-Facer, Golding et al. Manuscript in preparation).

This data suggests that *Arl* is similar to *Swl* in being unable to rescue SOD1 disease progression.

### **I.5.7 Axonemal dynein mutation**

Recently, it has been reported that the *Arl* mice contain a mutation in axonemal dynein, in addition to that in cytoplasmic dynein (Golding, unpublished data). The mutation is a point mutation in *Dnah11* (also known as left-right dynein, *lrd*) which is involved in establishing the left-right axis in developing embryos and is expressed in the embryonic node, essential for development of left-right asymmetry (Supp, Brueckner et al. 1999).

The situs inversus viscerum (*iv*) mouse is due to a mutation in *Dnah11*. Adult *iv/iv* mice show an incidence of approximately 50% of inverted visceral organ positioning, suggesting that *Dnah11* is involved in normal organ positioning. Without it, the process occurs randomly (Layton 1976).

This mouse model is similar to the human autosomal recessive condition, situs inversus, which causes the position of the visceral organs to be reversed in the body. 25% of situs inversus individuals also have a condition called primary ciliary dyskinesia (PCD), a dysfunction of the cilia during embryonic development. Normally, cilia are involved in determining the position of internal organs during development, so dysfunction of the cilia can lead to situs inversus (~50% of PCD patients also have situs inversus). Individuals suffering from both conditions are said to have Kartagener syndrome, which results in recurrent upper respiratory tract infections, and in males, infertility due to non-functioning cilia in spermatozoa (Afzelius 1976; Splitt, Burn et al. 1996).

The presence of an axonemal mutation in *Arl* mice was initially identified as abnormal cilia were noticed in the embryonic node of *Arl* embryos. Consequently, *Arl/iv* double heterozygotes were produced to check axonemal dynein function and were found to suffer from randomised situs inversus. Thus suggesting that *Arl* mice have impairment of axonemal dynein function that may result in a phenotype similar to that of *iv* mice. A point mutation of A6239T in *Dnah11* was identified, resulting in a change of aspartate to valine (Golding, unpublished data).

## **I.6 Aims of the project**

Previous investigations have shown that mutations in the heavy chain of cytoplasmic dynein can lead to a range of similar phenotypes in the mouse (Hafezparast, Klocke et al. 2003; Chen, Levedakou et al. 2007; Dupuis, Fergani et al. 2009). *Arl* is a novel mutation in the heavy chain of cytoplasmic dynein, but unlike the other dynein mutations, *Arl* is located close to the motor domain so motor function of the protein may be impaired.

To investigate what effect the mutation has on the function of dynein, cell extracts from homogenised tissue have been used to determine whether protein levels are affected. Sucrose density gradient centrifugation has been used to establish if the integrity of the dynein complex is disrupted. Dynein protein has been isolated through a process of MT binding and release, then further purified on a continuous sucrose density gradient. This purified protein has been analysed to verify its purity and confirm that all subunits were present.

The purified dynein samples have been used in MT gliding assays to look for differences in MT movement between WT and *Arl*/+. In addition to this ATPase assays looked for an effect on the hydrolysis of ATP. Finally, MT binding assays investigated whether the mutation affects the binding of MTs by the dynein complex.

In addition to this, mouse embryonic fibroblasts (MEFs) isolated from WT and *Arl*/+ embryos have been used as an *in vitro* model system to investigate the effects of the *Arl* mutation on cargo transport. A range of dynein cargos have been tested, including the reassembly of Golgi after disruption, and the transport of endosomes using the internalisation of fluorescently tagged epidermal growth factor (EGF). Furthermore, the transport of mitochondria have been analysed to establish whether the mutation affected their cellular transport.

Moreover, transmission electron microscopy was used to ascertain the effects of *Arl* on neuronal cells from lumbar spinal cord of adult mice. Golgi and mitochondria morphology was investigated. Consequently, the function of mitochondria isolated from lumbar spinal cord tissue was also tested.

## **CHAPTER II**

**Chapter II****MATERIALS AND METHODS**

All chemicals are from Sigma-Aldrich, unless otherwise stated. All cell biology media are from Invitrogen, unless otherwise stated.

**II.1 Buffers and media**

- Lysis buffer
  - 0.1 M Tris
  - 0.2% (w/v) SDS
  - 0.2 M NaCl
  - 0.5 mM EDTA
  
- 2D lysis buffer
  - 7 M Urea
  - 2 M Thiourea
  - 4% (v/v) CHAPS
  - 65 mM DTT
  
- Sample buffer
  - 0.125 M Tris-Cl
  - 4% (w/v) SDS
  - 20% (v/v) Glycerol
  - 0.2 M DTT
  - 0.02% Bromophenol blue
  
- PBS<sup>-</sup>
  - Phosphate buffered saline without Mg<sup>2+</sup> or Ca<sup>2+</sup>
  
- Homogenisation buffer
  - pH 6.8
  - 80 mM KPIPES
  - 1 mM EGTA
  - 2 mM MgSO<sub>4</sub>

- BRB80 buffer                      pH 6.8  
80 mM KPIPES  
2 mM MgCl<sub>2</sub>  
0.5 mM EGTA
  
- Motility buffer                      pH 6.7  
20 mM KPIPES  
10 mM K-acetate  
4 mM MgSO<sub>4</sub>
  
- ATPase assay buffer              pH 7.5  
2 mM MgCl<sub>2</sub>  
1 mM DTT  
1 mM ATP  
3 mM Phosphoenol pyruvate  
0.2 mM NADH  
50 mM Tris-acetate  
1.75% (v/v) Pyruvate kinase/lactate dehydrogenase
  
- Complete DMEM                      DMEM (Dulbecco's modified eagles medium)  
1% (v/v) Penicillin/streptomycin  
1% (v/v) L-glutamine  
15% (v/v) Foetal calf serum (Hyclone)
  
- CO<sub>2</sub> Independent                      CO<sub>2</sub> independent medium  
medium                                      1% (v/v) Penicillin/streptomycin  
1% (v/v) L-glutamine
  
- Complete L-15                        L-15 medium  
medium                                      5% (w/v) Glucose  
1% (v/v) Penicillin/streptomycin  
20 nM Progesterone

2% (v/v) Horse serum  
5 µg/ml Insulin  
10 mM Putrescine  
10 µg/ml Coalbumin  
30 nM Sodium selenite

- Motor neuron medium Neurobasal medium  
2% (v/v) B27 supplement  
25 µM β-mercaptoethanol  
2% Horse serum  
25 µM Glutamine  
0.1% (v/v) Fungizone  
1% (v/v) Penicillin/streptomycin
- Tissue homogenisation buffer pH 7.5  
0.3 M Mannitol  
20 mM MOPS  
2 mM EDTA
- O<sub>2</sub> Electrode buffer pH 7.4  
0.2 M Mannitol  
1 mM K-Phosphate  
50 mM KCl  
1 mM MgCl<sub>2</sub>  
10 mM MOPS

Primary Antibody	Company	Order code	Concentration used
anti-Dynein heavy chain, rabbit polyclonal IgG	Santa Cruz Biotech	SC-9115	1/200 – Western blot
anti-Dynein intermediate chain, 74.1kDa mouse monoclonal	Dr Kevin Pfister	/	1/1000 – Western blot
anti-P150 <sup>Glued</sup> , mouse polyclonal IgG	BD Transduction Labs	610473	1/500 – Western blot
anti- $\alpha$ -tubulin, DM1A mouse monoclonal IgG	Upstate	05-829	0.5 $\mu$ g/ml – Western blot
anti-Giantin, rabbit polyclonal	Covance	PRB-114C	1/1000 - Immunofluorescence
Secondary Antibody			
Goat anti-rabbit IgG, Alkaline phosphatase (AP) linked	Sigma	A3812	1/10,000 – Western blot
Goat anti-mouse IgG, AP linked	Sigma	A3562	1/10,000 – Western blot
Rabbit anti-mouse polyclonal IgG, HRP linked	Dako Cytomation	P0260	1/30,000 – Western blot
Donkey anti-rabbit IgG, HRP linked	GE Healthcare	NA934	1/30,000 – Western blot
Fluorescent Antibody			
EGF-Alexa Fluor 555 streptavidin complex	Invitrogen	E35350	10ng/ml – Immunofluorescence
Alexa Fluor 488 conjugate goat anti-mouse IgG	Molecular Probes	A11029	1/200 – Immunofluorescence
Alexa Fluor 546 conjugate goat anti-rabbit IgG	Molecular Probes	A11035	1/200 - Immunofluorescence

**Table 2. Antibodies**

Table giving details of antibodies used during experiments and optimised concentrations. AP = alkaline phosphatase linked secondary antibody, HRP = horseradish peroxidase linked secondary antibody. AP-linked antibodies were used with the CDP-STAR chemiluminescence system (Sigma) to detect proteins, HRP-linked antibodies were used with the Supersignal West Dura substrate (Pierce) to detect proteins.

### **II.2.1 Genotyping**

For genotyping, adult tail biopsies were digested using tail lysis buffer and proteinase K overnight at 55°C. Samples were centrifuged to pellet undigested tissue. The supernatant containing genomic DNA was collected and diluted 50X in PCR grade water.

PCR used 1X Hotstart Taq Mastermix (Qiagen) and 0.5 µM each of forward and reverse primer (Arl-F: 5'-CAC TCC AGA TGC ACA GTG CTC TCC AAC CAC -3'; Arl-R: 5'- CCC ACT CAC CCT CGA TGT TGT CAA TGT AAA CCC -3').

After the initial denaturation of 95°C for 15 min, thirty five cycles of PCR were performed. Denaturation was at 94°C for 30 sec, primer specific annealing temperature of 63°C for 30 sec was used, and then extension of 72°C for 1 min. A final extension of 72°C for 10 min was then performed. 5 µl of PCR product was analysed on 1% agarose gel to check for amplification.

PCR products were digested for 1.5 hr at 37°C with *Ava*I (New England Biolabs) restriction enzyme and run on a 3% agarose gel. An *Ava*I restriction site is present in the mutant sequence only, allowing the mutant PCR product to be distinguished from wildtype PCR product after digestion. The wildtype genotype produces one band of 270 bp, heterozygotes produce three bands of 270 bp, 235 bp and 35 bp, while homozygous mutants produce two bands of 235 bp and 35 bp.

PCR to genotype for the axonemal dynein mutation used 1X Hotstart Taq Mastermix (Qiagen) and 0.5µM each of two forward (WT and mutant) and one common reverse primer (Axo-F Mut: 5'-TCA TGA GAG CAT TGA GGG A-3'; Axo-F WT: 5'-TCA TGA GAG CAT TGA GGG T-3' and Axo-R: 5'-TGA CTA TCG TAC AAA ATG CTT-3')

After the initial denaturation of 95°C for 15 min, thirty five cycles of PCR were performed. Denaturation was at 94°C for 30 sec, primer specific annealing temperature of 55°C for 30 sec was used, and then extension of 72°C for 1 min. A final extension of

72°C for 10 min was then performed. 5 µl of PCR product was analysed on 1% agarose gel to establish genotype.

### **II.2.2 SDS-PAGE and Western Blotting**

For SDS-PAGE analysis, protein samples were denatured by boiling for 5 minutes in 5X SDS sample buffer (final concentration 1% SDS). The protein samples were then separated by SDS-PAGE using either the Mini Protean gel electrophoresis system from Biorad using 4% and 10% gels (as indicated for each experiment), or the XCell Surelock MiniCell system from Invitrogen with 4-12% gradient gels. Electrophoresis was conducted at a constant voltage of 120V for approximately 1.5 hr (or until the dye front reached the bottom of the gel). Protein bands were either visualised by coomassie blue staining, following the manufacturers instructions (Sigma), or transferred to polyvinylidene difluoride (PVDF) membrane from GE Healthcare for Western blotting. Membranes were immersed in methanol for 30 sec, then rinsed in water, prior to transfer to improve the transfer of proteins into the membrane. The polyacrylamide gels and membranes were “sandwiched” together between filter paper and sponge pads that had been soaked in transfer buffer and then secured in the transfer cassette (sponge pad-filter paper-gel-membrane-filter paper-sponge pad). Frozen cooling units were placed into the transfer tanks with the cassettes to prevent significant temperature increase from the current and transfers were also conducted at 4°C for this reason. The transfers were conducted at 20V overnight (with an additional 30 min at 90V when transferring very large proteins such as DHC). Blots were disassembled, rinsed in PBS containing 0.5% Tween-20 (PBST) and incubated in 5% w/v non-fat milk at room temperature for 1 hr on a rocking plate. The membranes were then rinsed in PBST and labelled with the primary antibody (as indicated) at room temperature for 1 hr on a rocking plate. The membranes were washed with PBST 1 x 15 min and 3 x 5 min on a rocking plate and then labelled with secondary antibody at room temperature for 45 min on a rocking plate. The secondary antibody was removed and the membranes washed in PBST 3 x 15 min on a rocking plate. The proteins were detected using alkaline phosphatase-linked secondary antibodies with the CDP-STAR chemiluminescence system (Sigma), or the Horseradish Peroxidase-linked secondary antibodies with the Supersignal West Dura substrate (Pierce) (See Table 2 for antibody details). Multiple film exposures were taken from the membranes over a range of exposure times (between 10 sec and 10 min

depending on protein), and those below saturation were used for quantification. To quantify, the film images were scanned using an image scanner with ImageMaster Labscan V3.01 software (Amersham Biosciences). The signal from the bands was determined, and the background intensity from the film was subtracted using the ImageQuant TL 2005 software (Amersham Biosciences). GraphPad Prism software was used for statistical analysis using Mann-Whitney t test. Significance was set as  $p < 0.05$ .

### **II.2.3 Dynein Quantification in Brain Tissue**

Adult wildtype and *Arl/+* mice were sacrificed by terminal CO<sub>2</sub> anaesthetisation and the brains collected. The tissue was weighed, then homogenised using a tight glass hand held Teflon homogeniser. This was done in a 1:4 ratio of tissue to 2D lysis buffer at room temperature to prevent the urea from crystallising if performed on ice. After homogenisation, the homogenate was left at room temperature for 30 min to allow solubilisation of the proteins; it was then centrifuged at 13,000 rpm for 20 min. The supernatant was then collected and the protein concentration measured using the 2D Quant kit (GE Healthcare) following the manufacturer's protocol. The standard BCA kit (Pierce) could not be used to measure the protein concentration as the urea, CHAPS and DTT would interfere with the kit. The 2D Quant kit precipitates the protein, allowing for the removal of interfering substances in solution. 5 µg of each sample was boiled at 95°C for 10 min in 5 X sample buffer (SB), then loaded onto a 4% and 10% SDS-PAGE gel and Western blotting conducted as previously described, with detection for DHC and  $\alpha$ -tubulin and alkaline phosphatase (AP)-linked secondary antibodies (1/10,000) (See table 2).

### **II.2.4 Dynein Quantification in Spinal Cord**

Adult wildtype and *Arl/+* mice were sacrificed by terminal CO<sub>2</sub> anaesthetisation and the spinal cords collected. The tissue was weighed, then homogenised using a tight glass hand held Teflon homogeniser. This was done in a 1:3 ratio of tissue to 2D lysis buffer. After homogenisation, the homogenate was left at room temperature for 30 min to allow solubilisation of the proteins; it was then centrifuged at 13,000 rpm for 20 min. The supernatant was then collected and the protein concentration measured using the 2D

Quant kit following the manufacturer's protocol. 5 µg of each sample was boiled at 95°C for 10 min in 5 X SB, then loaded onto a 4% and 10% SDS-PAGE gel and Western blotting conducted as previously described, and labelled with DHC and  $\alpha$ -tubulin and alkaline phosphatase (AP)-linked secondary antibodies (1/10,000) (See table 2).

### **II.2.5 Sucrose Density Gradient Analysis**

Adult wildtype and *Arl/+* mice were sacrificed by terminal CO<sub>2</sub> anaesthetisation and the brains collected. The tissue was weighed, then homogenised on ice using a tight glass Teflon hand homogeniser, in PBS<sup>-</sup>, containing 1X protease inhibitors (Roche) in 1:4 tissue to buffer ratio. The homogenate was centrifuged at 13,000 rpm for 20 min at 4°C, the pellets discarded and the supernatant retained. The protein concentrations were established using the Pierce BCA Protein Assay kit, following the manufacturer's protocol. 2 mg of protein from each sample was loaded onto 5-25% linearised sucrose density gradients and centrifuged at 50,000 rpm (~303,800 x g<sub>max</sub>) at 4°C for 4 hr. Nine equal fractions were gently pipetted from the top of the gradient using wide bore pipette tips to minimise disturbance to the gradient. These fractions were snap frozen in liquid nitrogen (LN<sub>2</sub>), then 16 µl of each sample boiled at 95°C for 10 min in 5 X SB and then analysed on 4% and 10% SDS-PAGE gels and Western blotting (as previously described) then labelled for DHC (1/200) (Santa Cruz) and DIC (1/2000) (Gift from Dr Kevin Pfister) and alkaline phosphatase (AP)-linked secondary antibodies (1/10,000) (See table 2).

### **II.2.6 Dynein Purification**

Thirty adult wildtype and *Arl/+* mice were sacrificed by terminal CO<sub>2</sub> anaesthetisation and the brains dissected. The tissue was kept on ice in ice-cold PBS<sup>-</sup>, then drained and weighed. Any blood was rinsed away with PBS<sup>-</sup> and the tissue homogenised in homogenisation buffer with ATP (HB/ATP) using a polytron at 4°C. The wildtype and *Arl/+* homogenates were centrifuged in a Sorvall SS34 rotor at 11 krpm (~15,000 x g<sub>av</sub>) at 4°C for 1 hr. The pellets were discarded and the supernatants centrifuged at high speed to remove as much membrane material as possible, using a Beckman SW55Ti rotor at 32.5 krpm (~100,000 x g<sub>av</sub>) at 4°C for 1 hr. The supernatants were collected and

the pellets discarded. To remove most of the microtubule associated proteins (MAPS) from the supernatants, the endogenous tubulin was polymerised using GTP to aid polymerisation and taxol to polymerise irreversibly (0.25 mM GTP and 6  $\mu$ M taxol) and incubated at 30-35°C for 30 min. The supernatants were then centrifuged at 20 krpm ( $\sim 37,000 \times g_{av}$ ) at 28°C for 30 min, again in a Beckman SW55Ti rotor. The resulting pellets were discarded and to the supernatants apyrase, AMP.PNP and taxol were added (1 U/ml apyrase, 50  $\mu$ M AMP.PNP and 4  $\mu$ M taxol). This was to bind the dynein to the microtubules using the non-hydrolysable analogue of ATP; AMP.PNP. This was incubated at 35°C for 30 min. Approximately 2 ml of 20% sucrose in HB and taxol were used as a cushion in two 5 ml centrifuge tubes. The supernatants were layered over the cushions and centrifuged at 32.5 krpm ( $\sim 100,000 \times g_{av}$ ) for 45 min at 25°C in an SW55Ti rotor. The supernatants and cushions were aspirated (a sample was kept to check if dynein remained in this sample) and the remaining pellets resuspended in 1/10<sup>th</sup> the original volume of the high speed supernatant of HB using a small, hand-held, glass homogeniser. The resuspended pellets were layered over 10% sucrose cushions and centrifuged at 17.8 krpm ( $\sim 30,000 \times g_{av}$ ) for 30 min at 28°C. Again the supernatants and cushions were removed and samples kept to check if dynein remained. The pellets were resuspended using a small glass, hand-held homogeniser in 1/20<sup>th</sup> the original supernatant volume of HB/KCl/taxol/ATP. This was incubated for 30 minutes at 37°C to elute the kinesin and dynein. This time, without a cushion, the resuspended samples were centrifuged at 17.8 krpm ( $\sim 30,000 \times g_{av}$ ) for 30 min at 28°C and the resulting supernatants were collected and stored on ice at 4°C. These were labelled motor sample 1. The pellets were resuspended in 1/50<sup>th</sup> the original volume of HB/KCl/ATP and left on ice at 4°C overnight. 5-20% sucrose density gradients were poured and allowed to linearise overnight. The following morning, the resuspended pellets were centrifuged at 17.8 krpm ( $\sim 30,000 \times g_{av}$ ) for 30 min at 4°C, the supernatants collected and labelled as motor sample 2. All of the motor samples 1 and 2 were loaded onto individual sucrose gradients and centrifuged at 52krpm ( $\sim 255,800 \times g_{av}$ ) for 4 hr and 35 min at 4°C with the brake set to low. Once complete, 12 equal fractions were collected from each of the gradients and left on ice at 4°C before being assayed for motility under the microscope the following day. Samples from each of the fractions were run on a 4-12% gradient SDS-PAGE and Western blotted (as previously described) and labelled for dynein heavy chain and intermediate chain and alkaline phosphatase (AP)-linked secondary antibodies

(1/10,000), to check for the presence and location of the dynein in the samples (See table 2).

### **II.2.7 Tubulin Polymerisation**

MTs were polymerised using 10 µl aliquots of 5 mg/ml stock tubulin in BRB80 buffer. To this was added, 1 mM GTP, 1X protease inhibitors (Roche), then warmed to RT and 20 µM paclitaxel added to a final volume of 20 µl in BRB80 buffer. This was then incubated at 35°C for 30 min. The sample becomes viscous and bubbles may appear if MTs have successfully been formed.

### **II.2.8 MT Gliding Assay**

The MT gliding assays were performed using protocols kindly provided by Professor Viki Allan (University of Manchester) and Professor Rob Cross (Warwick University). Flow chambers were constructed from microscope slides, with two strips of high vacuum grease run along either side, and a coverslip placed on top. This produced a chamber of approximately 15-20 µl volume. To the chamber, 2.5 mg/ml casein was added to coat the glass coverslip, preventing denaturing of the dynein once added. The casein was incubated at room temperature for 2 min. This was then washed out using motility buffer. Approximately 15 µl of the purified dynein fraction was flowed into the chamber and incubated in a humid chamber at room temperature for 2-5 min. The chamber was rinsed with 2 X volumes of motility buffer containing 150 µg/ml casein and 1 mM DTT. The microtubule dilution was then flowed through the chamber, allowed to bind to the dynein for a minute and then viewed using an Olympus VE-DIC equipped, upright microscope with a 60X Plan Apo 1.4 numerical aperture DIC objective, through a Hamamatsu Argus image processor. Once MTs were identified and focussed upon, any moving ones were recorded for 1 min periods at 1 frame per second. After filming was completed, the videos were analysed to measure the velocities of the moving MTs using the Retrac program developed by Nick Carter in the laboratory of Rob Cross (previously of the Marie Curie Research Institute, now the Centre for Mechanochemical Cell Biology, Warwick University). Table 3 details optimisations that were made to this protocol to improve the levels of MT motility observed. These conditions were developed in conjunction with Dr Kuniyoshi Kaseda (previously of the

Marie Curie Research Institute, now at the Saravio Institute, Japan), based on his anecdotal evidence from using this protocol.

### **II.2.9 Microtubule-dependent ATPase Assay**

Tubulin was polymerised to MTs and stabilised with paclitaxel. The MTs were added to the purified dynein fraction in 1ml of ATPase assay buffer. This mixture was added to a quartz cuvette and placed in a spectrophotometer set at 37°C. The change in absorbance at 340 nm was measured and recorded over a 5 min timeframe.

### **II.2.10 MT Binding Assay**

To 20 µl of polymerised MT sample, 20 µg of purified dynein sample was added and gently mixed. To this, 50 µM AMP.PNP was added to bind the dynein to the MTs, and incubated at 30°C for 15 min. 500 µl of 10% sucrose was placed into a 2 ml centrifuge tube and the MT/dynein sample layered over the top. This was centrifuged at 30 krpm (106,500 x  $g_{av}$ ) for 40 min at 25°C. The top sample was removed (the combined volume of MTs and dynein sample) and labelled supernatant and the 500 µl of sucrose cushion removed and labelled cushion. The pellet was washed in 100 µl of BRB80 buffer and centrifuged again at 30 krpm (106,500 x  $g_{av}$ ) for 40 min at 25°C. The wash buffer was removed and discarded and the pellet solubilised in 20 µl of BRB80 buffer. Each sample was run on an SDS-PAGE and analysed by western blot (as previously described) for DHC, DIC and  $\alpha$ -tubulin (1/1000) (Upstate) and alkaline phosphatase (AP)-linked secondary antibodies (1/10,000) (See table 2) and quantified using Image Pro software.

### **II.3.1 Collection and Culture of Mouse Embryonic Fibroblasts**

Pregnant female *Ar1/+* mice were sacrificed by terminal CO<sub>2</sub> anaesthetisation and the uterine horns dissected out and placed in phosphate buffered saline, without bivalent cations (PBS<sup>-</sup>). Each embryo was separated from its placenta and the brain and red organs removed, then finely minced in PBS<sup>-</sup> using a razor blade. The tissue from each embryo was then digested in 2 ml of trypsin-EDTA (0.05% trypsin and 0.53 mM EDTA-4 Na) for 15 min, with occasional shaking. DMEM supplemented with 15%

serum was added to neutralise the trypsin and the cells recovered by centrifugation for 5 min at 1500 rpm. The cells from each embryo were transferred to 175 cm<sup>2</sup> cell culture flasks and grown in complete DMEM medium at 37°C in 5% CO<sub>2</sub> and 3% O<sub>2</sub>.

### **II.3.2 Golgi Reassembly**

MEFs were seeded at a density of  $2.0 \times 10^5$  cells/well in a 6 well plate, on round coverslips, in complete DMEM medium. The cells were allowed to proliferate at 37°C in 5% CO<sub>2</sub> and 3% O<sub>2</sub> until 70% confluency was reached. The medium was replaced with chilled complete DMEM with 15mM HEPES and the cells incubated on ice for 30 min. 10 µg/ml of nocodazol was added to each well and incubated for 3 hours at 37°C in 5% CO<sub>2</sub> and 3% O<sub>2</sub>. The nocodazol was aspirated and the 0 min timepoint cells immediately fixed. All other timepoints were washed five times with plain DMEM as quickly as possible. Complete medium was then added and the cells incubated at 37°C in 5% CO<sub>2</sub> and 3% O<sub>2</sub> to recover for the specified timepoints. To fix the cells, 2 ml of -20°C methanol was added to each well for 8 min, this was then aspirated and the cells were washed twice with phosphate buffered saline containing 0.2% gelatine from cold water fish skin (PBSG). The cells were stained for Golgi using an antibody against giantin (1/200) (Covance), a Golgi membrane protein, and  $\alpha$ -tubulin. Alexa-Fluor conjugated secondary antibodies were then used (1/10,000) (All from Invitrogen) (See table 2). All antibodies were diluted in PBS<sup>-</sup> (except anti-giantin which was diluted in PBSG), and incubated at room temperature for 30 min. The coverslips were mounted on glass slides using Prolong Gold mounting medium containing DAPI (Invitrogen), and left to cure for 24 hr, then stored at 4°C. The slides were imaged using a Deltavision Core inverted, widefield microscope system (Applied Precision Inc.) with an Olympus 60 x Plan Apo 1.4 numerical aperture (na) oil objective lens. Imaging was conducted using the SoftWorX image processing software (Applied Precision Inc.) with appropriate filters (DAPI and TRITC) at 100% neutral density, and exposure times of 0.2-0.5 sec. Images were then deconvolved in the SoftWorx imaging program.

### **II.3.3 Endosomal Trafficking**

Wildtype and *Arl*/<sup>+</sup> MEFs were plated at a density of  $2.0 \times 10^5$  cells/ well in a 6 well plate on round coverslips in complete DMEM. Cells were allowed to proliferate at 37°C

in 5% CO<sub>2</sub> and 3% O<sub>2</sub> until 80% confluency was reached. The cells were washed twice with PBS<sup>-</sup> and then incubated in starving medium (DMEM containing L-glutamine and penicillin and streptomycin, but without serum) for 2 hr at 37°C in 5% CO<sub>2</sub> and 3% O<sub>2</sub>, before being stimulated for 10 min in starving medium containing 10 ng/ml Alexa Fluor-555 conjugated EGF (Invitrogen) and 0.1% BSA. The cells were washed twice with PBS<sup>-</sup>, replaced with fresh serum-free medium and the internalised EGF then chased for the indicated timepoints. Cells were then washed in ice cold PBS<sup>-</sup> and fixed with 4% paraformaldehyde (PFA) (Electron Microscopy Science) for 15 min and permeabilised with 0.1% Triton X-100 for 5 min, then washed three times in PBS<sup>-</sup> and blocked for 30 min with 2% BSA. The cells were stained for  $\alpha$ -tubulin for 30 min at room temperature and mounted using Prolong Gold antifade with DAPI, left to cure for 24 hr and then stored at 4°C. The slides were imaged using a Deltavision Core inverted, widefield microscope system (Applied Precision Inc.) with an Olympus 60 x Plan Apo 1.4 numerical aperture (na) oil objective lens. Imaging was conducted using the SoftWorX image processing software (Applied Precision Inc.) with appropriate filters (FITC, DAPI and TRITC) at 100% neutral density, and exposure times of 0.2-0.5 sec. Images were deconvolved in the SoftWorX image processing software.

### **II.3.4 Endosomal Trafficking in Live Cells**

Wildtype and *Arl*<sup>+</sup> MEFs were plated at a density of  $0.5 \times 10^5$  cells/ well in a 2 well, live cell imaging chamber in DMEM. Cells were allowed to proliferate at 37°C in 5% CO<sub>2</sub> and 3% O<sub>2</sub> until 50% confluency was reached. The cells were washed twice with PBS<sup>-</sup> and then incubated in starving medium (DMEM containing L-glutamine and penicillin and streptomycin, but without serum) for 2 hr at 37°C in 5% CO<sub>2</sub> and 3% O<sub>2</sub>, before being stimulated for 10 min in starving medium containing 20 ng/ml Alexa Fluor-555 conjugated EGF (Invitrogen) and 0.1% BSA. The cells were washed once with PBS<sup>-</sup>, replaced with fresh serum-free CO<sub>2</sub> independent medium and the internalised EGF then chased for 1 min movies (at 1 frame per 2 sec), every 5 min for a total of 30 min. Images were captured using 2 channels; DIC and TRITC filters on a Personal Deltavision (pDV) widefield, live cell imaging microscope system (Applied Precision Inc.) using an Olympus 100X Plan Apo 1.4 na oil objective lens. Neutral density was set at 100% for the the DIC channel and 50% for the TRITC channel. The movies were captured using the SoftWorX imaging software (Applied Precision Inc.) and analysed

using Image J and Excel to determine the total number of moving endosomes and the average velocities of each of the endosome trajectories. To determine the average velocities of the endosomes by calculating the total distance travelled by the endosome, as determined by the x and y coordinates provided by Image J, over a set time calculated from the number of frames that movement was measured. This data was used in Excel and the following formula used to calculate the distance travelled by the endosome being tracked:

$$=\text{SQRT}(((x_2-x_1)*(x_2-x_1))+((y_2-y_1)*(y_2-y_1)))$$

Where x and y are the location coordinates of the endosome. The calculated distance was then divided by the amount of time the distance was measured over to give the speed of movement of the endosome.

### **II.3.5 Tracking of Mitochondria in Live Cells**

Wildtype and *Arl*<sup>+/+</sup> MEFs were plated at a density of  $0.5 \times 10^5$  cells/ well in a 2 well, live cell imaging chamber in DMEM. Cells were allowed to proliferate overnight at 37°C in 5% CO<sub>2</sub> and 3% O<sub>2</sub> until 50% confluency was reached. 50 nM of Mitotracker Green FM (Invitrogen) was added to the cells in fresh complete medium and incubated for 30 min at 37°C in 5% CO<sub>2</sub> and 3% O<sub>2</sub>. The medium was replaced with CO<sub>2</sub> independent medium and cells imaged using DIC and FITC channels on a Personal Deltavision (pDV) widefield, live cell imaging microscope system (Applied Precision Inc.) using an Olympus 100X Plan Apo 1.4 na oil objective lens. Neutral density was set at 100% for the the DIC channel and 50% for the FITC channel. The movies of the visualised mitochondria were captured using the SoftWorX imaging software (Applied Precision Inc.) and were recorded at 1 frame per 2 sec for lengths of 1 min. The movies were analysed using Image J and Excel to determine the average velocities of the mitochondria by calculating the total distance travelled by the mitochondria, as determined by the x and y coordinates provided by Image J, over a set time calculated from the number of frames that movement was measured. This data was used in Excel and the following formula used to calculate the distance travelled by the mitochondrion being tracked:

$$=\text{SQRT}(((x_2-x_1)*(x_2-x_1))+((y_2-y_1)*(y_2-y_1)))$$

Where  $x$  and  $y$  are the location coordinates of the mitochondrion. The calculated distance was then divided by the time the distance was measured over to give the speed of movement of the mitochondrion.

### **II.3.6 Culturing of motor neurons**

E13 embryos were dissected from the uterine horn and washed in PBS<sup>-</sup>. They were then removed from the embryonic sacs and kept in PBS<sup>-</sup> on ice. The brain and red organs were removed and the spinal cord dissected from the posterior of the embryo, ensuring all connective and membranous tissue was removed. The meninges and dorsal root ganglia were removed and the dorsal root of the spinal cord cut away and discarded. The remaining ventral root (containing the motor neurons) was cut into pieces and transferred to PBS<sup>-</sup> containing antibiotics (penicillin and streptomycin). Spinal cord pieces were allowed to settle and then transferred to a 10 ml Falcon tube containing 1 ml HBSS medium, antibiotics and 10  $\mu$ l trypsin. This was incubated for 10 min at 37°C, with gentle shaking. The spinal cord pieces were transferred to 800  $\mu$ l of complete L15 medium (L15, 100  $\mu$ l 4% BSA and 100  $\mu$ l DNaseI). The cells were dissociated through gentle trituration, then allowed to settle for 2 min. The supernatant was transferred to a separate tube and to the pellet was added 900  $\mu$ l of complete L15 medium (L15, 100  $\mu$ l 4% BSA and 20  $\mu$ l DNaseI) and gently triturated 8 times. This was allowed to settle for 2 min to separate remaining large pieces of tissue and the supernatant combined with the first supernatant. To the remaining pellet 900  $\mu$ l of complete medium was added and gently dissociated again by triturating 8 times. The supernatant was combined with the others and the pellet discarded. The supernatant was centrifuged through a 1 ml BSA cushion for 5 min at room temperature. The supernatant was aspirated and the pellet gently resuspended in 600  $\mu$ l of Motor neuron culture medium and 200  $\mu$ l seeded per well of 2 well live cell chambers. A further 800  $\mu$ l of Motor neuron culture medium was added to each well and the cells incubated at 37°C in 5% CO<sub>2</sub> and 3% O<sub>2</sub>.

#### **II.4.1 Perfusion Fixation Protocol**

Adult wildtype and *Arl/+* mice were terminally anaesthetised by injection with ketamine hydrochloride and medetomidine hydrochloride, then intra-cardiac perfusion-fixation was performed using 2.5% glutaraldehyde and 1.5% paraformaldehyde in 100 mM Na cacodylate buffer. The perfusion was carried out in two stages; 50 ml of 100 mM cacodylate, followed by 100 ml of fixative. Perfusion was performed on a down-draught table to comply with COSHH. Tissue and muscle was removed from the hindlimbs, and the sciatic nerves removed and placed in fixative. The spinal cord was exposed by dorsal laminectomy, sliced at 2-3 mm intervals to facilitate access to tissue by the fixative and then placed in fixative. All tissues were left in fixative for 48 hr to harden. Tissues were immersed in 2% aqueous osmium tetroxide (Electron Microscopy Science) for 2 hr at room temperature, then dehydrated sequentially in increasing concentrations of ethanol- 70% ethanol, 2 x 10 min; 90% ethanol, 2 x 10 min; 100% ethanol, 2 x 10 min. The tissues were then incubated at room temperature in propylene oxide (Agar Scientific) for 2 x 15 min. Following this, the tissues were infiltrated with resin consisting of 1 part polypropylene oxide: 1 part araldite resin (Agar Scientific) for one hr on a rotating wheel. This was discarded and replaced with 1 part polypropylene oxide: 2 parts araldite resin for one hr on a rotating wheel, then finally replaced with 100% pure resin and left overnight to allow tissues to fully infiltrate on a rotating wheel. The following morning, sample pot caps were half filled with resin, the tissue from each sample placed on top and resin added to cover the tissue. These were placed in an oven at 60°C for 48 hr to allow the resin to cure. Once the resin was cured, the samples were sectioned using a microtome to produce multiple 100 nm sections. Each section was placed on a nickel electron microscopy grid, allowed to dry then stained with uranyl acetate and lead citrate. The samples were imaged at 1000 x and 5000 x magnification using an Hitachi-7100 transmission electron microscope with an axially mounted Gatan Ultrascan 1000 CCD camera.

#### **II.4.2 Preparation of Mitochondria and O<sub>2</sub> Consumption Assay**

Five adult wildtype and *Arl/+* mice were sacrificed by terminal CO<sub>2</sub> anaesthetisation and the lumbar section of the spinal cords dissected. The tissue was kept on ice in Tissue homogenisation buffer (THB), then homogenised with a loose, glass, handheld

homogeniser in approximately 1 ml of buffer, supplemented with 1% BSA and 7 mM L-cysteine hydrochloride. The homogenate was centrifuged at 800 x g for 10 min at 4°C. The supernatants were transferred to a new tube and centrifuged at 10,000 x g for 10 min at 4°C. The pellets were resuspended in 1 ml of buffer with 1% BSA, but no L-cysteine hydrochloride and centrifuged again at 10,000 x g for 10 min at 4°C. The pellets were then resuspended in 50 µl of Oxygen electrode buffer (OEB) and kept on ice. Using a Rank oxygen electrode, the oxygen consumption of the mitochondria was measured. 20 µl of mitochondria, with 5 µl of ascorbate and 5 µl of TMPD were added to the electrode chamber in 400 µl of buffer and the rate of O<sub>2</sub> consumption measured and recorded. The protein concentration of each sample was then measured using the BCA protein quantification kit from Pierce. The rate of O<sub>2</sub> consumption was then calculated as nmol O<sub>2</sub>.min<sup>-1</sup>.mg<sup>-1</sup> and wildtype and *Arl*<sup>-/-</sup> mitochondria compared.

## **CHAPTER III**

## **Chapter III**

# **INVESTIGATING THE EFFECT OF THE *ARL* MUTATION ON DHC PROTEIN**

## **III.1 Introduction**

As previously explained in chapter I, the *Arl* mutation results in a change of the well conserved tryptophan at position 1206, to arginine in the cytoplasmic dynein heavy chain gene 1 (*Dync1h1*). This is in a region currently of unknown function, just N-terminal to the motor domain.

The *Arl* mutation has been shown to have a related, but more severe phenotype than *Loa* or *Cral*, with homozygotes dying by E10, and a more pronounced and earlier onset hindlimb clenching in the tail suspension test.

As the mutation is located in an area of unknown function, initial studies looked at the effect of the mutation on the protein and its function.

## **III.2 Effect of mutation on mice**

As the *Arl* mutation is embryonically lethal in homozygous mutants, any experiments using adult tissue could only compare WT to heterozygotes. This means that experiments using dynein from heterozygous adult tissue will contain a mixed population of WT homodimers, WT-*Arl* heterodimers and *Arl* homodimers, likely to be in a 1:2:1 ratio. As some experiments are unable to distinguish which population may be causing a particular phenotype it is important that this is taken in to account when interpreting data.

Limitations in breeding were encountered, meaning that embryonic tissue was difficult to obtain. Under normal circumstances, mice can be timed mated so that embryos of specific ages can be dissected. However, *Arl* mice proved to be very poor breeders, with very few embryos and normal mendelian ratios of genotypes were not attained.

More than 100 timed matings were set up between *Arl/+* and *Arl/+* mice, resulting in only 6 pregnancies. From these 6 litters, only 2 *Arl/Arl* embryos were acquired at E10. This suggests that lethality due to the mutation may be earlier in development than previously thought.

Experiments using timed matings to produce litters of different ages were planned to establish at what stage of development the *Arl/Arl* embryos are lost, as the developmental stage at which the homozygous mutants are no longer viable can provide information about how the mutation may be affecting the embryo development. However, due to the very low levels of breeding in these mice, this was not possible.

Mendelian ratios were not identified in litters from breeding stock. As *Arl* is a dominant mutation, ratios from F1 backcrosses of *Arl/+* x WT should result in approximately 1:1 ratios of genotypes. However, from 901 mice produced from these crosses, 265 were *Arl/+* and 636 were WT, giving a ratio of 1 : 2.4. This suggests that some *Arl/+* mice are lost *in utero*.

The recently identified axonemal dynein mutation in *Arl* may play a part in the breeding problems and embryonic loss seen in *Arl* mice, however, due to time constraints it was not possible to investigate this in detail. Nevertheless, it was important to establish whether this axonemal mutation was indeed present in the *Arl* colony used in this project and although it was not practical to re-genotype the entire colony, a random selection of samples already used in this project was tested to determine the presence of the mutation.

As shown in Figure 6, the axonemal mutation is present in some samples, but not all, suggesting that the axonemal and cytoplasmic dynein mutations in *Arl* are able to segregate and have randomly done so in some of the mice that were used in this project.

### **III.3 Dynein heavy chain protein**

To investigate whether the *Arl* mutation had any effect on the levels of dynein heavy chain protein in tissue samples, the brains of six mice (3 wildtype and 3 *Arl/+*) were

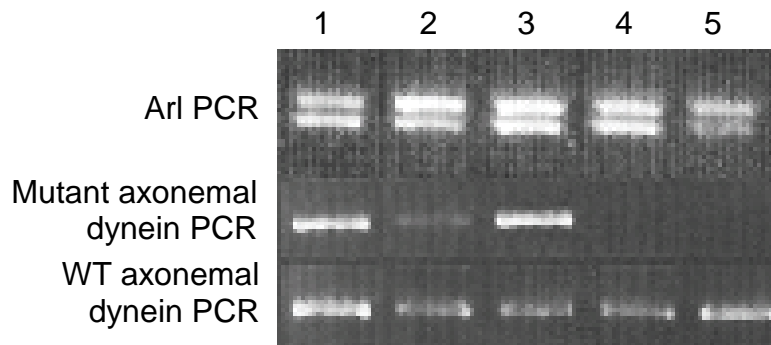


**Figure 6. Cytoplasmic and axonemal dynein genotypes of a selection of mice used during the project.**

Tissue from a sample of mice used during this project were genotyped for both the *Arl* mutation in cytoplasmic dynein, and the axonemal dynein mutation to identify whether all *Arl* mice contain the axonemal dynein mutation, or if the mutations can segregate. Samples 1-3 are *Arl*/+ and contain the axonemal dynein mutation. Samples 4 and 5 are *Arl*/+, but do not contain the axonemal dynein mutation.

dissected, homogenised in PBS<sup>-</sup> and 5µg of each analysed on a 4% SDS PAGE, with α-tubulin used as an internal loading control (Figure 7 A).

This was repeated using spinal cord tissue from six mice (as before, 3 wildtype and 3 *Arl/+*) which was homogenised and 5µg loaded onto a 4-12% gradient gel (Figure 7 B). Analysis of the proteins by western blotting showed no significant difference in the amount of DHC in *Arl/+* brain tissue or spinal cord tissue compared to wildtype littermates. This suggests that the *Arl* mutation does not affect the transcription or translation, or stability of the DHC protein.

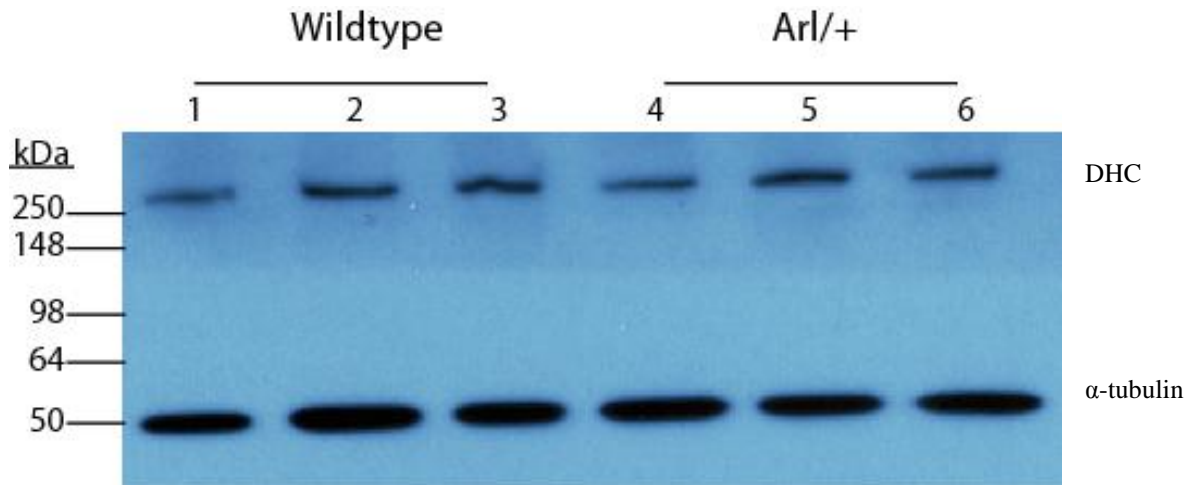
### **III.4 Integrity of the dynein complex**

The dynein complex is composed of two homodimerised heavy chains associated with a number of intermediate, light intermediate and light chains to form a fully functioning dynein motor protein. Despite the *Arl* mutation not being located within the region of homodimerisation of the heavy chains, or the areas of association of the accessory chains, it could, however, interfere with the stability of the complex causing a perturbation to its function.

To investigate this, sucrose density gradient centrifugation was used to see if the complex of dynein chains was affected by the *Arl* mutation. Brain tissue from wildtype and *Arl/+* mice was homogenised in PBS<sup>-</sup> and 2 mg of protein loaded onto 5-25% continuous sucrose density gradients and centrifuged at 303,800 x g<sub>max</sub> for 4 hr. Dynein chains that are associated in the complex would sediment together at approximately 20S, but any dynein not in the complex would sediment in much less dense fractions as it is “free” from the complex.

Equal fractions were removed from the gradients and analysed by SDS PAGE on 4% and 10% gels and western blotting to see if the sedimentation of the dynein chains was altered by the *Arl* mutation. Heavy chain and intermediate chain were labelled for as the mutation is contained within heavy chain, and intermediate chain is the least stable component of the complex (King 2009) and therefore the most likely to be affected by any disturbance to the complex. Despite this experiment using adult brain tissue, if the

A



B

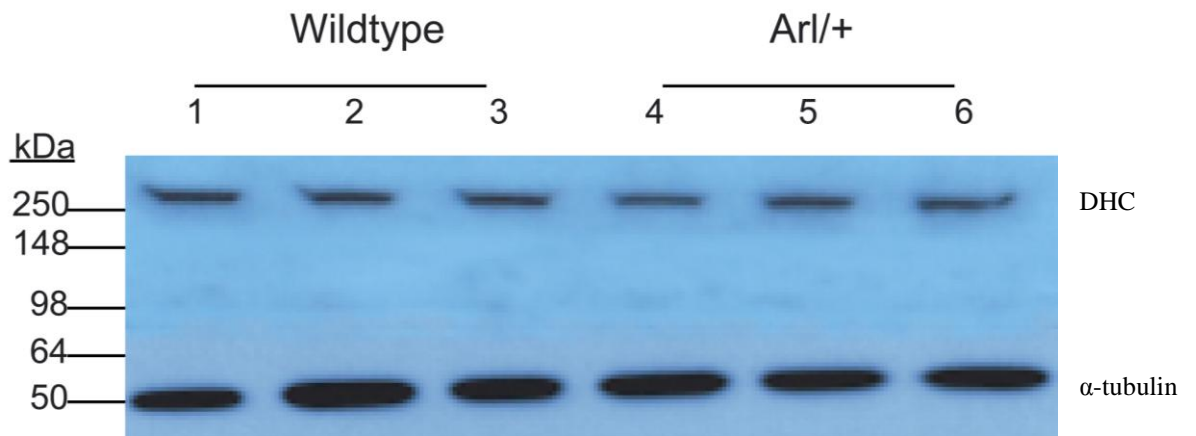


**Figure 7. Quantification of DHC in brain and spinal cord tissue from WT and *Arl/+* mice.**

- A. Brain tissue from 3 WT and *Arl/+* mice was homogenised in PBS<sup>-</sup> and 5 $\mu$ g of total protein loaded onto a 4% SDS PAGE, probed for DHC (1/200), with  $\alpha$ -tubulin (1/1000) used as an internal loading control.
- B. Spinal cord tissue from 3 WT and *Arl/+* mice was homogenised in PBS<sup>-</sup> and 5 $\mu$ g of total protein loaded onto a 4% SDS PAGE, probed for DHC (1/200), with  $\alpha$ -tubulin (1/1000) used as an internal loading control.

*Arl* mutation affected integrity of the complex, it would be expected that this would still be evident from the WB as the population of *Arl* homodimers is likely to make up approx. ¼ of the total heterozygous dynein sample. As can be seen from Figure 8, there is no difference in the distribution pattern of either the heavy chains or intermediate chains, suggesting that the integrity of the dynein complex is not affected by the mutation.

### **III.5 Purifying the dynein complex for analysis of its function**

As the dynein heavy chain is too large to practicably clone and express (~530kDa, ~4,500kb), purification of the complex from tissue was deemed to be the best way to obtain the protein for use in functionality assays (such as microtubule gliding assays). Dynein complex from wildtype and *Arl/+* was isolated to allow comparison of their function.

Brain tissue from approximately 35 mice of each genotype (WT and *Arl/+*) was collected and pooled together. This was homogenised and centrifugation steps used to purify the protein, with MT binding and centrifugation through a 20% and then 10% sucrose cushion and then release from the MTs with excess ATP. Pelleting of the MTs was used to isolate the MT based motor proteins (dynein and kinesin). This was then further purified on a 5-20% continuous sucrose density gradient to separate the motor proteins and equal fractions of the gradient were collected. These fractions were analysed by SDS PAGE on 4-20% gradient gels and coomassie staining and western blots were performed to identify the proteins in the fractions and which fraction contained the greatest amount of dynein complex for use in functionality assays. Samples from the supernatant of the sucrose cushions used in the purification were also analysed to estimate the efficiency of the MT binding dependent purification in these steps.

Despite there being a greater starting amount of total brain tissue in the *Arl/+* purification (~20 g of *Arl/+* v ~16 g wildtype), more dynein is apparent in the supernatant of the 20% cushion from the wildtype sample than the *Arl/+* (Figure 9). This would suggest that a greater amount of the wildtype dynein did not bind to MTs and was therefore unable to sediment through the sucrose cushion than that in the *Arl/+*

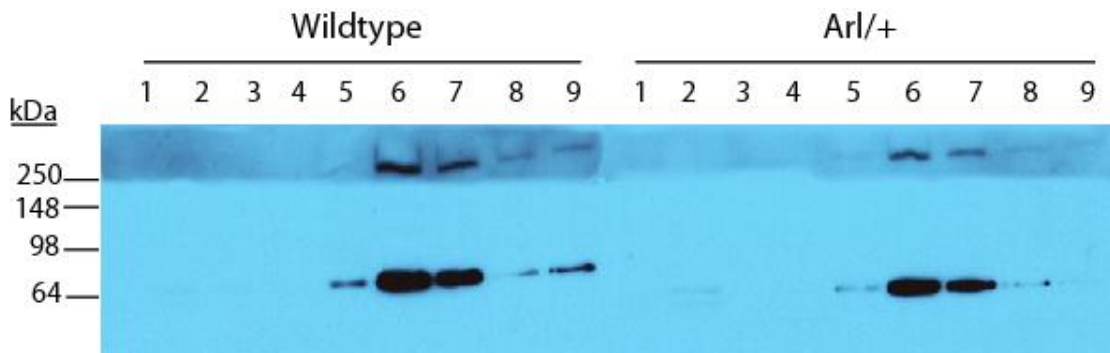
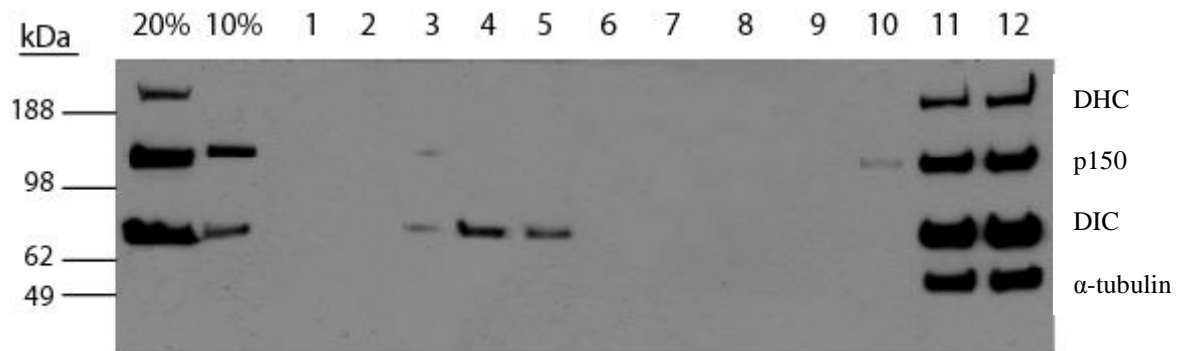


**Figure 8. Western blot of sucrose density gradient**

2 mg of tissue homogenate from WT and *Arl*<sup>+/+</sup> was loaded onto a 5-25% sucrose density gradient and centrifuged for 4 hr at 50,000 rpm ( $\sim 303,800 \times g_{\max}$ ). 9 equal fractions were removed and run on 4% and 10% gels and labelled for DHC (1/200) and DIC (1/1000). No difference in distribution between genotypes is seen.

A. Wildtype



B. *Arl*/+

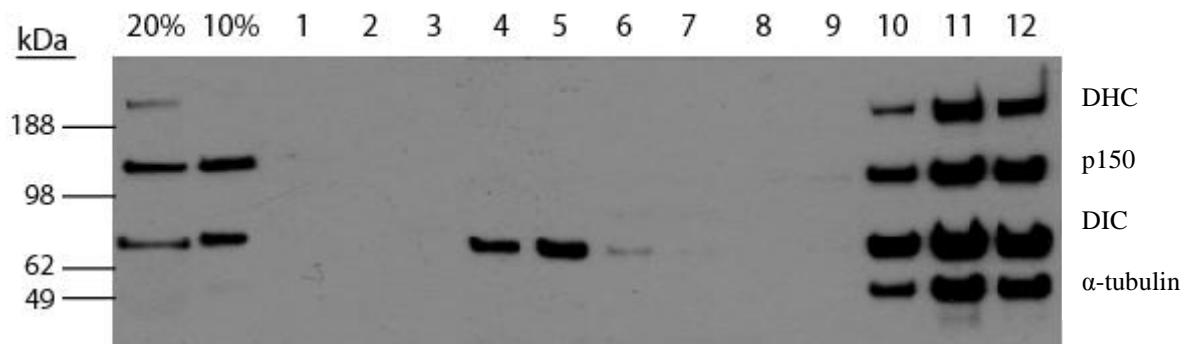


**Figure 9. Western blots of WT and *Arl*/+ dynein complex from dynein isolation.**

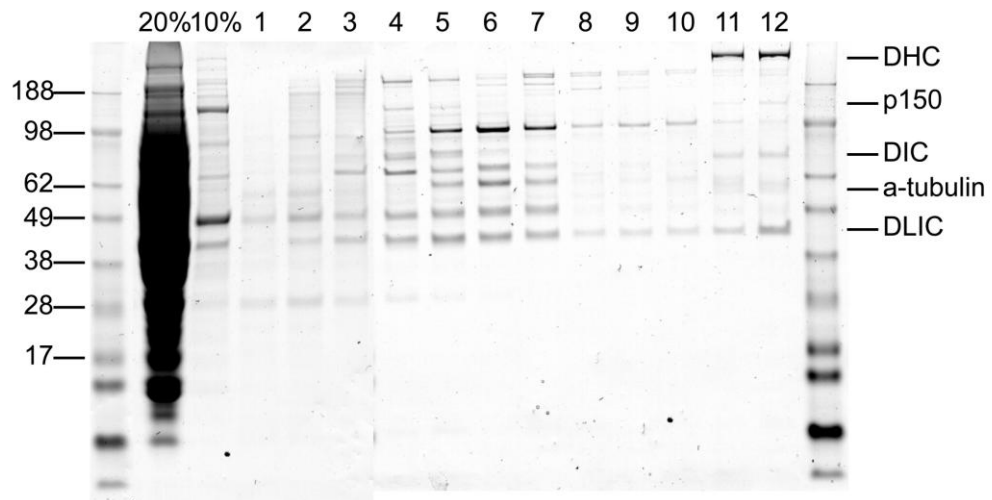
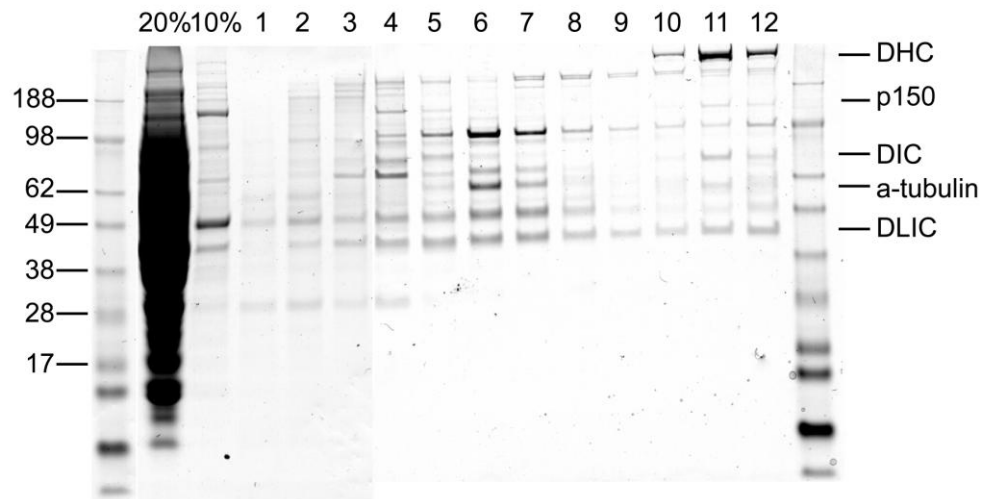
Brain tissue from approximately 35 mice was collected and pooled together. This was homogenised and centrifugation steps used to purify the protein, with MT binding and centrifugation through a 20% and then 10% sucrose cushion and then release from the MTs with excess ATP. This was then further purified on a 5-20% continuous sucrose density gradient to separate the motor proteins and 12 equal fractions of the gradient were collected. These fractions were analysed by SDS PAGE on 4-20% gradient gels and western blots performed to label for DHC, p150, DIC and  $\alpha$ -tubulin, and identify which fraction contained the greatest amount of dynein complex. A) Western blot from WT protein, B) western blot from *Arl*/+ protein.

sample. It has already been shown in Figure 7 A that there is no difference in the amount of dynein protein in brain tissue between wildtype and *Arl/+*, meaning if there was a greater amount of tissue used in *Arl/+*, then there should have been a greater amount of dynein protein than in the wildtype sample. This suggests that the difference in the amount of dynein able to sediment through the sucrose cushions is due to the ability of the dynein to bind to the MTs.

It is worth noting that due to the limited amount of *Arl/+* tissue available, this experiment was performed only once, and is thus a comparison between WT and *Arl/+* from 35 mice of each genotype on this one occasion.

The dynein complex is confined to fractions 11 and 12 in wildtype, but is seen in fractions 10, 11 and 12 in *Arl/+*. The reason for dynein being present in fraction 10 in the *Arl/+* sample is likely to be due to there being a larger amount of dynein present in these fractions which has caused it to “bleed” and overflow into fractions either side. This blot shows that the greatest amount of dynein is located in fraction 11 of both genotypes, with a lesser amount in fraction 12. This was confirmed by measuring the protein concentrations of fractions 11 and 12 of the purified wildtype and *Arl/+* dynein samples using a BCA kit. In WT, fractions 11 and 12 were found to be 0.95 mg/ml and 0.89 mg/ml respectively, and in *Arl* 1.23 mg/ml and 1.15 mg/ml. The difference in concentrations between the genotypes is accounted for by the differing starting amounts of tissue used. As fraction 11 contained the greatest amount of dynein in both genotypes it was therefore used for subsequent experiments.

Having identified which fractions contained the purified dynein complex, it was important to establish the purity of these samples. To do this the samples were run on 4-20% gradient gel and coomassie stained to identify all the proteins present in each fraction (Figure 10). In the main fractions containing dynein (11 and 12) the subunits of the dynein complex can be identified as well as dynactin and a small amount of tubulin. No other major bands that do not correspond with a dynein subunit appear to be present, suggesting that fractions 11 and 12 contain relatively pure dynein and are indeed suitable to use for experiments to investigate its function.

**A****B**

**Figure 10. Coomassie gels of WT and *Arl/+* dynein complex from dynein isolation.**

Brain tissue from approximately 35 mice was collected and pooled together. This was homogenised and centrifugation steps used to purify the protein, with MT binding and centrifugation through a 20% and then 10% sucrose cushion and then release from the MTs with excess ATP. This was then further purified on a 5-20% continuous sucrose density gradient to separate the motor proteins and 12 equal fractions of the gradient were collected. These fractions were analysed by SDS PAGE on 4-20% gradient gels and coomassie stained to identify the proteins present and which fraction contained the greatest amount of dynein complex. A) Coomassie gel of WT sample, B) coomassie gel of *Arl/+* sample, showing major proteins present in each sample.

## **Analysis of dynein function**

### **III.6 MT Gliding Assay**

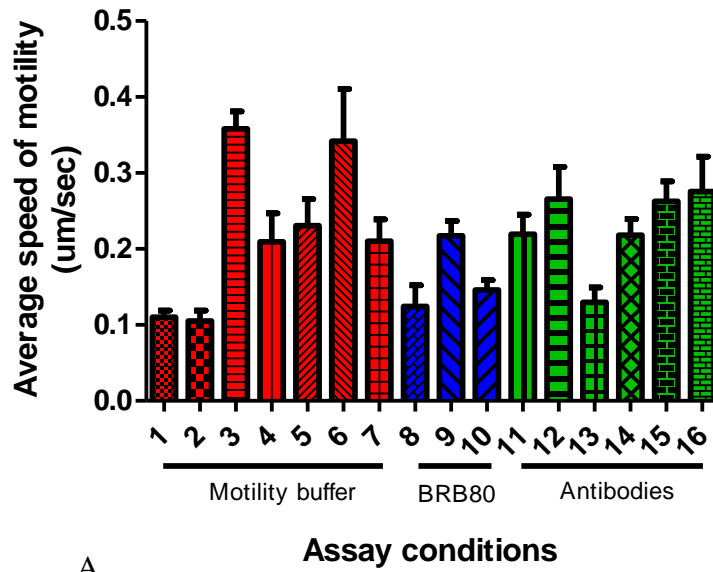
The dynein samples were used in microtubule gliding assays to try to determine if the *Arl/+* mutation affected the motility of the dynein. Microtubule gliding assays have previously been used to look at the speed of the dynein motor along MTs using video enhanced differential interference contrast (VE-DIC) microscopy. The wildtype dynein sample was used to optimise the system, so that the *Arl/+* sample could be measured and compared against it. The system requires flow chambers made from glass microscope slides and coverslips with two strips of vacuum grease in between to separate them, giving chambers of approximately 15-20  $\mu$ l volumes. Casein is flowed into the flow chambers and incubated to block the glass, coating it and preventing the dynein from denaturing upon attachment, the excess is then washed out using motility buffer. Next, the dynein is flowed into the chamber and incubated for at least 5 minutes in a humid chamber (to minimise evaporation of buffer from the small volume of the flow chamber). This allows time for the dynein to bind to the casein molecules, then short lengths of polymerised MTs are added to the dynein. The MTs bind to the dynein molecules and can be visualised using VE-DIC and the movements recorded and measured. The movement of the MTs is due to the dynein molecules and provides an indication of the level and speed of motility produced by the dynein. As the dynein used in this experiment is a comparison of WT with heterozygous, it is important that the individual velocities of many MTs are measured. This allows velocities of the different potential dynein populations to be investigated and distinguished between, as WT homodimers from the heterozygous dynein sample should have similar velocities to those from the WT dynein sample, and so any difference in velocity is likely to be due to the populations containing the mutant *Arl*.

The system proved difficult to optimise in spite of many different improvements being made. As can be seen from Table 3, 16 different conditions were tried, with some showing improvements over others, but none providing MT gliding velocities above  $\sim 0.3 \mu\text{m}/\text{sec}$  (Figures 11 A and B). In published data from this system dynein has shown MT gliding velocities of more than  $1 \mu\text{m}/\text{sec}$  (Paschal, Shpetner et al. 1987; Shimizu, Toyoshima et al. 1995). Of the conditions used that did produce MT gliding,

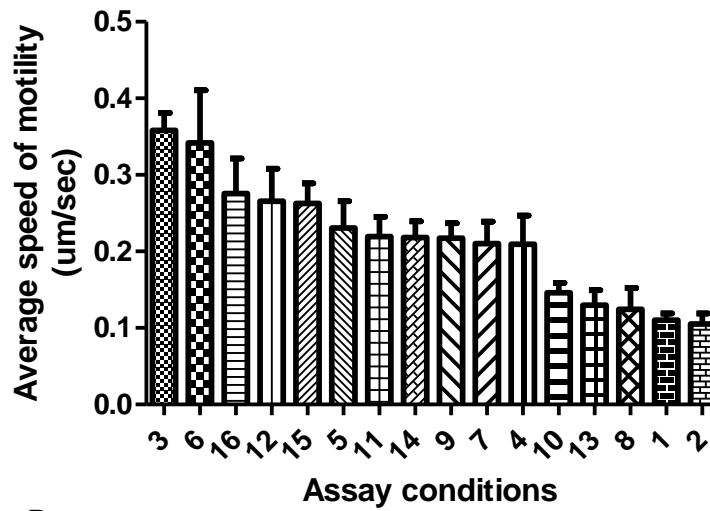
File no	Conditions	Movement	Av. Velocity (um/sec)
1	2x dyn dilution + motility buffer + 0.5mg/ml casein + 100uM taxol + 1mM DTT + ATP 1mM	MTs bound, but only 1-2 MTs moving v slowly	0.110012963
2	2x dyn dilution + motility buffer + 0.5mg/ml casein + 100uM taxol + 1mM DTT + 1mM ATP + 0.03% NP40	Fewer MTs bound, fewer than (1). Similar level of movement	0.105242
3	10x dyn dilution + motility buffer + 0.5mg/ml casein + 100uM taxol + 1mM DTT + ATP 1mM + 0.03% NP40	More MTs bound, greater no of MTs moving	0.357994074
4	10x dyn dilution + motility buffer + 0.5mg/ml casein + 100uM taxol + 1mM DTT + 4mM ATP + 0.03% NP40	Increased ATP=10x fewer MTs bound. Less movement	0.209417778
5	10x dyn dilution + motility buffer + 0.5mg/ml casein +100uM taxol + 1mM DTT + 0.2mM ATP + 0.03% NP40	Greatly decreased ATP= similar no of MTs as with 4mM ATP, some movement	0.230471667
6	10x dyn dilution + motility buffer + 0.5mg/ml casein + 100uM taxol + 1mM DTT + 1mM ATP + 0.03% NP40	Extra MTs added on top of first layer of MTs and dyn. More MTs bound and more movement	0.342031667
7	10x dyn dilution + motility buffer + 0.5mg/ml casein + 100uM taxol + 1mM DTT + 4mM ATP + 0.03% NP40	Same conditions, with extra MTs added, but less ATP= same amount of MTs bound, but less movement	0.21023
8	2x dyn dilution + BRB80 buffer + 0.5mg/ml casein + 100uM taxol + 1mM DTT + 1mM ATP	Different ionic strength of buffer, still see MT binding. Higher dyn conc (2x). Some MTs bound, lot of MT waving, but little movement	0.124198571
9	2x dyn dilution + BRB80 buffer + 0.5mg/ml casein + 100uM taxol + 1mM DTT + 4mM ATP + 0.03% NP40	A lot more MTs bound than with 10x dyn dil. Greater no of MTs moving	0.217337368
10	Undil. dyn + BRB80 buffer + 0.5mg/ml casein + 100uM taxol + 1mM DTT + 4mM ATP + 0.03% NP40 + GCO	Addition of oxygen scavenger system + increased ATP conc. Lots of MTs bound, but v little movement	0.146063333
11	10x dyn dil. + 0.03% NP40 + 0.5mg/ml casein + 100 uM taxol + 1mM DTT + 1mM ATP + p150 ab	MTs bound by addition of p150 antibody. Many more MTs bound, with some movement	0.21936
12	10x dyn dil. + 0.03% NP40 + 0.5mg/ml casein + 100 uM taxol + 4mM DTT + 1mM ATP + p150 ab	Increased ATP to 4mM, same MT binding, but decreased movement	0.265495714
13	2x dyn dil. + 0.03% NP40 + 0.5mg/ml casein + 100 uM taxol + 4mM DTT + 1mM ATP + DIC ab	DIC antibody= lots of MTs bound, but little movement	0.129905
14	10x dyn dil. + 0.03% NP40 + 0.5mg/ml casein + 100 uM taxol + 4mM DTT + 1mM ATP + DIC ab	Less dyn= similar amount of MTs bound, slightly more movement	0.218267143
15	10x dyn dil. + 0.03% NP40 + 0.5mg/ml casein + 100 uM taxol + 4mM DTT + 1mM ATP + DIC ab	Same conditions, but extra MTs added on top of denatured protein- more movement	0.2629145
16	10x dyn dil. + 0.03% NP40 + 0.5mg/ml casein + 100 uM taxol + 4mM DTT + 1mM ATP + p150 ab	Same conditions, but extra MTs added on top of denatured protein- more movement than with 2x dyn dil and w/o extra MTs added	0.27544

**Table 3. Motility assay conditions.**

Table giving details of motility assay conditions used, what effect they had and the resulting average motility speeds identified.



A



B

**Figure 11. Graphs showing average motility speeds from MT gliding assays**

- A) Graph of motility speeds from MT gliding assays, grouped by assay conditions used, either motility buffer, with varying dynein concentrations and ATP concentrations; or BRB80 buffer, with varying ATP concentration; or motility buffer with either anti-p150 (1/10) or anti-DIC (1/10) antibodies used to bind dynein to coverslip. Numbers below the graph relate to assay condition used (See table 1).
- B) Graph of motility speeds in order of motility speed achieved, from greatest speed to lowest. See table 1 for details of assay conditions used.

only a very small proportion of MTs were seen to be moving ( $\sim 1/10^{\text{th}}$  of the total number of MTs visible), far fewer than would be expected.

Despite this system having been used by other groups to measure the motility of dynein, it has generally used either recombinant dynein, meaning the samples were of extremely high purity, or dynein purified from bovine or porcine brain tissue. Using dynein purified from multiple murine brains, by means of protocols designed to purify dynein from bovine or porcine tissue may have affected the resulting motility.

As the gliding assay could not be optimised using wildtype dynein and as the protocol required such a large amount of brain tissue to obtain the purified dynein, and with the number of *Arl*/<sup>+</sup> mice limited due to their poor breeding, it was concluded that only limited data could be obtained from this experiment. It was decided that the *Arl*/<sup>+</sup> mice would be used to purify dynein, but that it would be better used to check other aspects of the dynein function, such as MT binding and ATPase assays.

### **III.7 ATPase Assay**

To investigate whether the *Arl* mutation had an affect on the ATPase function of the motor, the MT dependent spectrophotometric ATP/NADH coupled assay was used. This reaction is based on the conversion of phosphoenolpyruvate (PEP) to pyruvate by pyruvate kinase (PK) coupled to the conversion of pyruvate to lactate by lactate dehydrogenase (LDH). The second part of the reaction requires NADH which is oxidised to  $\text{NAD}^+$ . NADH absorbs strongly at 340 nm, but  $\text{NAD}^+$  does not, so the oxidisation of NADH can be followed by monitoring the absorbance at 340 nm. The decrease in  $\text{OD}_{340}$  can then be converted into ATPase activity where 1 molecule of NADH oxidised to  $\text{NAD}^+$  corresponds to the production of 1 molecule of ADP by the motor ATPase (Huang and Hackney 1994).

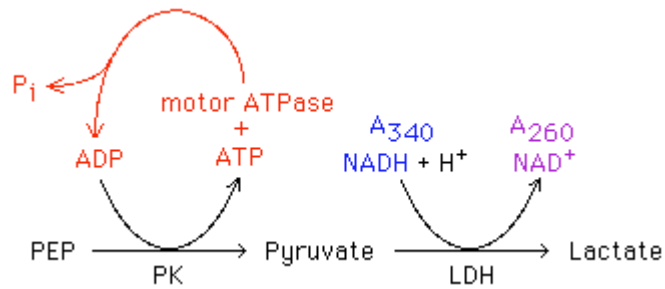


**Figure 12. Summary of ATP/NADH coupled assay.** (Adapted from (Huang and Hackney 1994))

To optimise the reaction and ensure that it worked, the wildtype purified dynein protein was used. A baseline reading was obtained using only reaction buffer (no dynein or MTs), then the ATPase activity of dynein without MTs was measured to estimate any non-MT dependent activity that may be present. The reaction was then conducted, initially using 20  $\mu\text{g}$  of dynein and 25  $\mu\text{g}$  of MTs. No rates of reaction at OD<sub>340</sub> were observed, indicating that the reaction was not occurring as expected. The ATPase activity of dynein is MT dependent (Huang and Hackney 1994), and so the amount of MTs and dynein added to the reaction was varied, using 20  $\mu\text{g}$  of dynein and 50  $\mu\text{g}$  of MTs; 20  $\mu\text{g}$  of dynein and 75  $\mu\text{g}$  of MTs. Then, in case the amount of dynein being used was too small for the reaction volume, 40  $\mu\text{g}$  of dynein and 50  $\mu\text{g}$  of MTs, then 40  $\mu\text{g}$  of dynein and 100  $\mu\text{g}$  of MTs were tried. However, this had no effect on the assay and no rates were recorded using any of the combinations.

Availability of both the purified dynein and the purchased tubulin were limiting factors in being able to optimise this assay as large volumes of both were required, restricting the number of times the assay could be repeated to allow optimisation. Another difficulty was the absence of a suitable positive control to ensure that the assay system was working correctly. Because of these factors, the ATPase activity of the wildtype purified dynein could not be measured.

### **III.8 MT Binding Assay**

Despite being unable to measure the ATPase activity of the dynein, the binding to MTs can be determined by incubating dynein with MTs and centrifuging through a sucrose cushion. Only dynein bound to MTs is dense enough to sediment through the cushion

and pellet at the bottom of the tube, thus giving an indication of the efficiency of the binding of the dynein to MTs.

When tested with WT purified dynein this method worked well, so the *Arl* dynein sample was used to compare against the wildtype. Using the pooled dynein samples, the pull-down was repeated three times for each genotype. 20 µg of dynein sample was incubated for 30 min at 37°C with 50 µg of polymerised MTs, then layered over a 20% sucrose cushion and centrifuged for 40 min at 30,000 rpm ( $77,100 \times g_{max}$ ). The top supernatant fraction was removed, then the cushion fraction. The pellet was washed and re-centrifuged and the pellet re-suspended and collected. Samples from each fraction were run on 4-12% gradient gels and blotted for DHC, DIC and  $\alpha$ -tubulin.

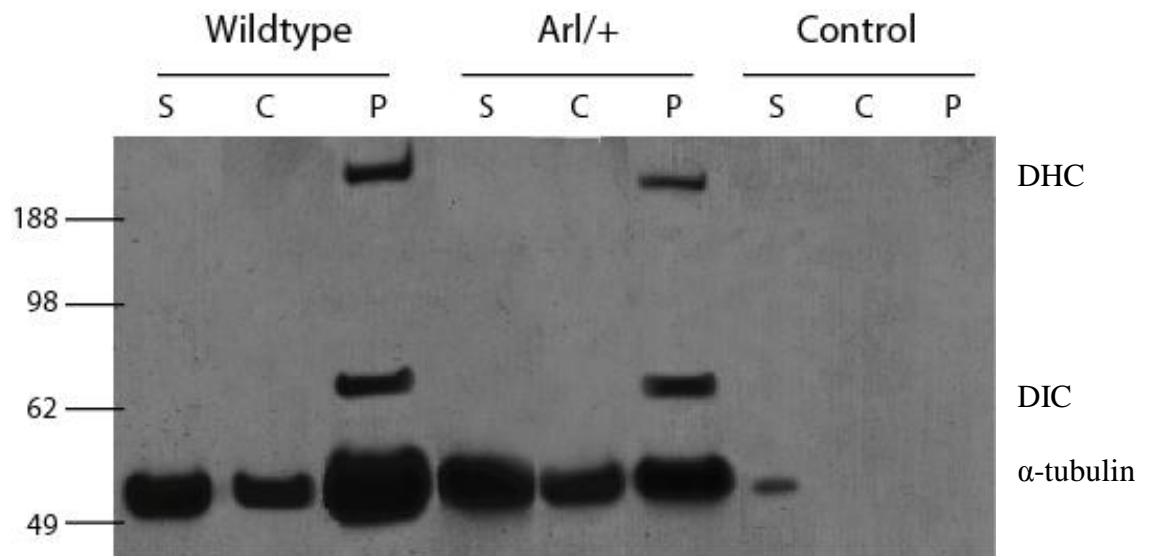
As can be seen from Figure 13 A, the greatest amount of dynein pulled down, relative to the amount of MTs, is in the *Arl* sample, suggesting that the binding of dynein to MTs is stronger or more efficient in *Arl* than WT. To quantify this, the dynein signal was measured and compared against the tubulin signal for each sample. By comparing the amount of dynein pelleted against the amount of tubulin pelleted, it disregarded any differences in the efficiency of tubulin polymerisation into MTs and therefore the total starting amount of MTs that were available to bind dynein.

Using the MT binding of WT as a reference, the binding of *Arl* was compared against it. As shown in Figure 13 B, the MT binding of the dynein is significantly greater in *Arl* than in WT ( $p=0.03$ ), suggesting that the *Arl* mutation increases the affinity of dynein for MTs.

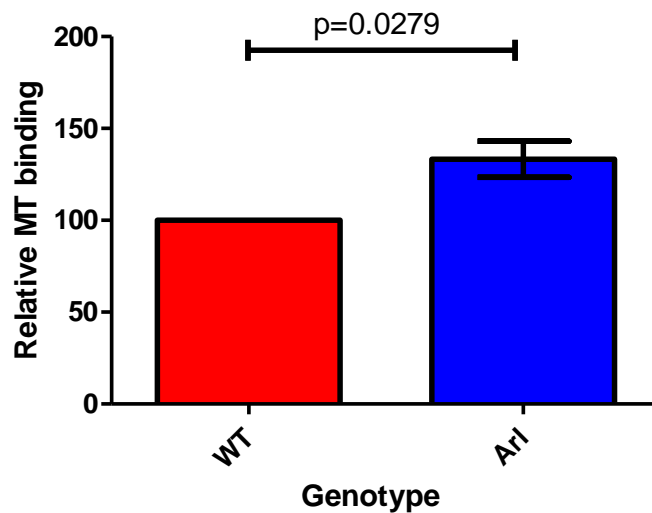
This data, together with the larger amount of dynein seen after centrifugation through sucrose cushions during the dynein purification suggests that the *Arl* mutation increases the binding of dynein to MTs compared to WT dynein.

### **III.9 Discussion**

The recently identified axonemal dynein mutation in *Arl* may be involved in the reduced breeding and embryonic loss of *Arl* seen in this colony. Axonemal dynein type 11 is mutated and this is known to be involved in positioning of organs during



A)



B)

**Figure 13. Binding of dynein to MTs in WT and Arl/+**

- A) Purified dynein complex was incubated with polymerised MTs and layered over a 20% sucrose cushion, centrifuged and supernatant (S), cushion (C) and pellet (P) fractions collected for both WT and Arl/+. Samples were run on a 4-12% gradient gel, western blotted and labelled for DHC, DIC and  $\alpha$ -tubulin. A range of exposures were taken, but only those not overexposed were used for quantification purposes. The tubulin in this figure is to demonstrate the relative amounts of dynein to tubulin only, and the tubulin signal was not used for quantification.
- B) Relative binding of DIC to  $\alpha$ -tubulin in Arl/+ was compared to WT reference. 3 samples of each genotype were measured.

development. When crossed with *iv* mice (a model for the human condition, situs invertus), the phenotype similar to that of *iv/iv* mice is seen. In human situs inversus, a common underlying cause is PCD which results in non-functioning spermatozoa in males. Therefore, further investigations into the effects of the axonemal dynein mutation on *Arl* mice are required and should include analysis of spermatozoa function to determine whether this is the cause of the reduced breeding seen in *Arl* mice.

As details of this mutation were only recently made available, it was out of the scope of this project to investigate in detail the possible involvement in the *Arl* phenotype. However, because of the specific roles played by cytoplasmic and axonemal dynein, it is unlikely that the axonemal mutation would affect the cytoplasmic dynein functions investigated in this thesis.

The *Arl* mutation is located in an area of unknown function, N-terminal to the motor domain, but C-terminal to the sites of both homodimerisation and accessory chain binding. Therefore, it was unlikely that the integrity of the complex would be perturbed by the mutation. However, as the function of the heavy chain region containing the mutation is unknown, it was possible any structural change caused by the mutation could affect the heavy chain and possibly have a knock on effect on the structure of the complex. Although it was important to check for any effects on the complex integrity, none were identified. This suggests that *Arl* does not affect the complex and also indicates that the area of unknown function is not involved in maintaining the structure or composition of the complex.

The amount of dynein recovered during the purification suggests a difference in the amount of dynein able to sediment through the sucrose cushions (Figure 9), possibly due to a difference in affinity for MTs. However, the samples had been incubated with AMP.PNP, a non-hydrolysable analogue of ATP, so the dynein complex would not have been in its maximal MT binding conformation. That a greater amount of *Arl*/+ dynein is seen in the pellet, having centrifuged through the sucrose cushion compared to WT, suggests that even in low MT binding state, the *Arl* dynein may still bind MTs more than WT dynein.

As shown in Figure 9, all the components of the dynein complex are present after purification, in both WT and *Arl/+* samples. However, despite all the different conditions tried, the purified dynein was unable to move a significant proportion of short lengths of MTs, or at a sufficient velocity, compared to published data. No dynein positive control was available, however, the kinesin positive control was used to initially set up the system and MT gliding was identified, indicating that none of the reagents involved were at fault (for example, the ATP which can become unstable and become hydrolysed to ADP). This suggests that the purified dynein may not have been functioning fully. This is most likely as the dynein used in the gliding assay was WT, and so there should be no other reason for it to be unable to move the MTs. The optimisation of the system was conducted on separate occasions, each time with freshly prepared dynein sample, so an isolated problem with one sample cannot be the cause.

The dynein purification is based on a protocol first established for purifying dynein from either bovine or porcine brain. It has not previously been used to purify dynein from multiple murine brains, and this difference may be where the problem lies. During the purification procedure, the activity of the dynein may be compromised, but the integrity of the complex maintained.

This is supported by the lack of ATPase activity recorded from the WT dynein sample. Again, no suitable dynein positive control was available to ensure the assay system was working, and there may have been an issue with the assay that prevented it from identifying enzyme activity, or the assay may not have been sensitive enough, with ATPase levels too small to be detected. However, this seems unlikely as it is a well established and published protocol, which has successfully been used to measure the basal ATPase activity of dynein, without MTs. Once stimulated by MT binding, ATPase activity has been shown to increase approximately sevenfold (King and Schroer 2000). Even if the assay was unable to detect a small ATPase activity before MT stimulation, it seems unlikely that it would also not be sensitive enough to detect an activity seven times greater. Together, it suggests that there was no ATPase activity to detect, supporting the theory that the protocol for purifying the dynein sample affects its ATPase activity.

A positive control would need to be identified to ensure the assay was properly functioning and to identify the level of sensitivity to then definitively determine whether the dynein sample maintained any ATPase activity. Based on this, possible alterations to the purification protocol could be investigated with the aim of resolving the loss of ATPase activity. Once this problem was rectified, the *Arl*/<sup>+</sup> dynein could be tested to identify any difference in ATPase activity compared to WT.

The possible lack of ATPase activity does not appear to affect the MT binding of either the WT or *Arl*/<sup>+</sup> dynein samples. Both genotypes show binding of MTs, but with greater levels identified in *Arl*/<sup>+</sup> compared to WT, suggesting that the *Arl* mutation may cause the dynein to have a greater affinity for MTs compared to WT.

The binding of dynein to MTs is dictated by the affinity state of the MTBD, and this affinity is linked to the binding, hydrolysis and release of ADP/ATP in the AAA domains of the motor ring. As discussed in chapter I, the difficulty of the large distance between the sites of ATP hydrolysis and MT binding is thought to be overcome by conformational changes around the AAA domains which change the registry of the coiled-coils of the stalk. This change in relative position of the coiled-coils is thought to regulate the affinity of the MTBD for MTs.

The proposed linker domain below the motor head is suggested to mediate the swing of the powerstroke after ATP hydrolysis. As the *Arl* mutation is located just C-terminal to the proposed location of the linker domain, it may affect the powerstroke. The linker domain is suggested to be close to the first AAA domain, one of the main sites of ATP hydrolysis, so if *Arl* caused an unknown structural change that affects the flexibility of the linker, it could have a knock-on effect of disrupting the conformational change around the ring structure, in the coiled-coil and ultimately in the MTBD. As the *Arl*/<sup>+</sup> dynein appears to increase the affinity of dynein for MTs compared to WT, this would suggest that a conformational change causes the MTBD to be maintained in a higher affinity conformation, compared to WT.

This proposed mechanism relies on the ATPase activity being established, so the assay is extremely important in identifying if the *Arl* mutation affects nucleotide binding and/or hydrolysis. It is also vital to establish whether a change in structure is brought

about by the mutation. As the location of the *Arl* mutation is currently of unknown structure and function, cloning of the area, expression and crystallisation to allow the structure of both *Arl* and WT to be determined and compared by x-ray crystallography is important in establishing the effect of the *Arl* mutation on the heavy chain.

Current work has included isolating mRNA from *Arl*/+ brain tissue, reverse transcription PCR to obtain cDNA of both *Arl* and WT, and PCR with primers specific for an area of the heavy chain containing the mutation (Pfam-B 8363 region consisting of residues 1032-1282). This has been cloned into a tagged expression vector, but further work will include expression of the protein, establishing its solubility and purifying using the tag. Crystal trials will then be set up, and any resulting crystals used to obtain diffraction patterns, from which the structures of the *Arl* and WT can be established. This information will allow *Arl* and WT structures to be compared and identify if the mutation causes significant structural perturbation.

## **CHAPTER IV**

## **Chapter IV**

### **INVESTIGATING THE EFFECT OF THE *ARL* MUTATION ON CARGO TRANSPORT**

#### **IV.1 Introduction**

As discussed in Chapter I, intracellular organelle transport is essential for a large number of cellular processes. The ability of a motor to transport its cargo provides an indication of the functioning of that motor.

As shown in Chapter III, *in vitro* assays of dynein function have proved difficult to obtain useful data from. An alternative method is to track the movements of cargos in cultured cells to investigate the effect of the *Arl* mutation on the cargo transport functions of cytoplasmic dynein.

In mammalian cells, the Golgi is positioned near the centrosome in a perinuclear distribution. The membranes require dynein and kinesin to maintain their position, as loss of dynein activity causes dispersal away from the centrosome and loss of kinesin causes compaction around the centrosome. Dysfunction in Golgi localisation can severely affect the organisation of the secretory pathway. This makes the Golgi an ideal cargo to investigate the effect of *Arl* on dynein's ability to transport a major and important cargo.

Endocytosis is an important mechanism in mammalian cells that involves internalisation of extracellular nutrients, regulation of cell surface receptor expression and antigen presentation for example. The best characterised mechanism of endocytosis is clathrin dependent receptor mediated, which is used by a large number of extracellular ligands that have different cell surface receptors, such as EGF, transferrin, antibodies and LDL. The binding and internalisation of the ligand-receptor complex into endosomes results in their trafficking through the endosomal pathway,

either for degradation (e.g. EGF) or recycling (e.g. transferrin) (Benmerah and Lamaze 2007; Parkar, Akpa et al. 2009).

Dynein is responsible for the trafficking of endosomes through the degradative endosomal pathway to the lysosomes and so tracking of EGF positive endosomes provides a way of investigating dynein's ability to transport an important cargo.

Mitochondria are translocated along MTs by members of the kinesin family and cytoplasmic dynein, as well as actin tracks driven most likely by myosin V. Their transport is modulated in response to physiological signals and local energy requirements. For example, in active neuronal growth cones, mitochondria move into them and become stationary, however, when growth cone activity is lower, the mitochondria switch to retrograde movement (Frederick and Shaw 2007).

Dysfunctional mitochondria are moved towards the cell body to be repaired by fusion with healthy mitochondria, or for degradation by mitophagy. In the cell body mitochondrial fission produces healthy mitochondria that are the correct size which are then transported down axons towards the synapses (Frederick and Shaw 2007).

So there are a number of situations where mitochondrial movement is required and retrograde transport is therefore extremely important. The importance of mitochondrial transport makes them an ideal cargo to utilise in the investigation of dynein-dependent transport.

#### **IV.2 In vitro cell system**

MEFs are an excellent model system for studying cellular function. Primary MEFs are easily cultured from E13 embryos and can be passaged a number of times without the need for immortalisation. However, because MEFs are derived from mesenchymal tissue (derived from all three germ layers), it means that gastrulation needs to have occurred for embryos to be used to culture MEFs from. As *Arl/Arl* embryos are not viable after E10 (during embryo gastrulation), it means that MEFs cannot be cultured from *Arl/Arl* embryos. WT E10 embryos were tested to see if any cell culture could be

established from such an early stage, but this was unsuccessful, meaning that cellular function of *Arl/Arl* cannot be investigated *in vitro*.

### **IV.3 Golgi Reassembly**

Cytoplasmic dynein is involved in the maintenance of the location of Golgi within the cell. Previously it has been shown that disruption of the MTs causes the dispersion of Golgi throughout the cell, as the dynein is unable to maintain its location (Hafezparast, Klocke et al. 2003). Once the MTs are able to re-polymerise, the dynein is responsible for re-assembling the Golgi. Because of this, the Golgi is useful in studying the ability of dynein to transport its cargo.

The experiment was conducted in MEFs as they are a well characterised and robust model cell system. This experiment has been extensively studied, particularly in *Loa* cells (Hafezparast, Klocke et al. 2003), so was useful to compare against the severity of the *Arl* mutation. *Arl* and *Loa* mice were crossed, and the resulting embryos were used to derive primary MEF cultures of all 4 possible genotypes (WT, *Arl*/+, +/-*Loa* and *Arl/Loa*).

Normally in cells, Golgi is maintained in a perinuclear region as shown by the untreated cells in Figure 14. In this experiment the cells were treated with cold and nocodazole (NZ) to depolymerise the MTs, resulting in the Golgi fragmenting throughout the cell, the NZ was washed out and the cells allowed to recover over a timecourse of 50 min. As shown by the WT cells in Figure 14, at 0 min, straight after the NZ has been washed out, the Golgi is fragmented around the cell, but by 30 min the Golgi has reassembled back into stacks of cisternae.

However, in the cells containing dynein mutations, the re-assembly of the Golgi is incomplete at 30 min, and it is not until 50 min that the dynein has transported the Golgi fragments back to form stacks around the nucleus. The compound heterozygotes are the most severely affected, with the reassembly far from complete by 30 min. The Golgi re-assembly is not rescued in the compound heterozygotes, demonstrating the *Arl* and *Loa* mutations do not show complementation, suggesting they may be allelic. The

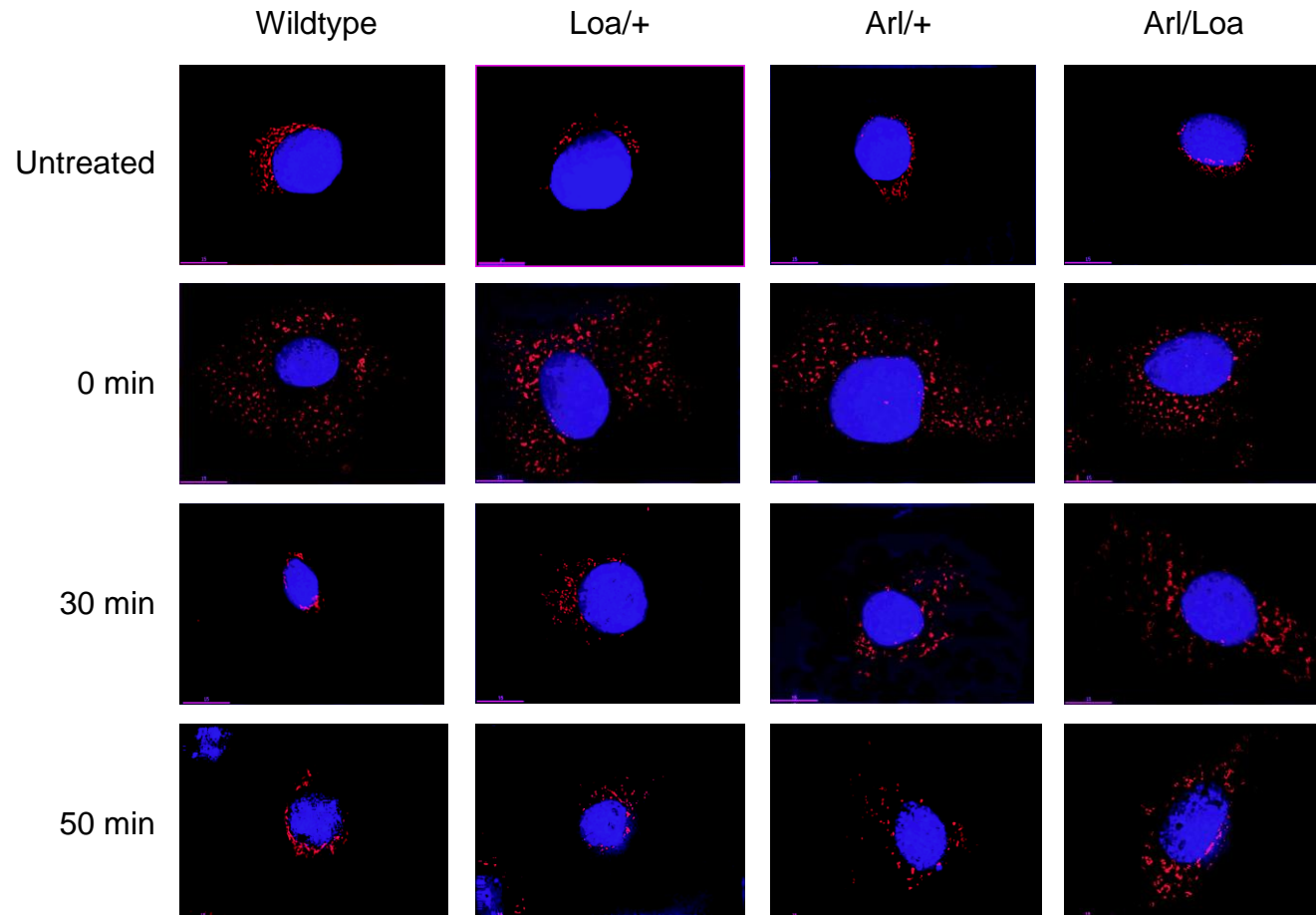


**Figure 14. Golgi reassembly after disruption with nocodazole in WT, *Loa*+, *Arl*+ and *Arl/Loa* MEFs.**

MEFS were treated with cold (4°C) for 30 min and nocodazole for 3 hr, washed and then allowed to recover at 37°C for the times indicated. Golgi here is shown in red and nuclei in blue (DAPI). The scale bar here represents 30µm, n=10

reassembly of the Golgi in the *Arl* cells is less complete than in the *Loa* cells, suggesting the *Arl* mutation impairs the function of dynein more so than *Loa*. By 50 min the recovery is more advanced, although not complete in the cells containing the dynein mutations. This data agrees with data previously obtained from *Loa* and indicates that the *Arl* mutation also impairs dynein's ability to transport Golgi after it has been fragmented around the cell.

To quantify this data, Image J was used to count the total number of Golgi fragments and measure the total area of Golgi in each cell. This was used to calculate ratios of the number of fragments against the total area and used to compare between the genotypes at each timepoint (n=10). A number of methods for analysis of this data were investigated, such as comparing total Golgi signal or number of remaining fragments between cells of each genotype. However, the cells analysed were of a range of sizes, meaning that direct comparison of total Golgi signal or number of fragments were not suitable methods of comparison. By calculating a ratio of the number of Golgi fragments against the total signal, the differences in the sizes of the cells measured was not a factor, and comparisons of the ratios could be used to determine the degree of reassembly in the cells of different genotypes.

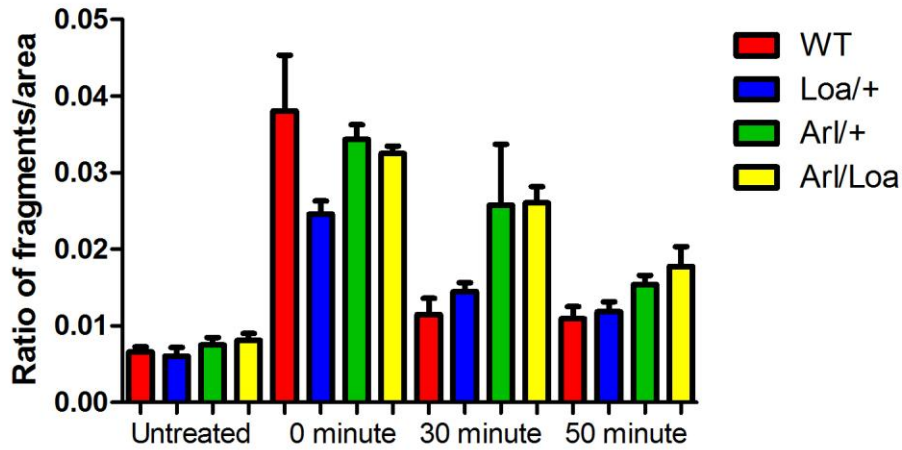
While full reassembly of the Golgi is complete by 30 min in WT (Figures 15 A and 15 B), Golgi in cells containing mutant dynein (both *Arl* and *Loa*) is not completely reassembled, even after 50 min of recovery. In *Loa*/+ the Golgi is nearing complete recovery, compared to untreated control cells (p=0.013), however, in *Arl*/+ cells the recovery is less complete by this stage (p=0.001). This suggests that the *Arl* mutation impairs the transport of Golgi more severely than *Loa*.

#### **IV.4 Fixed Cell EGF Trafficking**

Dynein function is well established in the trafficking of epidermal growth factor (EGF), so it is useful in investigating the effect of the *Arl* mutation on cytoplasmic dynein's role in the endocytic trafficking pathway.

MEFs were starved for 2 hr, then pulsed for 10 min with Alexa-fluor 555 conjugated EGF, washed twice and chased for 50 min. As shown in Figure 16, after the 10 min

## Reassembly of Golgi



A)

Mann-Whitney Test		
Comparison	p value	Significance
WT-C → WT-0min	0.0002	***
WT-C → WT-30min	0.1903	ns
WT-C → WT-50min	0.0599	ns
Loa/+-C → Loa/+0min	0.0002	***
Loa/+-C → Loa/+30min	0.0008	***
Loa/+-C → Loa/+50min	0.0127	*
Arl/+-C → Arl/+0min	0.0001	***
Arl/+-C → Arl/+30min	0.0001	***
Arl/+-C → Arl/+50min	0.0013	**
Arl/Loa-C → Arl/Loa-0min	0.0003	***
Arl/Loa-C → Arl/Loa-30min	0.0001	***
Arl/Loa-C → Arl/Loa-50min	0.0081	**

B)

**Figure 15. Quantification of Golgi reassembly after disruption with nocodazole in WT, *Loa/+*, *Arl/+* and *Arl/Loa* MEFs.**

- A)** Using the Image J program the total number of discrete spots and the total area of Golgi complex were measured, to calculate the ratio of spots/total area per cell in untreated, control cells and at 0 minute, 30 minute and 50 minute timepoints of recovery after nocodazole wash out.
- B)** Table of p values showing levels of significance in differences in recovery of Golgi between genotypes at different timepoints. n=10 cells

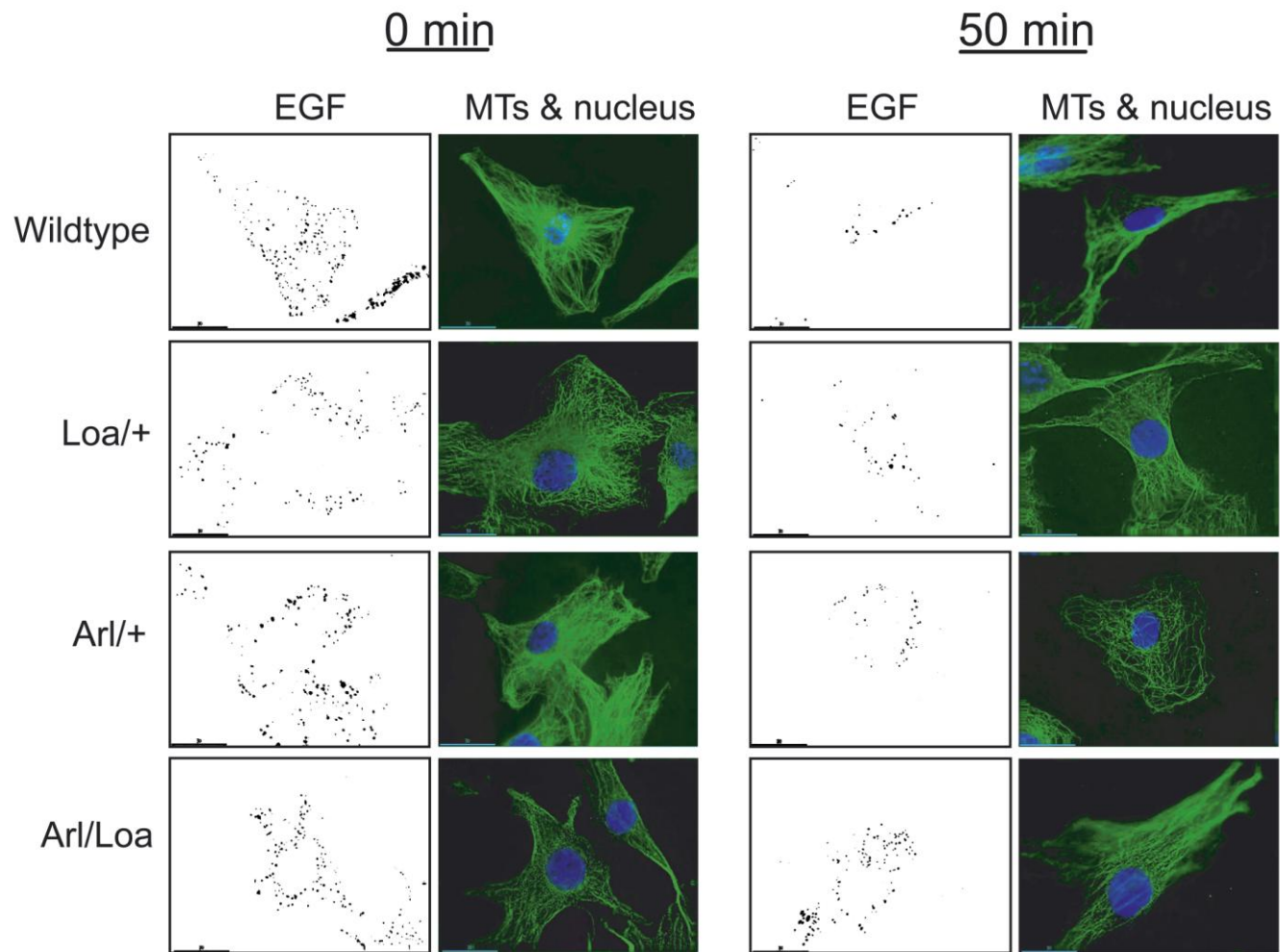


**Figure 16. Endosomal trafficking chase of Alexa Fluor 555 conjugated EGF in wildtype, *Loa*+, *Arl*+ and *Arl/Loa* MEFs**  
 MEFs were pulsed with EGF for 10 minutes and chased at 37°C for the times indicated. EGF is shown in pseudo-coloured inverted greyscale, the cytoskeleton ( $\alpha$ -tubulin) in green and nuclei in blue (DAPI). The scale bar represents 30 $\mu$ m.

pulse, most of the EGF-positive endosomes are accumulated around the cell periphery, where it has been internalised. After 50 min, in WT cells there are far fewer EGF-positive endosomes suggesting the majority of the EGF has been trafficked through the endosomal pathway towards the lysosomes for degradation. In the cells containing the *Loa* and *Arl* mutations, there are a greater number of EGF-positive endosomes remaining after 50 min compared to WT, with the compound heterozygotes containing the most.

To quantify this data Image J was used to count the total number of EGF-positive endosomes in each cell at each timepoint. From Figure 17 it can be seen that after 50 min there are significantly more EGF-positive endosomes remaining in the cells containing either the *Loa* or *Arl* or both mutations, compared to WT ( $p=0.023$ ,  $0.011$  and  $<0.001$  respectively). These endosomes are yet to reach the lysosomes to be degraded, suggesting that their transport has been delayed compared to WT due to the mutations in cytoplasmic dynein ( $n=15$  cells).

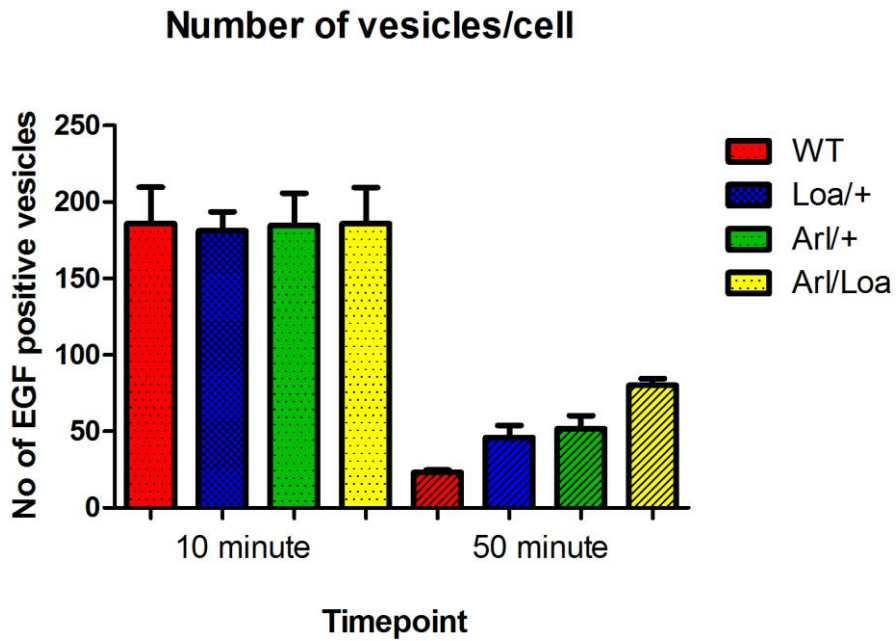
Together with the data from the Golgi reassembly this indicates that the *Loa* and *Arl* mutations do not show complementation and thus suggests they may be allelic. In addition, a number of *Arl/Loa* crosses were allowed to proceed to full term and littering. Of 17 litters, comprising 89 pups, no compound heterozygotes were detected, supporting the notion that the *Loa* and *Arl* mutations do not complement each other and thus the two mutations are allelic.

#### **IV.5 Live Cell EGF Trafficking**

In order to better understand the delay in EGF trafficking seen in the fixed cell experiment, live cell imaging was used which allows the movement of individual vesicles to be tracked and analysed.

As the allelism between *Loa* and *Arl* had been established through the lack of complementation seen in the experiments looking at Golgi reassembly and EGF trafficking in fixed cells, and the phenotype of the *Arl* mutation has been compared to that of the *Loa* mutation, experiments were now only conducted using *Arl/+* and WT cells.

A.



B.

Unpaired t-test		
Comparison	p value	Significance
WT 0 min → Loa 0 min	0.8619	ns
WT 0 min → Arl 0 min	0.9659	ns
WT 0 min → Arl/Loa 0 min	1.000	ns
WT 50 min → Loa 50 min	0.0226	*
WT 50 min → Arl 50 min	0.0106	*
WT 50 min → Arl/Loa 50 min	<0.0001	***

**Figure 17. Quantification of number of EGF-positive vesicles remaining in WT, *Loa/+*, *Arl/+* and *Arl/Loa* MEFs after indicated timepoints.**

- A. Image J was used to count the number of EGF-positive vesicles remaining in MEFs after 10 minute EGF pulse and 50 minute chase. n=15 cells.
- B. Table of p values showing level of significance in difference between numbers of EGF-positive vesicles in different genotypes at indicated timepoints.

MEFs were starved for 2 hr and stimulated with EGF as already described, then filmed for 1 min periods at set points in a 30 min timecourse at 1 frame every 2 sec. An Image J plug-in, Particle Tracker (Sbalzarini and Koumoutsakos 2005), was used to track the trajectories of the EGF-positive endosomes and this data was used to determine the total distance travelled by each endosome over a particular number of frames (Figure 18 A and 18 B). This allowed the speed of each endosome to be calculated and compared between genotypes. Figure 19 A shows that there is a significant difference in the average speed of the endosomes, with WT moving at a greater speed than *Arl*/+. This explains the delay in endosomes reaching the lysosomes for degradation in the fixed cell experiment, as the endosomes are being transported more slowly by *Arl*/+ dynein.

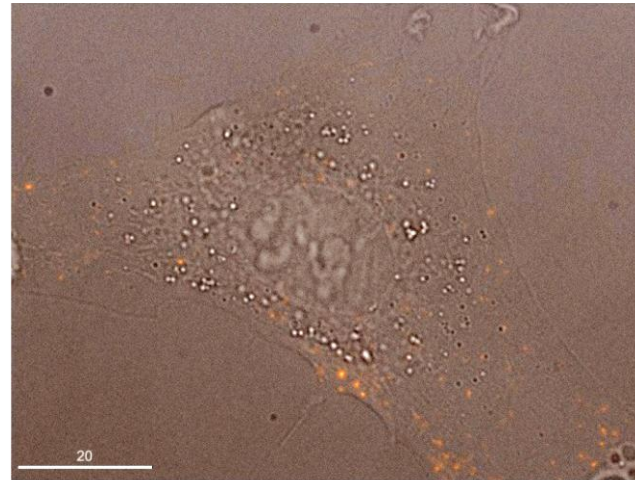
To investigate whether the endosomes behaved differently over the course of their transport through the pathway, the trajectories were analysed separately at different points throughout the timecourse (1 min, 15 min and 30 min). As shown by Figure 19 B, there is a significant difference in the speeds of the *Arl* endosomes compared to WT at each of the timepoints ( $p= 0.034$ ,  $0.012$  and  $0.019$  respectively), but no difference between the timepoints in the same genotype. This suggests that the impairment of dynein transport in *Arl*/+ cells is maintained throughout the endosome transport pathway and is not affected by where the endosome is located within the pathway.

#### **IV.6 Transport of Mitochondria**

To determine whether the *Arl* mutation affected dynein-dependent retrograde transport of mitochondria, MEFs were grown in coverslip chambers, suitable for live cell imaging. The cells were incubated with 50 nM mitotracker for 30 min, washed and then imaged using the FITC channel on the Deltavision pDV live cell imaging microscope. Movies of 1 min length were filmed at 1 frame/2 sec to record the movement of the labelled mitochondria (See Figure 20).

To quantify the movement of the mitochondria, the Image J plug-in, ParticleTracker, was used to track the trajectories of the movement ( $n=3$  cells). This was used to determine the total distances travelled over each movie and thus the speed at which the mitochondria were moving in each genotype. As seen in Figure 21, the mean speed of

Wildtype



Arl/+

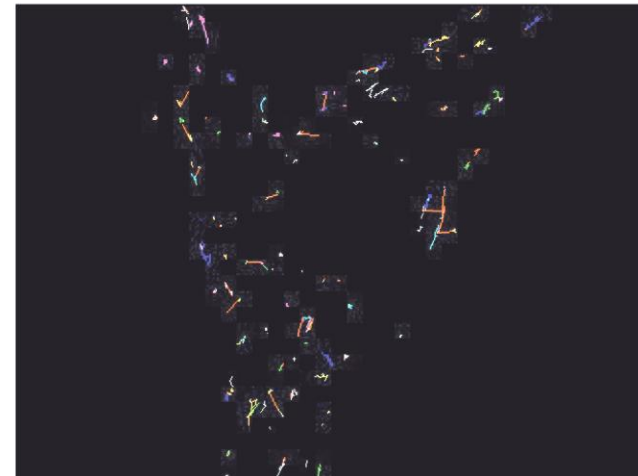
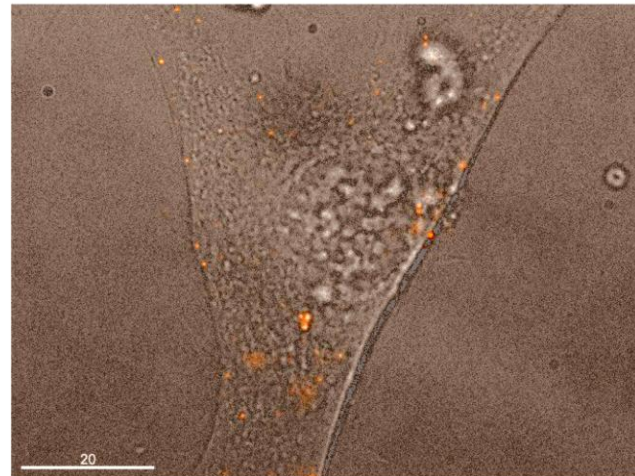
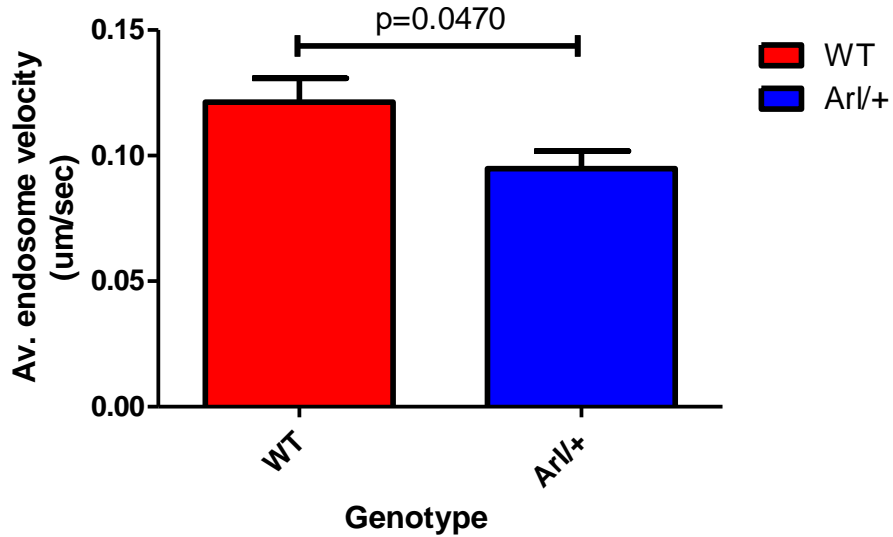


**Figure 18. Endosomal trafficking of Alexa-555 conjugated EGF in WT and *Arl*/+ MEFs**

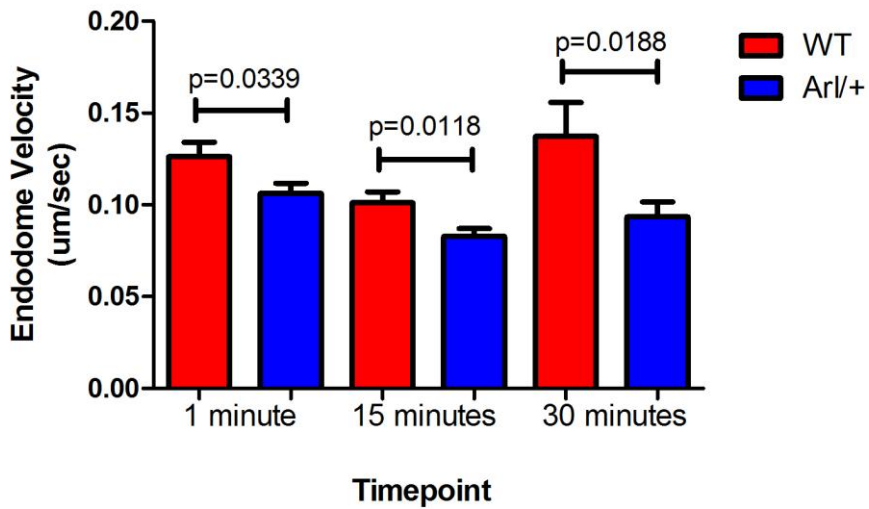
- A) Still frames from movies tracking movement of EGF in WT and *Arl*/+ MEFs. MEF cells shown using DIC channel and EGF in red.  
B) Image J Particle Tracker plug in used to track the trajectories of EGF-positive endosome movement over duration of movies.

### Average Endosome Velocity



A)

### Endosome Velocities

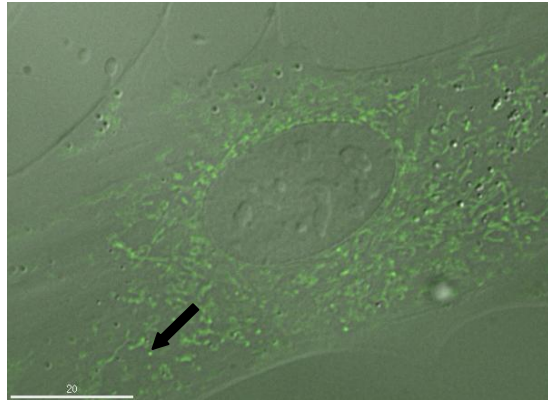


B)

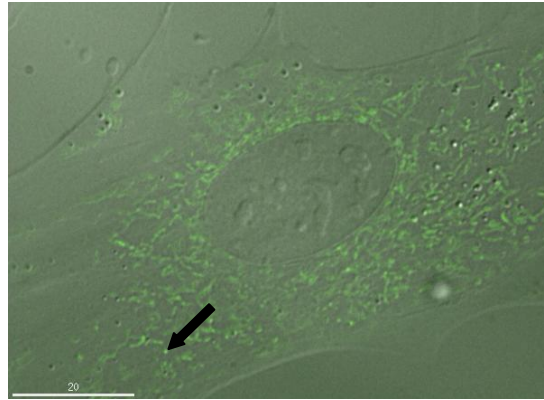
#### Figure 19. Quantification of speed of endosome movement in WT and Arl/+ MEFs

- A) Trajectories of endosome movements were used to calculate total distance travelled over specified frames to give over all average speeds of EGF-positive endosomes in WT and Arl/+ MEFs.
- B) Speeds of EGF-positive endosomes were calculated from movies at specified timepoints throughout chase to identify any differences in endosome speed between WT and Arl/+ at different points in the endosomal pathway. n=5 cells (approx. 150 endosomes per cell).

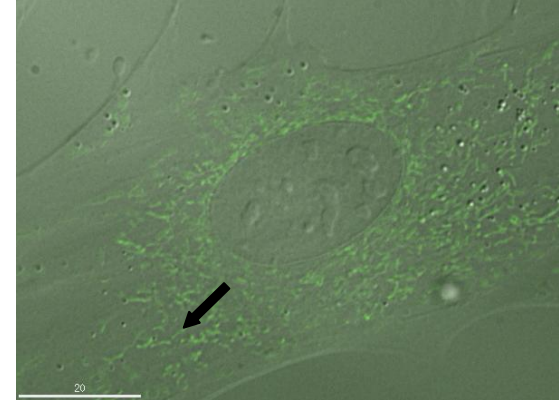
Wildtype



00.00 sec

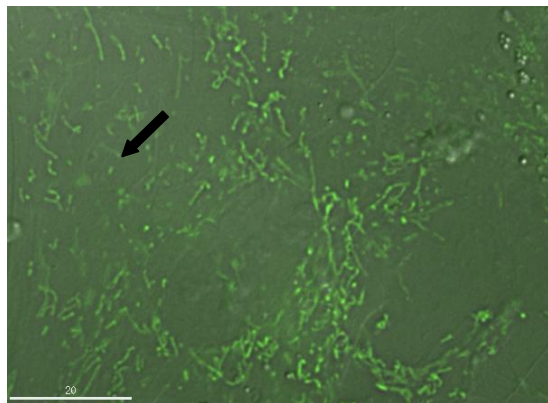


00.10 sec

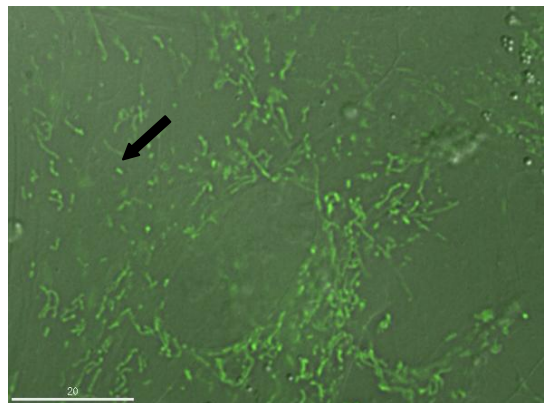


00.20 sec

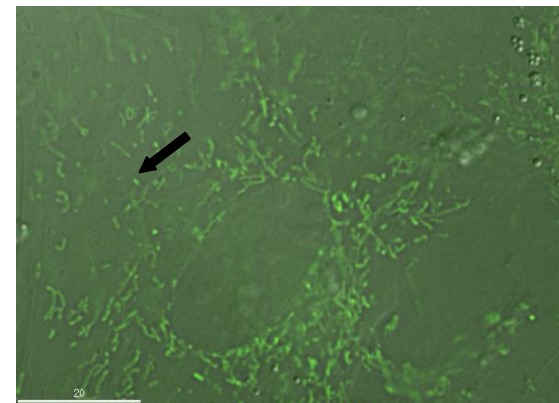
Arl/+



00.00 sec



00.10 sec



00.20 sec

**Figure 20. Still frames from movies showing movement of mitochondria in WT and *Arl/+* MEFs.**

MEFs were incubated with 50nM Mitotracker Green FM for 30 min at 37°C, replaced with CO<sub>2</sub> independent medium and filmed at 1 frame /2 sec. Arrows track movement of individual mitochondrion in each genotype. Still frames taken from movies at 0, 10 and 20 sec. Greater distance travelled over timeframe in WT compared to *Arl/+*. Scale bar = 20µm

mitochondria is slower in *Arl*<sup>+/+</sup> compared to WT, however, this difference is not significant (p=0.36).

#### **IV.7 Transport of cargo in motor neurons**

MEFs make a robust model cell system, but it is important to identify if similar cargo transport delays are also seen in *Arl* neurons, specifically, motor and sensory neurons. To do this, neurons were cultured from E13 embryos. The neurons can only be cultured from E13 embryos as in younger embryos neurogenesis has not progressed sufficiently for differentiated neurons to be present. Neural tissue can be cultured, but would need to be directed to differentiation *in vitro*. Utilising embryos of ~E13 stage of development allows dissection of differentiated neurons, meaning either motor or sensory neurons can be dissected and cultured. As studies using other cytoplasmic dynein mutations, such as *Loa*, *Cral* and *Swl* have identified differences in motor and sensory deficiencies, it is important to determine how these neurons are affected in *Arl*.

Due to the very low levels of breeding in *Arl* mice, only one set of embryos were obtained for use in neuron culture. Unfortunately, after the culture of motor neurons from this litter of embryos, genotyping revealed that only WT embryos had successfully produced neuron cultures. No further embryos were able to be obtained to repeat the culture of motor neurons, or try the culture of sensory neurons.

#### **IV.8 Discussion**

Intracellular transport of many organelles is extremely important for proper functioning of the cell. As dynein has been shown to be responsible for retrograde transport in cells, any impairment to its function could have a significant impact on its ability to transport cargo, which could severely impact the function of the cell.

The effects of *Arl* on some of dynein's major cargo show similar phenotypes, with differing degrees of significance, except for the movement of mitochondria. This suggests that the effect of *Arl* on cargo transport may not be specific to particular cargo, and so is not a problem with tethering of cargo. As the location of the mutation is not near the N-terminal site of cargo interaction, this is not unexpected. The decrease in

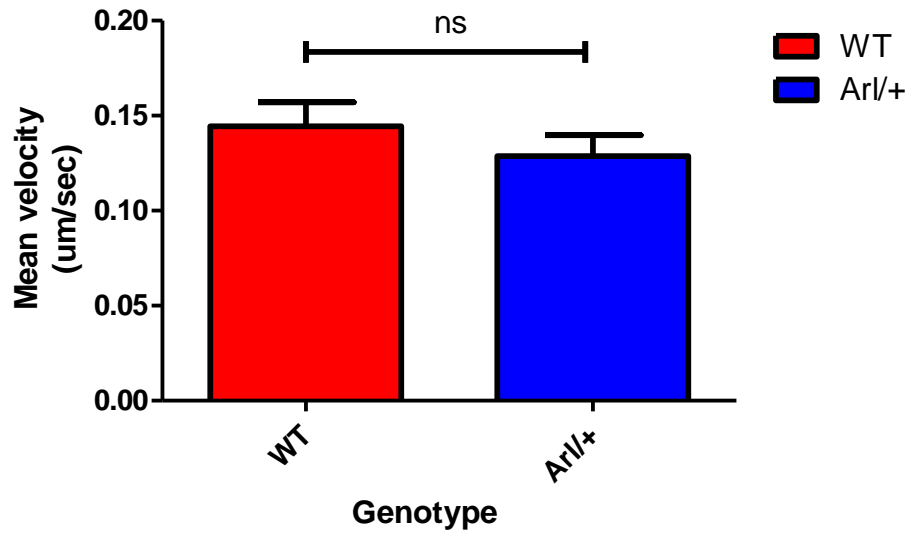


**Figure 21. Graph showing mean mitochondrial speed in WT and *Arl*/+ MEFs.** MEFs were incubated with 50nM Mitotracker for 30 min at 37°C, then replaced with CO<sub>2</sub> independent media and imaged for 1 min movies at 1 frame/2 sec to record the speed of mitochondrial movement. n=3 cells. p= 0.36 using unpaired t-test.

cargo transport speeds is more likely to be due to problems with dynein movement which results in the slower movement of cargo.

The lack of significant difference in mitochondria speed between WT and *Arl*/<sup>+</sup> may be that *Arl* affects cargo transport of mitochondria differently to other cargos, or the measurements could be affected by kinesin transport. Due to the nature of the MT arrays in fibroblasts, it can be difficult to distinguish directionality of cargo moving along them. This is not a problem when looking at uni-directional cargo (such as reassembly of disrupted Golgi, or endosomes), but mitochondrial movement is bi-directional, with dynein transporting in a mainly retrograde direction, and kinesin mainly anterogradely. If some of the mitochondrial measurements were of kinesin dependent movement, then this may have affected the measurements. Because of this, it is important for this experiment to be repeated in cells where direction of movement along the MTs can be easily determined, such as along neuronal axons. This would allow a direct comparison of dynein dependent mitochondrial movement to be made between WT and *Arl*/<sup>+</sup>.

## **CHAPTER V**

## **Chapter V**

# **INVESTIGATING THE EFFECT OF THE *ARL* MUTATION ON THE GOLGI APPARATUS AND MITOCHONDRIA USING TRANSMISSION ELECTRON MICROSCOPY**

## **V.1 Introduction**

In order to better understand the effects of the *Arl* mutation on the Golgi apparatus and mitochondria, and identify other possible cellular disruptions caused by the mutation, transmission electron microscopy (TEM) was employed. This method of microscopy allows high magnification images to be obtained showing great cellular detail. TEM images are taken of cross sections of either cells or tissue that have been fixed and stained with heavy metals. The differing affinity of structures for these heavy metals makes some appear electron-dense (high affinity), while others are electron-weak (low affinity), producing the high level of detail.

## **V.2 Ultrastructural Analysis of the Golgi Apparatus**

Adult WT and *Arl*/+ mice were perfusion fixed using gluteraldehyde and paraformaldehyde. The spinal cord was exposed by laminectomy and removed in sections and allowed to post-fix for 48 hr, immersed in osmium tetroxide and then sequentially dehydrated. The spinal cord sections were finally embedded in resin, then sectioned using a microtome to produce 100 nm transverse sections of spinal cord.

Images of neuronal cells from lumbar spinal cord sections were taken at 1000 x magnification to capture detail of the entire cell body, and then higher magnification (5,000 and 10,000 x) images obtained greater detail of specific areas of interest within the cell. Lumbar spinal cord was selected as the clenching phenotype in the *Arl* mouse is confined to the hindlimbs, suggesting that any possible neuronal defects are located in this area of the spinal cord.

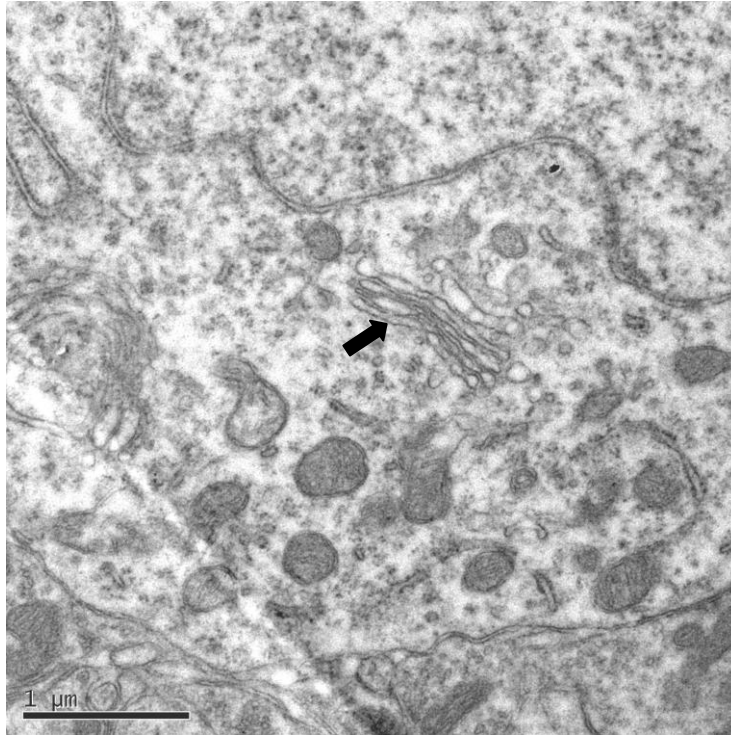
Although the reassembly of Golgi after disruption was impaired, as discussed in Chapter IV, the untreated control cells did not show any impairment due to the *Arl* mutation. However, immunocytochemistry cannot detect fine structural defects, only larger positioning issues. Therefore TEM is ideal to check the ultrastructure of the Golgi membrane and look for any problems with the organisation of the cisternae.

The lower magnification images (1000 x) were used to check the general amount and location of the Golgi in WT and *Arl*/+ neuronal cells. In general, the Golgi appeared to be of normal structure and location in WT cells, with the stacks of flattened membranes mainly near the centre of the cells, around the nucleus.

Using higher magnification (5,000 and 10,000 x) images were taken to look at the Golgi in greater detail (Figure 22). In WT the Golgi appears as would be expected, with well structured flattened membranes, often in a semicircular shape. Vesicles are apparent near the *trans*-Golgi network suggesting that the Golgi is properly functioning in processing molecules for transport - likely to be secretory vesicles containing neurotransmitters.

In *Arl*/+ cells, much of the Golgi appears normal, similar to that seen in the WT cells. However, as shown in Figure 22, some of the cisternae are very loosely packed, with large gaps between the stacks of membrane, suggesting that dynein is unable to maintain the normal fine structure. Such large spaces between the stacks of membranes may affect the movement of macromolecules between the *cis* and *trans* faces of the Golgi network. This in turn could cause problems with modification and/or labelling of proteins received from the rough endoplasmic reticulum (rER), possibly leading to incorrectly modified proteins or incorrect secretion. In neuronal cells these proteins could include neurotransmitters, essential for the proper communication between neurons.

A



B

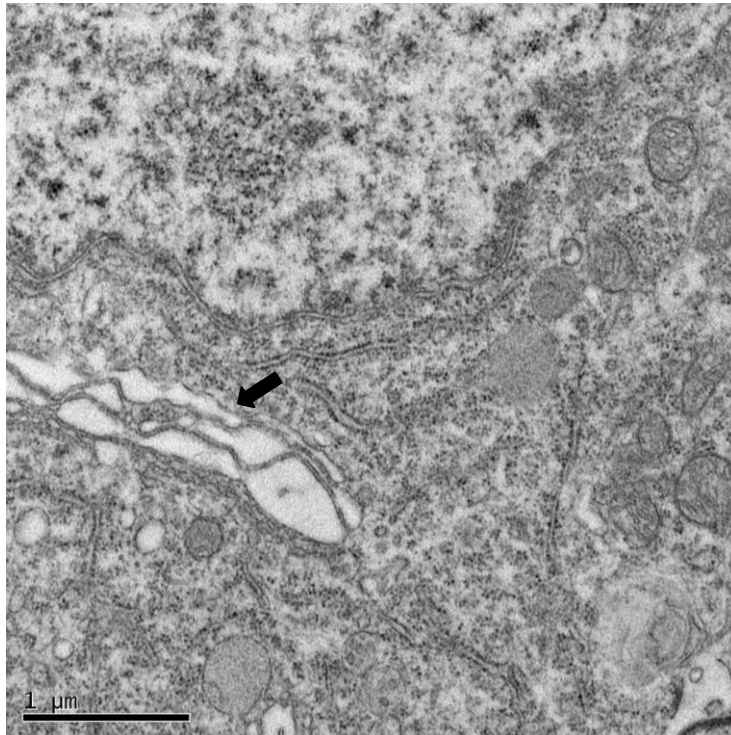


**Figure 22. TEM micrographs showing Golgi structure in WT and *Arl/+* cells**

TEM sections were imaged at 5000x magnification. Arrows indicate Golgi apparatus.

- A) Typical Golgi apparatus morphology in a WT neuronal cell with closely packed membranes
- B) Typical Golgi apparatus morphology in an *Arl/+* neuronal cell, with very loosely packed membranes with large gaps. Scale = 1 μm

### **V.3 Ultrastructural Analysis of the Mitochondria**

Another major cargo of cytoplasmic dynein is mitochondria, which are required to travel large distances, particularly in neurons, from axons to the cell body for recycling and degradation. This retrograde movement is mediated by dynein and therefore may be perturbed by the *Arl* mutation. Highly polarised cells, such as neurons, are particularly sensitive to defects in mitochondrial movement and so are ideal for studying the effects of possible transport defects.

To check for possible transport defects, the number of mitochondria in the cell body of neuronal cells, imaged at 1000 x magnification, were counted and compared between the genotypes of TEM sections. As can be seen from Figure 23, there is an overall trend for a greater number of mitochondria in WT cells compared to *Arl/+* cells, however this difference is not significant ( $p=0.2037$ ,  $n=15$ ).

The greater number of mitochondria present in WT cells compared to *Arl/+* cells suggests that the transport of mitochondria from axons to the cell body for degradation may be slightly impaired in *Arl/+* compared to WT, or the rate of degradation of mitochondria by autophagy may be increased. If there is a constant turnover of mitochondria, then a decrease in dynein transport, but continued levels of kinesin anterograde transport, would have the net effect of decreasing the number of mitochondria at the cell body. This difference could also be due to smaller sized neurons.

Recent studies in *Arl* (Bros-Facer, Golding et al. Manuscript in preparation) have identified a change in the size of motor neurons, from lumbar spinal cord, towards a greater number of smaller neurons, compared to WT. Smaller neuron size could explain fewer mitochondria identified in the cell bodies of these neurons. To determine whether this was the case, the diameter of the soma of the neurons were measured from the TEM micrographs, using Image J and compared between WT and *Arl/+*. As shown in Figure 24, the *Arl/+* neuronal soma are significantly smaller in diameter compared to WT ( $p=0.03$ ). This indicates that the reduced number of mitochondria seen in *Arl/+* neurons could be due to the reduced size of the neurons.

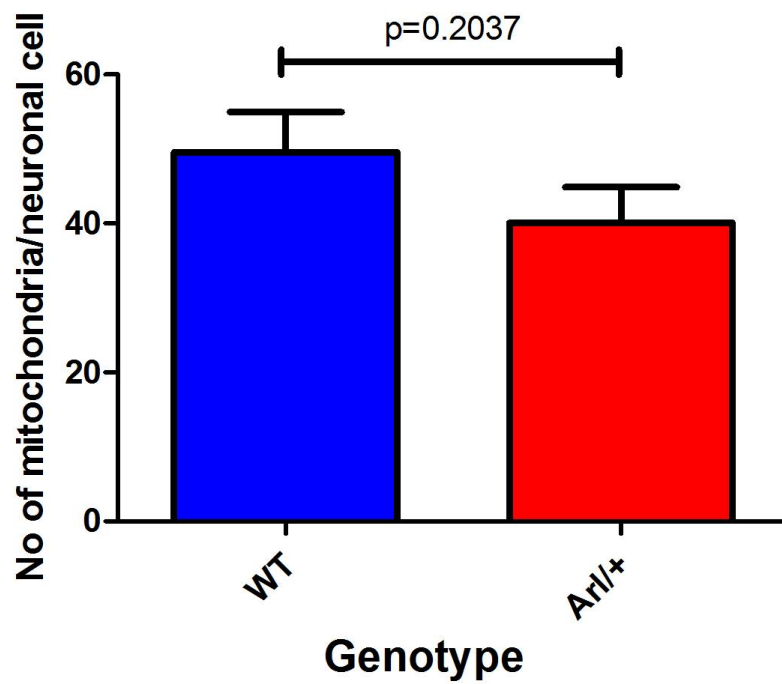


**Figure 23. Graph of quantification of number of mitochondria in cell body of WT and *Arl/+* neuronal cells.**

The number of mitochondria present in the cell body of neuronal cells from low magnification TEM images were counted and compared between WT and *Arl/+* cells. n=15

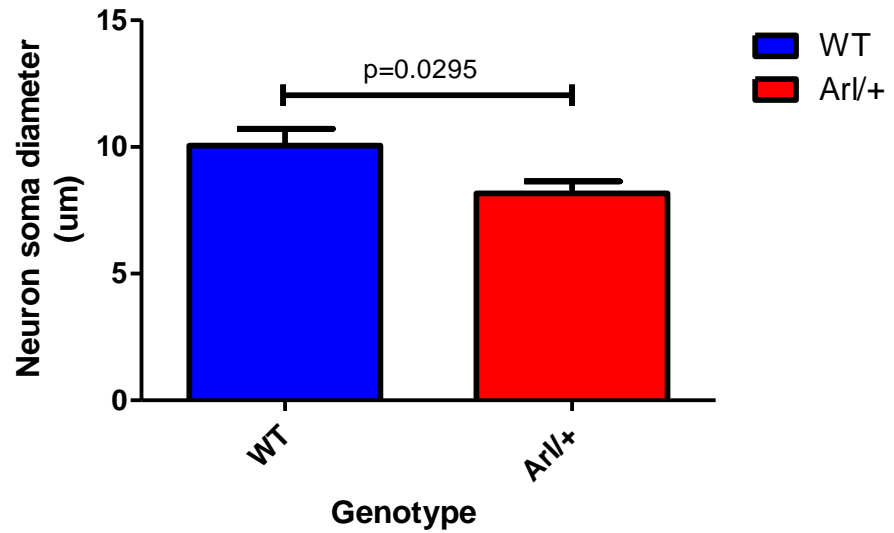


**Figure 24. Graph showing average neuron soma diameter in WT and *Arl/+* spinal cord neurons.**

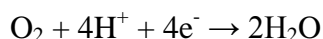
The diameter of the neuronal cell soma were measured using image J in WT and *Arl/+* neuronal cell TEM micrographs and compared. *Arl/+* neuronal soma are significantly smaller compared to WT ( $p=0.03$ ) ( $n=15$ ).

At greater magnification (5,000 and 10,000 x) the mitochondria show a difference in morphology between the two genotypes, with a number of the *Arl/+* mitochondria displaying an enlarged, elongated, deflated appearance, with less clearly defined cristae, compared to the WT (Figure 25). The WT cells contain compact, mainly oval mitochondria.

#### **V.4 Measuring Rates of Respiration**

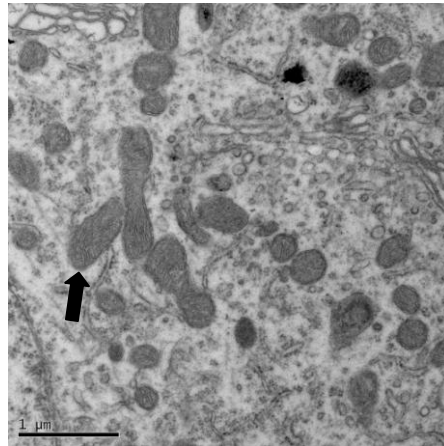
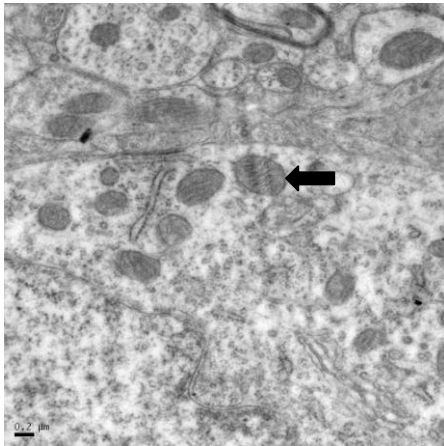
To investigate whether the morphological changes seen in the mitochondria affected the function, O<sub>2</sub> consumption assays were performed to identify the rates of respiration in mitochondria from each genotype. Using mitochondria, isolated from WT and *Arl/+* lumbar spinal cord by centrifugation, the rate of O<sub>2</sub> consumption was measured on a Rank O<sub>2</sub> electrode and the rates expressed as nmol O<sub>2</sub>.min<sup>-1</sup>.mg of protein<sup>-1</sup>. The mitochondria were isolated from lumbar spinal cord to ensure the mitochondria measured were comparable to those looked at using TEM. The isolated mitochondria were pooled together from the lumbar spinal cords of five mice, and each experiment was repeated three times.

Ascorbate and TMPD (tetramethyl pheylen diamine) are used to feed electrons to complex IV, cytochrome *c* oxidase. TMPD is an artificial electron carrier which is reduced by ascorbate and oxidised by cytochrome *c* to feed electrons to complex IV. Cytochrome *c* oxidase is a large membrane bound dimeric enzyme, with each half consisting of 13 protein chains. The complex acts as the terminal mitochondrial electron acceptor in the electron transport chain by accepting 4 electrons from cytochrome *c*, reducing an oxygen molecule.



This is coupled to the transfer of 4 protons across the mitochondrial membrane, to produce a membrane potential ( $\Delta\psi$ ), which is used to drive the synthesis of ATP. Thus, the consumption of O<sub>2</sub> at complex IV is a measure of the synthesis of ATP and the overall rate of respiration of the mitochondrion.

Wildtype



*Arl/+*

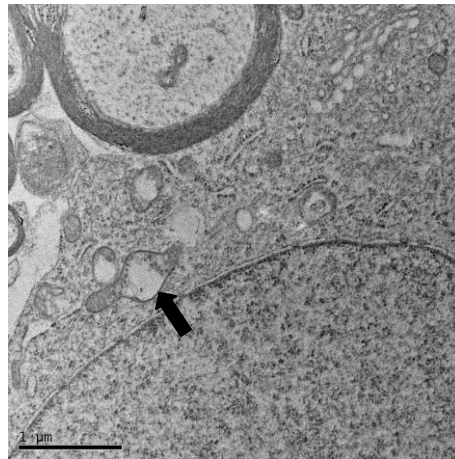
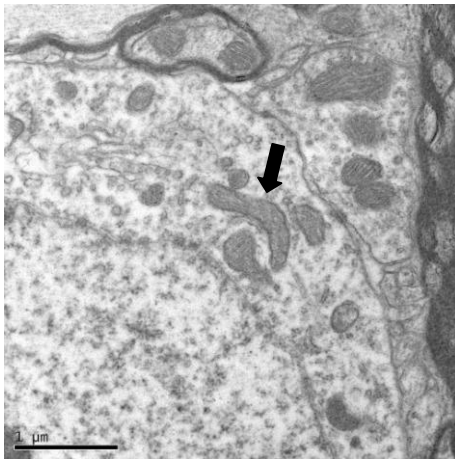


**Figure 25. TEM micrographs of mitochondria in WT and *Arl/+* neuronal cells.** In WT mitochondria are mainly oval shaped with clearly defined cristae, however, in *Arl/+* cells, mitochondria are often elongated in shape and have ill-defined cristae. Arrows indicate example mitochondria. Scale bar = 1  $\mu\text{m}$ .

As can be seen from Figure 26, the rate of respiration is significantly higher in the *Arl/+* compared to the WT ( $p=0.0156$ ). This data suggests that there may be a greater energy requirement in the lumbar spinal cord neurons from *Arl/+* compared to WT.

### **V.5 Discussion**

In TEM Golgi appeared normal, with correct structure and location, suggesting fixation and dissection procedures did not perturb tissue. At higher magnification, Golgi appears to be functioning normally, with secretory vesicles visible near the *trans*-Golgi. A large proportion of the Golgi appears normal in *Arl/+* sections compared to the WT cells. However, some cisternae are loosely packed with gaps between the stacks of membranes, suggesting that the *Arl* mutation affects dynein's ability to maintain the normal fine structure of the Golgi.

Such large gaps between the membranes of the Golgi could increase the distance between the *cis* and *trans* faces of the Golgi network and disrupt transport through the network. Golgi is important for modification and labelling of proteins which are then packaged, at the *trans* Golgi network (TGN), for transport to the plasma membrane (e.g. for exocytosis) or secretory pathways. Disruption of the structure of the Golgi could affect the labelling or modification of proteins, or impede their transport through the network. This could lead to incorrectly modified proteins, or incorrect or reduced secretion. In neuronal cells, the proteins secreted can include neurotransmitters, so any disruption to the Golgi could lead to perturbed neuronal function.

To test the functioning of the Golgi, despite the disrupted structure, transport through the ER-Golgi pathway could be investigated. Disruption to the function of the Golgi due to structural upset could affect the movement of proteins from the ER to the Golgi and subsequent transport through secretory or exocytic pathways. This could be investigated by transfecting WT and *Arl/+* cells with GFP-cDNA of a protein of interest. The expressed GFP-protein will then be transported through the ER-Golgi pathway and can be tracked using live cell imaging to determine whether the *Arl/+* cells are impaired in this transport compared to WT.

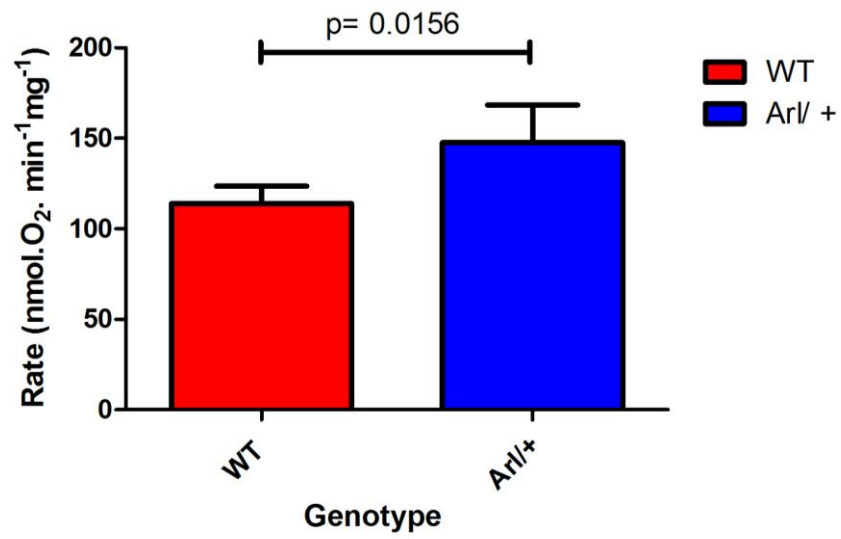


**Figure 26. Graph showing O<sub>2</sub> consumption of WT and Arl/+ mitochondria**

Mitochondria were isolated from WT and Arl/+ lumbar spinal cord and O<sub>2</sub> consumption assays performed to identify any difference between the genotypes. Assay was performed 3 times on mitochondria isolated from 5 mice each time and shows that Arl/+ mitochondria consume significantly greater amounts of O<sub>2</sub> compared to WT.

Dynein has been shown to be important for cellular distribution of mitochondria, and disruption of axonal transport leads to non-uniform distribution of mitochondria along the axon. The retrograde transport of mitochondria is important for degradation and recycling and so dynein is essential in ensuring only functional mitochondria remain in cells.

Although there is no significant difference in the number of mitochondria present in the cell bodies of *Arl/+* compared with that in the WT it is important to determine whether this is true throughout the entire cell, or just the cell body. Transport of mitochondria from axons to the cell body for degradation and the rate of degradation of mitochondria by autophagy should be investigated. The mitochondrial biogenesis is a balance between synthesis and degradation and determines the number of mitochondria in a cell. If autophagy of mitochondria is increased, but synthesis levels remain static, then overall numbers of mitochondria will decrease. To determine this, the number of mitochondria in entire neurons would need to be established to see if either the distribution of mitochondria between axons and cells bodies is different or the total number of mitochondria is different, or whether there is no difference between genotypes.

A decrease in dynein retrograde transport, but continued levels of kinesin anterograde transport would have the net effect of decreasing the number of mitochondria at the cell body. However, studies have shown that perturbed dynein transport can have an effect on kinesin, so rates of both anterograde and retrograde transport in *Arl/+* and WT neurons would need to be established to determine the balance of transport (Gross, Welte et al. 2002).

Unpublished data from Bros-Facer et al. (Bros-Facer, Golding et al. Manuscript in preparation) have shown a shift towards a greater number of smaller motor neurons in *Arl/+* lumbar spinal cord. These motor neurons were 20% smaller in *Arl/+* compared to WT. This trend was also identified in the neurons from the lumbar spinal cords used for TEM, which were measured and showed that *Arl/+* neuronal soma were significantly smaller than WT.

The mitochondria were then analysed at greater magnification to determine if the *Arl* mutation has an effect on mitochondria morphology. At 5000 x and 10000 x magnification the mitochondria show a difference in morphology between the two genotypes. While the majority of WT mitochondria maintain an oval, turgid appearance with well defined cristae, a number of *Arl/+* mitochondria display an enlarged, elongated appearance with some also exhibiting less well defined cristae.

The elongated, tubular appearance of these mitochondria in *Arl/+* cells could be due to increased fusion of unhealthy mitochondria with healthy ones, to produce healthy, functional mitochondria. Alternatively, the enlarged mitochondria may be unhealthy, particularly those with less well defined cristae, and awaiting degradation by autophagy, rather than repair through fusion.

Large mitochondria can arise during fission as new ones are produced. Dynein has been implicated in mitochondrial fission by transporting the dynamin related protein Drp1 which is necessary for mitochondrial fission. Varadi et al (Varadi, Johnson-Cadwell et al. 2004) have shown that disrupting dynein function in HeLa cells results in the movement of mitochondria from the cell periphery to the cell centre. It also results in the formation of long, and sometimes interconnected, mitochondria. Drp1 is recruited to the outer membrane of mitochondria for fission to occur, but when the dynein complex is disrupted (either through disruption of DIC, or disruption of dynamitin to affect dynactin) it results in the repositioning of Drp1 from the mitochondria to other cytoplasmic membranes. Therefore, the elongated, tubular mitochondria identified in *Arl/+* cells could be due to mislocation of Drp1 resulting from impaired dynein function.

To identify whether Drp1 is being relocated from mitochondrial membranes due to the *Arl* mutation, immunogold labelling TEM could be employed. This technique allows samples to be fixed and processed such that the antigenicity of the proteins is maintained. Sections can then be labelled with a primary antibody (in this case, against Drp1) and then with a secondary antibody conjugated to small gold particles (~5-10 nm in diameter). When imaged using the TEM, the gold particles are visible, revealing the location of the proteins of interest. This would provide information on the location of Drp1 and indicate whether the *Arl* mutation is resulting in mislocated Drp1.

To determine whether the morphological changes identified in mitochondria from *Arl*/<sup>+</sup> cells affect their function, O<sub>2</sub> consumption assays were utilised. This assay indicates the rate of respiration from the mitochondria tested.

Mitochondria were isolated from lumbar spinal cord of *Arl*/<sup>+</sup> and WT mice to ensure the mitochondria used were comparable to those analysed by TEM.

The *Arl*/<sup>+</sup> mitochondria showed a significantly higher rate of respiration compared to WT. This suggests that there is a greater energy requirement in lumbar spinal cord neurons from *Arl*/<sup>+</sup> than WT. This data is similar to that seen in *Loa*/<sup>+</sup> mice, where mitochondrial respiration is increased in *Loa*/<sup>+</sup> compared to WT (El-Kadi, Bros-Facer et al. 2010). Together these data suggest a gain-of-function by mutant cytoplasmic dynein which results in higher functioning mitochondria. However, the reasons for this increase are yet to be fully understood and further investigations are required.

The *Loa* mutation rescues the SOD1<sup>G93A</sup> phenotype, and specifically has been shown to rescue mitochondrial defects in respiration and membrane potential. However, *Arl*/<sup>+</sup> has not been shown to significantly ameliorate SOD1<sup>G93A</sup> phenotype. Although it is worth noting that only muscle force, motor neuron units and fatigue profiles were assessed and other specific SOD1<sup>G93A</sup> phenotypes may show improvement if tested.

Measurements of *Arl*/SOD1<sup>G93A</sup> rates of respiration would need to be established to identify if any increase in respiration can rescue this particular phenotype of SOD1. It may be that mitochondrial dysfunction plays only a small part in the raft of phenotypes caused by SOD1, and that rescue of it produces only a minimal overall improvement. This could explain *Arl* showing a similar increase in respiration as *Loa*, over WT, but not showing a global amelioration of phenotype when crossed with SOD1 as *Loa* does. There may be other phenotypes in SOD1 that *Loa* is able to rescue, but *Arl* is not, resulting in an overall improvement in *Loa*/SOD<sup>G93A</sup> that is not seen in *Arl*/SOD<sup>G93A</sup>. Further analyses on both *Loa* and *Arl* with SOD1 are required to establish how the mutations interact.

Interestingly, Miller and Sheetz (Miller and Sheetz 2004) have shown that ~90% of mitochondria with a high membrane potential move anterogradely in neurons. While ~80% of mitochondria exhibiting a low membrane potential move in a retrograde direction. As the mitochondria in the *Ar1/+* lumbar spinal cord preparations have increased ATP production, indicated by the increased O<sub>2</sub> consumption, their membrane potentials must be high to allow for the increased ATP production. This may mean that anterograde transport of mitochondria is increased in *Ar1/+* mitochondria, resulting in fewer remaining in the cell body. However, as no significant difference in mitochondrial number in the cell body was seen between genotypes, the total numbers would need to be established throughout the neuronal cells.

Mitochondria with a low membrane potential may not be functioning correctly, and so an increase in their retrograde transport would deliver them to the cell body for degradation. Tctex1 has been shown to interact with VDAC in the outer membrane of mitochondria (Schwarzer, Barnikol-Watanabe et al. 2002) and this interaction may regulate the binding of dynein, and therefore the retrograde transport of mitochondria, with a low membrane potential, for degradation.

A recent study from Cleveland's lab (Israelson, Arbel et al. 2010) has shown that mutant SOD1 directly binds to VDAC1 (a VDAC isoform), inhibiting conductance of the channel. The reduced activity decreases the survival of SOD1 mice through accelerated disease onset.

As reduced conductance by VDAC1 will decrease ATP synthesis and reduce membrane potential, this data correlates with the reduced O<sub>2</sub> consumption and thus ATP synthesis identified in SOD1 (El-Kadi, Bros-Facer et al. 2010). Spectrophotometric assays have corroborated this, by showing a decrease in complex IV activity in SOD1 compared to WT (Philpott, unpublished data). This assay measures the redox changes of cytochrome c added to complex IV and provides an accurate assessment of its activity (Benit, Goncalves et al. 2006).

This data suggests that binding of mutant SOD1 to VDAC1 plays a large role in the mitochondrial phenotype identified in SOD1 mice. As already discussed, dynein has been shown to interact with VDAC, via Tctex1, and recent data has shown increased

affinity of Tctex1 for the dynein complex in *Loa* (Deng, unpublished data). As *Loa* has been shown to partially rescue mitochondrial function and increase SOD1 lifespan, it suggests that increased binding of mutant dynein, via Tctex1, at VDAC may counteract the effects of mutant SOD1 binding.

Amelioration of SOD1 phenotype in mitochondria may be brought about by increased respiration rates in *Arl*, however, effects of *Arl* on SOD1 in mitochondria have yet to be investigated. As the *Arl* mutation is not near regions of accessory chain association or cargo binding, similar effects as *Loa* may not be expected.

## **CHAPTER VI**

## **Chapter VI**

### **FINAL DISCUSSION**

#### **VI.1 Summary of data**

As the main retrograde motor protein in cells, cytoplasmic dynein is responsible for transporting a wide range of cargo towards the minus end of MTs. Mutations in the heavy chain of dynein, such as *Loa*, *Cral* and *Swl*, have demonstrated that interfering with this motor protein can lead to disruptions in a broad array of cellular functions.

This study has demonstrated that a new heavy chain mutation, located in a region away from the other well characterised mutations, also causes disruption to cellular transport. *Arl* is located in an area of unknown function, N-terminal to the motor domain. Analysis of DHC protein showed no difference in the levels present in brain or spinal cord of *Arl/+* and WT and no effect on the integrity of the complex was identified using sucrose density gradient centrifugation of homogenised adult brain tissue.

The dynein complex was purified from adult brain tissue, with all subunits present; however, ATPase activity and MT gliding could not be measured. Using purified dynein, MT binding was found to be greater in *Arl/+* than WT, suggesting that the mutation may affect the structure of the motor domain resulting in a higher affinity for MTs.

Studies of cargo transport in MEFs revealed that in situations of cellular stress, dynein dependent reassembly of Golgi is impaired in *Arl/+* compared to WT. The trafficking of endosomes in MEFs was investigated using fluorophore-tagged EGF in fixed cells, which showed a delay in the endosomes reaching the lysosomes for degradation in *Arl/+* compared to WT. In addition to this, live cell imaging of EGF positive endosomes revealed that in *Arl/+* the average speed of transport is significantly slower compared to WT. To further investigate the effects of the mutation on dynein cargo, mitochondria were labelled with Mitotracker, a mitochondrial specific fluorophore, and their movement tracked by live cell imaging. Although not significant, a trend towards slower movement in *Arl/+* compared to WT was identified. Nevertheless, these studies

have shown that dynein transport is impaired across a range of cargos, suggesting that the effects of *Arl* on cargo transport are not specific to a particular cargo.

The effects of the mutation were further examined in spinal cord neurons from tissue sections using TEM. Small perturbations to Golgi structure were identified in *Arl/+* neuronal cells, with the cisternae appearing loosely stacked and large gaps in between some of the stacks of membranes. The untreated control MEFs used in the Golgi reassembly studies did not show any disruption, suggesting that *Arl* dynein is able to maintain the global positioning of Golgi, but unable to maintain the fine structure and organisation of the membranes.

Mitochondria were found to have altered morphology in *Arl/+* neurons, compared to WT, with an enlarged, elongated appearance. In a number of these mitochondria, the cristae were less well defined. No significant difference in the number of mitochondria in the cell centre was identified between *Arl/+* and WT cells. The *Arl/+* mitochondria were found to have significantly higher rates of respiration, compared to WT, suggesting a greater energy requirement in these neurons.

## **VI.2 Significance of results and conclusions**

A conformational change in AAA1 results from nucleotide hydrolysis, and causes knock-on conformational changes to neighbouring AAA domains. This results in the movement of CC1, relative to CC2 in the stalk and the change in registry between the two coiled-coils dictates the affinity of the MTBD for MTs (Gibbons, Garbarino et al. 2005). The proposed linker domain that is suggested to swing across the face of the ring is close to the site of the *Arl* mutation.

The mutation results in a change from hydrophobic tryptophan to the compact, polar arginine and is predicted to lie between two helices. It is therefore reasonable that the mutation could cause the structure to twist and affect the stability of the structure. A change in the structure at this location could affect the linker domain. A change in the positioning of the linker domain could affect the conformational state of the AAA1 domain, which is directly C-terminal to it. Perturbation of the conformation of AAA1 could alter the knock-on conformational change around the ring, thus affecting the stalk

and the affinity of the MTBD. Furthermore, if the movement of the linker domain is affected by the mutation, it may impede the powerstroke and thus the movement of dynein.

Under zero load, dynein mainly moves in steps of 24 nm and 32 nm. Under load, size step can decrease to 8 nm, suggesting that dynein can act as a molecular gear (Mallik, Carter et al. 2004). The model for this gear suggests that load-induced ATP binding tightens the AAA ring, resulting in a smaller but stronger step of the motor. Hence, any alteration in the conformation of the AAA domains due to the mutation could affect the step size (see Figure 27 below).

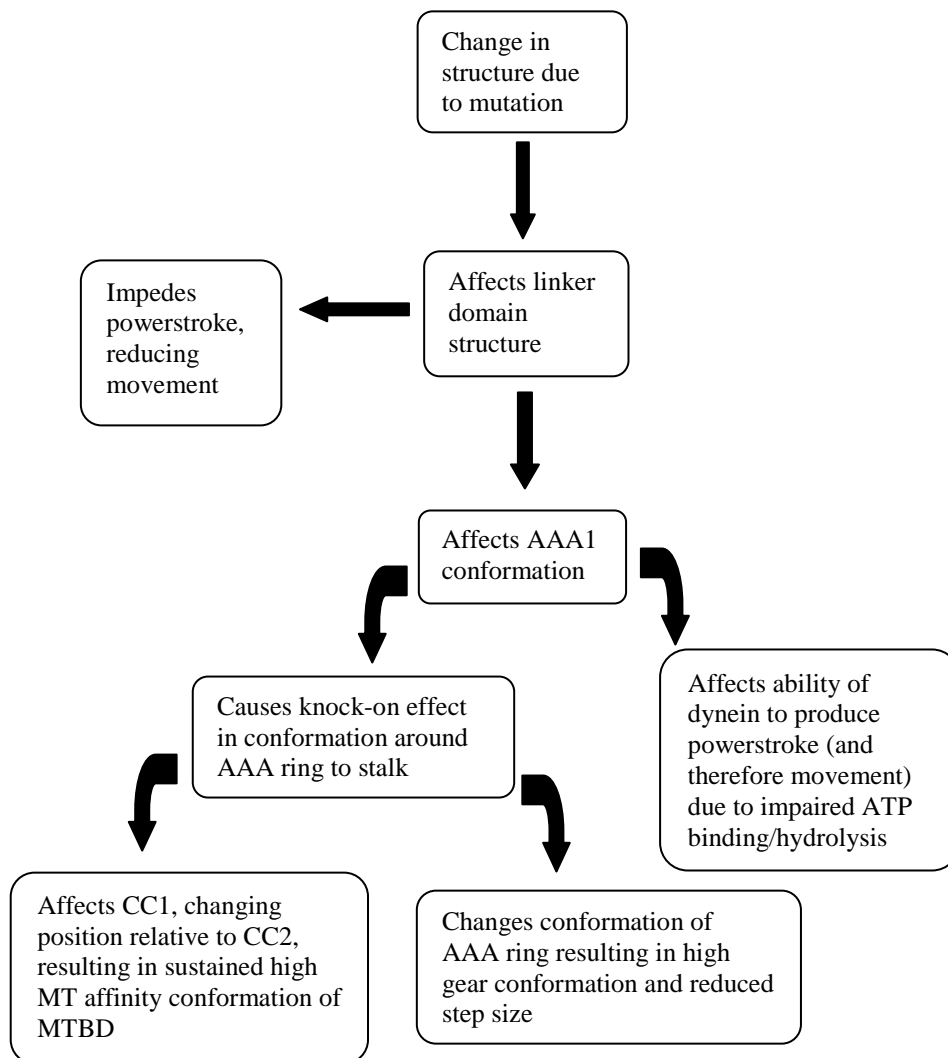


**Figure 27. Flow chart of suggested effects of mutation on dynein structure and function.**

The impairment in cargo transport seen in MEFs is unlikely to result from problems with cargo binding as the mutation is not near the area of cargo binding, meaning that decreased speed of dynein movement along the MT is more plausible. However, there are a number of possibilities (see Figure 28), such as:

- Increased MT binding (due to conformational changes detailed above), therefore slowing movement along the MT.
- Problems with ATP binding and/or hydrolysis due to conformational changes therefore affecting the ATP dependent powerstroke, and impeding the movement.
- The mutation affecting movement of the linker domain and therefore resulting in powerstroke swing impairment.
- The proposed gear system of dynein may be affected, causing dynein to move in smaller steps along the MT, thus resulting in a slower speed.

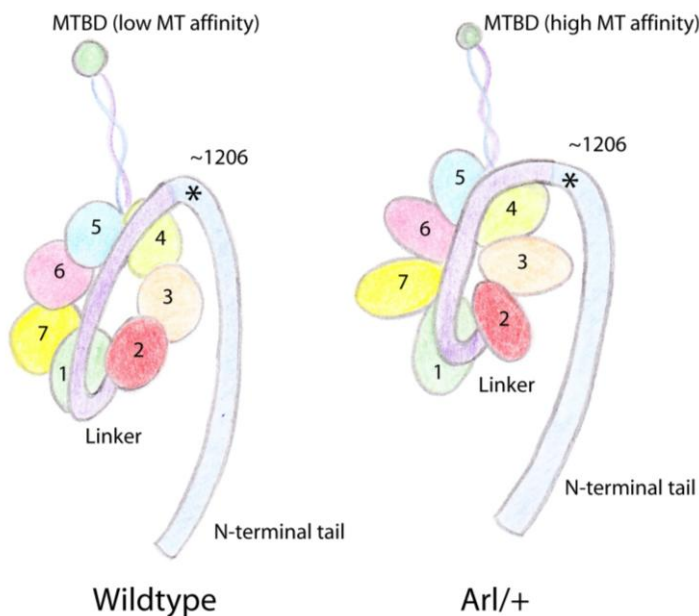


**Figure 28. Schematic of dynein showing proposed effect of *Arl* mutation.**

Asterisk denotes location of residue 1206, the location of the mutation in *Arl*. The mutation may cause the chain to twist, thus affecting the normal structure. This could have a knock-on effect on the flexibility of the linker domain (shown in purple), preventing it from bending at its normal angle. This could alter the angle at which the linker domain joins the first AAA domain, and may cause a change in conformation which has a knock-on effect to neighbouring AAA domains. The change in conformation of the ring of AAA domains may result in a change in the alignment of the coiled-coils. This change in alignment of CC1 and CC2 may cause the MTBD to bind MTs with a higher affinity.

Mitochondria with a high membrane potential have been shown to move in a predominantly anterograde direction, while low membrane potential mitochondria move in a mainly retrograde direction (Miller and Sheetz 2004). As *Arl*<sup>+/+</sup> mitochondria have been shown to have increased rates of respiration, and therefore increased membrane potential, it suggests that these mitochondria would be undergoing higher levels of anterograde transport. However, further studies are needed to identify any differences in kinesin- and dynein-dependent mitochondrial movement between genotypes.

In conclusion, this study provides evidence for increased affinity of *Arl*<sup>+/+</sup> dynein for MTs, and that this reduces the speed at which cargo can be transported in MEFs. In addition to this, mitochondria are mislocated with abnormal morphology in *Arl*<sup>+/+</sup> spinal cord neurons and demonstrate increased rates of respiration compared to WT. This study also demonstrates that a mutation in dynein at a location far from other well characterised dynein mutations can result in similar phenotypes, highlighting the importance of the proper functioning of this protein.

### **VI.3 Future directions**

To determine how the mutation is affecting the protein, it is important to identify what effect the mutation has on the structure. The region containing the mutation has been cloned from *Arl* and WT, but needs to be expressed and crystallised to allow x-ray diffraction patterns to be obtained. From these, structures can be determined and any effect due to the mutation ascertained. An alternative method to determine the effect of the mutation of the structure is the use of single molecule EM. This would allow the structure of the molecule to be established in different conformations, thereby determining its three-dimensional structure and allowing any effect of the mutation to be identified.

As AAA1 is the main site of ATP binding and hydrolysis, it is important to establish whether ATP hydrolysis is affected in *Arl*. The ATPase assay in Chapter III is an ideal system to utilise, but dynein needs to be purified that is fully functioning and a suitable positive control must be identified. Alternatively, other methods of measuring ATPase activity could be used, such as radioactive assays that measure  $^{32}\text{P}$  hydrolysed from ATP, or non-radioactive methods such as the spectrophotometric assay using malachite green.

To establish whether the mutation causes the dynein to move in smaller steps along the MTs, studies using an optical trap should be utilised. This would allow the step size of dynein to be determined in *Arl* and WT, and compare any differences in the force exerted by the motor. This would provide information on whether the gear mechanism of dynein is affected by the mutation.

As the mutation appears to affect the movement of dynein, rather than its association with cargo, it suggests that transport of all cargo would be affected. Further studies to determine the effect on other cargo could be performed, such as transport of MTs as cargo and whether there is an effect on mitosis. As transport of endosomes has been shown to be impaired, then downstream signalling could be disrupted by delayed trafficking of signalling factors. EGFR signalling is vital for a large number of signalling pathways and detailed examination could be performed to identify possible cellular effects of delayed signalling.

Currently, all *in vitro* studies of cargo transport have been performed using MEFs. Due to the large distances in neurons, particularly the axons, they can be more susceptible to defects in transport mechanisms. Studies on cargo transport should therefore be performed using both motor and sensory neurons, to determine the effects of the mutation on these cells.

The increased rate of respiration in *Arl* mitochondria, compared to WT, is similar to results obtained from *Loa* (El-Kadi, Bros-Facer et al. 2010). Further studies are required to determine why and how respiration is increased and comparisons with *Loa* could be useful in this respect. Additional analyses of *Arl*/SOD1 interactions may also help determine the nature of the effects of dynein mutations on mitochondria. Experiments such as dissecting the electron transport chain (ETC) would allow the function of each complex of the ETC to be checked, helping to identify the reason for increased respiration.

## **REFERENCES**

## References

- Afzelius, B. A. (1976). "A human syndrome caused by immotile cilia." Science **193**(4250): 317-9.
- Ahmad-Annur, A., P. Shah, M. Hafezparast, H. Hummerich, A. S. Witherden, K. E. Morrison, P. J. Shaw, J. Kirby, T. T. Warner, A. Crosby, C. Proukakis, P. Wilkinson, R. W. Orrell, L. Bradley, J. E. Martin and E. M. Fisher (2003). "No association with common Caucasian genotypes in exons 8, 13 and 14 of the human cytoplasmic dynein heavy chain gene (DNCHC1) and familial motor neuron disorders." Amyotroph Lateral Scler Other Motor Neuron Disord **4**(3): 150-7.
- Alberts, B., A. Johnson, J. Lewis, M. Raff, K. Roberts and P. Walter (2002). Molecular Biology of the Cell, Garland Science.
- Banks, G. T., V. Bros-Facer, H. P. Williams, R. Chia, F. Achilli, J. B. Bryson, L. Greensmith and E. M. Fisher (2009). "Mutant glycyI-tRNA synthetase (Gars) ameliorates SOD1(G93A) motor neuron degeneration phenotype but has little affect on Loa dynein heavy chain mutant mice." PLoS One **4**(7): e6218.
- Benit, P., S. Goncalves, E. Philippe Dassa, J. J. Briere, G. Martin and P. Rustin (2006). "Three spectrophotometric assays for the measurement of the five respiratory chain complexes in minuscule biological samples." Clin Chim Acta **374**(1-2): 81-6.
- Benmerah, A. and C. Lamaze (2007). "Clathrin-coated pits: vive la difference?" Traffic **8**(8): 970-82.
- Boldogh, I. R. and L. A. Pon (2007). "Mitochondria on the move." Trends Cell Biol **17**(10): 502-10.
- Bros-Facer, V., M. Golding, N. Nirmalanathan, R. Chia, A. Philpott, A. M. Flenniken, I. Vukobrodovic, L. R. Osborne, S. L. Adamson, J. Rossant, D. Boerio-Gueguen, E. Stoddart, H. Bostock, E. M. Fisher, G. Schiavo, L. Greensmith and M. Hafezparast (Manuscript in preparation). "Motor neuron and sciatic nerve pathology caused by a novel mutation in cytoplasmic dynein."
- Bruijn, L. I., M. K. Houseweart, S. Kato, K. L. Anderson, S. D. Anderson, E. Ohama, A. G. Reaume, R. W. Scott and D. W. Cleveland (1998). "Aggregation and motor neuron toxicity of an ALS-linked SOD1 mutant independent from wild-type SOD1." Science **281**(5384): 1851-4.
- Bruijn, L. I., T. M. Miller and D. W. Cleveland (2004). "Unraveling the mechanisms involved in motor neuron degeneration in ALS." Annu Rev Neurosci **27**: 723-49.

- Burgess, S. A., M. L. Walker, H. Sakakibara, P. J. Knight and K. Oiwa (2003). "Dynein structure and power stroke." Nature **421**(6924): 715-8.
- Burkhardt, J. K., C. J. Echeverri, T. Nilsson and R. B. Vallee (1997). "Overexpression of the dynamitin (p50) subunit of the dynactin complex disrupts dynein-dependent maintenance of membrane organelle distribution." J Cell Biol **139**(2): 469-84.
- Chen, X. J., E. N. Levedakou, K. J. Millen, R. L. Wollmann, B. Soliven and B. Popko (2007). "Proprioceptive sensory neuropathy in mice with a mutation in the cytoplasmic Dynein heavy chain 1 gene." J Neurosci **27**(52): 14515-24.
- Culver-Hanlon, T. L., S. A. Lex, A. D. Stephens, N. J. Quintyne and S. J. King (2006). "A microtubule-binding domain in dynactin increases dynein processivity by skating along microtubules." Nat Cell Biol **8**(3): 264-70.
- Driskell, O. J., A. Mironov, V. J. Allan and P. G. Woodman (2007). "Dynein is required for receptor sorting and the morphogenesis of early endosomes." Nat Cell Biol **9**(1): 113-20.
- Duchen, L. W. (1974). "A dominant hereditary sensory disorder in the mouse with deficiency of muscle spindles: the mutant Sprawling." J Physiol **237**(2): 10P-11P.
- Dupuis, L., A. Fergani, K. E. Braunstein, J. Eschbach, N. Holl, F. Rene, J. L. Gonzalez De Aguilar, B. Zoerner, B. Schwalenstocker, A. C. Ludolph and J. P. Loeffler (2009). "Mice with a mutation in the dynein heavy chain 1 gene display sensory neuropathy but lack motor neuron disease." Exp Neurol **215**(1): 146-52.
- Echeverri, C. J., B. M. Paschal, K. T. Vaughan and R. B. Vallee (1996). "Molecular characterization of the 50-kD subunit of dynactin reveals function for the complex in chromosome alignment and spindle organization during mitosis." J Cell Biol **132**(4): 617-33.
- El-Kadi, A. M., V. Bros-Facer, W. Deng, A. Philpott, E. Stoddart, G. Banks, G. S. Jackson, E. M. Fisher, M. R. Duchon, L. Greensmith, A. L. Moore and M. Hafezparast (2010). "The legs at odd angles (Loa) mutation in cytoplasmic dynein ameliorates mitochondrial function in SOD1G93A mouse model for motor neuron disease." J Biol Chem **285**(24): 18627-39.
- Frederick, R. L. and J. M. Shaw (2007). "Moving mitochondria: establishing distribution of an essential organelle." Traffic **8**(12): 1668-75.
- Gaudette, M., M. Hirano and T. Siddique (2000). "Current status of SOD1 mutations in familial amyotrophic lateral sclerosis." Amyotroph Lateral Scler Other Motor Neuron Disord **1**(2): 83-9.
- Gee, M. A., J. E. Heuser and R. B. Vallee (1997). "An extended microtubule-binding structure within the dynein motor domain." Nature **390**(6660): 636-9.

- Gibbons, I. R., J. E. Garbarino, C. E. Tan, S. L. Reck-Peterson, R. D. Vale and A. P. Carter (2005). "The affinity of the dynein microtubule-binding domain is modulated by the conformation of its coiled-coil stalk." J Biol Chem **280**(25): 23960-5.
- Gibbons, I. R., A. Lee-Eiford, G. Mocz, C. A. Phillipson, W. J. Tang and B. H. Gibbons (1987). "Photosensitized cleavage of dynein heavy chains. Cleavage at the "V1 site" by irradiation at 365 nm in the presence of ATP and vanadate." J Biol Chem **262**(6): 2780-6.
- Goodenough, U. and J. Heuser (1984). "Structural comparison of purified dynein proteins with in situ dynein arms." J Mol Biol **180**(4): 1083-118.
- Grissom, P. M., E. A. Vaisberg and J. R. McIntosh (2002). "Identification of a novel light intermediate chain (D2LIC) for mammalian cytoplasmic dynein 2." Mol Biol Cell **13**(3): 817-29.
- Gross, S. P., M. A. Welte, S. M. Block and E. F. Wieschaus (2002). "Coordination of opposite-polarity microtubule motors." J Cell Biol **156**(4): 715-24.
- Hafezparast, M., R. Klocke, C. Ruhrberg, A. Marquardt, A. Ahmad-Annuar, S. Bowen, G. Lalli, A. S. Witherden, H. Hummerich, S. Nicholson, P. J. Morgan, R. Oozageer, J. V. Priestley, S. Averill, V. R. King, S. Ball, J. Peters, T. Toda, A. Yamamoto, Y. Hiraoka, M. Augustin, D. Korthaus, S. Wattler, P. Wabnitz, C. Dickneite, S. Lampel, F. Boehme, G. Peraus, A. Popp, M. Rudelius, J. Schlegel, H. Fuchs, M. Hrabe de Angelis, G. Schiavo, D. T. Shima, A. P. Russ, G. Stumm, J. E. Martin and E. M. Fisher (2003). "Mutations in dynein link motor neuron degeneration to defects in retrograde transport." Science **300**(5620): 808-12.
- Harada, A., Y. Takei, Y. Kanai, Y. Tanaka, S. Nonaka and N. Hirokawa (1998). "Golgi vesiculation and lysosome dispersion in cells lacking cytoplasmic dynein." J Cell Biol **141**(1): 51-9.
- Heerssen, H. M., M. F. Pazyra and R. A. Segal (2004). "Dynein motors transport activated Trks to promote survival of target-dependent neurons." Nat Neurosci **7**(6): 596-604.
- Hollenbeck, P. J. and W. M. Saxton (2005). "The axonal transport of mitochondria." J Cell Sci **118**(Pt 23): 5411-9.
- Holleran, E. A., L. A. Ligon, M. Tokito, M. C. Stankewich, J. S. Morrow and E. L. Holzbaaur (2001). "beta III spectrin binds to the Arp1 subunit of dynactin." J Biol Chem **276**(39): 36598-605.
- Howell, B. J., B. F. McEwen, J. C. Canman, D. B. Hoffman, E. M. Farrar, C. L. Rieder and E. D. Salmon (2001). "Cytoplasmic dynein/dynactin drives kinetochore protein transport to the spindle poles and has a role in mitotic spindle checkpoint inactivation." J Cell Biol **155**(7): 1159-72.

- Huang, T. G. and D. D. Hackney (1994). "Drosophila kinesin minimal motor domain expressed in Escherichia coli. Purification and kinetic characterization." J Biol Chem **269**(23): 16493-501.
- Ilieva, H. S., K. Yamanaka, S. Malkmus, O. Kakinohana, T. Yaksh, M. Marsala and D. W. Cleveland (2008). "Mutant dynein (Loa) triggers proprioceptive axon loss that extends survival only in the SOD1 ALS model with highest motor neuron death." Proc Natl Acad Sci U S A **105**(34): 12599-604.
- Imamura, K., T. Kon, R. Ohkura and K. Sutoh (2007). "The coordination of cyclic microtubule association/dissociation and tail swing of cytoplasmic dynein." Proc Natl Acad Sci U S A **104**(41): 16134-9.
- Israelson, A., N. Arbel, S. Da Cruz, H. Ilieva, K. Yamanaka, V. Shoshan-Barmatz and D. W. Cleveland (2010). "Misfolded mutant SOD1 directly inhibits VDAC1 conductance in a mouse model of inherited ALS." Neuron **67**(4): 575-87.
- Jaarsma, D., F. Rognoni, W. van Duijn, H. W. Verspaget, E. D. Haasdijk and J. C. Holstege (2001). "CuZn superoxide dismutase (SOD1) accumulates in vacuolated mitochondria in transgenic mice expressing amyotrophic lateral sclerosis-linked SOD1 mutations." Acta Neuropathol **102**(4): 293-305.
- Jordens, I., M. Marsman, C. Kuijl and J. Neefjes (2005). "Rab proteins, connecting transport and vesicle fusion." Traffic **6**(12): 1070-7.
- Julien, J. P. and J. Kriz (2006). "Transgenic mouse models of amyotrophic lateral sclerosis." Biochim Biophys Acta **1762**(11-12): 1013-24.
- Kardon, J. R., S. L. Reck-Peterson and R. D. Vale (2009). "Regulation of the processivity and intracellular localization of Saccharomyces cerevisiae dynein by dynactin." Proc Natl Acad Sci U S A **106**(14): 5669-74.
- Kardon, J. R. and R. D. Vale (2009). "Regulators of the cytoplasmic dynein motor." Nat Rev Mol Cell Biol **10**(12): 854-65.
- Karki, S., B. LaMonte and E. L. Holzbaur (1998). "Characterization of the p22 subunit of dynactin reveals the localization of cytoplasmic dynein and dynactin to the midbody of dividing cells." J Cell Biol **142**(4): 1023-34.
- Kieran, D., M. Hafezparast, S. Bohnert, J. R. Dick, J. Martin, G. Schiavo, E. M. Fisher and L. Greensmith (2005). "A mutation in dynein rescues axonal transport defects and extends the life span of ALS mice." J Cell Biol **169**(4): 561-7.
- Kim, H., S. C. Ling, G. C. Rogers, C. Kural, P. R. Selvin, S. L. Rogers and V. I. Gelfand (2007). "Microtubule binding by dynactin is required for microtubule organization but not cargo transport." J Cell Biol **176**(5): 641-51.
- King, S. J., M. Bonilla, M. E. Rodgers and T. A. Schroer (2002). "Subunit organization in cytoplasmic dynein subcomplexes." Protein Sci **11**(5): 1239-50.

- King, S. J. and T. A. Schroer (2000). "Dynactin increases the processivity of the cytoplasmic dynein motor." Nat Cell Biol **2**(1): 20-4.
- King, S. M. (2000). "AAA domains and organization of the dynein motor unit." J Cell Sci **113** ( Pt **14**): 2521-6.
- King, S. M. (2009). "Purification of axonemal dyneins and dynein-associated components from *Chlamydomonas*." Methods Cell Biol **92**: 31-48.
- King, S. M., E. Barbarese, J. F. Dillman, 3rd, S. E. Benashski, K. T. Do, R. S. Patel-King and K. K. Pfister (1998). "Cytoplasmic dynein contains a family of differentially expressed light chains." Biochemistry **37**(43): 15033-41.
- Kuta, A., W. Deng, A. Morsi El-Kadi, G. T. Banks, M. Hafezparast, K. K. Pfister and E. M. Fisher (2010). "Mouse cytoplasmic dynein intermediate chains: identification of new isoforms, alternative splicing and tissue distribution of transcripts." PLoS One **5**(7): e11682.
- Layton, W. M., Jr. (1976). "Random determination of a developmental process: reversal of normal visceral asymmetry in the mouse." J Hered **67**(6): 336-8.
- Lee, I. H., S. Kumar and M. Plamann (2001). "Null mutants of the neurospora actin-related protein 1 pointed-end complex show distinct phenotypes." Mol Biol Cell **12**(7): 2195-206.
- Levy, J. R. and E. L. Holzbaur (2006). "Cytoplasmic dynein/dynactin function and dysfunction in motor neurons." Int J Dev Neurosci **24**(2-3): 103-11.
- Liang, Y., W. Yu, Y. Li, Z. Yang, X. Yan, Q. Huang and X. Zhu (2004). "Nudel functions in membrane traffic mainly through association with Lis1 and cytoplasmic dynein." J Cell Biol **164**(4): 557-66.
- Maier, K. C., J. E. Godfrey, C. J. Echeverri, F. K. Cheong and T. A. Schroer (2008). "Dynamitin mutagenesis reveals protein-protein interactions important for dynactin structure." Traffic **9**(4): 481-91.
- Mallik, R., B. C. Carter, S. A. Lex, S. J. King and S. P. Gross (2004). "Cytoplasmic dynein functions as a gear in response to load." Nature **427**(6975): 649-52.
- Markus, S. M., J. J. Punch and W. L. Lee (2009). "Motor- and tail-dependent targeting of dynein to microtubule plus ends and the cell cortex." Curr Biol **19**(3): 196-205.
- McGrail, M., J. Gepner, A. Silvanovich, S. Ludmann, M. Serr and T. S. Hays (1995). "Regulation of cytoplasmic dynein function in vivo by the *Drosophila* Glued complex." J Cell Biol **131**(2): 411-25.
- McIlwain, D. L. (1991). "Nuclear and cell body size in spinal motor neurons." Adv Neurol **56**: 67-74.

- Mesngon, M. T., C. Tarricone, S. Hebbar, A. M. Guillotte, E. W. Schmitt, L. Lanier, A. Musacchio, S. J. King and D. S. Smith (2006). "Regulation of cytoplasmic dynein ATPase by Lis1." *J Neurosci* **26**(7): 2132-9.
- Mikami, A., S. H. Tynan, T. Hama, K. Luby-Phelps, T. Saito, J. E. Crandall, J. C. Besharse and R. B. Vallee (2002). "Molecular structure of cytoplasmic dynein 2 and its distribution in neuronal and ciliated cells." *J Cell Sci* **115**(Pt 24): 4801-8.
- Miller, K. E. and M. P. Sheetz (2004). "Axonal mitochondrial transport and potential are correlated." *J Cell Sci* **117**(Pt 13): 2791-804.
- Mukherjee, S., R. N. Ghosh and F. R. Maxfield (1997). "Endocytosis." *Physiol Rev* **77**(3): 759-803.
- Neuwald, A. F., L. Aravind, J. L. Spouge and E. V. Koonin (1999). "AAA+: A class of chaperone-like ATPases associated with the assembly, operation, and disassembly of protein complexes." *Genome Res* **9**(1): 27-43.
- Nurminsky, D. I., M. V. Nurminskaya, E. V. Benevolenskaya, Y. Y. Shevelyov, D. L. Hartl and V. A. Gvozdev (1998). "Cytoplasmic dynein intermediate-chain isoforms with different targeting properties created by tissue-specific alternative splicing." *Mol Cell Biol* **18**(11): 6816-25.
- Ogawa, K. (1991). "Four ATP-binding sites in the midregion of the beta heavy chain of dynein." *Nature* **352**(6336): 643-5.
- Parkar, N. S., B. S. Akpa, L. C. Nitsche, L. E. Wedgewood, A. T. Place, M. S. Sverdlov, O. Chaga and R. D. Minshall (2009). "Vesicle formation and endocytosis: function, machinery, mechanisms, and modeling." *Antioxid Redox Signal* **11**(6): 1301-12.
- Paschal, B. M., A. Mikami, K. K. Pfister and R. B. Vallee (1992). "Homology of the 74-kD cytoplasmic dynein subunit with a flagellar dynein polypeptide suggests an intracellular targeting function." *J Cell Biol* **118**(5): 1133-43.
- Paschal, B. M., H. S. Shpetner and R. B. Vallee (1987). "MAP 1C is a microtubule-activated ATPase which translocates microtubules in vitro and has dynein-like properties." *J Cell Biol* **105**(3): 1273-82.
- Pazour, G. J., B. L. Dickert and G. B. Witman (1999). "The DHC1b (DHC2) isoform of cytoplasmic dynein is required for flagellar assembly." *J Cell Biol* **144**(3): 473-81.
- Perrone, C. A., D. Tritschler, P. Taulman, R. Bower, B. K. Yoder and M. E. Porter (2003). "A novel dynein light intermediate chain colocalizes with the retrograde motor for intraflagellar transport at sites of axoneme assembly in chlamydomonas and Mammalian cells." *Mol Biol Cell* **14**(5): 2041-56.
- Petsko, G. A. and D. Ringe (2004). *Protein Structure and Function*. London, New Science Press Ltd.

- Pfister, K. K., E. M. Fisher, I. R. Gibbons, T. S. Hays, E. L. Holzbaur, J. R. McIntosh, M. E. Porter, T. A. Schroer, K. T. Vaughan, G. B. Witman, S. M. King and R. B. Vallee (2005). "Cytoplasmic dynein nomenclature." J Cell Biol **171**(3): 411-3.
- Porter, M. E., R. Bower, J. A. Knott, P. Byrd and W. Dentler (1999). "Cytoplasmic dynein heavy chain 1b is required for flagellar assembly in *Chlamydomonas*." Mol Biol Cell **10**(3): 693-712.
- Puls, I., C. Jonnakuty, B. H. LaMonte, E. L. Holzbaur, M. Tokito, E. Mann, M. K. Floeter, K. Bidus, D. Drayna, S. J. Oh, R. H. Brown, Jr., C. L. Ludlow and K. H. Fischbeck (2003). "Mutant dynactin in motor neuron disease." Nat Genet **33**(4): 455-6.
- Reaume, A. G., J. L. Elliott, E. K. Hoffman, N. W. Kowall, R. J. Ferrante, D. F. Siwek, H. M. Wilcox, D. G. Flood, M. F. Beal, R. H. Brown, Jr., R. W. Scott and W. D. Snider (1996). "Motor neurons in Cu/Zn superoxide dismutase-deficient mice develop normally but exhibit enhanced cell death after axonal injury." Nat Genet **13**(1): 43-7.
- Reck-Peterson, S. L. and R. D. Vale (2004). "Molecular dissection of the roles of nucleotide binding and hydrolysis in dynein's AAA domains in *Saccharomyces cerevisiae*." Proc Natl Acad Sci U S A **101**(39): 14305.
- Reiner, O., R. Carrozzo, Y. Shen, M. Wehnert, F. Faustinella, W. B. Dobyns, C. T. Caskey and D. H. Ledbetter (1993). "Isolation of a Miller-Dieker lissencephaly gene containing G protein beta-subunit-like repeats." Nature **364**(6439): 717-21.
- Roberts, A. J., N. Numata, M. L. Walker, Y. S. Kato, B. Malkova, T. Kon, R. Ohkura, F. Arisaka, P. J. Knight, K. Sutoh and S. A. Burgess (2009). "AAA+ Ring and linker swing mechanism in the dynein motor." Cell **136**(3): 485-95.
- Rosen, D. R., T. Siddique, D. Patterson, D. A. Figlewicz, P. Sapp, A. Hentati, D. Donaldson, J. Goto, J. P. O'Regan, H. X. Deng and et al. (1993). "Mutations in Cu/Zn superoxide dismutase gene are associated with familial amyotrophic lateral sclerosis." Nature **362**(6415): 59-62.
- Ross, J. L., K. Wallace, H. Shuman, Y. E. Goldman and E. L. Holzbaur (2006). "Processive bidirectional motion of dynein-dynactin complexes in vitro." Nat Cell Biol **8**(6): 562-70.
- Santel, A. and S. Frank (2008). "Shaping mitochondria: The complex posttranslational regulation of the mitochondrial fission protein DRP1." IUBMB Life **60**(7): 448-55.
- Sasaki, S., A. Shionoya, M. Ishida, M. J. Gambello, J. Yingling, A. Wynshaw-Boris and S. Hirotsune (2000). "A LIS1/NUDEL/cytoplasmic dynein heavy chain complex in the developing and adult nervous system." Neuron **28**(3): 681-96.

- Sbalzarini, I. F. and P. Koumoutsakos (2005). "Feature point tracking and trajectory analysis for video imaging in cell biology." J Struct Biol **151**(2): 182-95.
- Schroer, T. A. (2004). "Dynactin." Annu Rev Cell Dev Biol **20**: 759-79.
- Schwarzer, C., S. Barnikol-Watanabe, F. P. Thinner and N. Hilschmann (2002). "Voltage-dependent anion-selective channel (VDAC) interacts with the dynein light chain Tctex1 and the heat-shock protein PBP74." Int J Biochem Cell Biol **34**(9): 1059-70.
- Shah, P. R., A. Ahmad-Annuar, K. R. Ahmadi, C. Russ, P. C. Sapp, H. R. Horvitz, R. H. Brown, Jr., D. B. Goldstein and E. M. Fisher (2006). "No association of DYNC1H1 with sporadic ALS in a case-control study of a northern European derived population: a tagging SNP approach." Amyotroph Lateral Scler **7**(1): 46-56.
- Shaw, P. J. (2001). "Genetic inroads in familial ALS." Nat Genet **29**(2): 103-4.
- Shimizu, T., Y. Y. Toyoshima, M. Edamatsu and R. D. Vale (1995). "Comparison of the motile and enzymatic properties of two microtubule minus-end-directed motors, ncd and cytoplasmic dynein." Biochemistry **34**(5): 1575-82.
- Short, B., C. Preisinger, J. Schaletzky, R. Kopajtich and F. A. Barr (2002). "The Rab6 GTPase regulates recruitment of the dynactin complex to Golgi membranes." Curr Biol **12**(20): 1792-5.
- Silvanovich, A., M. G. Li, M. Serr, S. Mische and T. S. Hays (2003). "The third P-loop domain in cytoplasmic dynein heavy chain is essential for dynein motor function and ATP-sensitive microtubule binding." Mol Biol Cell **14**(4): 1355-65.
- Splitt, M. P., J. Burn and J. Goodship (1996). "Defects in the determination of left-right asymmetry." J Med Genet **33**(6): 498-503.
- Starr, D. A., B. C. Williams, T. S. Hays and M. L. Goldberg (1998). "ZW10 helps recruit dynactin and dynein to the kinetochore." J Cell Biol **142**(3): 763-74.
- Stehman, S. A., Y. Chen, R. J. McKenney and R. B. Vallee (2007). "NudE and NudEL are required for mitotic progression and are involved in dynein recruitment to kinetochores." J Cell Biol **178**(4): 583-94.
- Suen, D. F., K. L. Norris and R. J. Youle (2008). "Mitochondrial dynamics and apoptosis." Genes Dev **22**(12): 1577-90.
- Supp, D. M., M. Brueckner, M. R. Kuehn, D. P. Witte, L. A. Lowe, J. McGrath, J. Corrales and S. S. Potter (1999). "Targeted deletion of the ATP binding domain of left-right dynein confirms its role in specifying development of left-right asymmetries." Development **126**(23): 5495-504.

- Taub, N., D. Teis, H. L. Ebner, M. W. Hess and L. A. Huber (2007). "Late endosomal traffic of the epidermal growth factor receptor ensures spatial and temporal fidelity of mitogen-activated protein kinase signaling." Mol Biol Cell **18**(12): 4698-710.
- Teuchert, M., D. Fischer, B. Schwalenstoecker, H. J. Habisch, T. M. Bockers and A. C. Ludolph (2006). "A dynein mutation attenuates motor neuron degeneration in SOD1(G93A) mice." Exp Neurol **198**(1): 271-4.
- Turner, B. J. and K. Talbot (2008). "Transgenics, toxicity and therapeutics in rodent models of mutant SOD1-mediated familial ALS." Prog Neurobiol **85**(1): 94-134.
- Tynan, S. H., M. A. Gee and R. B. Vallee (2000). "Distinct but overlapping sites within the cytoplasmic dynein heavy chain for dimerization and for intermediate chain and light intermediate chain binding." J Biol Chem **275**(42): 32769-74.
- Vaisberg, E. A., P. M. Grissom and J. R. McIntosh (1996). "Mammalian cells express three distinct dynein heavy chains that are localized to different cytoplasmic organelles." J Cell Biol **133**(4): 831-42.
- Vale, R. D. (2003). "The molecular motor toolbox for intracellular transport." Cell **112**(4): 467-80.
- Vallee, R. B. and P. Hook (2006). "Autoinhibitory and other autoregulatory elements within the dynein motor domain." J Struct Biol **156**(1): 175-81.
- Varadi, A., L. I. Johnson-Cadwell, V. Cirulli, Y. Yoon, V. J. Allan and G. A. Rutter (2004). "Cytoplasmic dynein regulates the subcellular distribution of mitochondria by controlling the recruitment of the fission factor dynamin-related protein-1." J Cell Sci **117**(Pt 19): 4389-400.
- Vaughan, K. T. and R. B. Vallee (1995). "Cytoplasmic dynein binds dynactin through a direct interaction between the intermediate chains and p150Glued." J Cell Biol **131**(6 Pt 1): 1507-16.
- Vaughan, P. S., J. D. Leszyk and K. T. Vaughan (2001). "Cytoplasmic dynein intermediate chain phosphorylation regulates binding to dynactin." J Biol Chem **276**(28): 26171-9.
- Vaughan, P. S., P. Miura, M. Henderson, B. Byrne and K. T. Vaughan (2002). "A role for regulated binding of p150(Glued) to microtubule plus ends in organelle transport." J Cell Biol **158**(2): 305-19.
- Waterman-Storer, C. M., S. B. Karki, S. A. Kuznetsov, J. S. Tabb, D. G. Weiss, G. M. Langford and E. L. Holzbaur (1997). "The interaction between cytoplasmic dynein and dynactin is required for fast axonal transport." Proc Natl Acad Sci U S A **94**(22): 12180-5.

- Williamson, T. L. and D. W. Cleveland (1999). "Slowing of axonal transport is a very early event in the toxicity of ALS-linked SOD1 mutants to motor neurons." Nat Neurosci **2**(1): 50-6.
- Woodman, P. G. (2000). "Biogenesis of the sorting endosome: the role of Rab5." Traffic **1**(9): 695-701.
- Yamada, M., S. Toba, Y. Yoshida, K. Haratani, D. Mori, Y. Yano, Y. Mimori-Kiyosue, T. Nakamura, K. Itoh, S. Fushiki, M. Setou, A. Wynshaw-Boris, T. Torisawa, Y. Y. Toyoshima and S. Hirotsune (2008). "LIS1 and NDEL1 coordinate the plus-end-directed transport of cytoplasmic dynein." Embo J **27**(19): 2471-83.

PUBLICATIONS

## The Legs at odd angles (*Loa*) Mutation in Cytoplasmic Dynein Ameliorates Mitochondrial Function in SOD1<sup>G93A</sup> Mouse Model for Motor Neuron Disease<sup>✦</sup>

Received for publication, March 31, 2010, and in revised form, April 8, 2010. Published, JBC Papers in Press, April 9, 2010; DOI: 10.1074/jbc.M110.129320

Alli Morsi El-Kadi<sup>1</sup>, Virginie Bros-Facer<sup>3</sup>, Wenhan Deng<sup>1</sup>, Amella Philpott<sup>1</sup>, Eleanor Stoddart<sup>1</sup>, Gareth Banks<sup>1</sup>, Graham S. Jackson<sup>4</sup>, Elizabeth M. C. Fisher<sup>4</sup>, Michael R. Duchon<sup>5</sup>, Linda Greensmith<sup>6</sup>, Anthony L. Moore<sup>2</sup>, and Majid Hafezparast<sup>1</sup>

From the <sup>1</sup>Biochemistry and Biomedical Science, School of Life Sciences, University of Sussex, Brighton BN1 9QG, the <sup>2</sup>Sobell Department of Motor Neuroscience and Movement Disorders and the <sup>3</sup>Department of Neurodegenerative Disease, UCL Institute of Neurology, London WC1N 3BG, and the <sup>4</sup>Cell and Developmental Biology, UCL Division of Biosciences, London WC1B 6BT, United Kingdom

Amyotrophic lateral sclerosis (ALS) is a debilitating and fatal late-onset neurodegenerative disease. Familial cases of ALS (FALS) constitute ~10% of all ALS cases, and mutant superoxide dismutase 1 (SOD1) is found in 15–20% of FALS. SOD1 mutations confer a toxic gain of unknown function to the protein that specifically targets the motor neurons in the cortex and the spinal cord. We have previously shown that the autosomal dominant *Legs at odd angles* (*Loa*) mutation in cytoplasmic dynein heavy chain (*Dync1h1*) delays disease onset and extends the life span of transgenic mice harboring human mutant SOD1<sup>G93A</sup>. In this study we provide evidence that despite the lack of direct interactions between mutant SOD1 and either mutant or wild-type cytoplasmic dynein, the *Loa* mutation confers significant reductions in the amount of mutant SOD1 protein in the mitochondrial matrix. Moreover, we show that the *Loa* mutation ameliorates defects in mitochondrial respiration and membrane potential observed in SOD1<sup>G93A</sup> motor neuron mitochondria. These data suggest that the *Loa* mutation reduces the vulnerability of mitochondria to the toxic effects of mutant SOD1, leading to improved mitochondrial function in SOD1<sup>G93A</sup> motor neurons.

targets motor neurons in the cortex, brainstem, and the anterior horn of the spinal cord, leading to paralysis and eventually death, typically within 5 years of diagnosis (1–5). The majority of ALS cases are sporadic, and ~10% are familial, although the etiology of ALS is largely unknown. Between 15 to 20% of familial ALS and ~1% of sporadic ALS are caused by dominant gain-of-toxic function mutations in the gene coding for Cu,Zn superoxide dismutase 1 (SOD1) (6–8).

Transgenic mice overexpressing mutant forms of human SOD1 have been invaluable in providing insights into the pathogenesis of ALS and in highlighting the cellular functions that are targeted in the disease (for reviews, see Refs 9 and 10). Formation of intracellular protein aggregates in motor neurons is a common characteristic of all ALS cases and is also observed in SOD1 transgenic mouse models. Biochemical and immunohistochemical studies have shown that SOD1 and ubiquitin aggregates are present in SOD1-mediated familial ALS cases and their transgenic mouse models and that TDP-43 and ubiquitin aggregates are seen in most ALS inclusions, including sporadic ALS (3, 10–12).

Mutant SOD1-mediated motor neuron death is thought to be due to a gain of aberrant chemistry in copper and zinc active sites, making them highly reactive with subsequent damage to other proteins, but Wang *et al.* (13) showed that mutant SOD1 proteins with significantly reduced affinity to copper, but with propensity to aggregation, induced disease similar to those variants that stably bind copper. However, mutant SOD1 toxicity could be the result of toxicity of the intracellular aggregates through aberrant chemistry, sequestration of other proteins into the aggregates, proteasome overload, and damage to specific organelles such as mitochondria (3, 14).

In addition, impaired axonal transport has been highlighted in motor neuron death in ALS, and we and others have shown that axonal transport defects are one of the earliest pathological events observed in motor neurons of mutant SOD1 transgenic mice (15–20). Furthermore, *in vivo* experiments involving injection of a neurotracer have shown that transport from muscle to motor neurons is impaired in SOD1<sup>G93A</sup> mice and that there is an association of dynein with mutant SOD1 aggregates in the motor neurons of these mice (21). Two recent studies have reported that there is a direct “gain-of-interaction”

Amyotrophic lateral sclerosis (ALS)<sup>2</sup> is a debilitating late-onset, progressive form of motor neuron disease that primarily

<sup>1</sup> This work was supported by the Medical Research Council (to M. H., A. M. E.-K., and E. S.), the Biotechnology and Biological Sciences Research Council (to M. H., W. D., and A. L. M.), the Amyotrophic Lateral Sclerosis Association and Robert Packard Center for ALS Research at Johns Hopkins (to M. H., L. G., E. M. C. F., and V. B.-F.), the Brain Research Trust (to L. G.), The Wellcome Trust (to G. S. J. and E. M. C. F.), and the University of Sussex (to A. P.).

<sup>2</sup> Author's Choice—Final version full access.

<sup>3</sup> The on-line version of this article (available at <http://www.jbc.org>) contains supplemental Figs. 1–10.

<sup>4</sup> To whom correspondence should be addressed. Tel.: 44-1273-678214; Fax: 44-1273-872663; E-mail: m.hafezparast@sussex.ac.uk.

<sup>5</sup> The abbreviations used are: ALS, amyotrophic lateral sclerosis; SOD1, Cu,Zn superoxide dismutase 1; Dync1h1 and DHC, cytoplasmic dynein heavy chain 1; DIC, dynein intermediate chain; p150, dynein p150<sup>Gluc</sup>; *Loa*, *Legs at odd angles*; TGN38, trans-Golgi network 38; HB, homogenization buffer; IP, immunoprecipitation; BDG, buoyant density gradient; PK, proteinase K; IMS, intermembrane space; FCCP, cyanide-p-trifluoromethoxyphenylhydrazone; TMRM, tetramethylrhodamine methyl ester perchlorate; GST, glutathione S-transferase; ER, endoplasmic reticulum; TWS, tissue wash buffer; RIPA buffer, radioimmune precipitation assay buffer; MOPS, 4-morpholinopropanesulfonic acid; PBS, phosphate-buffered saline.

### Cytoplasmic Dynein Mutation Rescues Mitochondrial Defects

between aggregate-prone variants of mutant, but not wild-type, SOD1 (including SOD1<sup>G93A</sup>), and cytoplasmic dynein in glutathione S-transferase (GST) pulldown and immunoprecipitation assays and that disruption of cytoplasmic dynein function abolishes this interaction (22, 23).

Cytoplasmic dynein is a motor protein involved in diverse cellular processes including nuclear movement, positioning of mitotic spindles, Golgi apparatus and endoplasmic reticulum, and retrograde axonal transport of mitochondria and endocytic membranes containing neurotrophic factors in neurons (24–28). This multisubunit protein complex consists of two homodimerized heavy chains, DYNC1H1, here referred to as DHC, and several intermediates (DYNC1I), here referred to as DIC, light intermediates (DYNC1LI), and light (DYNL) chains (25, 29). Dynein function is regulated by another multisubunit protein, dynactin, which through its p150 subunit also plays a significant role as a docking protein for some of the various cargos transported by dynein (30). We have previously shown that an autosomal dominant point mutation causing F580Y substitution in DHC gives rise to a progressive motor deficit in heterozygous *Loa* (*Dync1h1*<sup>Loa/+</sup>) mice (31–33) and that in cultured motor neurons isolated from E13.5 homozygous embryos this mutation impairs retrograde axonal transport leading to motor neuron degeneration and death of the pups within a day after birth (31). In addition, others have shown that the *Loa* mutation causes  $\gamma$ -motor neuron and proprioceptive sensory neuron degeneration in heterozygous *Dync1h1*<sup>Loa/+</sup> mice which is thought to be the cause of the phenotype in these mice (34, 35). Interestingly, when we crossed *Dync1h1*<sup>Loa/+</sup> with SOD1<sup>G93A</sup> mice to investigate a possible link between dynein and mutant SOD1, the SOD1<sup>G93A</sup>;*Dync1h1*<sup>Loa/+</sup> progeny from this cross showed a wild-type phenotype with regard to muscle force, motor unit, and motor neuron survival at 120 days when their SOD1<sup>G93A</sup> littermates exhibited severe defects (17). Moreover, the average lifespan of SOD1<sup>G93A</sup>;*Dync1h1*<sup>Loa/+</sup> mice increased by 28% compared with their SOD1<sup>G93A</sup> littermates ( $p \leq 0.001$ ). In addition, the *Loa* allelic mutation Y1055C in *Dync1h1*<sup>Y1055C/+</sup> mice has also been shown to delay disease onset and increase the life span of SOD1<sup>G93A</sup> mice by 14% (36). Subsequently Chen *et al.* (34) and Ilieva *et al.* (35) replicated these in mice bearing the *Loa* mutation and found increases in life span of 21% ( $p < 0.01$ ) and 9% ( $p = 0.002$ ), respectively.

Both (34) and Ilieva *et al.* (35) also reported significant loss of proprioceptive sensory neurons in *Dync1h1*<sup>Loa/+</sup> mice. The loss of sensory neurons in *Dync1h1*<sup>Loa/+</sup> mice prompted Ilieva *et al.* (35) to propose that the rescue of SOD1<sup>G93A</sup> is a result of reduced glutamate excitotoxicity brought about by the loss of the glutamatergic proprioceptive sensory neurons (35). However, the *Sprawling* (*Dync1h1*<sup>Spr/+</sup>) mouse with a G1040-T1043delinsA mutation in the dynein heavy chain shows even greater proprioceptive sensory neuron loss than the *Loa*, but it is not able to rescue the SOD1<sup>G93A</sup> phenotype (34). Moreover, the W1206R mutation in *Abnormal rear leg* (*Arl*) mouse, which is allelic to *Loa*, confers loss of sensory neuron fibers in the *Dync1h1*<sup>Arl/+</sup> mice, but it has no effect on the disease onset or

life span in the double mutant SOD1<sup>G93A</sup>;*Dync1h1*<sup>Arl/+</sup> mice.<sup>3</sup> These findings, therefore, do not support the hypothesis that the protection of motor neurons in SOD1<sup>G93A</sup>;*Dync1h1*<sup>Loa/+</sup> mice is solely the result of reduced glutamatergic sensory neuron input by the *Loa* mutation.

The above findings do, however, suggest a link between cytoplasmic dynein and SOD1<sup>G93A</sup> toxicity. In this report we present evidence to suggest that the *Loa* mutation in dynein affects the subcellular distribution of mutant SOD1 protein in SOD1<sup>G93A</sup>;*Dync1h1*<sup>Loa/+</sup> mice after, but not before, the onset of the disease. Furthermore, the *Loa* mutation in dynein weakens the association of SOD1<sup>G93A</sup> protein with the mitochondria in the cortex of the brain and spinal cord. We also present data showing severe defects in respiration and membrane potential of SOD1<sup>G93A</sup> mitochondria, which are ameliorated in mitochondria isolated from SOD1<sup>G93A</sup>;*Dync1h1*<sup>Loa/+</sup> mice. In addition, the results of this study show that there is no direct interaction between dynein and SOD1<sup>G93A</sup> and that SOD1<sup>G93A</sup> protein does not disrupt the dynein complex.

#### EXPERIMENTAL PROCEDURES

**Animals and Tissue Collection.**—Congenic heterozygous *Dync1h1*<sup>Loa/+</sup> female mice, maintained on a C57BL/6 (Harlan UK) genetic background, were crossed with male transgenic mice expressing human SOD1<sup>G93A</sup>, maintained on an F1 (SJL x C57BL/6) genetic background, to produce four genetically distinct groups of littermates: *Dync1h1*<sup>+/+</sup>, *Dync1h1*<sup>Loa/+</sup>, heterozygote, SOD1<sup>G93A</sup> hemizygote, and SOD1<sup>G93A</sup>;*Dync1h1*<sup>Loa/+</sup> double-heterozygote (represented in the figures as +/+, *Loa*+, SOD1<sup>G93A</sup>, and SOD1<sup>G93A</sup>/*Loa*, respectively) mice. The SJL mice were purchased from Harlan UK. All mice were identified by genotyping for the *Loa* mutation in the cytoplasmic dynein heavy chain gene *Dync1h1* and the human SOD1 transgene from tail genomic DNA (31, 37). Tissues were harvested from mice at different ages and/or different stages of disease. The early stage was when the mice showed a body weight loss of less than 10% accompanied by shaky hind limbs; the late stage was characterized by a 10–15% reduction in body weight accompanied by an apparent muscle wasting and paralysis of hind limbs; the end stage was when the mice lost their righting reflex and showed 20% reduction of their body weight compared with that before becoming symptomatic. Mice were killed by a schedule I killing, and brains and spinal cords were dissected, washed with appropriate ice-cold buffers, and either used fresh or snap-frozen in liquid nitrogen and stored at –80 °C. All animal experiments were conducted in accord with the UK Animal (Scientific Procedures) Act (1986).

**Chemicals, Reagents, and Antibodies.**—All chemicals and reagents were obtained from Sigma unless otherwise stated. Phosphate-buffered saline (PBS<sup>-Ca-Mg</sup>) was from Invitrogen; RIPA was from Upstate Biotechnology; protein A-Sepharose 4B beads were from Zymed Laboratories Inc.; protein A- and protein B-agarose beads were from Roche Applied Science;

<sup>3</sup>V. Bros-Facser, M. Golding, D. Boërio-Guégan, N. Nirmalanathan, R. Chla, A. Philpott, A. M. Flannick, I. Vukobrodovic, L. R. Osborn, S. L. Adamson, J. Rossant, E. Stoddart, E. M. C. Fibbet, H. Bostock, G. Schlavo, L. Greensmith, and M. Hafzparast, manuscript in preparation.

## Cytosolic Dynein Mutation Rescues Mitochondrial Defects

proteinase K was from New England Biolabs; BS<sup>3</sup> and the BCA protein assay kit were from Pierce. The following antibodies were used in this study: mouse monoclonal anti-dynein intermediate chain 74.1 (generously provided by Dr. K. Pfister, University of Virginia or Santa Cruz, sc-13524), FL-154 rabbit polyclonal anti-SOD1, H-300 rabbit polyclonal anti-dynactin p150<sup>ctd</sup>, R-325 rabbit polyclonal anti-dynein heavy chain, 20-E8 mouse monoclonal anti-Cox4, C-20 goat polyclonal anti-calnexin, C-15 goat polyclonal anti-TGN38, (Santa Cruz Biotechnology, sc-11407, sc-11363, sc-9115, sc-58348, sc-6465, sc-27680, respectively), NCL-SOD1 mouse monoclonal anti-SOD1 (Novo Castra), mouse monoclonal anti-p150<sup>ctd</sup> (BD Transduction Laboratories, 610473), and mouse monoclonal anti- $\alpha$ -tubulin (Upstate Biotechnology, 05-829).

**Immunoprecipitation and Cross-linking**—Homogenization of the mouse brain or spinal cord tissues and immunoprecipitation experiments were carried out after either the procedure we developed in our laboratories (see "Results") or as described elsewhere (22). Brains and spinal cords were homogenized in a range of homogenization buffers (HBs) (see "Results" for details). The homogenates were clarified by centrifugation at  $16,000 \times g$  for 15 min at 4 °C, and their protein contents were determined using the BCA kit. Approximately 2.0 mg of homogenate proteins were cleared by incubation with beads for 1 h with shaking at 4 °C, and the beads then removed by centrifugation. The cleared homogenates were then incubated with a range of different beads (protein G-agarose, protein A-agarose, or protein A-Sepharose 4B beads or TrueBlot<sup>TM</sup> anti-mouse Ig IP beads from eBioscience) linked with anti-DIC, anti-dynactin p150, or anti-SOD1 antibodies or with anti-hemagglutinin antibody or IgG as the negative control for time periods that varied between 3 h to overnight with shaking at 4 °C. The immunoprecipitated complexes on beads were retrieved by brief centrifugation and washed four times with HB and once with water. Protein complexes on beads were resuspended in 1 $\times$  SDS loading buffer, heated for 5 min at 95 °C, and analyzed by SDS-PAGE and Western blotting detecting for DIC, DHC, p150, and SOD1. Chemical cross-linking with BS<sup>3</sup>, the water soluble analogue of disuccinimidyl suberate, was performed according to the manufacturer's recommendations and Zhang *et al.* (22).

**Sucrose Density Gradient Analysis**—A 4.8-ml 5–40% continuous sucrose gradient in PBS<sup>-Ca/Mg</sup> was established overnight at 4 °C in Beckman Ultra-Clear Centrifuge tubes (Beckman, Palo Alto, CA). Brains and spinal cords of *Dync1h1<sup>+/+</sup>*, *Dync1h1<sup>low/+</sup>*, *SOD1<sup>G235A</sup>*, and *SOD1<sup>G235A</sup>;Dync1h1<sup>low/+</sup>* mice at different postnatal stages were homogenized in PBS<sup>-Ca/Mg</sup> containing 0.1% Triton X-100 and protease and phosphatase inhibitors. Homogenates were spun at  $800 \times g$  for 15 min. Protein contents of the supernatants were determined, and the equivalent to 1.5–2 mg of protein of tissue homogenate was layered onto the gradient. After centrifugation at  $237,000 \times g$  in a SW-55 Ti rotor (Beckman) for 4 h at 4 °C, 16 equal-volume fractions were collected, and equal volumes of each fraction were loaded onto 4–12% gradient SDS-PAGE gels and analyzed by immunoblotting.

**Buoyant Density Analysis**—Buoyant density analysis was carried out essentially as described by Vande Velde *et al.* (38).

Briefly, cerebral cortices and spinal cords of late-stage *SOD1<sup>G235A</sup>* and *SOD1<sup>G235A</sup>;Dync1h1<sup>low/+</sup>* mice were collected and washed with PBS<sup>-Ca/Mg</sup> and then placed in an ice-cold HB containing 250 mM sucrose, 10 mM HEPES-NaOH (pH 7.4), 1 mM EDTA plus protease, and phosphatase inhibitors. Tissues were homogenized on ice with seven strokes of a glass-pestle homogenizer. Homogenates were centrifuged at  $1000 \times g$  for 10 min. Supernatants were collected, and the pellets were washed with 0.5 volumes HB and centrifuged again. Supernatants were pooled and centrifuged at  $16,000 \times g$  for 15 min to yield a crude mitochondrial pellet and post-mitochondrial supernatant. Crude mitochondria were gently resuspended in HB and then adjusted to 1.204 g/ml Optiprep (iodixanol) and loaded in the bottom of Beckman Ultra-Clear centrifuge tubes. Crude mitochondria were overlaid with an equal volume of 1.175 g/ml and 1.078 g/ml Optiprep in HB and centrifuged at  $50,000 \times g$  for 4 h in a Beckman SW-55 Ti rotor. During centrifugation, mitochondria along with any proteins tightly associated with them float up to their corresponding buoyant density of 1.13–1.15 g/ml, which bands at the interface between the 1.078- and 1.175-g/ml layers of the gradient. Under these conditions, soluble or aggregated proteins (density 1.26 g/ml) would not be able to break through the density barrier and should sediment downward. After centrifugation the mitochondria-enriched bands were collected and washed once with HB to remove the Optiprep. The protein contents of these fractions were then determined. Samples of the *SOD1<sup>G235A</sup>* and *SOD1<sup>G235A</sup>;Dync1h1<sup>low/+</sup>* cerebral cortex and spinal cord buoyant density gradient (BDG) fractions containing equal amounts of proteins were subjected to treatments with salt, alkali, and digestion with proteinase K in the presence and absence of detergents and then analyzed by SDS-PAGE and immunoblotting.

**Preparation of the Microsomes**—The post-crude mitochondrial supernatant obtained during sample preparation for the buoyant density analysis was used to obtain the microsomal fraction. The pellet (microsomal fraction) obtained after spinning the post-mitochondrial supernatant at  $60,000 \times g$  at 4 °C in the Beckman TL-100 ultracentrifuge was washed once with the HB, and the protein content was determined. Samples of the *SOD1<sup>G235A</sup>* and *SOD1<sup>G235A</sup>;Dync1h1<sup>low/+</sup>* cerebral cortex and spinal cord microsomal fractions containing equal amounts of proteins were subjected to chemical insults with salt and alkali and digestion with proteinase K in the presence and absence of detergents and then analyzed by SDS-PAGE and immunoblotting.

**Treatment with Alkali**—Samples from the BDG fractions and the microsomal fraction were incubated with 0.1 M Na<sub>2</sub>CO<sub>3</sub> (pH 11.5) for 30 min on ice and then centrifuged at  $16,000 \times g$  for 15 min. Supernatants were collected, and pellets were washed once and then resuspended in homogenization buffer. Supernatants and pellets were analyzed by SDS-PAGE and immunoblotting.

**Extraction with High Salt**—Samples from the BDG fractions and the microsomal fraction containing equal amounts of proteins were incubated sequentially in 0.2, 0.5, and 1.0 M KCl for 20 min on ice then centrifuged at  $16,000 \times g$  for 15 min. Pellets

### Cytoplasmic Dynein Mutation Rescues Mitochondrial Defects

were washed once. Pellets and supernatants were analyzed by SDS-PAGE and immunoblotting.

**Treatment with Proteinase K**—Samples from the BDG fractions and the microsomal fraction containing equal amounts of proteins were treated with 100  $\mu$ g/ml proteinase K for 15 min at room temperature in the absence or presence of differing combinations of 0.5–1% Triton X-100 and 1% SDS. Proteinase K was inactivated by adding 10 mM phenylmethylsulfonyl fluoride for 10 min on ice. Digestions were analyzed by SDS-PAGE and immunoblotting.

**Preparation of Mitochondria-enriched Fractions for Polarographic Studies and Measurement of Oxygen Consumption**—Brain cortex and spinal cord tissues were dissected and washed once in ice-cold tissue wash buffer (TWB; 0.3 M mannitol, 20 mM MOPS, 2 mM EDTA (pH 7.5)) then homogenized with a loose pestle in  $\sim$ 1 ml of TWB supplemented with 1% bovine serum albumin and 7 mM L-cysteine hydrochloride monohydrate. Homogenates were centrifuged at  $800 \times g$  for 10 min at 4 °C. The supernatants were transferred into new tubes and centrifuged at  $10,000 \times g$  for 10 min at 4 °C. The pellets were gently resuspended in  $\sim$ 1 ml of TWB supplemented with 1% bovine serum albumin but without L-cysteine and re-centrifuged as above; the pellets (mitochondrial fractions) were then gently resuspended in the minimum amount of TWB supplemented with 1% bovine serum albumin, and protein concentrations were determined.

Oxygen consumption was measured polarographically in a Rank oxygen electrode containing 0.4 ml of 0.3 M mannitol, 10 mM potassium phosphate, 10 mM KCl, 5 mM  $MgCl_2$ , and 10 mM HEPES (pH 7.4). Cytochrome c oxidase activity was determined after the addition of 10 mM sodium ascorbate and 1 mM tetramethyl-*p*-phenylenediamine. Rates are expressed as nmol of  $O_2$   $min^{-1}$   $mg$  of protein $^{-1}$ .

**Subfractionation of the Mitochondria**—Three freshly isolated mouse cortices of each genotype were homogenized and subjected to buoyant density gradient centrifugation to isolate floated mitochondria that were free from protein aggregates, as described above. We then used Pallotti and Lenaz (39) method to fractionate the mitochondria. Briefly, the mitochondria were resuspended in hypotonic 15 mM KCl and allowed to swell for 10 min on ice before centrifugation at  $105,000 \times g$  for 15 min. The supernatants, intermembrane space (IMS) fractions, were kept, and the pellets (mitoplasts) were resuspended in 150 mM KCl followed by incubation on ice for 10 min. The mitoplast suspensions were then subjected to centrifugation at  $105,000 \times g$  for 15 min. The supernatants (S2) were kept, and the mitoplast pellets were then resuspended in 250 mM sucrose and 10 mM Hepes-NaOH (pH 7.4) with 1 mM EDTA plus proteases and phosphatase inhibitors followed by drastic sonication at 150 Watt for a total of 10 min, with 30-s bursts and 30-s off cycles. The sonicated suspensions were then centrifuged at  $26,000 \times g$  for 15 min to remove large particles. The resulting supernatants were pooled and ultracentrifuged at  $152,000 \times g$  for 40 min. The supernatants (matrix fractions) were collected, and the pellets (membrane fractions) were resuspended in the above sucrose buffer and kept frozen at  $-80$  °C for Western blot analysis.

**Primary Motor Neuron Cultures**—Mixed motor neuron cultures were prepared from SOD1<sup>G93A</sup> mice (40). Briefly, embry-

onic spinal cords (E13) were removed, and the ventral horns were isolated. Genotype was determined, and wild type, *Loa*<sup>+</sup>, SOD1<sup>G93A</sup>, or SOD1<sup>G93A</sup>/*Loa* ventral horns were pooled and cultured separately. Motor neurons were seeded at  $2.5 \times 10^4$  cells/cm<sup>2</sup>. Cells were maintained in complete neurobasal medium (supplemented with 2% B-27 supplement, 0.5 mM glutamine, 0.05% mercaptoethanol, and 2% horse serum (all Invitrogen), 0.1 ng/ml glial-derived neurotrophic factor, 0.5 ng/ml ciliary neurotrophic factor, and 0.1 ng/ml brain derived neurotrophic factor (all Caltag, Silverstone, UK), 50 units/ml penicillin, 50  $\mu$ g/ml streptomycin, and 2.5  $\mu$ g/ml amphotericin B (all Sigma)) in a 37 °C, 5% CO<sub>2</sub> humidified incubator for 7 days. Motor neurons were distinguished from interneurons using the following morphological criteria: a cell body diameter  $\geq$ 15  $\mu$ m and the presence of a minimum of three neuritic processes (for details see Bilsland *et al.* (41)).

**Fluorescent Measurement of Mitochondrial Membrane Potential ( $\Delta\Psi_m$ )**—Confocal images were obtained using a Zeiss 510 confocal laser scanning microscope (Oberkochen, Germany) equipped with 40 $\times$  and 63 $\times$  plan-apochromat objective lenses. Cells were loaded with 30 nM tetramethylrhodamine methyl ester (TMRM from Molecular Probes, Paisley, UK) for 30 min and incubated at 37 °C in a HEPES-buffered salt solution (recording medium) composed of 156 mM NaCl, 3 mM KCl, 2 mM  $MgSO_4$ , 1.25 mM  $KH_2PO_4$ , 2 mM  $CaCl_2$ , 10 mM glucose, and 10 mM HEPES (pH 7.35; all Sigma) for the measurement of  $\Delta\Psi_m$ . Fluorescence was excited using the 543 nm laser line, and emitted fluorescence was measured above 560 nm. Measurements were made from a compressed z stack to avoid bias from confocal sampling from a single image plane (41).

**Image Analysis**— $\Delta\Psi_m$  was analyzed using LSM software (Carl Zeiss GmbH in association with EMBL, Heidelberg, Germany). In all experiments the analysis was made by measuring the mean TMRM fluorescence intensity in mitochondria excluding all background signals, so that the signal was not influenced by mitochondrial mass.

**GST Tagging, Bacterial Expression, and GST Pulldown of SOD1**—Wild type SOD1, SOD1<sup>A6V</sup>, SOD1<sup>G93A</sup>, and SOD1<sup>G93A</sup> in the pET28 expression vector (42) were subcloned in-frame into the GST pGEX-4T-1 (Amersham Biosciences) bacterial expression vector using BamHI/XhoI restriction sites. *Escherichia coli* BL21 (DE3) bacteria were transfected with the GST-tagged SOD1 constructs or pGEX-4T-1 vector, and the proteins were expressed by isopropyl 1-thio- $\beta$ -D-galactopyranoside induction (43). After lysing the cells, the expressed GST and GST-tagged SOD1 proteins were purified using S-linked glutathione-agarose beads (Sigma). The captured GST and GST-SOD1 proteins on beads were then incubated with brain homogenate prepared from a non-transgenic C57BL/6 mouse. Beads were then washed 4 times with homogenization buffer then heated in 1 $\times$  SDS sample loading buffer at 95 °C for 5 min. The pull-down assays were then analyzed by SDS-PAGE and Western blotting.

**Statistical Analysis**—We used GraphPad Prism and SigmaStat to analyze our data by two-way analysis of variance followed by Bonferroni post tests, for mitochondrial respiratory function studies, Wilcoxon matched-pairs test, for Western blots, the Mann-Whitney *U* test, Student's *t* test and analysis of variance, for motor neuron studies. Significance was set at  $p < 0.05$ .

## Cytoplasmic Dynein Mutation Rescues Mitochondrial Defects

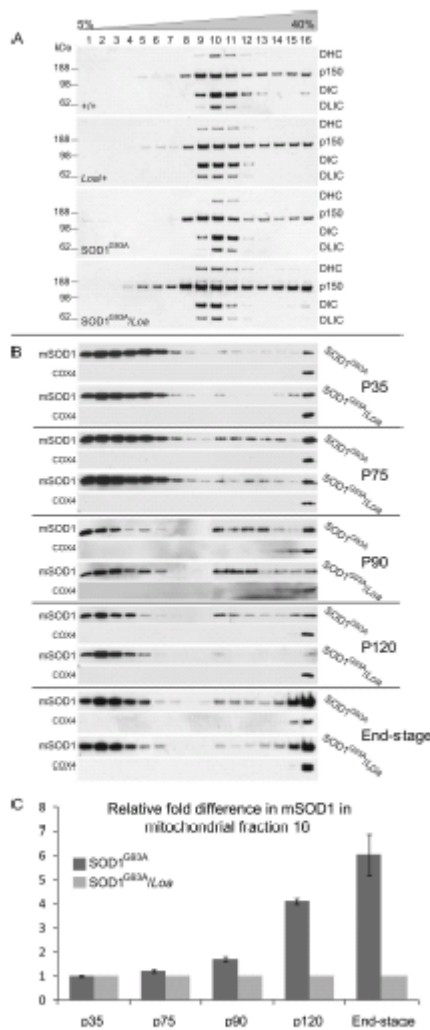


**FIGURE 1.** The integrity and sucrose sedimentation pattern of the dynein complex is not compromised in SOD1<sup>G83A</sup> and SOD1<sup>G83A/Lox</sup>, but the *Lox* mutation in dynein alters the sedimentation of mutant SOD1 in SOD1<sup>G83A/Lox</sup> mice. **A**, Brain homogenates of equal protein contents prepared from +/+, *Lox*/+, SOD1<sup>G83A</sup>, and SOD1<sup>G83A/Lox</sup> mice (at end stage of disease in the SOD1<sup>G83A</sup> and SOD1<sup>G83A/Lox</sup> mice) were sedimented in 5–40% continuous sucrose gradient by centrifugation at 237,000 × g for 4 h at 4 °C as

## RESULTS

**The Integrity and Sucrose Sedimentation Pattern of the Dynein Complex Are Not Compromised in SOD1<sup>G83A</sup> and SOD1<sup>G83A/Lox</sup> Dync1h1<sup>Lox/+</sup> Mice.**—We have previously shown that dynein-mediated retrograde axonal transport is impaired in cultured motor neurons isolated from SOD1<sup>G83A</sup> embryos and that the *Lox* mutation rescues this defect (17). We, therefore, crossed *Dync1h1*<sup>Lox/+</sup> mice with the SOD1<sup>G83A</sup> transgenic mice to generate SOD1<sup>G83A</sup>;*Dync1h1*<sup>Lox/+</sup> double mutants, SOD1<sup>G83A</sup>, *Dync1h1*<sup>Lox/+</sup>, and *Dync1h1*<sup>+/+</sup> progeny and examined whether mutant SOD1 disrupts the dynein complex and, if so, whether the *Lox* mutation confers any resistance to this disruption in SOD1<sup>G83A</sup>;*Dync1h1*<sup>Lox/+</sup> mice, giving rise to delayed disease and extended life span. To investigate this possibility we analyzed the sedimentation of the dynein complex using 5–40% continuous sucrose gradient density sedimentation assays on brain and spinal cord homogenates of late-stage SOD1<sup>G83A</sup> (120 days old) and SOD1<sup>G83A</sup>;*Dync1h1*<sup>Lox/+</sup> (150 days old) and *Dync1h1*<sup>Lox/+</sup> and *Dync1h1*<sup>+/+</sup> at 150 days of age (Fig. 1A).

These data show that the bulk of the dynein complex, represented by DHC, DIC, and dynein light intermediate chain, sediments in fractions 9, 10, and 11 and that their sedimentation patterns in wild-type (+/+) brain matched those of SOD1<sup>G83A</sup> brain, and likewise, the sedimentation patterns of these polypeptides from *Dync1h1*<sup>Lox/+</sup> brain matched those from SOD1<sup>G83A</sup>, *Dync1h1*<sup>Lox/+</sup>. However, we note that there is a slight *Lox*-dependent shift of the dynein complex toward lighter fraction 9 in *Dync1h1*<sup>Lox/+</sup> and SOD1<sup>G83A</sup>;*Dync1h1*<sup>Lox/+</sup>, as evident from DIC and dynein light intermediate chain signals in fractions 11 and 12 versus those in fraction 9 of all the genotypes (Fig. 1A). We will discuss these data further under “Discussion.” As only a subpopulation of the p150 subunit of dynein is associated with the dynein complex, there was a wider sucrose gradient density distribution of this polypeptide, but there were no significantly reproducible differences between the genotypes for p150. Together, these data indicate that the dynein complex in brain and spinal cord of transgenic mice is neither perturbed by the presence of mutant SOD1 nor is it involved in higher molecular weight complexes, such as SOD1<sup>G83A</sup> aggregates.

**The *Lox* Mutation in Dynein Alters the Sedimentation of Mutant SOD1 in SOD1<sup>G83A</sup>;*Dync1h1*<sup>Lox/+</sup> Mice.**—As the mutant SOD1 did not affect the sedimentation pattern of the

described under “Experimental Procedures.” Then 16 equal-volume fractions were collected from top to bottom and analyzed by SDS-PAGE and Western blotting detection for DHC, p150, DIC, and dynein light intermediate chain (DLC) as representatives of the dynein-dynactin complex. **B**, shown are brain homogenates of equal protein contents prepared from SOD1<sup>G83A</sup> and SOD1<sup>G83A/Lox</sup> littermates at the postnatal stages; P35 (before disease onset), P75 (onset of disease), P90 (early stage of disease), P120 (late stage of disease), and end-stage, were sedimented in 5–40% continuous sucrose gradient by centrifugation at 237,000 × g for 4 h at 4 °C as described under “Experimental Procedures.” Then 16 equal-volume fractions were collected from top to bottom and analyzed by SDS-PAGE and Western blotting detection for SOD1 (to avoid overexposure caused by much higher levels of mutant SOD1 (mSOD1) protein in the lighter fractions of the gradient, we loaded 3 μl of fractions 1–3, 8 μl of fractions 5–7, 10 μl of fractions 8–9, and 20 μl of fractions 11–16; supplemental Fig. 3 shows the true representations of equal loadings of the fractions on SDS-PAGE immunoblots). **C**, -fold difference ( $n = 3–6$ ) in mutant SOD1 protein in fraction 16 of the SOD1<sup>G83A</sup> mice was quantified relative to that in SOD1<sup>G83A/Lox</sup> mice using COX4 as the internal control.

### Cytoplasmic Dynein Mutation Rescues Mitochondrial Defects

dynein complex, we decided to look at the effect of mutant dynein on the sedimentation pattern of SOD1<sup>G93A</sup> in brains and spinal cords at P35 (postnatal day 35; before symptom onset), P75 (at symptom onset), P90 (early stage disease), P120 (late stage disease), and end-stage (when both SOD1<sup>G93A</sup> and SOD1<sup>G93A</sup>;Dync1h1<sup>low/+</sup> mice show hind limb paralysis and delayed righting reflex). Fig. 1B shows representative data from brain homogenates and demonstrates that the mutant dynein does not affect the sedimentation of SOD1<sup>G93A</sup> at P35 (i.e. before the onset of the disease). However, at P75, the sedimentation of mutant SOD1 protein in SOD1<sup>G93A</sup> brain homogenate starts to show a different pattern than that from SOD1<sup>G93A</sup>;Dync1h1<sup>low/+</sup> in which the amount of the mutant SOD1 protein sedimented in the denser fractions of the gradient was less than that in the equivalent fractions from SOD1<sup>G93A</sup> brain homogenate. Interestingly, this difference increased as the disease progressed from the early stage toward the end-stage, when the difference was most prominent (see P90, p120, and end-stage in Fig. 1B). It is noteworthy that to avoid overexposure of the films due to significantly more mutant SOD1 in the lighter fractions, we loaded smaller amounts of protein in lanes 1–10 for SDS-PAGE (Fig. 1B).

Quantitative analyses of these data using the mitochondrial marker COX4 as the internal control are shown in Fig. 1C. Similar results were obtained from BDG centrifugation assays (data not shown) and from spinal cords (see supplemental Fig. 1), but the effect was more profound in the brains.

To test that this difference in sedimentation was not due to differences in expression of SOD1<sup>G93A</sup> protein in SOD1<sup>G93A</sup>;Dync1h1<sup>low/+</sup> and SOD1<sup>G93A</sup> or in the protein contents loaded onto the sedimentation columns, various amounts of proteins from the same brain homogenates used for sedimentation experiments were analyzed by SDS-PAGE followed by Western blotting using antibodies against SOD1 and  $\alpha$ -tubulin. As shown in supplemental Fig. 2, the expression levels of SOD1<sup>G93A</sup> protein are almost identical in SOD1<sup>G93A</sup>;Dync1h1<sup>low/+</sup> and SOD1<sup>G93A</sup> brains, as judged by the signal from the loading control protein,  $\alpha$ -tubulin. Together these data suggest that mutant dynein alters the sucrose gradient density distribution of SOD1<sup>G93A</sup>, clearing the protein away from the densest fractions of the gradient. This effect, as shown in Fig. 1, B and C, becomes more evident with the progression of the disease.

**The Loa Mutation Reduces the Amount of Mutant SOD1 in Subcellular Fractions Containing Mitochondria and Endoplasmic Reticulum (ER) Microsomes**—Next, we used more organelle-specific markers to look at the sedimentation patterns of different cell organelles in the above continuous sucrose gradients. As supplemental Fig. 3 shows, the distribution of the trans-Golgi marker TGN38 (type I integral trans-Golgi membrane protein) was confined to the lightest fractions of the gradient (supplemental Fig. 3, lanes 1–4). ER microsomes were spread across most of the gradient as judged by the signal from calnexin (type I integral ER membrane protein), an ER-specific marker (supplemental Fig. 3, lanes 3–16). Detection for Cox4 (an integral inner mitochondrial membrane protein), on the other hand, revealed that the mitochondria were sedimented solely in the densest fractions of the gradient (Fig. 1B and supplemental Fig. 3). The pattern of SOD1<sup>G93A</sup> and the

distribution of the mitochondria and ER in the sucrose gradients suggest that the mitochondria and/or ER could be involved in the effect exerted by Loa on SOD1<sup>G93A</sup> distribution.

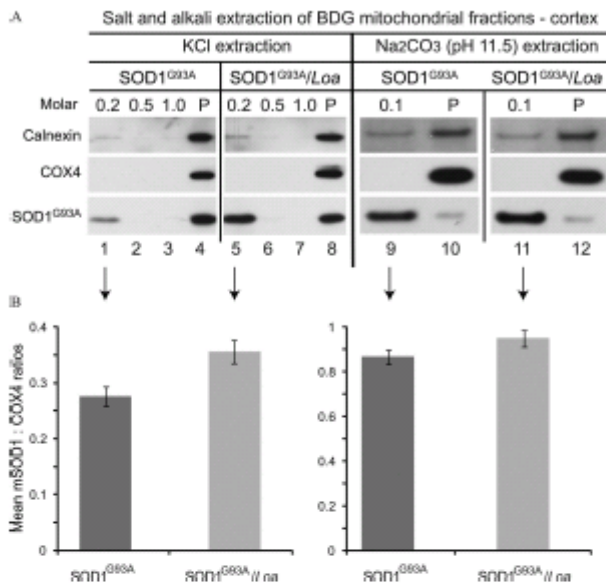
**Effect of the Loa Mutation on the Association of SOD1<sup>G93A</sup> Protein with Mitochondria and ER in the Brain Cortex**—The co-enrichment of mutant SOD1 aggregates with organelles such as mitochondria during fractionation, in which the samples were layered on top of a continuous gradient, has been suggested to be a contamination rather than genuine association of the mutant protein with this organelle (38). Thus, we have used a discontinuous iodixanol BDG centrifugation to circumvent this potential contamination problem. After centrifugation, the enriched floated mitochondrial fractions were collected. The iodixanol was removed, and the protein contents of these fractions and the 60,000  $\times$  g "microsomal" fraction obtained from the post-mitochondrial supernatant (for details, see "Experimental Procedures") were then determined. Subsequently, the association of SOD1<sup>G93A</sup> with the organelles contained in these fractions was tested by subjecting samples of equal protein content from all fractions to salt extraction and alkali treatment. These treatments dissociate mutant SOD1 and other peripheral membrane proteins that form electrostatic or hydrogen bonds with the cytoplasmic face of the mitochondrial outer membrane.

Fig. 2A shows representative results of the sequential salt (KCl) or alkali (Na<sub>2</sub>CO<sub>3</sub>) extractions from the mitochondria-enriched fractions to release the peripheral membrane proteins. These samples, containing equal amounts of protein, were subjected to increasing concentrations of 0.2, 0.5, and 1.0 M KCl or 0.1 M Na<sub>2</sub>CO<sub>3</sub> (pH 11.5). After incubation with each salt or alkali concentration, the samples were centrifuged down to obtain soluble and insoluble fractions. All fractions were then analyzed by SDS-PAGE and Western blotting. The Western blotting analyses in Fig. 2A show positive signals for Cox4 and calnexin (Fig. 2A, lanes 4, 8, 10, and 12), thus indicating the presence of mitochondria as well as the microsomal ER in the mitochondria-enriched fraction of the buoyant density gradient. Moreover, treatment of these membranes with 0.2 M KCl followed by quantification analysis of the signals using COX4 as the internal control revealed that compared with SOD1<sup>G93A</sup> mice, the release of membrane-associated mutant SOD1 protein from SOD1<sup>G93A</sup>;Dync1h1<sup>low/+</sup> brain cortex was significantly higher ( $p = 0.05$ ,  $n = 6$ ) (Fig. 2, A, lanes 1 and 5, and B, left panel). Increasing the salt concentration did not induce further release of SOD1<sup>G93A</sup> from brain cortex in any of the samples (Fig. 2A, lanes 2 and 3 and lanes 6 and 7).

Representative data showing the alkali extraction of SOD1<sup>G93A</sup> are demonstrated in Fig. 2 (right panels). Quantification analysis of these data (Fig. 2B, right panel) showed increased levels of mutant SOD1 released from the membranes of SOD1<sup>G93A</sup>;Dync1h1<sup>low/+</sup> (Fig. 2A, lanes 11 and 12) than from SOD1<sup>G93A</sup> (Fig. 2A, lanes 9 and 10). This increase, however, did not reach statistical significance ( $p = 0.1$ ,  $n = 4$ ).

Thus, the mutant SOD1 protein association with the organelle membranes in the mitochondria-enriched fraction seems to be more sensitive to salt and alkali in the cerebral cortex of SOD1<sup>G93A</sup>;Dync1h1<sup>low/+</sup> compared with that from SOD1<sup>G93A</sup> mice. Moreover, this fraction contains microsomal

## Cytoplasmic Dynein Mutation Rescues Mitochondrial Defects



**FIGURE 2. SOD1<sup>G93A</sup> is less strongly associated with the mitochondria and ER in the brain cortex of SOD1<sup>G93A/Loa</sup> mice.** A, samples containing equal protein amounts of the BDG mitochondrial fractions prepared from brain cortices of SOD1<sup>G93A</sup> and SOD1<sup>G93A/Loa</sup> littermates at the late-stage of disease were sequentially incubated with 0.2, 0.5, and 1.0 M KCl or 0.1 M Na<sub>2</sub>CO<sub>3</sub> (pH 11.5) for 20 or 30 min, respectively, on ice then centrifuged at 16,000 × g for 15 min after each incubation to obtain soluble and insoluble (P) fractions that were then analyzed by SDS-PAGE and Western blotting detection for calnexin, Cox4, and SOD1. B, the amounts of mutant SOD1 released after treatment were quantified (n = 4) using COX4 as the internal control for salt extraction, 0.2 M KCl and 0.1 M Na<sub>2</sub>CO<sub>3</sub>, as indicated by the arrows. Wilcoxon matched-pairs analysis showed that more mutant SOD1 is released from SOD1<sup>G93A/Loa</sup> compared with SOD1<sup>G93A</sup>, reaching statistical significance for salt (p = 0.03), but not for alkali (p = 0.13) extractions.

al-ER as indicated by signals from calnexin (Fig. 2A). Some of calnexin, or at least its cytoplasmic domain, can be seen stripped off the membranes and is, therefore, detected in the soluble fractions (Fig. 2A, lanes 1 and 5 and lanes 9 and 11). It is worth noting that calnexin is a type I integral membrane protein with its COOH terminus exposed on the cytoplasmic side, and the antibody used in these experiments was raised against the cytoplasmic domain, hence, suggesting that the cytoplasmic domain of calnexin might have been cleaved off the membranes by the salt and alkali insults. Together these data suggest that the SOD1<sup>G93A</sup> protein associates with mitochondria and/or microsomes and that the *Loa* mutation weakens this association.

**Organelle-associated SOD1<sup>G93A</sup> Is Largely Protease- and Detergent-resistant.**—The organelle-associated SOD1<sup>G93A</sup> protein in BDG fractions isolated from SOD1<sup>G93A</sup> and SOD1<sup>G93A/Loa</sup>; *Dync1h1*<sup>Loa/+</sup> spinal cord and brain homogenates was also tested for its protease and detergent sensitivity. Supplemental Fig. 4A shows representative data obtained by incubating the mitochondria-enriched fractions of these samples with proteinase K (PK) in

the absence (lanes 1 and 3) or presence (lanes 2 and 4) of 0.5% Triton X-100, which solubilizes the organelle membranes. Incubating the organelles present in this fraction with PK alone did not have any significant effect on SOD1<sup>G93A</sup> protein or organelles as indicated by the presence of signals from mutant SOD1 and the organelle-specific integral membrane proteins calnexin, TGN38, and Cox4 (supplemental Fig. 4A, lanes 1 and 3). However, in the presence of 0.5% Triton X-100, PK digested the organelle specific markers, but it was still unable to digest mutant SOD1 protein (supplemental Fig. 4A, lanes 2 and 4). The presence of Triton X-100 at this concentration was clearly not sufficient to completely solubilize the inner mitochondrial membrane, as some of the Cox4 protein could still be detected in the presence of the detergent (supplemental Fig. 4A, lanes 2 and 4). Moreover, the *Loa* mutation did not appear to have any effect on the PK sensitivity of mutant SOD1 in the presence or absence of 0.5% Triton X-100.

Thus, we analyzed the PK digestion of mitochondrial SOD1<sup>G93A</sup> in two BDG fractions, 1 and 3, of spinal cord by increasing the concentration of Triton X-100 to 1% and adding SDS (1%) to the reaction. Under these conditions the inner mitochondrial membrane was completely dissolved, thereby making the intramitochondrial SOD1<sup>G93A</sup> accessible to PK digestion (supplemental Fig. 4B). As a result, the intramitochondrial SOD1<sup>G93A</sup> protein was largely but not totally digested compared with the reactions without the detergents (supplemental Fig. 4B, lanes 2, 4, 6, and 8). These data show that some PK-sensitive SOD1<sup>G93A</sup> protein is in the matrix or associated with mitochondrial membranes; however, there is still a large proportion of the mutant SOD1 protein, most likely in an aggregated form, that is not degraded by PK. Moreover, we did not detect any difference between SOD1<sup>G93A</sup> and SOD1<sup>G93A/Dync1h1</sup><sup>Loa/+</sup> genotypes in these assays (supplemental Fig. 4B), suggesting that the *Loa* mutation does not alter the nature of mutant SOD1 protein in the mitochondria.

***Loa* Mutation Alters SOD1<sup>G93A</sup> Localization in the Mitochondria.**—To examine the effect of the *Loa* mutation on the redistribution of the mutant SOD1 protein, we focused on the mitochondria. Floated mitochondria were isolated from cerebral cortex of three SOD1<sup>G93A</sup> or SOD1<sup>G93A/Dync1h1</sup><sup>Loa/+</sup> mice and fractionated into IMS, matrix, or membrane fractions, as described under "Experimental Procedures."

## Cytoplasmic Dynein Mutation Rescues Mitochondrial Defects

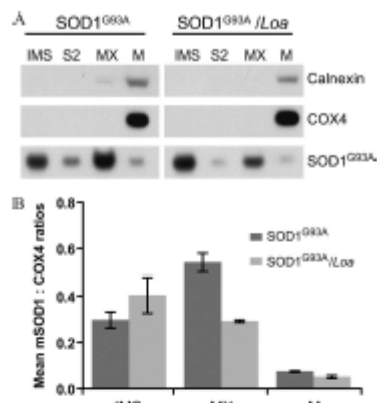


**FIGURE 3.** *Loa* mutation alters the localization of mutant SOD1 in the mitochondria. **A**, suspensions of freshly isolated mitochondria from cerebral cortex of these mice of each genotype were suspended in 0.015 M KCl and allowed to swell for 10 min on ice before centrifugation at  $105,000 \times g$  for 15 min. The supernatants containing mutant SOD1 in the mitochondrial IMS were kept, and the pellets were resuspended in 0.15 M KCl for 10 min on ice followed by centrifugation at  $105,000 \times g$  for 15 min. The supernatants (S2) were kept, and the pellets (mitoplasts) were then resuspended in 0.25 M sucrose and 10 mM Hepes-NaOH (pH 7.4) with 1 mM EDTA plus proteases and phosphatase inhibitors. The mitoplasts were then harshly sonicated with 30-s bursts followed by 30-s off cycles at 150 Watt for a total of 10 min. The sonicated suspension was centrifuged at  $26,000 \times g$  for 15 min to remove large particles. The resulting supernatants containing mitochondrial matrix (MX) were ultracentrifuged at  $152,000 \times g$  for 40 min. The supernatants were collected as matrix (M), and the pellets, membranes (M), were suspended in the above sucrose buffer followed by SDS-PAGE and Western blot analysis. **B**, quantitative analysis ( $n = 3$ ) using COX4 as the internal control and the Wilcoxon matched-pairs test of the mitochondrial subfractions revealed the presence of significantly higher ( $p < 0.02$ ) and lower ( $p = 0.016$ ) levels of mutant SOD1 (mSOD1) in the IMS and matrix, respectively, of SOD1<sup>G93A/Loa</sup> mitochondria compared with those in SOD1<sup>G93A</sup>. The mutant SOD1 associated with the membrane subfractions tended to be higher in the SOD1<sup>G93A</sup>, but it did not reach statistical significance ( $p = 0.25$ ).

As shown in Fig. 3, in SOD1<sup>G93A</sup> mitochondria most of the mutant protein is in the matrix. In contrast, the mutant SOD1 is mainly in the IMS of the SOD1<sup>G93A/Loa</sup> mitochondria (Fig. 3A). Quantitative analysis of these data using COX4 as internal control revealed that the IMS of SOD1<sup>G93A/Loa</sup> contained significantly less mutant protein compared with that in SOD1<sup>G93A</sup> mitochondria ( $p = 0.03$ ,  $n = 3$ ). The matrix and membrane fractions of SOD1<sup>G93A/Loa</sup> mitochondria, however, contained higher levels of the SOD1<sup>G93A</sup> protein, reaching statistical significance for the matrix ( $p = 0.02$  and  $0.25$ , respectively,  $n = 3$ ) (Fig. 3B).

**Mitochondrial Respiration and Membrane Potential Are Severely Impaired in SOD1<sup>G93A</sup> Mice, but They Are Ameliorated in SOD1<sup>G93A/Loa</sup> Mice—Collectively,** the above data suggested differential association of mutant SOD1 with mitochondria from SOD1<sup>G93A/Loa</sup> versus those from SOD1<sup>G93A</sup> mice. Moreover, there is growing evidence that the mitochondrial localization of mutant SOD1 may play an important role in the pathogenesis of ALS (14, 41). Therefore, given the limited amount of the protein in mitochondrial preps

and as cytochrome *c* oxidase (complex IV) activity is a sensitive indicator of mitochondrial function, we assessed mitochondrial function at the cytochrome *c* oxidase level in mitochondrial fractions from brain cortex and spinal cord of the four possible genotypes (wild-type *Dync1h1*<sup>+/+</sup>, heterozygous *Dync1h1*<sup>Loa/+</sup>, hemizygous SOD1<sup>G93A</sup>, and double mutants SOD1<sup>G93A/Loa</sup>; *Dync1h1*<sup>Loa/+</sup>). In these experiments cytochrome *c* oxidase activity was assayed polarographically by measuring oxygen consumption rate in the presence of ascorbate and tetramethyl-*p*-phenylenediamine. Our data indicate that the respiratory rate of the mitochondria from 120-day (late stage) SOD1<sup>G93A</sup> brain is substantially reduced compared with that of their wild-type littermates (gray bars in Fig. 4A).

Interestingly, mitochondrial oxygen consumption in *Dync1h1*<sup>Loa/+</sup> exceeds that of the wild type and it is improved in SOD1<sup>G93A/Loa</sup>; *Dync1h1*<sup>Loa/+</sup> relative to SOD1<sup>G93A</sup> (gray bars in Fig. 4A). The subsequent addition of FCCP to obtain the maximal respiratory activity resulted in significant respiratory stimulations in mitochondria from the wild type, *Dync1h1*<sup>Loa/+</sup>, and SOD1<sup>G93A/Loa</sup>; *Dync1h1*<sup>Loa/+</sup> but not with the SOD1<sup>G93A</sup> mitochondria (black bars in Fig. 4A). Statistical analysis of these data using two-way analysis of variance followed by Bonferroni post tests revealed that the mitochondrial response to FCCP stimulation is not consistent for all genotypes ( $p = 0.012$ , degrees of freedom = 15) and that this stimulatory response is significant in wild type ( $p < 0.001$ ), *Dync1h1*<sup>Loa/+</sup> ( $p < 0.001$ ), and SOD1<sup>G93A/Loa</sup>; *Dync1h1*<sup>Loa/+</sup> ( $p < 0.05$ ) but not in SOD1<sup>G93A</sup> ( $p > 0.05$ ).

These data indicate that in SOD1<sup>G93A</sup> mitochondria cytochrome *c* oxidase activity is impaired and that the *Loa* mutation appears to partially restore this defect. This amelioration of complex IV function by the *Loa* mutation is consistent with our confocal microscopy imaging data obtained from examining the mitochondrial membrane potential in cultured primary motor neurons using TMRM. The data from these assays are shown in Fig. 4B and reveal that, compared with motor neurons from wild-type littermates ( $n = 55$ ), the mitochondrial membrane potential ( $\Delta\Psi_m$ ) in SOD1<sup>G93A</sup> motor neurons ( $n = 54$ ) is significantly depolarized ( $p < 0.0001$ ) and that this defect is ameliorated in motor neurons of SOD1<sup>G93A/Loa</sup>; *Dync1h1*<sup>Loa/+</sup> mice ( $n = 71$ ). In contrast, the  $\Delta\Psi_m$  of *Dync1h1*<sup>Loa/+</sup> motor neurons ( $n = 48$ ) was not significantly different from the  $\Delta\Psi_m$  of wild type motor neurons ( $n = 55$ ).

**Mutant SOD1<sup>G93A</sup> Does Not Show Interactions with Cytoplasmic Dynein in Immunoprecipitation (IP) Assays—**The redistribution of mutant SOD1 protein, the amelioration of mitochondrial function, and the previously observed increased life span and delayed disease onset in SOD1<sup>G93A/Loa</sup>; *Dync1h1*<sup>Loa/+</sup> double mutant mouse strains suggested a possible interaction between components of the dynein complex and SOD1<sup>G93A</sup> protein. We, therefore, analyzed the mutant SOD1 protein and components of the dynein complex in the spinal cord and brain homogenates from SOD1<sup>G93A/Loa</sup>; *Dync1h1*<sup>Loa/+</sup> double mutants, SOD1<sup>G93A</sup>; *Dync1h1*<sup>Loa/+</sup>, and *Dync1h1*<sup>+/+</sup> mice at varying stages of the disease. The interaction between dynein-dynactin and SOD1<sup>G93A</sup> was investigated by IP assays.

Co-IP analysis of the brain homogenate of an end-stage SOD1<sup>G93A</sup> mouse (125 days old) revealed that the polyclonal

## Cytoplasmic Dynein Mutation Rescues Mitochondrial Defects

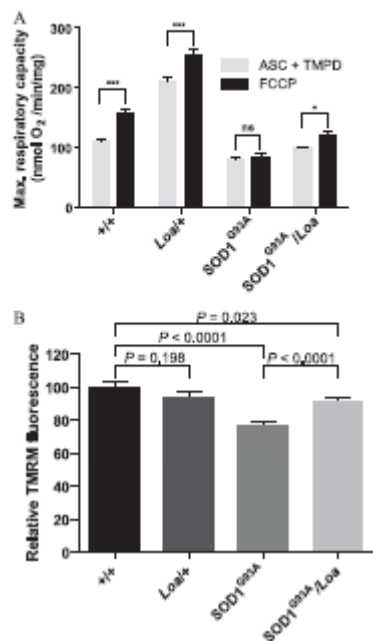


**FIGURE 4.** *Lox* mutation ameliorates defects in oxygen consumption rate and membrane potential of SOD1<sup>G23A</sup> mitochondria. **A**, brain mitochondria were purified from homogenates in TWB buffer supplemented with 1% bovine serum albumin and 7 mM L-cysteine hydrochloride monohydrate as described under "Experimental Procedures." Oxygen consumption rates of mitochondria were measured in an oxygen electrode in the presence of ascorbate (ASC) and tetramethyl-p-phenylenediamine (TMPD; gray bars). Respiration was stimulated by the addition of 1  $\mu$ M FCCP (black bars). As expected, the addition of FCCP significantly stimulated oxygen consumption in +/+ ( $p < 0.001$ ) and *Dync1h1*<sup>+/+</sup> ( $p < 0.001$ ) SOD1<sup>G23A</sup> mitochondria, on the other hand, failed to produce any significant response to FCCP. However, SOD1<sup>G23A</sup>/*Lox* mitochondria showed increased respiration after the addition of FCCP, which was statistically significant ( $p < 0.05$ ). Two-way analysis of variance (degrees of freedom = 15) followed by Bonferroni post tests were used for statistical analysis of these data. ns, not significant; \*,  $p < 0.05$ ; \*\*,  $p < 0.001$ ; \*\*\*,  $p < 0.0001$ . **B**, mitochondria in motor neurons from SOD1<sup>G23A</sup> mice are depolarized, but this effect is abolished in motor neurons of SOD1<sup>G23A</sup>/*Lox* mice. TMRM is a potentiometric indicator with a single delocalized positive charge, and thus, it becomes sequestered in mitochondria as a result of the electrochemical potential gradient that exists between the cytosol and mitochondria. Using TMRM and confocal microscopy, mitochondrial membrane potentials ( $\Delta\psi_m$ ) were measured in cultured motor neurons isolated from E13 embryos of each genotype. The  $\Delta\psi_m$  of SOD1<sup>G23A</sup> motor neurons was 23% lower than the  $\Delta\psi_m$  of motor neurons from wild-type littermates ( $p < 0.001$ ), indicating that mitochondria from SOD1<sup>G23A</sup> motor neurons are depolarized. However, in motor neurons from SOD1<sup>G23A</sup>/*Lox* mice,  $\Delta\psi_m$  was 10% lower ( $p = 0.023$ ) than that in motor neurons of wild-type littermates, indicating that the *Lox* mutation is able to ameliorate the defect in  $\Delta\psi_m$  present in SOD1<sup>G23A</sup> motor neurons.

anti-SOD1 antibody could precipitate only a small amount of the SOD1<sup>G23A</sup> protein, but considerable amounts of p150 and DIC were present in the IP sample (supplemental Fig. 5A, lane 3). On the other hand, neither anti-dynactin p150 nor anti-DIC anti-

body was successful in co-immunoprecipitating SOD1<sup>G23A</sup> from the same brain homogenate (supplemental Fig. 5A, lanes 8 and 13). A weaker signal from DIC and p150 was also found in the negative control IP, in which the brain homogenate was incubated with beads only (supplemental Fig. 5A, lane 4). However, the difference in signal intensities obtained from sample and negative control IPs was big enough to suggest the pull-down may be specific, at least for the p150 (supplemental Fig. 5A, lane 3).

To test this further, the IP experiment was repeated on brain homogenate prepared from another end-stage mouse using mouse monoclonal or rabbit polyclonal anti-SOD1 and mouse monoclonal anti-p150 as IP antibodies. As shown in supplemental Fig. 5B, lanes 4 and 8, only the polyclonal and not the monoclonal anti-SOD1 antibody co-immunoprecipitated p150, suggesting that the interaction of SOD1<sup>G23A</sup> and p150 is not direct and may be in part due to temporal entrapment of p150 protein and possibly other soluble proteins within SOD1<sup>G23A</sup> aggregates. Once again, the anti-p150 antibody was not able to pull down SOD1<sup>G23A</sup> (supplemental Fig. 5B, lane 12).

To verify the specificity of SOD1-DIC interaction observed in supplemental Fig. 5A, we conducted more IP experiments on brain homogenates prepared from several end-stage SOD1<sup>G23A</sup> mice using antibodies against DIC and SOD1. The anti-DIC antibody was only able to specifically co-IP some of the SOD1<sup>G23A</sup> protein with dynein in one mouse brain homogenate (supplemental Fig. 5C, lane 3). On the other hand, when a reciprocal IP was conducted, a mouse monoclonal anti-SOD1 antibody failed to co-IP any dynein along with SOD1<sup>G23A</sup> from the same brain homogenate (supplemental Fig. 5C, lane 5).

Lack of reproducible data for interaction between SOD1<sup>G23A</sup> and dynein prompted us to try a series of different homogenization and binding buffers and conditions. Supplemental Fig. 5D shows that none of these conditions was able to co-IP SOD1 with dynein (lanes 3–5) even when all dynein present in the sample was immunoprecipitated (lane 9).

This lack of dynein and SOD1<sup>G23A</sup> interaction contradicts the report by Zhang *et al.* (22) in which IP assays show a progressive interaction between these two proteins, which correlated with the disease progression in SOD1<sup>G23A</sup> transgenic mice. Thus, we sought to investigate these interactions in brains and spinal cords of end-stage SOD1<sup>G23A</sup> mice when, according to the above report, dynein and SOD1<sup>G23A</sup> interact with high affinity (22).

We used the Zhang *et al.* (22) RIPA buffer for homogenization and binding reactions as well as our IP protocol that utilizes PBS<sup>-Ca<sup>2+</sup>/Mg</sup>. Fig. 5 shows representative data from these assays on brain and spinal cord homogenates from end-stage SOD1<sup>G23A</sup> mice. As shown in Fig. 5A, we successfully pulled down DHC and DIC using the 74.1 antibody against DIC in PBS as homogenization and binding buffer, but no SOD1<sup>G23A</sup> protein could be detected in the pull-down assays (Fig. 5A, lanes 6–9). Likewise, the anti-SOD1 antibody did not IP DHC, DIC, or p150 (Fig. 5A, lanes 2–5). In addition, using the same RIPA buffer and IP antibody and conditions as reported by Zhang *et al.* (22), DHC and DIC were successfully immunoprecipitated, but we did not detect any co-IP of SOD1<sup>G23A</sup> protein with

## Cytosolic Dynein Mutation Rescues Mitochondrial Defects

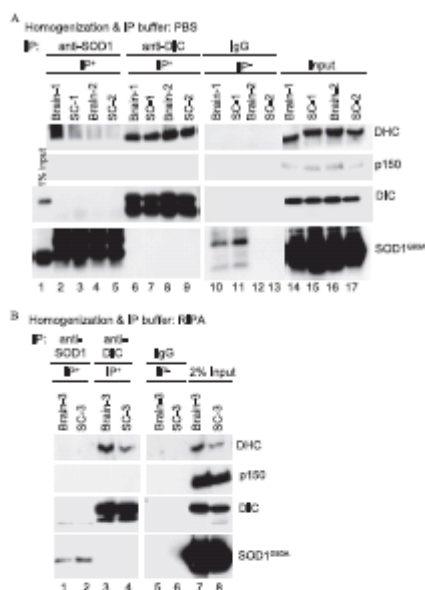


**FIGURE 5. Immunoprecipitation of the dynein-dynactin complex and mutant SOD1 from brains and spinal cords of end-stage SOD1<sup>G93A</sup> mice using two different IP buffers.** Homogenates of brains and spinal cords (SC) from three end-stage transgenic mice (SC-1–3) prepared in PBS without  $\text{Ca}^{2+}$  and  $\text{Mg}^{2+}$  (A) or in RIPA buffer containing 50 mM Tris-HCl (pH 7.4), 150 mM NaCl, 0.25% deoxycholic acid, 1% Nonidet P-40, 1 mM EDTA (B) were incubated with anti-DIC, anti-SOD1 antibody, or with IgG as a negative control, and the IP procedure was conducted as described by Zhang *et al.* (22). The IP products along with 2% of the input were analyzed by SDS-PAGE and Western blotting.

dynein (Fig. 5B, lanes 3 and 4). The anti-SOD1 antibody did not IP DHC, DIC, or p150 in this buffer either (Fig. 5B, lanes 1 and 2). It is noteworthy that the DIC74.1 antibody is currently the most efficient antibody available for IP of the dynein complex, but as its epitope is in the p150 binding domain of DIC, it appears to disrupt dynein-p150 interactions (44–46), and hence, as shown in Fig. 5, this antibody does not efficiently pull down p150.

To ensure that the above lack of interaction between dynein and SOD1<sup>G93A</sup> in our IP experiments is not due to the dissociation of DIC from the dynein complex and to ascertain the oligomerization of mutant SOD1, we analyzed SOD1<sup>G93A</sup> and SOD1<sup>G93A</sup>:Dync1h1<sup>L260/+</sup> brain and spinal cord homogenates prepared in PBS or RIPA buffer in non-denaturing and non-reducing gradient PAGE (4–15%) (supplemental Fig. 6). As shown in the left panel of supplemental Fig. 6, DIC in these samples is part of large molecular weight complexes indicating that the DHC-DIC interactions are intact in these samples. Moreover, SOD1<sup>G93A</sup> shows stretched ladders/smears that are consistent with its tendency to form oligomers and aggregates

(supplemental Fig. 6, right panel). These data clearly show that the methods used to prepare the samples for IP did not affect the complexity of dynein or the heterogeneity of the mutant SOD1 protein.

We also tested the likelihood of interactions between dynein and SOD1<sup>G93A</sup> in the spinal cord of symptomatic (hind limbs paralyzed) against asymptomatic (no apparent muscle wasting or paralysis in the hind limbs) SOD1<sup>G93A</sup> and non-transgenic mice aged 131, 118, and 100 days, respectively. Supplemental Fig. 7 shows representative examples of the data using anti-DIC antibody to pull down the dynein complex from the spinal cord homogenates in RIPA buffer. The anti-DIC antibody efficiently pulled down the dynein complex represented by DIC and DHC in all samples, but no SOD1<sup>G93A</sup> was pulled down, as shown in supplemental Fig. 7, lanes 2, 5, and 8.

**Cross-linking Buffer Causes Disruption of Dynein Complex and Nonspecific Pulldown of Spinal Cord SOD1<sup>G93A</sup> Protein.**—Cross-linking and immunoprecipitation of proteins in cell lysates from SOD1<sup>A4V</sup>-expressing NSC34 motor neuron-like cells has been reported to co-IP DHC with the SOD1<sup>A4V</sup>-containing high molecular weight complexes (22), suggesting a possible transient/weak interaction between mutant SOD1 and dynein that could be stabilized by cross-linking. To test this possibility we cross-linked spinal cord proteins using BS<sup>3</sup> followed by IP with the DIC74.1 antibody and immunoblotting to detect DHC, DIC, and SOD1<sup>G93A</sup> (supplemental Fig. 8A).

Immunoprecipitation was also carried out on spinal cord homogenates prepared for cross-linking but lacking the cross-linker BS<sup>3</sup>, i.e. the cross-linking conditions were met but without including the cross-linker itself. We found that cross-linking had two effects on the IP of the dynein complex. First, the IP of DIC was less efficient from the cross-linked versus the un-cross-linked samples (supplemental Fig. 8A, DIC bands in lanes 2 versus 3; and 5 versus 6). Second, in the cross-linked samples, DHC was not co-immunoprecipitated by anti-DIC antibody (supplemental Fig. 8A, lanes 3 and 6). Moreover, SOD1<sup>G93A</sup> was non-specifically precipitated whether the samples were cross-linked or not, suggesting that the SOD1<sup>G93A</sup> precipitation was solely due to the presence of the cross-linking buffer (supplemental Fig. 8A, lanes 5–7).

This nonspecific pulldown of SOD1<sup>G93A</sup> seems to be intrinsic to the mutant human SOD1 as mouse SOD1 protein was not found in the pulldown of the cross-linked homogenates from non-transgenic mice (supplemental Fig. 8A, lanes 2 and 3). These data indicate that BS<sup>3</sup> cross-linking disrupts DHC-DIC interactions and that the cross-linking buffer used in this assay promotes nonspecific pulldown of SOD1<sup>G93A</sup>. Furthermore, the dissociation of the DHC-DIC complex by cross-linking was independent of the presence of the mutant SOD1 as it also occurred in the samples prepared from non-transgenic mice.

In the above experiments we followed the procedure recommended by Zhang *et al.* (22) in which after incubation of the homogenates with the antibodies for 3 h to overnight, the beads were washed 3 times with the IP buffer. To further test the specificity of the SOD1<sup>G93A</sup> that was co-immunoprecipitated with dynein in the cross-linking buffer (supplemental Fig. 8A), we repeated the above experiments in duplicate; spinal cord homogenates from 100 day old transgenic mice were prepared

## Cytoplasmic Dynein Mutation Rescues Mitochondrial Defects

in cross-linking buffer lacking BS<sup>5</sup>. In one set of the IP samples the beads were washed three times, as recommended by Zhang *et al.* (22), and in the other set they were washed four times instead of three. Supplemental Fig. 8B shows that the non-specifically pulled down SOD1<sup>G93A</sup> in lanes 2 and 3 was completely removed simply by introducing a fourth wash as shown in lanes 5 and 6. These data confirm that IP assays do not detect specific interactions between SOD1<sup>G93A</sup> and dynein.

**Human Wild-type and Different Mutant SOD1-GST Fusion Proteins Do Not Pull Down Dynein in Vitro**—We expressed GST-tagged human wild-type SOD1, SOD1<sup>A4V</sup>, SOD1<sup>G27E</sup>, SOD1<sup>G85S</sup>, and SOD1<sup>G93A</sup> in bacteria for *in vitro* pulldown experiments. After purification, the GST or the GST-SOD1 proteins captured on glutathione-agarose beads were incubated with brain homogenate prepared from a non-transgenic mouse. After washing four times with homogenization buffer, the pulled-down proteins on beads were analyzed by SDS-PAGE and Western blotting, detecting for SOD1 and DIC. In these pulldown experiments neither the wild-type SOD1 (see supplemental Fig. 9, lane 5) nor any of the mutant SOD1 proteins (lanes 6–9) was able to pull down dynein.

**The *Loa* Mutation Does Not Induce Novel Interaction between Dynein and SOD1<sup>G93A</sup>**—To investigate whether the *Loa* mutation promotes any interaction between dynein and SOD1, we tested brain and spinal cord homogenates prepared from SOD1<sup>G93A</sup>, SOD1<sup>G93A</sup>;*Dync1h1*<sup>Loa/+</sup>, *Dync1h1*<sup>Loa/+</sup>, and *Dync1h1*<sup>Loa/+</sup> littermates at a late stage (120 days) of the disease using the IP protocol described by Zhang *et al.* (22). Fig. 6 shows a representative of our IP assays using DIC74.1 antibody for IP of the dynein complex and its associated proteins. As shown in Figs. 6, A and B, lanes 2, 5, 8, and 11), although DIC is successfully pulled down, neither the endogenous mouse SOD1 nor the transgenic mutant SOD1<sup>G93A</sup> co-IP with DIC. Interestingly, we also noted that in some cases SOD1<sup>G93A</sup> protein is pulled down non-specifically in the negative controls containing anti-hemagglutinin antibody only from spinal cord (see lane 9 in Fig. 6A) and to some extent from brain homogenates of the SOD1<sup>G93A</sup> but not SOD1<sup>G93A</sup>;*Dync1h1*<sup>Loa/+</sup> mice.

As our earlier data had shown that the *Loa* mutation in SOD1<sup>G93A</sup>;*Dync1h1*<sup>Loa/+</sup> mice rescued the retrograde axonal transport defect observed in embryonic SOD1<sup>G93A</sup> motor neurons in culture (17), we examined the possibility of a likely interaction between SOD1 and dynein during embryonic development. We tested this possibility at embryonic stage E16.5 in IP assays using brain tissues and an antibody against human SOD1 to pull down the mutant SOD1 and any associated components of the dynein-dynactin complex (supplemental Fig. 10). The anti-SOD1 antibody efficiently pulled down SOD1<sup>G93A</sup> protein from the samples, but DHC, DIC, and p150 were not co-immunoprecipitated with SOD1<sup>G93A</sup> (see supplemental Fig. 10, lanes 12 and 16). Although a faint signal of DHC was observed in IP from the non-transgenic *Dync1h1*<sup>Loa/+</sup> and from SOD1<sup>G93A</sup> homogenates (supplemental Fig. 10, lanes 4 and 12), these were regarded as nonspecific as a similar signal for DHC was also found in the IP from the negative control IP in which the IP antibody was not included (data not shown). Collectively these data indicate that there is no IP-detectable interaction

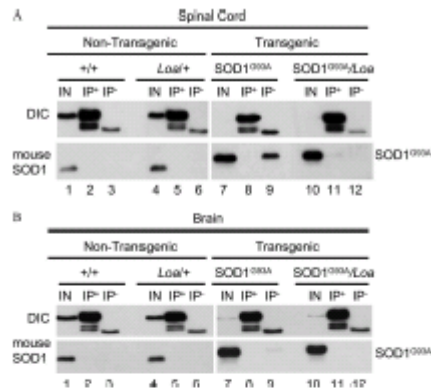


**FIGURE 6. Dynein *Loa* mutation does not induce novel interaction between dynein and SOD1<sup>G93A</sup>.** Spinal cords (A) and brains (B) of 100-day-old mice representing the four different genotypes produced by crossing SOD1<sup>G93A</sup> with *Loa*<sup>+/+</sup> mice were homogenized in lysis buffer then subjected to IP as described (22) using anti-DIC antibody or anti-hemagglutinin antibody as the negative control. The IP products along with 1% or 0.2% of the input (IN) from non-transgenic and transgenic homogenates, respectively, were analyzed by SDS-PAGE and Western blotting.

between SOD1<sup>G93A</sup> and dynein in brain homogenates prepared from E16.5 embryos of the *Dync1h1*<sup>Loa/+</sup> x SOD1<sup>G93A</sup> mouse cross.

## DISCUSSION

Data from studies on conditional transgenic mice with cell-specific expression of mutant SOD1 suggest that motor neuron death in ALS is non-cell autonomous. These studies have shown that the deleterious effects of mutant SOD1 within motor neurons determines disease onset, but it is the expression of mutant SOD1 in astrocytes and microglia that accelerates later disease progression independent of the disease onset (47–50). Therefore, because the *Loa* mutation delays disease onset without changing disease progression, it is possible that the amelioration of the disease induced by the *Loa* mutation occurs at the level of the motor neuron, suggesting that there may be a functional interaction between mutant SOD1<sup>G93A</sup> and the *Loa* mutation within motor neurons.

Moreover, Perlson *et al.* (51) have recently shown that the retrograde trafficking of trophic factors is defective in both *Dync1h1*<sup>Loa/+</sup> and SOD1<sup>G93A</sup> mice, but a significant shift from survival retrograde signaling to stress/death signaling is possibly responsible for the rapid demise of the motor neurons in SOD1<sup>G93A</sup> mice.

The recent proposition (35) that the amelioration of the disease in SOD1<sup>G93A</sup>;*Dync1h1*<sup>Loa/+</sup> mice might be a result of reduced excitotoxicity brought about by the loss of sensory neurons in *Dync1h1*<sup>Loa/+</sup> is unlikely to be the sole explanation, as *Dync1h1*<sup>266/+</sup>, *Dync1h1*<sup>Cma1/+</sup>, and *Dync1h1*<sup>As1/+</sup> mice also show similar or greater sensory neuronal loss but do not ameliorate the SOD1<sup>G93A</sup> disease phenotype.

### Cytoplasmic Dynein Mutation Rescues Mitochondrial Defects

The shift in the sedimentation of the dynein complex to the lighter fractions (Fig. 1A) in sucrose gradient density is only in the presence of the *Loa* mutant dynein. We have also observed this in newborn mice from the *Loa* colony and have examined and confirmed this difference in detail. A manuscript describing these data and the role of the *Loa* mutation in the assembly of the dynein complex is in preparation.

There is mounting evidence that mutant SOD1 protein associates with mitochondria, leading to mitochondrial dysfunction in familial ALS and its rodent transgenic models of familial ALS (Ref. 38; for review, see Manfredi and co-workers (52)). Moreover, it has been shown that mitochondrial respiration is generally impaired in SOD1<sup>G93A</sup> mice (53, 54), and increased levels of mutant SOD1 in mitochondria of transgenic mice appear to adversely affect disease progression (55). In addition, Mattiazzi *et al.* (56) found deficits in complex I, II, III, and IV activities in spinal cord mitochondria from symptomatic SOD1<sup>G93A</sup> mice, and Kirkinetzos *et al.* (57) observed losses in complex IV activity within the brain and spinal cord of paralyzed SOD1<sup>G93A</sup> mice. However, the mechanism by which mitochondrial dysfunction plays a role in the death of motor neurons in SOD1 transgenic mice is not yet fully understood.

It is, therefore, intriguing that, as shown here, decreased levels of mutant SOD1 in the mitochondrial matrix and membranes (Fig. 3) plus a reduction in the association of total mutant SOD1 protein with SOD1<sup>G93A</sup>; *Dync1h1*<sup>Loa/+</sup> mitochondria, compared with those of SOD1<sup>G93A</sup> mice (Fig. 1, B and C), correlates with amelioration of the defects in mitochondrial respiration and membrane potential in these mice. Therefore, the amelioration of disease in SOD1<sup>G93A</sup> mice by the *Loa* mutation could be due to some as yet unknown gain-of-function by mutant cytoplasmic dynein, which is manifested by better equipped mitochondria and possibly ER to resist the toxic effects of mutant SOD1 protein in motor neurons.

Mitochondria are one of many transported cargos whose distribution in the cell body and axons is regulated by retrograde and anterograde motors. Recently, it has been reported that the anterograde mitochondrial transport is defective in motor neurons of SOD1<sup>G93A</sup> mice (20). This defect has been shown to elicit an imbalance in the anterograde and retrograde transport of the mitochondria along motor axons, giving rise to more sparse mitochondrial populations in the axons. Thus, an explanation for the rescue of the SOD1<sup>G93A</sup> phenotype by *Loa* could be the partial restoration of the balance in retrograde and anterograde axonal transport by slowing the retrograde transport of the mitochondria.

The data in the present study together with those from other groups show that mutant SOD1 not only accumulates within the mitochondrial matrix and the intermembrane space but also associates with mitochondrial outer membrane (38). As a result, mutant SOD1 could change mitochondrial structure and membrane composition and render the interaction of the molecular motors with their docking site on the mitochondrial membrane less efficient. By reducing the amount of mutant SOD1 in the mitochondria, as we have shown here, the *Loa* mutation could improve the docking of the molecular motors to the mitochondria, and this could subsequently restore their trafficking.

However, in our earlier studies, using a fluorescently labeled fragment of the tetanus toxin, we have shown that in cultured embryonic motor neurons retrograde transport is also impaired in the SOD1<sup>G93A</sup> motor neurons (17). But in the presence of heterozygous *Loa* mutation the speed of retrograde axonal transport in SOD1<sup>G93A</sup> motor neurons improved dramatically (17). Analyses of the mitochondrial transport in motor neurons of SOD1<sup>G93A</sup>; *Dync1h1*<sup>Loa/+</sup> and SOD1<sup>G93A</sup> are, therefore, required to shed further light on the possible restoration of the balance between the anterograde and retrograde transports in these mice.

Varadi *et al.* (60) show that the disruption of dynein function results in the dissociation of dynamin-related protein (Drp1) from the mitochondrial outer membrane, causing significant morphological changes to the mitochondria and the excessive accumulation of the mitochondria in the perinuclear region of the cells. Drp1 is involved in mitochondrial fission, and it has been shown to interact with dynein-dynactin, suggesting that the delivery of Drp1 to the mitochondrial membrane could be mediated by dynein (58, 59, 60). Our data and the evidence from the Varadi *et al.* study (60) could, therefore, provide a plausible explanation for the improvement in disease phenotype induced in SOD1<sup>G93A</sup> mice by the *Loa* mutation.

The data presented in this paper clearly indicate that, contrary to the conclusion of Zhang *et al.* (22), the interaction between mutant SOD1<sup>G93A</sup> and dynein is not direct or at least is not detectable by immunoprecipitation.

According to Zhang *et al.* (22), there are direct interactions between cytoplasmic dynein and mutant SOD1, but not wild-type SOD1, and that these interactions increase with disease progression. However, analyzing brain and spinal cord tissue homogenates isolated from animals at different stages of the disease and using a range of IP antibodies, buffers, and protocols, including those described by Zhang *et al.* (22), we did not detect any evidence that could conclusively indicate direct interactions between SOD1<sup>G93A</sup> protein and cytoplasmic dynein in SOD1<sup>G93A</sup> or SOD1<sup>G93A</sup>; *Dync1h1*<sup>Loa/+</sup> mice. This is despite ensuring that the dynein complex is intact in our experiments, as tested in native gel and sucrose density gradient sedimentation assays. In fact when we used the cross-linking method used by Zhang *et al.* (22) to show the interaction between dynein and SOD1<sup>A4V</sup>, the cross-linking buffer dissociated dynein heavy chain from the intermediate chain, and more importantly, the cross-linking buffer in the absence of dynein or SOD1 antibody mediated nonspecific pulldown of SOD1<sup>G93A</sup> protein.

In conclusion, our data suggest that mutant dynein in SOD1<sup>G93A</sup>; *Dync1h1*<sup>Loa/+</sup> mice protects motor neurons and delays disease onset at least in part by conferring subtle morphological and structural modifications to the mitochondria, rendering them less prone to association with toxic SOD1<sup>G93A</sup> and consequently resulting in a significant improvement in mitochondrial respiration and the overall function of this vital organelle. Future studies aimed at understanding the underlying molecular mechanisms of the mutant-dynein-mediated protection of the mitochondria from toxic SOD1<sup>G93A</sup> protein and restoration of mitochondrial function in SOD1<sup>G93A</sup>; *Dync1h1*<sup>Loa/+</sup> will be invaluable

## Cytoplasmic Dynein Mutation Rescues Mitochondrial Defects

in elucidating the molecular pathology of ALS, which in turn may highlight novel therapeutic pathways.

**Acknowledgments**—We thank Dr. Kevin Pfister (Dept. of Cell Biology, School of Medicine, University of Virginia) for providing the anti-DIC antibody and the detailed protocol for immunoprecipitating the dynein complex. We also thank Dr. Haining Zhu (Dept. of Molecular and Cellular Biochemistry, University of Kentucky) for providing the detailed protocol for co-immunoprecipitating dynein-SOD1.

## REFERENCES

- Rowland, L. P., and Shneider, N. A. (2001) *N. Engl. J. Med.* 344, 1688–1700
- Brown, R. H., Jr. (1995) *Curr. Opin. Neurobiol.* 5, 841–846
- Bruijn, L. I., Miller, T. M., and Cleveland, D. W. (2004) *Annu. Rev. Neurosci.* 27, 723–740
- Cleveland, D. W., and Rothstein, J. D. (2001) *Nat. Rev. Neurosci.* 2, 806–819
- Shaw, P. J. (1999) *BMJ* 318, 1118–1121
- Deng, H. X., Hentati, A., Timmer, J. A., Iqbal, Z., Cayabyab, A., Hung, W. Y., Getzoff, E. D., Hu, P., Hersfeldt, B., and Ross, R. P. (1998) *Science* 261, 1047–1051
- Rosen, D. R., Siddique, T., Patterson, D., Figlewicz, D. A., Sapp, P., Hentati, A., Donaldson, D., Gotto, J., O'Fallon, J. P., and Deng, H. X. (1993) *Nature* 362, 59–62
- Paiselli, P., and Brown, R. H. (2006) *Nat. Rev. Neurosci.* 7, 710–723
- Shibata, N. (2001) *Neuropathology* 21, 82–92
- Turner, B. J., and Talbot, K. (2008) *Prog. Neurobiol.* 85, 94–134
- Shaw, B. F., and Valentini, J. S. (2007) *Trends Biochem. Sci.* 32, 78–85
- Banks, G. T., Kato, A., Isaacs, A. M., and Fisher, E. M. (2008) *Mamm. Genome* 19, 299–305
- Wang, J., Casiano-Yarman, A., Rodriguez, A., Scheurmann, J. P., Slunt, H. H., Cao, X., Griffin, J., Hart, P. J., and Borchelt, D. R. (2007) *J. Biol. Chem.* 282, 345–352
- Manfredi, G., and Xu, Z. (2005) *Mitochondrion* 5, 77–87
- Bressan, A. C., Lynn, M. P., Atkinson, M. B., Chou, S. M., Wilborn, A. J., Marks, K. E., Calver, J. E., and Flogler, E. J. (1987) *Neurology* 37, 738–748
- Jablonska, S., Witos, S., and Sendtner, M. (2004) *J. Neurobiol.* 58, 272–286
- Kieran, D., Hafnerparast, M., Bohner, S., Dick, J. R., Martin, J., Schiavo, G., Fisher, E. M., and GreenSmith, L. (2005) *J. Cell Biol.* 169, 561–567
- Rao, M. V., and Nixon, R. A. (2003) *Neurochem. Res.* 28, 1041–1047
- Williamson, T. L., and Cleveland, D. W. (1999) *Nat. Neurosci.* 2, 50–56
- De Vos, K. J., Chapman, A. L., Tennant, M. E., Manser, C., Tudor, E. L., Lau, K. F., Brownlee, L., Ackerley, S., Shaw, P. J., McLoughlin, D. M., Shaw, C. E., Leigh, P. N., Miller, C. C., and Grierson, A. J. (2007) *Hum. Mol. Genet.* 16, 2720–2728
- Ligon, L. A., LaMonte, B. H., Wallace, K. E., Weber, N., Kalb, R. G., and Holzbaur, E. L. (2005) *Neuroreport* 16, 533–536
- Zhang, F., Ström, A. L., Fukuda, K., Lee, S., Hayward, L. J., and Zhu, H. (2007) *J. Biol. Chem.* 282, 16691–16699
- Ström, A. L., Shi, P., Zhang, F., Gai, J., Kirby, R., Hayward, L. J., and Zhu, H. (2008) *J. Biol. Chem.* 283, 22795–22805
- King, S. M. (2000) *Biochim. Biophys. Acta* 1496, 60–75
- Pfister, K. K., Shah, P. R., Hummerich, H., Basso, A., Cotton, J., Anwar, A. A., King, S. M., and Fisher, E. M. (2006) *PLoS Genet* 2, e1
- Vale, R. D. (2005) *Cell* 112, 467–480
- Vilios, R. B., Williams, J. C., Varma, D., and Barnhart, L. E. (2004) *J. Neurobiol.* 58, 189–200
- Yano, H., Lee, F. S., Kong, H., Chuang, J., Aronava, J., Perez, P., Sung, C., and Chan, M. V. (2001) *J. Neurosci.* 21, RC125
- Pfister, K. K., Fisher, E. M., Gibbons, I. R., Hays, T. S., Holzbaur, E. L., McIntosh, J. R., Porter, M. E., Schroter, T. A., Vaughan, K. T., Witman, G. B., King, S. M., and Vallee, R. B. (2005) *J. Cell Biol.* 171, 411–413
- Schmer, T. A. (2004) *Annu. Rev. Cell Dev. Biol.* 20, 759–779
- Hafnerparast, M., Kloke, R., Fuhrberg, C., Marquardt, A., Ahmad-Annuar, A., Bowen, S., Lall, G., Witherden, A. S., Hummerich, H., Nicholson, S., Morgan, P. J., Oezguer, R., Priestley, J. V., Averill, S., King, V. R., Ball, S., Peters, J., Toda, T., Yamamoto, A., Hirakawa, Y., Augustin, M., Korthaus, D., Watzler, S., Walnitz, P., Dickmeis, C., Lampel, S., Boehme, F., Peraus, G., Popp, A., Rudolph, M., Schlegel, J., Fuchs, H., Hrabec de Angelis, M., Schiavo, G., Shima, D. T., Basso, A. P., Stamm, G., Martin, J. E., and Fisher, E. M. (2005) *Science* 300, 808–812
- Hafnerparast, M., Ahmad-Annuar, A., Wood, N. W., Tahiri, S. J., and Fisher, E. M. (2007) *Lancet Neurol.* 1, 215–224
- Ruggers, D. C., Peters, J., Martin, J. E., Ball, S., Nicholson, S. J., Witherden, A. S., Hafnerparast, M., Latcham, J., Robinson, T. L., Quilter, C. A., and Fisher, E. M. (2001) *Neurosci. Lett.* 306, 89–92
- Chen, X. J., Levoulakou, E. N., Miller, K. J., Wollmann, R. L., Soliven, B., and Popko, B. (2007) *J. Neurosci.* 27, 14515–14524
- Ilieva, H. S., Yamanaka, K., Mallmar, S., Kakinohara, O., Takah, T., Marzala, M., and Cleveland, D. W. (2008) *Proc. Natl. Acad. Sci. U.S.A.* 105, 12599–12604
- Tauchert, M., Fischer, D., Schwakenstorfer, B., Habich, H. J., Böckers, T. M., and Ludolph, A. C. (2006) *Exp. Neurol.* 198, 271–274
- Gurney, M. E., Fu, H., Chiu, A. Y., Dal Canto, M. C., Polchow, C. Y., Alexander, D. D., Caliendo, J., Hentati, A., Kwon, Y. W., and Deng, H. X. (1994) *Science* 264, 1772–1775
- Vande Veldt, C., Miller, T. M., Cashman, N. R., and Cleveland, D. W. (2008) *Proc. Natl. Acad. Sci. U.S.A.* 105, 4022–4027
- Pallotti, F., and Lenaz, G. (2007) *Methods Mol. Biol.* 80, 3–44
- Arcot, V., Garcia, A., de Bovis, B., Filippi, P., Henderson, C., Pettmann, B., and delapierre, O. (1999) *J. Neurosci. Res.* 55, 119–126
- Bilal, L. G., Nirmalanathan, N., Yip, J., GreenSmith, L., and Duchon, M. E. (2008) *J. Neurochem.* 107, 1271–1283
- Stevens, J. C., Chia, R., Hendrick, W. T., Brue-Facer, V., van Minnen, J., Martin, J. E., Jackson, G. S., GreenSmith, L., Schiavo, G., and Fisher, E. M. C. (2010) *PLoS ONE* 5, e9541
- Guan, K. L., and Dixon, J. E. (1991) *Anal. Biochem.* 192, 262–267
- King, S. M., Barbarese, F., Dillman, J. F., 3rd, Patel-King, R. S., Carson, J. H., and Pfister, K. K. (1996) *J. Biol. Chem.* 271, 19368–19366
- Beil, L. B., 2nd, and Pfister, K. K. (2000) *Methods* 22, 307–316
- Pfister, K. K., Benaabadi, S. E., Dillman, J. F., 3rd, Patel-King, R. S., and King, S. M. (1998) *Cell Motil. Cytoskeleton* 41, 154–167
- Boillie, S., Yamanaka, K., Lohsiger, C. S., Copeland, N. G., Jenkins, N. A., Kassiotis, G., Kollias, G., and Cleveland, D. W. (2006) *Science* 312, 1389–1392
- Clement, A. M., Nguyen, M. D., Roberts, E. A., Garcia, M. L., Boillie, S., Rute, M., McMahon, A. P., Doucette, W., Stwek, D., Ferrante, R. J., Brown, R. H., Jr., Julien, J. P., Goldstein, L. S., and Cleveland, D. W. (2003) *Science* 302, 113–117
- Yamanaka, K., Boillie, S., Roberts, E. A., Garcia, M. L., McAlonis-Dennis, M., Mikas, O. R., Cleveland, D. W., and Goldstein, L. S. (2008) *Proc. Natl. Acad. Sci. U.S.A.* 105, 7594–7599
- Yamanaka, K., Chun, S. J., Boillie, S., Fujimori-Tonosu, N., Yamashita, H., Gutmann, D. H., Takahashi, R., Mizuno, H., and Cleveland, D. W. (2008) *Nat. Neurosci.* 11, 251–253
- Perbon, E., Jeong, G. B., Ross, J. L., Dick, R., Wallace, K. E., Kalb, R. G., and Holzbaur, E. L. (2009) *J. Neurosci.* 29, 9903–9917
- Hervias, L., Beal, M. F., and Manfredi, G. (2006) *Muscle Nerve* 33, 598–608
- Browne, S. E., Bowling, A. C., Baik, M. J., Gurney, M., Brown, R. H., Jr., and Beal, M. F. (1998) *J. Neurochem.* 71, 281–287
- Martin, J. J., Liu, Z., Chen, K., Price, A. C., Pan, Y., Swaby, J. A., and Golden, W. C. (2007) *J. Comp. Neurol.* 500, 20–46
- Deng, H. X., Shi, Y., Furukawa, Y., Zhu, H., Fu, R., Liu, E., Gorrie, G. H., Khan, M. S., Hung, W. Y., Bigio, E. H., Lukacs, T., Dal Canto, M. C., O'Halloran, T. V., and Siddique, T. (2006) *Proc. Natl. Acad. Sci. U.S.A.* 103, 7142–7147
- Mattiazzi, M., D'Aurelio, M., Gajewski, C. D., Martushova, K., Kiasi, M., Beal, M. F., and Manfredi, G. (2002) *J. Biol. Chem.* 277, 29626–29633
- Kirkinezos, I. G., Bacman, S. R., Hernandez, D., Oca-Cossio, J., Arias, L. J., Perez-Pinzon, M. A., Bradley, W. G., and Moraes, C. T. (2005) *J. Neurosci.* 25, 164–172
- Karbowsky, M., and Yuste, R. J. (2003) *Cell Death Differ.* 10, 870–880
- Smirnova, E., Geiparic, L., Sturland, D. L., and van der Bliek, A. M. (2001) *Mol. Biol. Cell* 12, 2245–2256
- Varadi, A., Johnson-Cadwell, L. I., Cirilli, V., Yoon, Y., Allan, V. J., and Rutter, G. A. (2004) *J. Cell Sci.* 117, 4389–4400



## Behavioral and Other Phenotypes in a Cytoplasmic Dynein Light Intermediate Chain 1 Mutant Mouse

Gareth T. Banks,<sup>1\*</sup> Matilda A. Haas,<sup>2\*</sup> Samantha Line,<sup>6</sup> Hazel L. Shepherd,<sup>6</sup> Mona AlQatari,<sup>7</sup> Sammy Stewart,<sup>7</sup> Ida Rishal,<sup>8</sup> Amella Philpott,<sup>9</sup> Bernadett Kalmar,<sup>2</sup> Anna Kuta,<sup>1</sup> Michael Groves,<sup>3</sup> Nicholas Parkinson,<sup>1</sup> Abraham Acevedo-Arozena,<sup>10</sup> Sebastian Brandner,<sup>3,4</sup> David Bannerman,<sup>6</sup> Linda Greensmith,<sup>2,4</sup> Majid Hafezparast,<sup>7</sup> Martin Koltzenburg,<sup>2,4,7</sup> Robert Deacon,<sup>6</sup> Mike Fainzilber,<sup>8</sup> and Elizabeth M. C. Fisher<sup>1,4</sup>

<sup>1</sup>Department of Neurodegenerative Disease, <sup>2</sup>Sobell Department of Motor Science and Movement Disorders, <sup>3</sup>Division of Neuropathology, and <sup>4</sup>Medical Research Council (MRC) Centre for Neuromuscular Diseases, University College London (UCL) Institute of Neurology, London WC1N 3BG, United Kingdom, <sup>5</sup>MRC National Institute for Medical Research, London NW7 1AA, United Kingdom, <sup>6</sup>Department of Experimental Psychology, University of Oxford, Oxford OX1 3UD, United Kingdom, <sup>7</sup>UCL Institute of Child Health, London WC1N 1EH, United Kingdom, <sup>8</sup>Department of Biological Chemistry, Weizmann Institute of Science, 76100 Rehovot, Israel, <sup>9</sup>School of Life Sciences, University of Sussex, Brighton BN1 9QG, United Kingdom, and <sup>10</sup>MRC Mammalian Genetics Unit, Harwell OX11 0RD, United Kingdom

The cytoplasmic dynein complex is fundamentally important to all eukaryotic cells for transporting a variety of essential cargoes along microtubules within the cell. This complex also plays more specialized roles in neurons. The complex consists of 11 types of protein that interact with each other and with external adaptors, regulators and cargoes. Despite the importance of the cytoplasmic dynein complex, we know comparatively little of the roles of each component protein, and in mammals few mutants exist that allow us to explore the effects of defects in dynein-controlled processes in the context of the whole organism. Here we have taken a genotype-driven approach in mouse (*Mus musculus*) to analyze the role of one subunit, the dynein light intermediate chain 1 (*Dync1li1*). We find that, surprisingly, an N235Y point mutation in this protein results in altered neuronal development, as shown from *in vivo* studies in the developing cortex, and analyses of electrophysiological function. Moreover, mutant mice display increased anxiety, thus linking dynein functions to a behavioral phenotype in mammals for the first time. These results demonstrate the important role that dynein-controlled processes play in the correct development and function of the mammalian nervous system.

### Introduction

In mammals cytoplasmic dynein 1 is a large complex of proteins whose constituent members are defined by their molecular weights: the heavy chain (encoded by a single gene *Dync1h1*); the intermediate chains (*Dync1i1*, *Dync1i2*); the light-intermediate chains (*Dync1li1*, *Dync1li2*); the light chains (*Dynl1*, *Dynl3*, *Dynlrb1*, *Dynlrb2*, *Dynlrl1*, *Dynlrl2*) (Pfister et al., 2005, 2006; Hook and Vallee, 2006; Levy and Holzbauer, 2006). The stoichiometry of the intact complex is not known exactly, but at its core lies a homodimer of heavy chains, which binds to microtubules enabling cytoplasmic dynein to move in an ATP-dependent man-

ner (Gennerich et al., 2007). The other subunits are thought to maintain the stability of the complex, to modulate its activity, and to interact with accessory and cargo proteins. However, while it has been established that the individual dynein subunits can have complex cell-specific splicing patterns (Pfister et al., 1996a,b; Salata et al., 2001; Ha et al., 2008; Kuta et al., 2010), we know comparatively little regarding the specific functions of the separate subunits.

One way to study dynein function is to investigate individual genes/protein mutations, however, in mammals the only DYNC1 (cytoplasmic dynein) mutations so far described are four alleles of mouse *Dync1h1*, one of which is a knock-out (Harada et al., 1998; Hafezparast et al., 2003; Chen et al., 2007). The point mutants (all detected in phenotype-driven screens) give highly informative phenotypes compared with those seen in knock-out animals and have uncovered roles that are not detected in null animals (Harada et al., 1998; Hafezparast et al., 2003; Kieran et al., 2005; Chen et al., 2007; Banks and Fisher, 2008; Ilieva et al., 2008; Dugulis et al., 2009).

To further investigate the role of individual dynein subunits, we have used a genetic technique, random chemical mutagenesis, and then taken a genotype-driven approach using a mouse with a point mutation in the dynein light intermediate chain 1, DYNC1LI1. We chose this subunit because it binds important cargoes including pericentrin (Tynan et al., 2000) and Na<sup>+</sup> chan-

Received Oct. 6, 2010; revised Jan. 18, 2011; accepted Jan. 25, 2011.

This work was funded by the Wellcome Trust, UK Medical Research Council and Biotechnology and Biological Sciences Research Council, the BIOXX-IT1 Research and Training Network funded by the European Union, the State Research Trust, Isaac Newton Foundation and Legacy Foundation programs in neurodegenerative research, and the National Alliance for Research on Schizophrenia and Depression. We are grateful to Christiana Rubberg for developmental analysis of embryos and thank Ray Young for graphics. The *Dync1li1*<sup>N235Y</sup> mouse line is freely available via the European Mouse Mutant Archive.

\*G.T.B. and M.A.H. contributed equally.

The authors declare no competing financial interest.

This article is freely available online through the JNeurosci Open Choice option.

Correspondence should be addressed to Elizabeth M. C. Fisher, Department of Neurodegenerative Disease, MRC Centre for Neuromuscular Diseases, 351 Institute of Neurology, London WC1N 3BG, UK. E-mail: e.m.c.fisher@ucl.ac.uk.

DOI:10.1523/JNEUROSCI.2244-10.2011

Copyright © 2011 the authors 0270-6474/11/315483-12\$15.00/0

nels (Zheng et al., 2008), and in *Aspergillus* DYNC1LI1 stabilizes the interaction of heavy and intermediate chains (Zhang et al., 2009). Thus it is likely that dynein light intermediate chains play critical roles within the cell and therefore in the organism as a whole. However, at the time of writing no mammalian model of light intermediate chain dysfunction has been published.

We identified and characterized a mouse carrying a point mutation in *Dync1li1*. We find mutant mice have increased anxiety-like behavior, changes in cortical and peripheral neuronal outgrowth and branching, hypotrophy of sensory neurons and electrophysiological defects and at the cellular level defects in Golgi reassembly and endosome sorting and trafficking. Thus this genotype-driven approach, characterizing a mouse with a relatively subtle point mutation, has revealed a range of unsuspected essential functions dependent on the cytoplasmic dynein complex.

## Materials and Methods

### Animal studies

Wherever possible, all methods were undertaken blind to mouse genotype, which was decoded after the results were collected. The animal studies were performed under guidance issued by the UK Medical Research Council in *Responsibility in the Use of Animals for Medical Research* (1993) and under license from the UK Home Office.

### Heteroduplex screening the MRC Mammalian Genetics Unit ENU DNA archive

The *Dync1li1*<sup>N235Y</sup> mutation arose in an ENU mutagenesis experiment at the MRC Mammalian Genetics Unit, MRC Harwell, UK (Nolan et al., 2000). Briefly, BALB/cAnN male mice are treated with ENU which results in random point mutations in the sperm of these animals. These males are crossed with C3H/HeH females to produce F1 (C3H/HeH × BALB/cAnN) progeny carrying heterozygous random point mutations. Genomic DNAs are archived from F1 (C3H/HeH × BALB/cAnN) males for subsequent screening; sperm samples are archived in parallel for re-derivation of mouse lines. Genomic DNAs from archive were analyzed by heteroduplex analysis following the protocols outlined in (Qiu et al., 2004). Please see supplemental material (available at [www.jneurosci.org](http://www.jneurosci.org)) for primer sequences and complete methodology.

### Re-derivation and genotyping of *Dync1li1*<sup>N235Y</sup> mouse strain

Frozen sperm from the *Dync1li1*<sup>N235Y</sup> mutant F1 male mouse was used for *in vitro* fertilization (IVF) with C57BL/6J females we used 50 two-cell stage embryos for implantation into two pseudo-pregnant C57BL/6J females, resulting in 12 animals, of which 3 females and 1 male were heterozygotes and were used as founders for our *Dync1li1*<sup>N235Y</sup> colony. Subsequently the sex of the *Dync1li1*<sup>N235Y</sup> heterozygote animal used in backcrosses was alternated for each generation so that nuclear, mitochondrial and Y chromosome DNA was all of C57BL/6J origin.

DNA was extracted from mouse tail biopsies using a genomic DNA isolation kit (Promega UK Ltd). Genotyping was performed by allele-specific PCR. Two amplifications were performed per genomic DNA sample: one PCR amplified the wild-type *Dync1li1* allele only (DLC1WT forward: ATCTCTGCGCCCAAGTCC; DLC1WT reverse: AGCACTGGTAGGCCAGATT) generating a fragment of 427 bp. The second PCR amplified the *Dync1li1*<sup>N235Y</sup> allele only (DLC1N235Y forward: TTACCACTGAGCCATCTCTG; DLC1N235Y reverse: AGCACTGGTAGGCCAGGTA) generating a fragment of 440 bp. Both reactions also contained primers to amplify an unrelated DNA fragment of 590 bp from *Dync1l2* (control forward: GTTCACAGCAITTAATTGGCC; control reverse: TGTGACAATGGCAAGTCCAG). PCRs were performed for 35 cycles, annealing temperature 66°C, using MegMix Gold (Microzone) according to the manufacturer's instructions. Products were visualized on a 2% agarose gel. If the control fragment was absent, the reaction was "failed." If the control fragment was present samples in which the wild-type *Dync1li1* allele and not the *Dync1li1*<sup>N235Y</sup> allele amplified were genotyped as *Dync1li1*<sup>+/+</sup>; those with the *Dync1li1*<sup>N235Y</sup> allele and not the wild-type allele were scored as *Dync1li1*<sup>N235Y/N235Y</sup>;

samples in which both the wild-type allele and the *Dync1li1*<sup>N235Y</sup> allele amplified were genotyped as *Dync1li1*<sup>N235Y/+</sup>.

### Behavioral tests

Please see supplemental material (available at [www.jneurosci.org](http://www.jneurosci.org)) for methods for open field behavior, food and water intake, glucose preference, wheel running, accelerating rotarod, modified SHIRPA, spontaneous alternation and water maze.

**Spontaneous locomotor activity.** Spontaneous locomotor activity was assessed in transparent plastic cages with two horizontal photocell beams located along the long axis of each cage, during a single 2 h test session (without habituation to the test cage). Female mice were used only and were placed individually into the activity cages, and the total number of beam breaks made by each mouse was recorded.

**Plus maze.** The plus maze had four arms (each 27.5 × 5.5 cm) arranged in a cross formation: two "closed" arms bordered by 30-cm-high walls and two "open" arms without walls. The maze was elevated 50 cm above the ground and illuminated by bright white light. Female mice were used only and were placed at the distal end of a closed arm and their movements were recorded for 5 min. Behavioral analysis was performed using an automated tracking system (Ethovision XT) which measured the time spent in each region, the number of entries to each region, the latency to enter an open arm and the distance traveled.

**Successive alleys.** The successive alleys apparatus consisted of four increasingly anxiogenic, linearly connected wooden alleys. Each alley was 45 cm in length. The alleys had the following dimensions: alley 1 = 9 cm wide, 29-cm-high walls, painted black; alley 2 = 9 cm wide, 2.5-cm-high walls, painted gray; alley 3 = 6.7 cm wide, 0.5-cm-high walls, painted white; alley 4 = 5 cm wide, 0.3-cm-high walls, painted white. A 2 cm step down led from alley 2 to alley 3, with a further 0.5 cm step down between alleys 3 and 4. The apparatus was elevated 1 m above the floor in a well lit laboratory. Female mice used only and were placed individually at the closed end of Alley 1, facing the wall. Each trial lasted for 300 s, during which time the latency to first enter, the total time spent in, and the number of entries into, each section were recorded.

**Weight lifting.** Strength testing was performed using a set of seven weights of linearly increasing mass. Each mouse was held by the tail, and its forepaws were allowed to grasp a ball of wire mesh to which a weight was attached; female mice were used only. If the mouse lifted this weight for 3 s it was tested on progressively heavier ones. The weight lifting score was calculated from the heaviest weight lifted and the number of seconds for which the weight was held.

**CatWalk.** Female mice were used only and were allowed to walk spontaneously up and down the glass CatWalk walkway while images were collected by a video camera placed below. Three crosses of the walkway were analyzed for each animal and the data averaged. A number of parameters were examined, including footprint sequence, front and hind base of support, regularity, and paw print size, angle and intensity.

### Cortical neuron dendrite analysis

Uterine horns were removed from time-mated heterozygous *Dync1li1*<sup>N235Y/+</sup> mice at embryonic day 15 (E15) under anesthesia (isoflurane, 2.5 L/min). Approximately 0.5 μl of solution containing enhanced green fluorescent protein (GFP)-pCIG2 expression plasmid (2 μg/μl) and Fast Green dye was injected into the lateral ventricle using a microinjection needle (Femtojet, Eppendorf). Electroporation paddles were oriented to target GFP incorporation to neurons eventually populating the PFC. Electroporated embryos were placed back into the mother and allowed to develop normally, until either E17 or postnatal day 15 (P15). Embryos harvested at E17 were used to prepare dissociated cortical neuron cultures, according to established methods (Banker and Goslin, 1998); briefly, dissected cortices were trypsinized (0.125%, Invitrogen), dissociated and plated into the wells of poly-L-lysine (0.01%, Sigma)-coated Labtek chamber slides at a density of 1 × 10<sup>5</sup> cells per chamber. Cultures were maintained in Neurobasal medium with supplements (B-27, Glutamax and penicillin/streptomycin, Invitrogen), until they were fixed at 10 days *in vitro* (DIV) with 4% paraformaldehyde (PFA) and immunolabeled with an antibody to GFP (1:100, Morpho-Sys). Up to 20 GFP-labeled neurons per embryo were imaged using a

DeltaVision microscope and Softworks software. NeuroTrace software was used to trace photographed neurons and analyze dendritic characteristics in wild-type and *Dync1li1<sup>CG2597/CG2597</sup>* neurons. In all cases data were checked for normal distribution using the D'Agostino and Pearson test, then compared for statistical differences using the *t* test or nonparametric Mann–Whitney *U* test.

Alternatively, GFP-expressing mice at P15 were transcardially perfused with 0.9% saline, followed by 4% paraformaldehyde. Brains were removed, postfixed for 1 h in 4% PFA, then vibratome cut coronal sections (100  $\mu$ m) were imaged using an SP5 Multiphoton, Leica confocal system to observe the architecture of the cortex, in particular the organization of layer II/III projection neurons and their dendritic arbors. Confocal images were collected using Leica software and were processed using Velocity, NIH ImageJ, and Photoshop (Adobe) software. Fluorescence intensity was plotted using NIH ImageJ, as a measure of GFP-positive neuron position within the neocortex.

#### Conditioning lesion and sensory neuron cultures

Mice of either sex were subjected to unilateral sciatic nerve crush at mid-thigh level. Three days after injury, dissociated cultures were prepared from the L4–5 dorsal root ganglia (DRGs) ipsilateral and contralateral to the nerve crush as described previously (Hanzel et al., 2003). The dissociated DRGs were plated in DMEM/F12 medium supplemented with N1 and 10% horse serum on laminin-coated glass coverslips at a density of 2–5 neurons/mm<sup>2</sup>. After 20 h cultures were fixed in 4% paraformaldehyde, stained with anti-NFH (neurofilament heavy chain) and number of branches per neuron was measured using MetaMorph software on digital images captured by ImageXpressMicro (Molecular Devices) fluorescent automatic microscope at 10 $\times$  magnification.

#### Conduction studies and dorsal root ganglion histology

**Skin-nerve preparation.** Animals of either sex, 3–4 months of age, 7 wild-type and 8 *Dync1li1<sup>CG2597/CG2597</sup>* littermates were killed by cervical dislocation. There were no obvious gross morphological differences of the nerves on dissection. The skin-nerve preparation was performed as described previously (Koltzenberg et al., 1997). The saphenous nerve with the skin of the hind leg attached was dissected free and placed “inside-up” in an organ bath. The preparation was superfused (15 ml/min) with an oxygen-saturated modified synthetic interstitial fluid solution containing the following (in mM): 123 NaCl, 3.5 KCl, 0.7 MgSO<sub>4</sub>, 1.7 NaH<sub>2</sub>PO<sub>4</sub>, 2.0 CaCl<sub>2</sub>, 9.5 sodium gluconate, 5.5 glucose, 7.5 sucrose, and 10 HEPES at a (mean  $\pm$  SD) pH of 7.4  $\pm$  0.05 and a temperature of 32.0  $\pm$  0.5°C.

Recordings of A- and C-fiber sensory nerve compound action potentials (SNAP) were made using a low noise custom-made amplifier and HP 1 Hz, LP 1 kHz filter setting without a notch filter. The nerve was stimulated with a fine monopolar steel needle as cathode and the anode placed close by in the organ bath. Voltages given are mean  $\pm$  SEM. Statistical comparison was made with a nonpaired *t* test.

**Muscle nerve conduction velocity studies.** Animals of either sex, 4–5 months of age, 5 wild-type and 5 *Dync1li1<sup>CG2597/CG2597</sup>* littermates were studied *in vivo*. Mice were anesthetized with isoflurane and studied using a Viking Qest EMG machine (generously donated by Carefusion). Compound action potentials were recorded from small foot muscles with needle electrodes and 10 Hz HP and 10 kHz LP filters. The recording electrode was inserted perpendicularly through the plantar skin midway between the metatarsal-phalangeal joints and the ankle. The reference electrode was inserted into the hallux. The tibial nerve was stimulated at the ankle and the sciatic nerve at the sciatic notch using a pair of monopolar needle electrodes. Needle EMG was obtained with a thin (30 ga, “facial”) concentric needle electrode with a recording area of 0.03 mm<sup>2</sup> from intrinsic foot muscles or the medial gastrocnemius muscle using 10 Hz HP and 10 kHz LP filters. Voltages given are mean  $\pm$  SEM. Statistical comparison with made with a nonpaired *t* test.

**Histochemical analyses of DRGs.** Animals of either sex, 3–4 months of age, 4 wild-type and 3 *Dync1li1<sup>CG2597/CG2597</sup>* littermates were used in this

analysis. Cervical and lumbar DRGs were fixed in a 4% PFA and subsequently soaked in a sterile 10% sucrose solution (in PBS) for 2 h and then successively transferred to increasing concentrations of 20% sucrose for a further 2 h and finally a 30% solution overnight at 4°C. Cryoprotected lumbar or cervical DRGs were embedded in OCT and sectioned on a cryostat at 10  $\mu$ m.

**Fixed or unfixed skin.** Analysis of epidermal nerve fiber density using PGP9.5 (a marker for unmyelinated fibers) (Achilli et al., 2009), Merkel cells (using cytokeratin 18), and large myelinated fibers stained for neurofilament heavy chain (NF2) was undertaken. Sections were double immunostained at room temperature following permeabilization with Triton-X and blockade with donkey serum either using a mouse IgG1 monoclonal anti-neurofilament 200 (NF2, Sigma) antibody and a rabbit polyclonal anti-peripherin antibody (Millipore Bioscience Research Reagents, AB1530) or using the mouse IgG1 monoclonal anti-parvalbumin (Z35 Swant) or a rabbit polyclonal antiserum to calcitonin gene-related peptide (CGRP) (1134, Biomed International). Primary antibodies were applied overnight, secondary antibodies were an Alexa Fluor 488 donkey anti-rabbit IgG (Invitrogen, A21206) and a Cy3 donkey anti-mouse IgG (Jackson ImmunoResearch) and applied for 2 h. Slides were mounted using a Vectashield mounting media with a nuclear DAPI stain and viewed on a Zeiss Axiohot 2. Images were taken at a 20 $\times$  fluor objective and captured using appropriate filters.

#### Data analysis

**Cell counts for NFH/peripherin immunostaining.** Lumbar and cervical DRGs from each animal were analyzed separately. Captured images were viewed in Adobe Photoshop CS4. A minimum of 200 cell profiles, constituting approximately three dorsal root ganglion (DRG) sections, were analyzed for each animal and the number of cell profiles positive for each marker was recorded. Of those profiles showing nuclei, the areas and perimeters of at least 50 cells positive for each marker were recorded using a 21-inch LCD (liquid crystal display) digitizing tablet with Adobe Photoshop software. The mean data from individual animals was then combined so that group data from mutant animals could be compared with the data from the wild-type animals.

**Cell counts for parvalbumin/CGRP immunostaining.** As with the NFH/peripherin immunostaining, the lumbar and cervical DRGs were analyzed separately. A minimum of 400 cell profiles were counted for each animal and areas were recorded for those profiles which showed immunoreactivity for each marker using the same software as for the NFH/peripherin counts. The nuclei of parvalbumin and CGRP-immunoreactive cells were not always visible so the areas of all the immunoreactive cell profiles were measured as opposed to just those profiles that had been sectioned in the nuclear plane.

#### Mouse embryonic fibroblast protocols

**Creation of mouse embryonic fibroblasts.** A pregnant female was sacrificed at day 13.5 postcoitum by cervical dislocation, embryos were separated and kept in L-15 medium on ice (Invitrogen) before processing. Head and visceral organs were removed and tissues were minced using razor-blades and suspended in 1.5 ml of 0.05% trypsin (Invitrogen) in DPBS supplemented with 10 mM MgCl<sub>2</sub> and DNase I (200 U, Invitrogen). Tissue was incubated at 37°C, 20 min, transferred into 4 ml of warm medium [DMEM supplemented with 10% FBS and 1:100 (v/v) penicillin/streptomycin]. Remaining pieces of tissue were allowed to settle to the bottom of the tube and cell suspension was transferred into cell culture flasks (Nunc).

**Golgi reassembly after disruption with nocodazole.** E13 mouse embryonic fibroblasts (MEFs) were grown to 70% confluence on round coverslips in 6 well plates in standard DMEM at 37°C, 3% O<sub>2</sub>. Standard DMEM was replaced by ice-cold standard DMEM containing 15 mM HEPES, cells were left on ice for 30 min. This was replaced with DMEM containing 10  $\mu$ M nocodazole, and cells were incubated at 37°C, 3 h, 3% O<sub>2</sub>. Nocodazole was washed from the cells 5 times in DMEM and cells returned to 3% O<sub>2</sub>, 37°C incubator to recover for 0, 30 and 50 min before being fixed in –20°C methanol, 8 min. The cells were then washed 3 times in PBS containing 0.2% gelatin from coldwater fish skin (PBSC). Samples were stained for Golgi using rabbit polyclonal anti-giantin (1:

1000) (Covance) and cytoskeleton using mouse monoclonal anti- $\alpha$ -tubulin (1:200) (Millipore); secondary antibodies were Alexa Fluor 546-conjugated goat anti-rabbit IgG (1:200) (Invitrogen) and Alexa Fluor 488-conjugated goat anti-mouse IgG (1:200) (Invitrogen). Antibodies were diluted in either PBSC (anti-giantin) or PBS- (PBS without magnesium or calcium) for 30 min, room temperature. Finally, cells were mounted on glass slides using ProLong Gold antifade mounting medium, containing 4',6'-diamidino-2-phenylindole dihydrochloride (DAPI) (Invitrogen), and allowed to cure for 24 h at room temperature, then stored at 4°C.

#### Endosomal trafficking chase of Alexa Fluor-conjugated epidermal growth factor

E13 MEFs were grown to 80% confluence on rotund coverslips in 6 well plates in standard DMEM at 37°C, 3% O<sub>2</sub> and then washed twice with PBS, without calcium or magnesium (PBS-). Cells were starved for 2 h in starving medium (DMEM, penicillin/streptomycin, and t-glyceraline) at 37°C, 3% O<sub>2</sub>, before stimulation for 10 min with warmed starving medium containing 8 ng/ml Alexa Fluor 555-conjugated epidermal growth factor (EGF) (Invitrogen) and 0.1% BSA. Cells were washed twice with ice-cold PBS- and the internalized EGF was chased for 0, 20, and 40 min. Samples were then fixed at the given time points with 4% PFA for 15 min, and permeabilized for 5 min in 0.1% Triton X-100 and blocked in 2% BSA, 1 h. Samples were then mounted on glass slides using ProLong Gold antifade mounting medium containing DAPI (Invitrogen) and allowed to cure for 24 h, room temperature, then stored at 4°C.

## Results

### Origin and inheritance of *Dync1li1*<sup>N255Y</sup> mutation

An archive of genomic DNAs from novel mice with random point mutations has been created at the MRC Mammalian Genetics Unit, UK in an *N*-ethyl-*N*-urea (ENU) driven mutagenesis program (Nolan et al., 2000). To take a genotype driven approach to understanding dynein subunit function, we screened this archive for *Dync1li1* exon 5 since it is one of the largest protein coding exons in the gene and the larger the stretch of DNA screened, the higher the probability that a mutation will be found. We amplified a 248 bp fragment (including complete 170 bp of exon 5), multiplexed at four DNA samples per well. A heteroduplex screen of 1248 amplicons (i.e., 4992 pools) showed a possible mutation in one DNA pool (supplemental Fig. S1A, available at [www.jneurosci.org](http://www.jneurosci.org) as supplemental material); sequencing revealed the single mutant DNA sample (supplemental Fig. S1B, available at [www.jneurosci.org](http://www.jneurosci.org) as supplemental material). Thus in our amplicon we detected 1 mutation per  $1.24 \times 10^6$  bp, of which  $0.85 \times 10^6$  bp were protein coding.

The *Dync1li1* mutation was an A to T change at base pair 795 (cDNA numbering; Mouse Genome Informatics accession number MGI:2135610) causing an asparagine to tyrosine change at the highly conserved residue 235: *Dync1li1*<sup>N255Y</sup> (Fig. 1). This mutation was not found in either parental strain, BALB/cAnN or C3H/HeH, confirming it is not a single-nucleotide polymorphism (nor is it found in C57BL/6).

The *Dync1li1*<sup>N255Y</sup> mouse line was rederyed by IVF and 4 animals (3 female, 1 male) were used as the founders for our *Dync1li1*<sup>N255Y</sup> colony. These mice were crossed to C57BL/6J mice and subsequent generations were backcrossed to produce a congenic strain or intercrossed to produce homozygous animals. At N5, 8 *Dync1li1*<sup>N255Y/+</sup> heterozygous males were crossed with 14 *Dync1li1*<sup>N255Y/+</sup> heterozygous females, producing 37 litters with an average size of 8 pups per litter. The sex ratio did not vary from normal (143 males, 147 females;  $\chi^2 = 0.09$ ). Homozygous animals were viable and the genotype ratios were not significantly altered from Mendelian norms (79 wild type, 140 heterozygote,

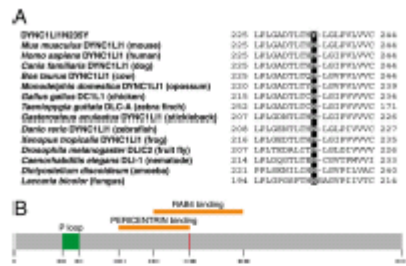


**Figure 1.** Partial sequence and domains of wild-type and mutant *Dync1li1*. **A**, Multiple sequence alignment of cytoplasmic dynein light intermediate chain 1. Asparagine 235 is mutated in the *Dync1li1*<sup>N255Y</sup> mouse but is highly conserved throughout the animal kingdom and also in amoebae and fungi. **B**, Protein domain map of *Dync1li1*, showing the location of the *Dync1li1*<sup>N255Y</sup> mutation as a red bar. The map was created using the domains identified by Billi et al. (2001), Hughes et al. (1995), and Yuan et al. (2000).

71 homozygotes;  $\chi^2 = 2.86$ ). Homozygotes were fertile—two intercrosses of homozygous males and females produced litters of 11 and 7 homozygous pups.

We went on to test the mutant mice for phenotypic differences: all phenotyping was performed blind to genotype on wild-type and homozygous age-, sex-matched littermates. Note that although the backcross generation of mice used varied between experiments, all mice within each experiment were of the same generation on C57BL/6J.

### Behavioral analysis and histology of brain and spinal cord

To determine whether the *Dync1li1* mutation plays a role in behavior, female mice (12 wild type, 11 *Dync1li1*<sup>N255Y/N255Y</sup> homozygotes, N4) were assessed. We found no difference between genotypes in open field behavior, food and water intake, glucose preference or wheel running (supplemental Fig. S2A, B, available at [www.jneurosci.org](http://www.jneurosci.org) as supplemental material). However, when placed in a novel environment *Dync1li1*<sup>N255Y/N255Y</sup> mice displayed lower levels of spontaneous locomotor activity than wild-type littermates ( $F_{(1,21)} = 4.35$ ;  $p < 0.05$ ) (Fig. 2A).

Next, anxiety was examined using the elevated plus maze. Compared with wild types, *Dync1li1*<sup>N255Y/N255Y</sup> mice had a longer latency to first enter an open arm ( $U_{(1,12)} = 29.0$ ;  $p < 0.05$ ), spent less time in the aversive open arms ( $U_{(1,12)} = 100.5$ ;  $p < 0.05$ ) and more in the closed arms ( $U_{(1,12)} = 13.0$ ;  $p < 0.01$ ) (Fig. 2B) and made fewer entries to the open arms ( $U_{(1,12)} = 103.0$ ;  $p < 0.05$ ) and the closed arms ( $U_{(1,12)} = 112.5$ ;  $p < 0.005$ ) (Fig. 2C). However, the distance moved by the *Dync1li1*<sup>N255Y/N255Y</sup> mice did not differ from that of wild types ( $t_{(21)} = -1.50$ ;  $p = 0.15$ ), suggesting that the reduced exploration of the open arms could not be explained by hypoactivity. In addition, *Dync1li1*<sup>N255Y/N255Y</sup> mice displayed significantly increased defecation during the task compared with wild types ( $U_{(1,12)} = 28.0$ ;  $p < 0.05$ ).

Anxiety was further examined using the successive alleys task (Deacon et al., 2003). Again, *Dync1li1*<sup>N255Y/N255Y</sup> mice were slower to move into the more aversive second alley ( $U_{(1,12)} = 26.0$ ;  $p < 0.05$ ), spent less time in the second alley ( $U_{(1,12)} = 106.0$ ;  $p < 0.05$ ) (Fig. 2D) and made fewer entries into the second alley ( $U_{(1,12)} = 110.0$ ;  $p < 0.01$ ) (Fig. 2E). The small number of animals (4 wild type, 0 *Dync1li1*<sup>N255Y/N255Y</sup>) that

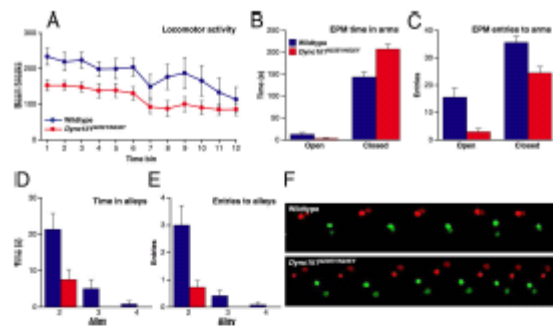


**Figure 2.** Behavior of *Dync1li1*<sup>N253Y/N253Y</sup> mice. **A**, *Dync1li1*<sup>N253Y/N253Y</sup> mice displayed significantly lower levels of spontaneous locomotor activity compared with wild-type littermates. **B**, On the elevated plus maze (EPM), the *Dync1li1*<sup>N253Y/N253Y</sup> mice spent significantly less time in the open arms and more time in the closed arms. **C**, They also made significantly fewer entries to both the open and closed arms. **D**, On the successive alleys task *Dync1li1*<sup>N253Y/N253Y</sup> mice spent less time in the more aversive alleys compared with wild types. **E**, They also made fewer entries to these alleys (the *Dync1li1*<sup>N253Y/N253Y</sup> mice did not make any entries to alleys 3 or 4). **F**, Footprint analysis using the CatWalk system found that compared with wild types, *Dync1li1*<sup>N253Y/N253Y</sup> mice displayed a significantly greater difference between the BOS of their front legs and hind legs due to a relative narrowing of the front BOS and a widening of the hind BOS; a representative sample from one animal is shown. Green, right front foot; dark green, right hind foot; red, left front foot; dark red, left hind foot. Animals walked from right to left.

ventured beyond the second alley meant that valid analyses could not be performed on alleys 3 and 4. Thus the results of the plus maze and successive alleys tasks suggest that the *Dync1li1*<sup>N253Y/N253Y</sup> mice display increased anxiety compared with their wild-type littermates.

At 6 months of age the performance of *Dync1li1*<sup>N253Y/N253Y</sup> mice on the accelerating rotarod did not differ from that of wild types ( $t_{(21)} = 0.47$ ;  $p = 0.64$ ). However, *Dync1li1*<sup>N253Y/N253Y</sup> mice tended to be slightly stronger than wild types on a weightlifting test of grip strength ( $U_{(11,12)} = 35.5$ ;  $p = 0.06$ ) (supplemental Fig. S2C, available at [www.jneurosci.org](http://www.jneurosci.org) as supplemental material). In addition, examination of gait using the CatWalk analysis system found that the ratio of forepaw base of support (BOS) to hindpaw BOS was significantly reduced in the homozygous mutant animals ( $t_{(21)} = 3.21$ ;  $p < 0.005$ ) compared with wild-type littermates. This was due to a relative narrowing of the forepaw BOS coupled with an increase in the hindpaw BOS (Fig. 2F). We performed the modified SHIRPA test (Rogers et al., 1997, 2001), which included further rotarod and grip strength measurements, upon male and female mice up to 52 weeks of age but found no difference between homozygotes and wild-type controls (supplemental material, supplemental Fig. S2I, J, available at [www.jneurosci.org](http://www.jneurosci.org) as supplemental material) and no differences in tests of hippocampal spatial working memory (spontaneous alternation) (supplemental Fig. S2D, available at [www.jneurosci.org](http://www.jneurosci.org) as supplemental material), or reference memory acquisition and reversal (supplemental material, supplemental Fig. S2D–H, available at [www.jneurosci.org](http://www.jneurosci.org) as supplemental material).

Given the behavioral and gait abnormalities, brain and cervical and lumbar spinal cord were assessed histologically. Attention was paid to prefrontal cortex (PFC), hippocampus, striatum and cerebellum, but we detected no differences between wild-type and mutant littermates in brain or spinal cord morphology or

motor neuron counts in the sciatic motor pool (supplemental material, supplemental Fig. S3A–D, available at [www.jneurosci.org](http://www.jneurosci.org) as supplemental material).

#### Cortical neuron dendrite outgrowth and branching

As axonal and dendritic development is known to be mediated by cytoplasmic dynein-dependent processes, we investigated the morphology of cortical neurons, including those in the PFC. A GFP expression plasmid was transfected into the cortex of embryos at E15 by *in utero* electroporation, selectively labeling neurons that would in the developed brain become layer II/III cortical projection neurons. Two days after electroporation dissociated cortical cultures were prepared from fluorescent hemispheres. Ten days later GFP-expressing cells were analyzed to determine patterns of dendritic outgrowth and branching (Fig. 3A). We found the mean dendritic tree length was significantly increased in *Dync1li1*<sup>N253Y/N253Y</sup> neurons (Fig. 3B); wild type,  $370.3 \pm 33.46 \mu\text{m}$ ; *Dync1li1*<sup>N253Y/N253Y</sup>,  $452.6 \pm 34.52 \mu\text{m}$ ;  $p = 0.0029$ ). Furthermore, individual dendrites terminated significantly further from the soma in *Dync1li1*<sup>N253Y/N253Y</sup> neurons than wild-type controls (Fig. 3B); wild type,  $170.9 \pm 4.637 \mu\text{m}$ ; *Dync1li1*<sup>N253Y/N253Y</sup>,  $182.6 \pm 4.411 \mu\text{m}$ ;  $p = 0.0281$ ). Thus homozygous mutant dendrites grew longer and extended further from the soma than those of wild-type animals, which may have implications for correct connectivity between neurons *in vivo*. Despite these differences in dendritic tree length, wild-type and *Dync1li1*<sup>N253Y/N253Y</sup> neurons had the same average number of dendritic trees (supplemental Fig. S4A, available at [www.jneurosci.org](http://www.jneurosci.org) as supplemental material; wild type,  $5.405 \pm 0.3388$ ; *Dync1li1*<sup>N253Y/N253Y</sup>,  $4.923 \pm 0.2807$ ;  $p = 0.4697$ ) and the trees displayed similar branching patterns: the average number of branch points, or nodes, per dendrite was not statistically different (supplemental Fig. S4B, available at [www.jneurosci.org](http://www.jneurosci.org) as supplemental material; wild type,  $3.985 \pm 0.3221$ ; *Dync1li1*<sup>N253Y/N253Y</sup>,  $4.236 \pm 0.2391$ ;  $p = 0.4697$ ). In addition, the frequency of nodes per dendritic tree was statistically indistinguishable between wild-type and *Dync1li1*<sup>N253Y/N253Y</sup> neurons. This indicates that the variability in branching patterns observed between neurons within each genotype, was consistent between the two genotypes (supplemental Fig. S4C, available at [www.jneurosci.org](http://www.jneurosci.org) as supplemental material). Finally, a Sholl analysis showed virtually identical number of intersections within given radii of the cell body for wild-type and *Dync1li1*<sup>N253Y/N253Y</sup> neurons (supplemental Fig. S4D, available at [www.jneurosci.org](http://www.jneurosci.org) as supplemental material). Therefore, increased dendrite outgrowth, but not increased branching, characterizes cortical neurons in *Dync1li1*<sup>N253Y/N253Y</sup> neuron cultures.

To determine whether dendritic branching and organization defects occur in *Dync1li1*<sup>N253Y/N253Y</sup> neurons *in vivo*, embryos subjected to electroporation with GFP at E15 were left to develop normally and brains were harvested at P15. In these experiments electroporation was targeted toward the PPC, an area that has been associated with anxiety studies in lesion studies (Deacon et

al., 2003). We found mutant phenotypes that could not be observed in *in vitro* cultures in the PFC of *Dync1li1*<sup>N253Y/N253Y</sup> animals more neurons that had migrated past their appropriate layer II/III position and into the uppermost part of the cortex (Fig. 3C,E; quantitation shown in H). More caudally (Fig. 3I,J) there was a marked increase in GFP-labeled neurons in the uppermost layer of the cortex in *Dync1li1*<sup>N253Y/N253Y</sup> mice. Many of these neurons displaced from layer II adopted abnormal orientation in *Dync1li1*<sup>N253Y/N253Y</sup> animals compared with wild types (Fig. 3D,F) and also a proportion within layer II/III showed abnormal orientation (Fig. 3G). Figure 3 shows that this misorientation was characterized by the apical dendrite not projecting radially, toward the pial surface, but instead to varying degrees tangentially. In addition we observed neurons with abnormal apical dendrite morphology including thickening of the dendrite and often irregular trajectories (Fig. 3K, arrow).

#### Adult sensory neuron branching

To establish whether the *Dync1li1*<sup>N253Y</sup> mutation affected neuronal branching in the periphery we examined neuronal cultures from wild-type and *Dync1li1*<sup>N253Y/N253Y</sup> DRGs. We also examined the possibility that the *Dync1li1* mutation might affect dynein-based retrograde injury signaling by performing conditioning lesion experiments as described previously (Hanz et al., 2003).

Two wild-type and two *Dync1li1*<sup>N253Y/N253Y</sup> male mice of 2–4 months old were used for each experiment, and three independent replicates were carried out. Mice were subjected to unilateral sciatic nerve crush at mid-thigh level; 3 d later, dissociated cultures were prepared from L4–5 DRGs ipsilateral and contralateral to the nerve crush. Neurons were fixed after 20 h in culture, stained with anti-NFH, and branching was measured. As shown in Figure 4A,B, in naive conditions NFH-positive sensory neurons from *Dync1li1*<sup>N253Y/N253Y</sup> mice had a greater number of branches than wild-type controls. We found similar results for neurons under injury conditions, although differences were less significant than for naive conditions, apparently due to a more marked injury response in wild-type neurons (47.6% increase in branching after injury, compared with 33.5% increase in the mutants).

To assess nerve branching in developing animals we performed whole-mount neurofilament immunohistochemistry in the limbs of E13.5 animals; we found no significant difference between wild-type and *Dync1li1*<sup>N253Y/N253Y</sup> animals in the number of branch points (supplemental material, supplemental Figure S4, available at [www.jneurosci.org](http://www.jneurosci.org) as supplemental

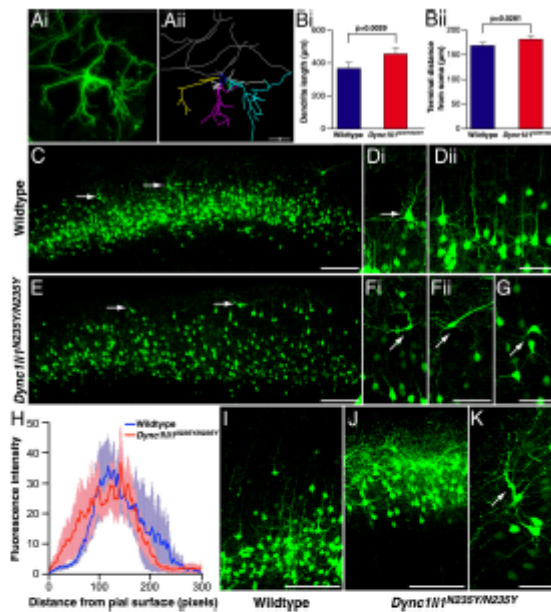


**Figure 3.** Morphology of wild-type and mutant *Dync1li1*<sup>N253Y/N253Y</sup> cortical neurons. **A**, Cortical neurons were electroporated *in vivo* at E15, then cultured *in vitro* from E17 embryos. At 10 DIV they were analyzed to compare morphology of wild-type and *Dync1li1*<sup>N253Y/N253Y</sup> cortical neurons. GFP-positive neurons (**B**) were hand-traced using NeuroLucida software (**B**). **B**, The length of dendritic trees for wild-type and *Dync1li1*<sup>N253Y/N253Y</sup> neurons, *in vitro*. **C**, *Dync1li1*<sup>N253Y/N253Y</sup> dendrites were significantly longer than wild-type dendrites ( $p = 0.0029$ ). **D**, *Dync1li1*<sup>N253Y/N253Y</sup> dendrites terminated significantly further from the soma than wild-type dendrites ( $p = 0.0081$ ). **E**, Low magnification of the cortex from a wild-type brain electroporated with GFP at E15 and harvested at P15. GFP-positive neurons occupy a discrete band corresponding to cortical layers II/III. **D**, **E**, Higher-magnification image showing the orientation of a pyramidal neuron in layer II/III. **F**, **G**, Neighboring neurons align in the same orientation with apical dendrites projecting toward the pial surface. **E**, The cortex from a *Dync1li1*<sup>N253Y/N253Y</sup> brain electroporated with GFP at E15 and harvested at P15 (rostrocaudally matched with **C**). Compared with **C**, GFP-positive cells were more distributed, with more neurons residing in the uppermost part of the cortex (arrow). **F**, The cell body and apical dendrite of neurons located closer to the pial surface in *Dync1li1*<sup>N253Y/N253Y</sup> mutants were mis-oriented. **G**, Neurons in layer II of *Dync1li1*<sup>N253Y/N253Y</sup> cortex also often displayed incorrect orientation. **H**, Comparison of the proportion of electroporated neurons located in upper layers of the neocortex, as measured by fluorescence intensity. **I**, Higher-magnification imaging from wild-type cortex in more caudal sections showed most GFP-positive neurons within layer II/III. **J**, In contrast to **I**, GFP-expressing cells in *Dync1li1*<sup>N253Y/N253Y</sup> cortex occupied a location much closer to the pial surface. **K**, The apical dendrite of neurons *Dync1li1*<sup>N253Y/N253Y</sup> cortex were often thickened and projected in an incorrect orientation. Scale bars: **A**, **C**, **E**, **I**, **J**, 100  $\mu$ m; **D**, **F**, **G**, **K**, 50  $\mu$ m.

material) and whole-mount neurofilament staining did not show any obvious abnormalities in the peripheral nervous system of homozygotes at P12.5 (Christiana Ruhrberg, personal communication).

#### Neurophysiology of sensory neurons and dorsal root ganglia histology

Mice with mutations in the dynein heavy chain 1 subunit have a loss of cutaneous and proprioceptive sensory neurons, and so for comparison we undertook sensory nerve conduction studies of the saphenous nerve on 8 wild-type and 7 *Dync1li1*<sup>N253Y/N253Y</sup> homozygous male littermates (3 months of age, N3). Recordings

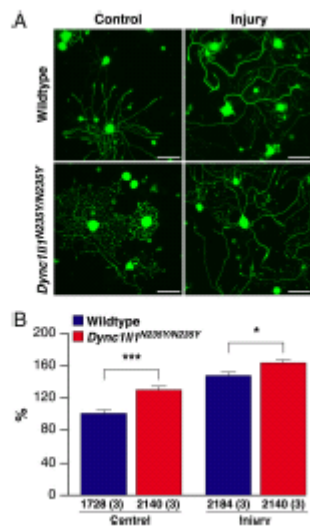


**Figure 4.** *Dync1li1*<sup>N235Y</sup> point mutation increases branching in cultured sensory neurons. **A**, Fluorescent images of DRG neurons from wild-type and *Dync1li1*<sup>N235Y</sup> homozygous mice under naive and injury conditions. Right leg sciatic nerves of wild-type and mutant mice were crush-injured 3 d before dissection of L4–S5 DRGs for primary culture of sensory neurons; corresponding contralateral DRGs were used for naive controls. Cultures were imaged by automated fluorescent microscopy after 20 h *in vitro*, to obtain 150 images per slide, at magnification 10 $\times$ . **B**, Quantification shows a significant increase in branching of naive sensory neurons from *Dync1li1*<sup>N235Y</sup> homozygous (25.4% increase over wild type). Increased branching was also observed in homozygous *Dync1li1*<sup>N235Y/N235Y</sup> sensory neurons after injury, although the difference is less pronounced than in naive neurons, apparently due to a more robust injury response in the wild-type neurons. \*\*\* $p < 10^{-6}$ , \*\* $p < 0.05$  (Student's *t* test). Scale bar, 100  $\mu$ m.

were taken of the A (myelinated)- or C (unmyelinated)-fiber SNAPs; we found a small but significant ( $p < 0.05$ ) reduction of the peak-to-peak amplitude of the A-fiber SNAP from  $3.2 \pm 0.3$  mV in wild types to  $2.5 \pm 0.2$  mV in homozygous mutants (Fig. 5A) but no difference in the conduction velocity (wild type,  $28.8 \pm 0.8$  m/s; *Dync1li1*<sup>N235Y/N235Y</sup>,  $27.1 \pm 1.2$  m/s;  $p > 0.2$ ). With respect to the C-fibers, we found no significant reduction of the peak-to-peak amplitude of the C-fiber SNAP (wild type,  $391 \pm 48$   $\mu$ V; *Dync1li1*<sup>N235Y/N235Y</sup>,  $385 \pm 61$   $\mu$ V,  $p > 0.4$ ) and no significant reduction of the conduction velocity (wild type,  $0.86 \pm 0.06$  m/s; *Dync1li1*<sup>N235Y/N235Y</sup>,  $0.92 \pm 0.04$  m/s;  $p > 0.4$ ).

To determine whether the sensory electrophysiological defect in A-fiber SNAP was reflected histologically, DRGs from the cervical and lumbar spinal cord were stained for NFH (a marker for myelinated fibers) and peripherin (a marker for thin myelinated and unmyelinated fibers) (supplemental Figure S5A, available at [www.jneurosci.org](http://www.jneurosci.org) as supplemental material). We found no differences in the NFH- and peripherin-immunoreactive cell profiles in cervical or lumbar DRGs of wild-type or mutant animals (supplemental Table S1, available at [www.jneurosci.org](http://www.jneurosci.org) as supplemental material). However, analysis of the size distribution of labeled neuronal profiles revealed a significant shift to the left (smaller neurons) in homozygous mutants compared with wild-

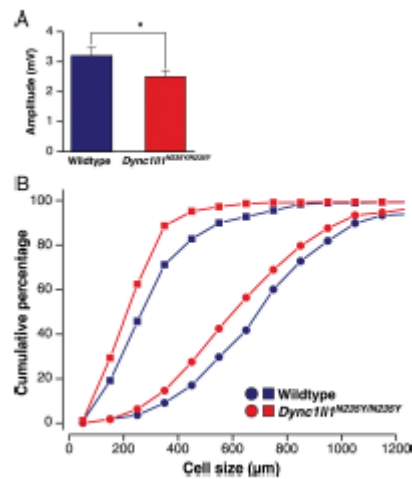


**Figure 5.** Neurophysiological and histological analysis of *Dync1li1*<sup>N235Y</sup> mice. **A**, *Dync1li1*<sup>N235Y/N235Y</sup> mice have a significant reduction of the peak-to-peak amplitude of A-fiber compound action potential in the saphenous nerve compared with wild-type littermates. \* $p < 0.05$ . **B**, (Scan plots of the neuronal profile area distribution of neurofilament-immunoreactive neurons (giving rise to large myelinated A-fibers; round symbols) and of peripherin-immunoreactive cells (giving rise to C-fibers; square symbols) in lumbar dorsal root ganglia. The cell profile size in both populations is reduced in *Dync1li1*<sup>N235Y</sup> mice compared with wild-type littermates.

type littermates in lumbar DRG. Changes in cervical DRGs were smaller which is compatible with a length-dependent effect as seen in many neuropathies (Fig. 5B; Table 1).

We also stained cervical and lumbar DRGs for calcitonin gene-related peptide (CGRP, a marker of peptidergic nociceptors) and parvalbumin (status proprioceptors and mechanoreceptors) (supplemental Fig. S5B, available at [www.jneurosci.org](http://www.jneurosci.org) as supplemental material). Similarly, we found no differences in the percentage of CGRP- and parvalbumin-immunoreactive cells in the cervical and lumbar DRGs of wild-type and mutant animals (supplemental Table S2, available at [www.jneurosci.org](http://www.jneurosci.org) as supplemental material), but there was a significant shift to smaller neurons in homozygous mutants compared with wild-type littermates (Table 2).

We found no loss of epidermal nerve fiber density between wild-type and mutant animals, and no reduction in the number of Merkel cells, whose survival depends on innervation by mechanoreceptive sensory neurons. Together these findings indicate that there is no distal degeneration of large myelinated or unmyelinated sensory neurons. To establish whether the *Dync1li1*<sup>N235Y</sup> mutation had any effect upon the saphenous nerve itself, a histological analysis was performed upon the saphenous nerves of 3 wild types and 3 homozygotes and we found no difference in average fiber size, fiber size distribution, g-ratio, or average axonal diameter (supplemental material, supplemental Fig. S5C–F, supplemental Table S3, available at [www.jneurosci.org](http://www.jneurosci.org) as supplemental material).

**Table 1.** Cell profile size distribution in cervical and lumbar DRGs for NFH- and peripherin-positive neurons in wild-type and *Dync1li1*<sup>N253Y/N253Y</sup> mice

	Cervical		Lumbar	
	Wild type (n = 3)	<i>Dync1li1</i> <sup>N253Y/N253Y</sup> (n = 4)	Wild type (n = 3)	<i>Dync1li1</i> <sup>N253Y/N253Y</sup> (n = 4)
Total number of NFH-positive profile areas measured	201	286	165	240
Mean NFH cell profile area	730 ± 80 (579–833)	676 ± 37 (568–739)	773 ± 46 (714–864)	680 ± 33 (595–734)
Total number of peripherin-positive profile areas measured	338	496	379	430
Mean peripherin cell profile area	330 ± 32 (279–387)	307 ± 6 (279–323)	351 ± 31 (294–299)	285 ± 18 (245–319)

For mean ± SEM values, the values in parentheses are ranges.

**Measurement:** There was no significant difference ( $p > 0.1$ , Kolmogorov–Smirnov test) in the distribution of the profile areas of cervical NFH-immunoreactive DRG neurons between wild-type mice (730 ± 80 μm<sup>2</sup>, mean ± SD;  $n_{\text{obs}} = 201$ ,  $n_{\text{expec}} = 1$ ) and *Dync1li1*<sup>N253Y/N253Y</sup> littermates (676 ± 37 μm<sup>2</sup>, mean ± SD;  $n_{\text{obs}} = 286$ ,  $n_{\text{expec}} = 4$ ). Data not shown. The distribution of the profile areas of lumbar NFH-immunoreactive DRG neurons is significantly different ( $p < 0.05$ , Kolmogorov–Smirnov test) between wild-type mice (773 ± 46 μm<sup>2</sup>, mean ± SD;  $n_{\text{obs}} = 165$ ,  $n_{\text{expec}} = 1$ ) and *Dync1li1*<sup>N253Y/N253Y</sup> littermates (680 ± 33 μm<sup>2</sup>, mean ± SD;  $n_{\text{obs}} = 240$ ,  $n_{\text{expec}} = 4$ ) (Fig. 5B).

**Peripherin:** The distribution of the profile areas of cervical peripherin-immunoreactive DRG neurons is significantly different ( $p < 0.05$ , Kolmogorov–Smirnov test) between wild-type mice (330 ± 32 μm<sup>2</sup>, mean ± SD;  $n_{\text{obs}} = 338$ ,  $n_{\text{expec}} = 1$ ) and *Dync1li1*<sup>N253Y/N253Y</sup> littermates (307 ± 6 μm<sup>2</sup>, mean ± SD;  $n_{\text{obs}} = 496$ ,  $n_{\text{expec}} = 4$ ). Data not shown. The distribution of the profile areas of lumbar peripherin-immunoreactive DRG neurons is significantly different ( $p < 0.005$ , Kolmogorov–Smirnov test) between wild-type mice (351 ± 31 μm<sup>2</sup>, mean ± SD;  $n_{\text{obs}} = 379$ ,  $n_{\text{expec}} = 1$ ) and *Dync1li1*<sup>N253Y/N253Y</sup> littermates (285 ± 18 μm<sup>2</sup>, mean ± SD;  $n_{\text{obs}} = 430$ ,  $n_{\text{expec}} = 4$ ) (Fig. 4C).

**Table 2.** Cell profile size distribution in cervical and lumbar DRG for CGRP- and parvalbumin-positive neurons

	Cervical		Lumbar	
	Wild type (n = 3)	<i>Dync1li1</i> <sup>N253Y/N253Y</sup> (n = 4)	Wild type (n = 3)	<i>Dync1li1</i> <sup>N253Y/N253Y</sup> (n = 3)
Total number of CGRP-positive profile areas measured	239	315	255	389
Mean CGRP cell profile area	459 ± 69 (378–595)	420 ± 27 (383–498)	485 ± 26 (469–502)	435 ± 26 (395–484)
Total number of parvalbumin-positive profile areas measured	264	285	233	339
Mean parvalbumin cell profile area	508 ± 26 (477–539)	477 ± 21 (476–509)	474 ± 7 (418–538)	378 ± 7 (364–388)

For mean ± SEM values, the values in parentheses are ranges.

**CGRP:** The distribution of the profile areas of cervical CGRP-immunoreactive DRG neurons is significantly different ( $p < 0.005$ , Kolmogorov–Smirnov test) between wild-type mice (459 ± 69 μm<sup>2</sup>, mean ± SD;  $n_{\text{obs}} = 239$ ,  $n_{\text{expec}} = 1$ ) and *Dync1li1*<sup>N253Y/N253Y</sup> littermates (420 ± 27 μm<sup>2</sup>, mean ± SD;  $n_{\text{obs}} = 315$ ,  $n_{\text{expec}} = 4$ ). Data not shown. The distribution of the profile areas of lumbar CGRP-immunoreactive DRG neurons is significantly different ( $p < 0.005$ , Kolmogorov–Smirnov test) between wild-type mice (485 ± 26 μm<sup>2</sup>, mean ± SD;  $n_{\text{obs}} = 255$ ,  $n_{\text{expec}} = 1$ ) and *Dync1li1*<sup>N253Y/N253Y</sup> littermates (435 ± 26 μm<sup>2</sup>, mean ± SD;  $n_{\text{obs}} = 389$ ,  $n_{\text{expec}} = 4$ ). Data not shown.

**Parvalbumin:** The distribution of the profile areas of cervical parvalbumin-immunoreactive DRG neurons is significantly different ( $p < 0.001$ , Kolmogorov–Smirnov test) between wild-type mice (508 ± 26 μm<sup>2</sup>, mean ± SD;  $n_{\text{obs}} = 264$ ,  $n_{\text{expec}} = 1$ ) and *Dync1li1*<sup>N253Y/N253Y</sup> littermates (477 ± 21 μm<sup>2</sup>, mean ± SD;  $n_{\text{obs}} = 285$ ,  $n_{\text{expec}} = 4$ ). Data not shown. The distribution of the profile areas of lumbar parvalbumin-immunoreactive DRG neurons is significantly different ( $p < 0.001$ , Kolmogorov–Smirnov test) between wild-type mice (474 ± 7 μm<sup>2</sup>, mean ± SD;  $n_{\text{obs}} = 233$ ,  $n_{\text{expec}} = 1$ ) and *Dync1li1*<sup>N253Y/N253Y</sup> littermates (378 ± 7 μm<sup>2</sup>, mean ± SD;  $n_{\text{obs}} = 339$ ,  $n_{\text{expec}} = 4$ ) (Fig. 5C).

As *Dync1li1*<sup>N253Y/N253Y</sup> animals have a different gait from wild-type littermates, motor nerve conduction velocity was assessed in wild-type and *Dync1li1*<sup>N253Y/N253Y</sup> littermates and we found no differences between genotypes (supplemental material, available at [www.jneurosci.org](http://www.jneurosci.org)). In aggregate these findings indicate that there is no loss of subpopulations of neurons, but a hypotrophy of all cell types and no dying back neuropathy of motor, or large and small diameter sensory neurons.

#### Dynein-controlled processes in *Dync1li1*<sup>N253Y/N253Y</sup> mouse embryonic fibroblasts

We studied the effect of the *Dync1li1*<sup>N253Y</sup> mutation on two important cellular processes known to involve cytoplasmic dynein: maintenance of Golgi integrity and endosomal movements. Golgi abnormalities have been reported in both *Dync1li1*<sup>200</sup> (Hafexparast et al., 2003) and in *Drosophila* with a mutation in the dynein light intermediate chain (Zheng et al., 2008; Palmer et al., 2009). We analyzed the effect of the *Dync1li1*<sup>N253Y</sup> mutation on reassembly of Golgi complex in MEFs, following exposure to nocodazole. We found Golgi reassembly progressed throughout the recovery time and was almost complete in wild-type cells within 50 min, thus there was no significant difference in the ratio of Golgi spots per unit area in wild-type cells compared with the corresponding untreated wild-type cells at the 50 min time point ( $p = 0.31$ ) (Fig. 6A, B; supplemental Fig. S6, available at [www.jneurosci.org](http://www.jneurosci.org) as supplemental material). However, there was a defect in Golgi complex reassembly in *Dync1li1*<sup>N253Y/N253Y</sup> cells, when untreated and treated cells at the 50 min recovery time point were compared ( $p = 0.008$ ). No statistically significant differences ( $p = 0.06$ ) were observed in the ratio of Golgi spots per unit area in heterozygous *Dync1li1*<sup>N253Y/+</sup> cells under these two conditions (supplemental Fig. S6, available at [www.jneurosci.org](http://www.jneurosci.org) as supplemental material).

As dynein is responsible for the trafficking and sorting of endosomes within the cell (Driskell et al., 2007) we investigated the effect of the *Dync1li1*<sup>N253Y</sup> mutation on endosomal dynamics. Wild-type and homozygous MEFs were pulsed with Alexa Fluor 555-conjugated EGF, then fixed at set time points (Fig. 7A, B), and the number of EGF-positive vesicles in each cell was counted. When we compared the number of EGF-positive vesicles, as a measure of their trafficking to the lysosome for degradation, at 20 and 40 min time points, we observed significant differences between wild-type and homozygous MEFs ( $p = 0.0032$  and  $p = 0.0007$  respectively) which may indicate a slower rate of degradation.

#### Dynein subunit levels and interactions

We generated antibodies against wild-type DYNC1L1, and the dynein intermediate chain protein 1, DYNC1I1 (supplemental material, supplemental Fig. S7, available at [www.jneurosci.org](http://www.jneurosci.org) as supplemental material). To investigate whether the DYNC1L1 mutation affected its stability or expression, or its interactions with other components of the dynein complex, we assessed various cytoplasmic dynein subunit levels in brain from 12-month old wild-type and *Dync1li1*<sup>N253Y/N253Y</sup> mice and found no differences in individual protein levels, except for a significant increase in the levels of DYNLT3 in *Dync1li1*<sup>N253Y/N253Y</sup> mice compared with wild-type controls ( $p = 0.001$ ; supplemental Fig. S8A, B; supplemental Table S4, available at [www.jneurosci.org](http://www.jneurosci.org) as supplemental material). Coimmunoprecipitation studies indicated DYNC1L1<sup>N253Y</sup> was still bound within the complex, and also that there was a significant decrease in the amount of coprecipitating DYNLL in mutant samples when compared with wild type ( $p = 0.000005$ ; supplemental material, supplemental Fig. S8C–E; supplemental Table S5, available at [www.jneurosci.org](http://www.jneurosci.org) as supplemental material). We found no differences in the autophagy

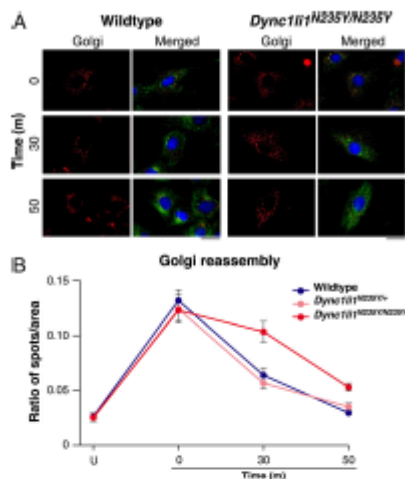


**Figure 6.** Golgi reassembly in wild-type and *Dync1li1<sup>N235Y/N235Y</sup>* MEFs. **A**, MEFs were treated with cold (4°C) for 20 min and nocodazole for 3 h, washed and then allowed to recover at 37°C for the times indicated. Golgi are shown in red, cytoskeleton in green ( $\alpha$ -tubulin) and nuclei in blue (DAPI). The scale bar represents 30  $\mu$ m. **B**, The total number of discrete spots and the total area of Golgi complex were measured to calculate the ratio of spots/total area per cell; 5 cells per genotype were assessed. In wild-type and heterozygous cells, after 50 min of recovery, the Golgi complex has reformed and is not significantly different from that in untreated cells. However, in the *Dync1li1<sup>N235Y/N235Y</sup>* homozygous mutant cells, the Golgi complex has a significant defect in recovery after 50 min compared with untreated cells and treated wild-type and heterozygous cells at the same time point.

marker LC3 II or in the cellular localization of DYNC1LI1 or its cargo RAB4 between wild-type and mutant animals in cortical neurons (supplemental material, supplemental Fig. S8 F–K, available at [www.jneurosci.org](http://www.jneurosci.org) as supplemental material).

### Discussion

We have identified and characterized a novel mouse line carrying an ENU-derived mutation causing an asparagine to tyrosine change in DYNC1LI1 at highly conserved residue 235. This is the first published mammalian mutant of a dynein light intermediate chain and allows us to assess aspects of dynein function that have not been highlighted thus far in the available mouse models of dynein dysfunction. *Dync1li1<sup>N235Y/N235Y</sup>* homozygote mice show increased anxiety-like behavior and altered gait in behavioral tests and have neurons with altered morphologies and electrophysiological properties. The *Dync1li1<sup>N235Y</sup>* mutation changes Golgi formation and endosomal trafficking, and the level expression and association of two other subunits of the dynein complex.

Our behavioral studies reveal that *Dync1li1<sup>N235Y/N235Y</sup>* homozygotes display greater levels of anxiety-like behavior than wild-type littermates on both the elevated plus maze and successive alleys task. Although these tasks can be influenced by changes in baseline levels of locomotor activity, the two groups did not differ in the distance traveled on the elevated plus maze, suggesting that the reduced exploration of the open arms by the

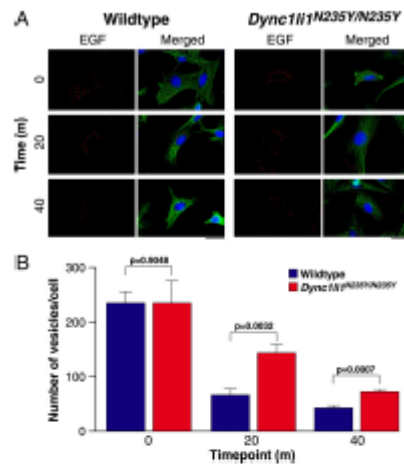


**Figure 7.** Endosomal trafficking chase of Alexa Fluor 555-conjugated EGF in wild-type and *Dync1li1<sup>N235Y/N235Y</sup>* MEFs. **A**, MEFs were pulsed with EGF for 10 min and chased at 37°C for the times indicated. EGF is shown in red, cytoskeleton ( $\alpha$ -tubulin) in green and nuclei in blue (DAPI). Ten cells per genotype per time point were assessed. Scale bar, 30  $\mu$ m. **B**, The number of EGF-positive vesicles per cell in wild-type and homozygous MEFs at 0, 20, and 40 min time points. At 0 min wild-type and *Dync1li1<sup>N235Y/N235Y</sup>* homozygous mutant cells have similar numbers of vesicles, however, after 20 and 40 min *Dync1li1<sup>N235Y/N235Y</sup>* homozygous mutant cells have significantly more vesicles remaining than wild-type cells.

*Dync1li1<sup>N235Y/N235Y</sup>* mice could not be explained by hypoactivity, and no hypoactivity was found in wheel running tests. Despite this, it is difficult to conclusively dissociate anxiety and locomotor activity as these two factors are closely linked (reduced locomotor activity potentially may result from increased anxiety as well as potentially acting as a confound in the measurement of anxiety) (Milner and Crabbe, 2008). Because of this difficulty, defecation was used as a non-locomotor measure of anxiety (DeFries et al., 1978). The increased defecation observed in *Dync1li1<sup>N235Y/N235Y</sup>* mice during behavioral testing supports the hypothesis that these animals display increased levels of anxiety.

*Dync1li1<sup>N235Y/N235Y</sup>* homozygotes have defects in cortical projection neuron morphology and the laminar positioning of this neuronal population, which indicates a migration defect affecting the cortex and prefrontal cortex. Alterations in neuronal morphology in the medial PFC have been found to be induced by chronic stress (Goldwater et al., 2009), as well as anxiety (Pascual and Zamora-León, 2007). Stress linked neuronal migration defects have also been observed in the hippocampus (Keays et al., 2007; Scoble et al., 2009) and basolateral amygdala (Kudo et al., 2007; Carim-Todd et al., 2009). A number of other mouse models with PFC-related behavioral deficits show defects in neuronal morphology or migration. However, linking behavior and migration defects is complex, for example migration defects observed in this study are similar to those in the *Lmx1a* (*dreher*) mutant mouse (overmigration of layer II neurons into layer I), but the two mouse lines show markedly different behavioral phenotypes—*dreher* mice show circling behavior, balance abnormal-

ties, hyperactivity and deafness, none of which we see in *Dync1li1<sup>N253Y/N253Y</sup>* homozygotes (Costa et al., 2001).

Dynein is involved in neuronal migration through its interactions with LIS1 (Tsat et al., 2007). *Lis1* mutant mice have severe defects in neuronal migration in the brain, including in the same cortical regions disrupted in *Dync1li1<sup>N253Y/N253Y</sup>* homozygotes (Hirotsune et al., 1998). However, *Lis1* mutant mice do not show changes in anxiety (Paylor et al., 1999) suggesting the interesting possibility that neuronal defects observed in *Dync1li1<sup>N253Y/N253Y</sup>* mice may be due to interactions with pathways other than those regulated by LIS1.

We note that Importins, transported by cytoplasmic dynein (Perry and Fainzilber, 2009), are involved in synapse-to-nucleus signaling downstream of NMDA receptors (Thompson et al., 2004; Dieterich et al., 2008; Jeffrey et al., 2009), and NMDA receptors are important mediators of anxiety (Barkas et al., 2010). It is possible the *Dync1li1<sup>N253Y</sup>* mutation affects Importin transport in response to NMDA receptor activation, thus altering anxiety in these mice.

Previous mouse studies have shown DYNC1H1 plays an important role in proprioception and sensory neuronal function (Chen et al., 2007; Ilieva et al., 2008). Similarly the *Dync1li1<sup>N253Y</sup>* mutation alters the firing properties, neuron size and morphology of sensory nerves. Thus as sensory nerve deficits have been found now in mouse models with mutations in two different cytoplasmic dynein subunits, possibly DRG neurons are more reliant on dynein-mediated processes than other neuron populations. Cell type specificity may be due to different cargos transported by dynein within the different cells—studies in *Drosophila* show the dynein light intermediate chain interacts with a class of degenerate/epithelial sodium channels (Zheng et al., 2008) that in mammals appear to be found exclusively in DRG (Benson et al., 2002).

Mutation of the light intermediate chain in *Drosophila* cause dendritic and axonal defects in neurons, such as branching defects and a reduction of the dendritic arbor (Sato et al., 2008; Zheng et al., 2008). However, these neuronal phenotypes differ from those found in the present study: in *Drosophila* mutations in the light intermediate chain cause a reduction in the length and number of dendrite branches (Sato et al., 2008; Zheng et al., 2008), whereas the *Dync1li1<sup>N253Y/N253Y</sup>* mice have an increase in dendrite length in cortical neurons (with no changes in branching) and an increase in the number of dendrite branches in DRG neurons. These differences may arise because the reported *Drosophila* mutations cause loss of function, while the *Dync1li1<sup>N253Y</sup>* may be a novel gain of function.

The light intermediate chains play an essential role in endosomal dynamics in cells through their interactions with the RAB protein family (Biell et al., 2001; Sato et al., 2008; Zheng et al., 2008). Studies of the cytoplasmic dynein light intermediate chain in *Drosophila* suggest the cellular machinery controlling dendrite branching is transported in endosomes and Golgi outposts (Sato et al., 2008; Zheng et al., 2008). Our data from the *Dync1li1<sup>N253Y</sup>* mutation support this view to some extent: we found the *Dync1li1<sup>N253Y</sup>* mutation reduces the trafficking of Golgi fragments and endosomes. However, while branching defects were observed in DRG neurons in *Dync1li1<sup>N253Y/N253Y</sup>* mice, we found no such defects in cortical neurons or in the peripheral nerves in the developing limb. In contrast, the cortical neurons of *Dync1li1<sup>N253Y/N253Y</sup>* mice showed other morphological abnormalities such as increased dendrite outgrowth. These results imply that dynein-mediated processes may mediate different aspects of neuronal morphology in different neuronal populations.

We also note that the *Dync1li1<sup>N253Y</sup>* mutation lies at the periphery of a known binding site for pericentrin. The primary function of pericentrin is thought to be the control of the mitotic spindle and the assembly of the centriole. Interestingly, a recent study of Cep120 (a centriole localized protein) hypothesized that defects in centriole formation may lead to alterations in neuronal migration (Mahjoub et al., 2010). Furthermore, there is also evidence to suggest that pericentrin may play a role in cillogenesis (Myoshi et al., 2006) and that ependymal cilia are responsible for directing CSF flow (Lang et al., 2006). Because abnormal CSF flow is linked to gait abnormalities (for example, in the human condition, normal pressure hydrocephalus (Gideon et al., 1994)), it is possible that the *Dync1li1<sup>N253Y</sup>* mutation causes abnormalities in pericentrin localization/function that affect cilia and CSF flow, and thus locomotion in this mouse. Future studies of the *Dync1li1<sup>N253Y</sup>* mutation should look at the interaction between the mutated light-intermediate chain 1 and pericentrin.

In *Dync1li1<sup>N253Y/N253Y</sup>* mice our quantified Western blot studies indicate increased levels of DYNLT3. We cannot tell whether this light chain lies within the complex or not from our westerns, but our immunoprecipitation experiments reveal that while the interaction of the intermediate chains in the core complex is maintained, (1) the increased DYNLT3 levels were not incorporated into the complete complex, and (2) there is a reduction in binding of the DYNLT3 light chains. Currently there is no evidence of a direct interaction between the dynein light intermediate and light chains. Instead the light chains are thought to interact with the intermediate chains within the core complex. It is possible the *Dync1li1<sup>N253Y</sup>* mutation alters the confirmation of the intermediate chains in the complex and this change affects the association of the light chains.

Our knowledge of the roles of the individual cytoplasmic dynein subunits comes from studies in nonmammalian organisms and in transfected cell lines, with the exception of the heavy chain, for which four mutant alleles are known in mouse: (1) a gene targeted knock-out; the point mutants (2) Legs at odd angles (*Dync1h1<sup>Loa</sup>*) and (3) Cramping 1 (*Dync1h1<sup>Cm1</sup>*); (4) a 9 bp coding deletion Sprawling (*Dync1h1<sup>Spw</sup>*) (Harada et al., 1998; Hafezparast et al., 2003; Chen et al., 2007). Homozygous knock-out (null) mice die early in embryogenesis and there is no reported phenotype for heterozygous knock-outs (Harada et al., 1998). In contrast *Dync1h1<sup>Loa</sup>*, *Dync1h1<sup>Cm1</sup>* and *Dync1h1<sup>Spw</sup>* heterozygotes have major defects in the proprioceptive system and locomotor abnormalities (homozygotes die in embryogenesis/at birth) (Harada et al., 1998; Hafezparast et al., 2003; Kieran et al., 2005; Chen et al., 2007; Banks and Pflieger, 2008; Ilieva et al., 2008; Dupuis et al., 2009). We note that the phenotype of the *Dync1li1<sup>N253Y</sup>* mouse strain is different from that of the four heavy chain mutants, particularly with respect to behavior. The heavy chain and *Dync1li1<sup>N253Y</sup>* mutants all give rise to defects in Golgi reassembly (Hafezparast et al., 2003) and EGF trafficking (Hafezparast et al., 2003; our unpublished data) both of which are known to be dynein-dependent processes. However, heterozygous *Dync1h1<sup>Loa</sup>* mice develop an obvious gait abnormality ("low-based, reptilian") easily visible by eye, plus significant defects in rotarod and grip-strength, none of which we find in the *Dync1li1<sup>N253Y/N253Y</sup>* mutants at comparable ages (Hafezparast et al., 2003). There are also significant reductions in axon numbers in the saphenous nerve of *Dync1h1<sup>Loa</sup>* mice and more profound neurophysiological changes in nerve conduction properties compared with the *Dync1li1<sup>N253Y/N253Y</sup>* mutants (AlQatari et al., 2009). We note that we did not find significant alterations in peripheral nerve branching at E13.5, whereas this was seen in both

heterozygous and homozygous *Dync1h1<sup>Loa</sup>* mutants. A deeper comparison of the different subunit mutants at the cellular level would shed more light on the role of specific subunits, versus the entire complex, and here we clearly show phenotypes that have not been described before for in any of the heavy chain mutants. We note that Ori-McKenney, Vallee and colleagues have recently shown altered processivity of dynein with the *Dync1h1<sup>Loa</sup>* heavy chain mutation (Ori-McKenney et al., 2010), such a change is unlikely in the *Dync1h1<sup>K2527</sup>* light intermediate chain mutation, which would presumably explain the somewhat different phenotypes of mutant mice, although this needs to be investigated.

Here we have used freely available mouse genetics resources to take a focused genotype-driven approach, working with a point mutation likely to be more informative than a knock-out, to analyzing one more of the 11 cytoplasmic dynein subunit proteins and have uncovered diverse roles at the level of the whole organism, nervous system and cell. The *Dync1h1<sup>K2527</sup>* mouse has opened up new avenues for investigation of the roles of cytoplasmic dynein and its individual components, and gives new insight into the functioning and architecture of the mammalian nervous system.

## References

- Achilli F, Bros-Facér V, Williams HP, Banks GT, AlQatari M, Chia R, Tucci V, Groves M, Nickols CD, Sebam KL, Kendall R, Cadar MZ, Talbot K, van Minsse J, Burgess RW, Brandner S, Martin JE, Koltzenburg M, Green-Smith L, Nolan PM, et al. (2009) A novel mouse model with a point mutation in glycyl-tRNA synthetase (*Gars*) has sensory and motor phenotypes and profoundly reduced enzyme activity in homozygotes. *Dis Mod Mech* 2:359–373.
- AlQatari M, Vastani N, Bros-Facér V, Groves M, Green-Smith L, Fisher EMC, Koltzenburg M (2009) Mutations of the cytoplasmic dynein heavy chain gene *Dync1h1* cause a severe sensory neuropathy. *J Peripher Nerv Syst* 14 (S2):6.
- Banker G, Goulán K (1998) *Culturing nerve cells*. Cambridge, MA: Massachusetts Institute of Technology.
- Banks GT, Fisher EM (2008) Cytoplasmic dynein could be key to understanding neurodegeneration. *Genome Biol* 9:214.
- Barkas C, McHugh SJ, Sprengel R, Seeburg PH, Rawlins JN, Sunnerman DM (2010) Hippocampal NMDA receptors and anxiety: at the interface between cognition and emotion. *Eur J Pharmacol* 626:49–56.
- Benson CL, Xie J, Wemmie JA, Price MP, Hens JM, Welsh MJ, Snyder PM (2002) Heteromultimers of DEG/ENAC subunits form H<sup>+</sup>-gated channels in mouse sensory neurons 1. *Proc Natl Acad Sci U S A* 99:2338–2343.
- Bielli A, Thörnqvist PO, Hendrick AG, Finn R, Fitzgerald K, McCaffrey MW (2001) The small GTPase Rab4A interacts with the central region of cytoplasmic dynein light intermediate chain-1. *Biochem Biophys Res Commun* 281:1141–1153.
- Carin-Todd L, Bath KG, Fulgenzi G, Yanpallewar S, Jing D, Barrick CA, Becker J, Buckley H, Dorsey SG, Lee FS, Tenarollo L (2009) Endogenous truncated TrkB: T1 receptor regulates neuronal complexity and TrkB kinase receptor function in vivo. *J Neurosci* 29:678–685.
- Chen XI, Levedakou EN, Millen KI, Wollmann RL, Soliven B, Popko B (2007) Proprioceptive sensory neuropathy in mice with a mutation in the cytoplasmic dynein heavy chain 1 gene. *J Neurosci* 27:14515–14524.
- Costa C, Harding B, Copp AJ (2001) Neuronal migration defects in the Dreher (*Lm1a*) mutant mouse: role of disorders of the glial limiting membrane. *Cereb Cortex* 11:498–505.
- Deacon RM, Penny C, Rawlins JN (2003) Effects of medial prefrontal cortex cytoskeletal lesions in mice. *Behav Brain Res* 139:139–155.
- DeFries JC, Gervais MC, Thomas EA (1978) Response to 30 generations of selection for open-field activity in laboratory mice. *Behav Genet* 8:3–13.
- Dieterich DC, Karpova A, Mikhaylova M, Zdobnova I, Ktnig L, Landwehr M, Kreuz M, Smalla KH, Richter K, Landgraf P, Reisser C, Boeckers TM, Zschentner W, Spilker C, Seidenbecher CI, Garner CC, Gundelfinger ED, Kreuz MR (2008) Caldesmon-1: a protein liaison that couples NMDA receptor signalling to the nucleus. *PLoS Biol* 6:e34.
- Driskell OJ, Mironov A, Allan VI, Woodman PG (2007) Dynein is required for receptor sorting and the morphogenesis of early endosomes. *Nat Cell Biol* 9:113–120.
- Dupain L, Fergani A, Braunstein KE, Eichbach I, Holln, Rane F, Gonzalez De Aguilar JL, Zorum B, Schwalmstocker B, Ludolph AC, Loeffler JP (2009) Mice with a mutation in the dynein heavy chain 1 gene display sensory neuropathy but lack motor neuron disease. *Exp Neurol* 215:146–152.
- Gennerich A, Carter AP, Reck-Peterson SL, Vale RD (2007) Force-induced bidirectional stepping of cytoplasmic dynein. *Cell* 131:952–965.
- Gideon P, Ståhlberg P, Thomsen C, Gjørris F, Sørensen PS, Henriksen O (1994) Cerebrospinal fluid flow and production in patients with normal pressure hydrocephalus studied by MRI. *Neuroradiology* 36:210–215.
- Goldwater DS, Pavlides C, Hunter RG, Bloss EB, Hof PR, McEwen BS, Morrison JH (2009) Structural and functional alterations to rat medial prefrontal cortex following chronic restraint stress and recovery. *Neuroscience* 164:798–808.
- Ha J, Lo KW, Myers KR, Carr TM, Humi MK, Basoul BA, Segal RA, Pfister KK (2008) A neuron-specific cytoplasmic dynein isoform preferentially transports TrkB signaling endosomes. *J Cell Biol* 181:1027–1039.
- Hafeezparast M, Klocke R, Ruhrberg C, Marquardt A, Ahmad-Amrur A, Bowen S, Lalis G, Witherden AS, Hummerich H, Nicholson S, Morgan PJ, Ouzagheer R, Priestley JV, Averill S, King VR, Ball S, Peters J, Toda T, Yamamoto A, Hiraoka Y, et al. (2003) Mutations in dynein link motor neuron degeneration to defects in retrograde transport. *Science* 300:808–812.
- Hanz S, Perlson E, Willis D, Zheng JQ, Manarwa R, Huerta JJ, Koltzenburg M, Kohler M, van Minsse J, Twiss JL, Fainzilber M (2003) Axoplasmic importins enable retrograde injury signaling in lesioned nerve. *Neuron* 40:1095–1104.
- Harauda A, Takai Y, Kamai Y, Tanaka Y, Norioka S, Hirokawa N (1998) Golgi vesiculation and lysosome dispersion in cells lacking cytoplasmic dynein. *J Cell Biol* 141:51–59.
- Hirotsune S, Fleck MW, Gambello MI, Eix GI, Chen A, Clark GD, Ledbetter DH, McBain CJ, Wymshaw-Boria A (1998) Graded reduction of Pafah1b1 (*Lis1*) activity results in neuronal migration defects and early embryonic lethality. *Nat Genet* 19:333–339.
- Höök P, Vallee RB (2006) The dynein family at a glance. *J Cell Sci* 119:4369–4371.
- Hughes SM, Vaughan KT, Herkowitz JS, Vallee RB (1995) Molecular analysis of a cytoplasmic dynein light intermediate chain reveals homology to a family of ATPases. *J Cell Sci* 108:17–24.
- Ilieva HS, Yamanaka K, Mallema S, Kakinohana O, Yakoh T, Marumoto M, Cleveland DW (2008) Mutant dynein (*Loa*) triggers proprioceptive axon loss that extends survival only in the SOD1 ALS model with highest motor neuron death. *Proc Natl Acad Sci U S A* 105:12599–12604.
- Jeffrey RA, Ch'ng TH, O'Dell TJ, Martin KC (2009) Activity-dependent anchoring of importin alpha at the synapse involves regulated binding to the cytoplasmic tail of the NR1-1a subunit of the NMDA receptor. *J Neurosci* 29:15613–15620.
- Keays DA, Tian G, Poirier K, Huang G, Siebold C, Clauk J, Oliver PL, Fray M, Harvey RI, Molnar Z, Piton MC, Duan N, Valdar W, Brown SD, Davies KE, Rawlins JN, Cowan NJ, Nolan P, Chelly J, Flint J (2007) Mutations in alpha-subunit cause abnormal neuronal migration in mice and lissencephaly in humans. *Cell* 128:45–57.
- Kieran D, Hafeezparast M, Bohner S, Dick JR, Martin J, Schiavo G, Fisher EM, Green-Smith L (2005) A mutation in dynein rescues axonal transport defects and extends the lifespan of ALS mice. *J Cell Biol* 169:561–567.
- Koltzenburg M, Stucky CL, Lewin GR (1997) Receptive properties of mouse sensory neurons innervating hairy skin. *J Neurophysiol* 78:1841–1850.
- Kudo T, Fujii T, Ikegami S, Inokuchi K, Takayama Y, Ikehara Y, Nishihara S, Togyachi A, Takahashi S, Tachibana K, Yama S, Nirimatsu H (2007) Mice lacking alpha-3-fucosyltransferase IX demonstrate disappearance of Lewis x structure in brain and increased anxiety-like behaviors. *Glycobiology* 17:1–9.
- Kuta A, Deng W, Morri El-Kadi A, Banks GT, Hafeezparast M, Pfister KK, Fisher EM (2010) Mouse cytoplasmic dynein intermediate chain: identification of new isoforms, alternative splicing and tissue distribution of transcripts. *PLoS One* 5:e11682.
- Lang B, Song B, Davidson W, MacKenzie A, Smith N, McCaig CD, Hammar AJ, Shen S (2006) Expression of the human PAC1 receptor leads to dose-dependent hydrocephalus-related abnormalities in mice. *J Clin Invest* 116:1924–1934.

- Levy JR, Holtbauer EL (2006) Cytoplasmic dynein/dynactin function and dysfunction in motor neurons. *Int J Dev Neurosci* 24:105–111.
- Mahjoub MR, Xie Z, Stearns T (2010) Cep120 is asymmetrically localized to the daughter centriole and is essential for centriole assembly. *J Cell Biol* 191:331–346.
- Milner LC, Crabbe JC (2008) Three murine anxiety models: results from multiple inbred strain comparisons. *Genes Brain Behav* 7:496–505.
- Miyoshi K, Onishi K, Asanuma M, Miyazaki I, Diaz-Corrales FI, Ogawa N (2006) Embryonic expression of pericentrin suggests universal roles in cilogenesis. *Dev Genes Evol* 216:537–542.
- Nolan PM, Peters J, Srivastava M, Rogers D, Hagan J, Spurr N, Gray JC, Vizar L, Brooker D, Whitehill E, Washbourne R, Hough T, Govenaway S, Hewitt M, Liu X, McCormack S, Pickford K, Selley R, Wells C, Tymowska-Lalanne Z, et al. (2000) A systematic, genome-wide, phenotype-driven mutagenesis programme for gene function studies in the mouse. *Nat Genet* 25:440–443.
- Ori-McKenney KM, Xu J, Gross SP, Vallee RB (2010) A cytoplasmic dynein tail mutation impairs motor processivity 1. *Nat Cell Biol* 12:1228–1234.
- Palmer KI, Hughes H, Stephens DJ (2009) Specificity of cytoplasmic dynein subunits in discrete membrane-trafficking steps. *Mol Biol Cell* 20:2885–2899.
- Pascual R, Zamora-León SP (2007) Effects of neonatal maternal deprivation and postweaning environmental complexity on dendritic morphology of prefrontal pyramidal neurons in the rat. *Acta Neurobiol Exp (Wars)* 67:471–479.
- Paylor R, Hirotsune S, Gambello MJ, Yava-Paylor L, Crawley JN, Wynshaw-Boris A (1999) Impaired learning and motor behavior in heterozygous *Pafah1b1* (*Lis1*) mutant mice. *Learn Mem* 6:521–537.
- Perry RB, Fainzilber M (2009) Nuclear transport factors in neuronal function. *Semin Cell Dev Biol* 20:600–606.
- Pfister KK, Salata MW, Dillman JF 3rd, Torre E, Lye RJ (1996a) Identification and developmental regulation of a neuron-specific subunit of cytoplasmic dynein. *Mol Biol Cell* 7:331–343.
- Pfister KK, Salata MW, Dillman JF 3rd, Vaughan KT, Vallee RB, Torre E, Lye RJ (1996b) Differential expression and phosphorylation of the 74-kDa intermediate chains of cytoplasmic dynein in cultured neurons and glia. *J Biol Chem* 271:1687–1694.
- Pfister KK, Fisher EM, Gibbons III, Hays TS, Holtbauer EL, McIntosh JR, Porter ME, Schroer TA, Vaughan KT, Witman GB, King SM, Vallee RB (2005) Cytoplasmic dynein nomenclature. *J Cell Biol* 171:411–413.
- Pfister KK, Shah PR, Hammerich H, Russ A, Cotton J, Annuar AA, King SM, Fisher EM (2006) Genetic analysis of the cytoplasmic dynein subunit families. *PLoS Genet* 2:e1.
- Qaswailid MM, Hugill A, Dear N, Vizar L, Wells S, Horner E, Fuller S, Weedon J, McMath H, Woodman P, Edwards D, Campbell D, Rodger S, Carey I, Roberts A, Glenister P, Lalanne Z, Parkinson N, Coghill EL, McKeone R, et al. (2004) A gene-driven ENU-based approach to generating an allelic series in any gene. *Mamm Genome* 15:585–591.
- Rogers DC, Fisher EM, Brown SD, Peters J, Hunter AJ, Martin JE (1997) Behavioral and functional analysis of mouse phenotype SHIRPA, a proposed protocol for comprehensive phenotype assessment. *Mamm Genome* 8:711–713.
- Rogers DC, Peters J, Martin JE, Ball S, Nicholson SJ, Withenden AS, Hafizparant M, Latchans J, Robinson TL, Quilley CA, Fisher EM (2001) SHIRPA, a protocol for behavioral assessment: validation for longitudinal study of neurological dysfunction in mice. *Neurosci Lett* 306:89–92.
- Salata MW, Dillman JF 3rd, Lye RJ, Pfister KK (2001) Growth factor regulation of cytoplasmic dynein intermediate chain subunit expression precedes neurite extension. *J Neurosci Res* 65:408–416.
- Sato D, Sato D, Tsuyama T, Saito M, Ohkura H, Rolls MM, Ishikawa F, Uemura T (2008) Spatial control of branching within dendritic arbors by dynein-dependent transport of Rab5-endosomes. *Nat Cell Biol* 10:1164–1171.
- Scobie KN, Hall BJ, Wilke SA, Klomparens KC, Fujii-Kuriyama Y, Ghosh A, Hen R, Sahay A (2009) Kruppel-like factor 9 is necessary for late-phase neuronal maturation in the developing dentate gyrus and during adult hippocampal neurogenesis 1. *J Neurosci* 29:9875–9887.
- Thompson KR, Okia KO, Chen DM, Zhao Y, O'Dell TJ, Martin KC (2004) Synapse to nucleus signaling during long-term synaptic plasticity: a role for the classical active nuclear import pathway. *Neuron* 44:997–1009.
- Tsai JW, Beemer KH, Vallee RB (2007) Dual subcellular roles for LIS1 and dynein in radial neuronal migration in live brain tissue. *Nat Neurosci* 10:970–979.
- Tyan SH, Parohita A, Dotsey SJ, Vallee RB (2000) Light intermediate chain 1 defines a functional subfraction of cytoplasmic dynein which binds to pericentrin. *J Biol Chem* 275:32763–32768.
- Zhang J, Li S, Musa S, Zhou H, Xiang X (2009) Dynein light intermediate chain in *Aspergillus nidulans* is essential for the interaction between heavy and intermediate chains. *J Biol Chem* 284:34760–34768.
- Zheng Y, Wildonger J, Ye B, Zhang Y, Kita A, Younger SH, Zimmerman S, Jan LY, Jan YN (2008) Dynein is required for polarized dendritic transport and uniform microtubule orientation in axons. *Nat Cell Biol* 10:1172–1180.